UNIVERSITÄT DUISBURG ESSEN

Offen im Denken

DISSECTION AND MODULATION OF (PATHO)BIOLOGICAL SURVIVIN FUNCTIONS BY SUPRAMOLECULAR LIGANDS

Dissertation

zur Erlangung des Doktorgrades

Dr. rer. nat.

der Fakultät für Biologie

an der Universität Duisburg-Essen

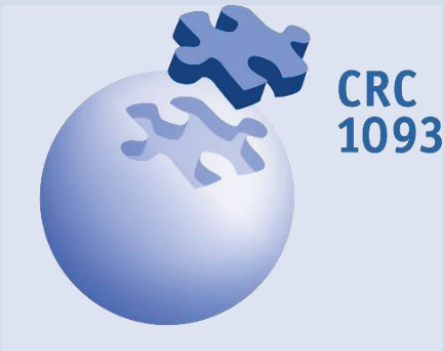

vorgelegt von

Sandra Bäcker

aus Löningen

Juni 2018

DOI: 10.17185/duepublico/47121
URN: urn:nbn:de:hbz:464-20211026-082806-4

Die der vorliegenden Arbeit zugrunde liegenden Experimente wurden am Zentrum für medizinische Biotechnologie in der Abteilung für Molekularbiologie II der Universität Duisburg-Essen durchgeführt.

1. Gutachter:	Prof. Dr. Shirley Knauer
2. Gutachter:	Prof. Dr. Peter Bayer
3. Gutachter:	
Vorsitzende des Prüfungsausschusses:	Prof. Dr. Elsa Sánchez-García
Tag der mündlichen Prüfung:	12.09.2018

TABLE OF CONTENTS

LIST OF ABBREVIATIONS

°C ..... degree Celsius
A ..... absorbance
A ..... adenine
A ..... ampere
Å ..... angstrom
aa ..... amino acid(s)
Ab ..... antibody
AF ..... Alexa Fluor
Amp ..... ampicillin
Apaf-1 ..... apoptotic protease activating factor 1
ApE ..... A plasmid Editor
Apo2L ..... Apo2 ligand
APS ..... ammonium persulfate
atm ..... atmosphere
AU ..... arbitrary unit
Bcl-2 ..... B-cell lymphoma-2
Bcl-XL ..... B-cell lymphoma-extra large
BEST ..... band-selective excitation short-transient
BIR ..... baculovirus IAP repeat
BIRC5 ..... baculovirus IAP repeat-containing protein 5
bp ..... base pair
BSA ..... bovine serum albumin
C ..... carbon
C ..... cytoplasmic
C ..... cytosine
c ..... centi
c ..... concentration
cal ..... calorie
Carb ..... carbenicillin
CARD ..... caspase-associated recruitment domain
CAS ..... cellular apoptosis susceptibility protein
caspase ..... cysteinyl-aspartate-specific protease
CBP ..... CREB-binding protein

CD ..... circular dichroism
CDK ..... cyclin-dependent kinase
c-IAP ..... cellular inhibitor of apoptosis protein
CMV ..... cytomegalovirus
CPC ..... chromosomal passenger complex
CRC ..... Collaborative Research Center
CREB ..... cyclic adenosine monophosphate response element-binding protein
CRIME ..... CRM1, importin-β etc.
CRM1 ..... chromosome region maintenance 1
C-term. ..... carboxy-terminal/terminus
d ..... deci
Da ..... dalton
deg ..... degree
dGTP ..... deoxyguanosine triphosphate
DIABLO ..... direct inhibitor of apoptosis protein-binding protein with low pI
DIM ..... dimerization
DISC ..... death-inducing signaling complex
DMEM ..... Dulbecco's Modified Eagle Medium
DNA ..... deoxyribonucleic acid
DNase ..... deoxyribonuclease
dNTP ..... deoxynucleotide triphosphate
DPBS ..... Dulbecco's Phosphate-Buffered Saline
DPSS ..... diode-pumped solid-state
DR4/5 ..... death receptor 4/5
DTT ..... dithiothreitol
ECL ..... enhanced chemiluminescence
E. coli ..... *Escherichia coli*
EDTA ..... ethylenediaminetetraacetic acid
e.g. ..... exempli gratia (for example)
et al. ..... *et alii*
etc. ..... et cetera
ExPASy ..... Expert Protein Analysis System
f ..... femto
f ..... forward
FADD ..... fas-associated death domain
FCS ..... fetal calf serum
for ..... forward
fw ..... forward

G ..... gap
G ..... Gibbs energy
G ..... guanine
g ..... gram
g ..... gravity (force)
GAP ..... GTPase-activating protein
GDP ..... guanosine diphosphate
GEF ..... guanine exchange factor
GSH ..... glutathione
GST ..... glutathione S-transferase
GTP ..... guanosine triphosphate
GTPase ..... guanosine triphosphatase
H ..... enthalpy
H ..... hydrogen
h ..... hour
HA ..... hemagglutinin
HBXIP ..... hepatitis B X-interacting protein
HEAT ..... huntingtin, elongation factor 3, protein phosphatase 2A and yeast kinase target of rapamycin kinase 1
HeLa ..... Henrietta Lacks
HRP ..... horseradish peroxidase
HSQC ..... heteronuclear single quantum correlation
Hz ..... hertz
I ..... intensity
IAP ..... inhibitor of apoptosis protein
ICCE ..... Imaging Center Campus Essen
IEC ..... ion exchange chromatography
IF ..... immunofluorescence
IgG ..... immunoglobulin G
ILP2 ..... inhibitor of apoptosis protein-like protein 2
INCENP ..... inner centromere protein
IPTG ..... isopropyl b-D-1-thiogalactopyranoside
ITC ..... isothermal titration calorimetry
J ..... joule
K ..... Kelvin
k ..... kilo
K_A ..... association constant
Kan ..... kanamycin

Kap ..... karyopherin
kb ..... kilobase
K_D ..... dissociation constant
KPi ..... potassium phosphate
l ..... liter
lac ..... lactose
LB ..... Luria-Bertani
LC ..... liquid chromatography
LGC ..... Laboratory of the Government Chemist
LMB ..... Leptomycin B
M ..... mega
M ..... mitosis
M ..... mol/liter
m ..... meter
m ..... milli
Mcl-1 ..... myeloid cell leukemia-1
MD ..... molecular dynamic
Mg ..... magnesium
min ..... minute
ML-IAP ..... melanoma-inhibitor of apoptosis protein
mRNA ..... messenger ribonucleic acid
mut ..... mutant
MW ..... molecular weight
N ..... nitrogen
N ..... nuclear
n ..... nano
NAIP ..... neuronal apoptosis inhibitory protein
NES ..... nuclear export signal
NF-κB ..... nuclear factor kappa-light-chain-enhancer of activated B cells
NLS ..... nuclear localization signal
NMR ..... nuclear magnetic resonance
NP-40 ..... Nonidet P-40
NPC ..... nuclear pore complex
N-term. ..... amino-terminal/terminus
NTF2 ..... nuclear transport factor 2
NUP ..... nucleoporin
O ..... oxygen
OD_{600} ..... optical density at 600 nm

Opti-MEM ..... Optimized Minimum Essential Medium
P ..... phosphorus
p ..... pico
Pa ..... pascal
PAGE ..... polyacrylamide gel electrophoresis
PBS ..... phosphate-buffered saline
PCB ..... PreScission protease cleavage buffer
PCR ..... polymerase chain reaction
PDB ..... protein data bank
PEI ..... polyethylenimine
pH ..... potentia Hydrogenii
PKI ..... protein kinase A inhibitor
PLA ..... proximity ligation assay
PMSF ..... phenylmethanesulfonylfluoride
PPI ..... protein–protein interaction
ppm ..... parts per million
PreSc ..... PreScission protease (recognition sequence)
Prom ..... promotor
PTM ..... post-translational modification
PVDF ..... polyvinylidene difluoride
QM/MM ..... quantum mechanics/molecular mechanics
R ..... resistance
® ..... registered trademark
r ..... reversed
Ran ..... Ras-related nuclear protein
RanBP ..... Ran-binding protein
Ras ..... rat sarcoma
RCC1 ..... regulator of chromosome condensation 1
rev ..... reversed
RING ..... really interesting new gene
RIPA ..... radioimmunoprecipitation assay
RNA ..... ribonucleic acid
rpm ..... revolutions per minute
RT ..... room temperature
S ..... entropy
S ..... synthesis
s ..... second
SAF ..... spindle assembly factor

SDS ..... sodium dodecyl sulfate
seq ..... sequencing
SINE ..... Selective Inhibitors of Nuclear Export
Smac ..... second mitochondria-derived activator of caspase
SOE ..... splice overlap extension
Surv ..... Survivin
SV40 ..... simian virus 40
T ..... temperature
T ..... thymine
T ..... tumor
TAE ..... Tris-acetate-EDTA
TAMRA 5-carboxytetramethylrhodamine
TBS ..... Tris-buffered saline
TBST ..... Tris-buffered saline and Tween 20
TEMED ..... tetramethylethylenediamine
Term ..... terminator
TM ..... trademark
TRAIL ..... tumor necrosis factor related apoptosis-inducing ligand
Tris ..... Tris(hydroxymethyl)aminomethane
Tris-HCl ..... Tris hydrochloride
tRNA ..... transfer ribonucleic acid
TROSY ..... transverse relaxation optimized spectroscopy
UV ..... ultraviolet
V ..... volt
v/v ..... volume per volume
WB ..... western blotting
w/o ..... without
WT ..... wild type
w/v ..... weight per volume
XIAP ..... X-linked inhibitor of apoptosis protein
YFP ..... yellow fluorescent protein
Zn ..... zinc
Δ ..... change/difference
δ ..... chemical peak shift
λ ..... wavelength
µ ..... micro

LIST OF FIGURES

LIST OF TABLES

SUMMARY

Targeted cancer therapy provides a promising approach to fight cancer, the second leading cause of death worldwide following cardiovascular diseases, and reduces or avoids harmful side effects occurring in conventional chemo- and radiotherapy. This therapy addresses specific targets, which are preferentially or exclusively expressed in cancer cells. Survivin, highly up-regulated in almost all cancer types, represents such a target. Its overexpression is associated with resistance against chemo- and radiotherapy, frequent recurrences and decreased patient survival. As a member of the inhibitor of apoptosis protein (IAP) family, Survivin plays a cytoprotective role by inhibiting cell death, but as part of the chromosomal passenger complex (CPC) it is also crucial for the regulation of mitosis. For both biological functions, an interaction with the nuclear export receptor CRM1, mediated by Survivin's highly conserved, leucine-rich nuclear export signal (NES), is pivotal. However, the mechanisms regulating Survivin's biological functions are still not completely resolved and a matter of scientific controversy. Thus, interference with the Survivin–CRM1 interaction could not only help to elucidate the distinct biological functions of Survivin but also to potentially inhibit cancer cell proliferation. Small molecule inhibitors of the export receptor CRM1 have already been identified. However, they supposedly also interfere with binding of CRM1 to other NES-bearing proteins, making them at most selective but clearly not specific.

Therefore, this work aims to signal-specifically target the NES of Survivin instead of the receptor and thereby to inhibit the interaction between the surface-exposed NES and CRM1 by supramolecular tweezer molecules, which are able to bind to surface-accessible lysine and arginine residues.

Establishing a robust protein expression and purification system enabled recombinant production not only of Survivin, but also of the high molecular weight export receptor CRM1 and its cofactor Ran for biochemical *in vitro* assays and structural analyses. Characterization of the purified proteins by circular dichroism (CD) spectroscopy revealed correct protein folding, while analytical gel filtration confirmed their theoretical molecular weight and demonstrated Survivin's dimerization state. To improve binding affinity and specificity towards Survivin, a short peptide (ELTL) and an elongated version (ELTLGEFL), both mimicking the C-terminus of the NES and the overlapping dimer interface of Survivin, were linked to the basic tweezer as a second binding motif. Binding of the unmodified and both peptide-linked tweezer molecules to Survivin was demonstrated by ITC analyses with affinities in the micromolar range (20–30 µM). As expected, the tweezer bearing the

elongated peptide ELTLGEFL had the highest affinity to Survivin. Moreover, NMR titration experiments confirmed tweezer binding to specific basic amino acids (K90/91, K103 and R106) within or near Survivin's NES. Considering additional MD and QM/MM results, the tweezer modified with the short peptide ELTL revealed indeed a higher specificity to Survivin. Biochemical pull-down assays demonstrated that tweezers were indeed able to interfere with the Survivin–CRM1 interaction *in vitro*. This could not only be shown using purified proteins but also in competition with a variety of other potential cargo proteins in eukaryotic cell lysates. The effective inhibiting concentrations were 10–50 µM, agreeing with the results from ITC measurements. Peptide modifications of the tweezer molecules enhanced their ability to interfere with Survivin–CRM1 complex formation. Unexpectedly, mutations of the basic amino acids K90/91 and K103, supposedly involved in tweezer binding, to serine residues revealed an enhanced binding affinity of the basic and ELTL-linked tweezer. As this Survivin mutant exhibited structural defects affecting ITC results, the search for other suitable mutations is required. Nevertheless, investigations of this Survivin mutant in cell lysates revealed that all three tweezer molecules could not interfere with the Survivin–CRM1 interaction, thus suggesting that tweezer molecules mediate their inhibitory effect by specifically targeting lysines in Survivin's NES and dimer interface.

In the future, the establishment of cellular assays for Survivin–CRM1 co-localization as well as the analysis of nuclear export activity enables cellular investigations of biological functions. Moreover, the discovery of cellular tweezer uptake will allow analyses of the effects a functional interference by supramolecular tweezers entails. A further improvement of binding affinity as well as specificity could be achieved by multivalency for example with a supramolecular ligand which combines two tweezer units anchored at two opposed sites of the NES and linked via an extended peptide sequence flanking and mimicking most of the NES. Moreover, nanoparticles and precision macromolecules covalently decorated with a combination of different Survivin NES-specific ligands would create additional hetero- and multiavidity.

To conclude, peptide modifications of supramolecular tweezer molecules seemed to be a promising strategy to successfully improve their affinity and specificity to Survivin as well as their ability to interfere with the Survivin–CRM1 interaction.

ZUSAMMENFASSUNG

Die zielgerichtete Krebstherapie bietet einen vielversprechenden Ansatz zur Bekämpfung von Krebs, der weltweit zweithäufigsten Todesursache nach Herz-Kreislauf-Erkrankungen, und verringert oder vermeidet dabei gesundheitliche Nebenwirkungen, die bei der konventionellen Chemo- und Strahlentherapie auftreten. Derartige Therapien adressieren spezifische Zielmoleküle, die bevorzugt oder ausschließlich in Krebszellen vorkommen. Survivin, das in fast allen Krebsarten hochreguliert ist, stellt ein solches Ziel dar. Die Überexpression von Survivin ist mit einer Resistenz gegen Chemo- und Strahlentherapie, einer erhöhten Rezidiv- sowie einer verminderten Überlebensrate der Patienten assoziiert. Als Mitglied der IAP-Proteinfamilie hemmt Survivin den Zelltod und besitzt somit eine zytoprotektive Aktivität, ist aber als Teil des CPC auch entscheidend an der Regulation der Mitose beteiligt. Für beide biologische Funktionen ist eine Interaktion mit dem nukleären Exportrezeptor CRM1 ausschlaggebend, die durch Survivins hochkonserviertes, Leucin-reiches NES vermittelt wird. Allerdings sind die Mechanismen, welche die biologischen Funktionen von Survivin regulieren, noch immer nicht vollständig geklärt und werden teilweise kontrovers diskutiert. Eine Inhibition der Survivin–CRM1-Interaktion könnte also nicht nur dazu beitragen, die biologischen Funktionen von Survivin aufzuklären, sondern zudem einen neuen Ansatz zur Hemmung der Krebszellproliferation darstellen. Inhibitoren des Exportrezeptors CRM1 wurden bereits identifiziert. Diese interferieren allerdings auch mit der Bindung von CRM1 an andere NES-tragende Proteine, was sie bestenfalls selektiv, aber nicht spezifisch wirksam macht.

Daher zielt diese Arbeit darauf ab, anstelle des Export-Rezeptors das NES von Survivin gezielt mit supramolekularen Pinzetten, die an oberflächenzugängliche Lysin- und Argininreste binden können, zu adressieren und dabei die aktivitätsvermittelnde Wechselwirkung zwischen Survivins oberflächenexponiertem NES und CRM1 zu stören.

Die Etablierung eines robusten Proteinexpressions- und Reinigungssystems ermöglichte die rekombinante Herstellung von Survivin, dem Exportrezeptor CRM1 sowie seinem Cofaktor Ran, die in biochemischen *in vitro* Experimenten und Strukturanalysen eingesetzt wurden. Durch die Charakterisierung aller gereinigten Proteine mittels CD-Spektroskopie konnte ihre korrekte Proteinfaltung nachgewiesen werden. Die analytische Gelfiltration bestätigte ihr theoretisches Molekulargewicht und die Dimerisierung von Survivin. Um die Bindungsaffinität und Spezifität gegenüber Survivin zu verbessern, wurden ein kurzes (ELTL) und ein verlängertes Peptid (ELTLGEFL), die sowohl den C-terminalen Teil des NES als auch die überlappende Dimerisierungsregion von Survivin nachahmen, als zweites Bindungsmotiv

kovalent an das Pinzetten-Grundmolekül gebunden. Die Bindung der unmodifizierten und der beiden Peptid-gebundenen Pinzetten an Survivin konnte durch ITC-Analysen mit Affinitäten im mikromolaren Bereich (20–30 µM) gezeigt werden. Tatsächlich wies die Pinzette mit dem verlängerten Peptid ELTLGEFL dabei die höchste Affinität zu Survivin auf. Darüber hinaus wurde die Bindung an bestimmte basische Aminosäuren (K90/91, K103 und R106) innerhalb oder in der Nähe des NES durch NMR-Titrationsexperimente nachgewiesen. Unter Berücksichtigung zusätzlicher Ergebnisse aus MD- sowie QM/MM-Studien konnte für die ELTL-gebundene Pinzette eine höhere Spezifität zu Survivin gezeigt werden. Biochemische *Pull-down*-Experimente konnten belegen, dass die Pinzetten die Survivin–CRM1-Interaktion *in vitro* hemmen. Dies konnte nicht nur mit gereinigten Proteinen bestätigt werden, sondern auch in eukaryotischen Zelllysaten, in denen Survivin mit vielen anderen potenziellen Frachtproteinen von CRM1 konkurrierte. Die effektiven Inhibitorkonzentrationen lagen in Einklang mit den ITC-Ergebnissen zwischen 10 und 50 µM. Darüber hinaus zeigten die Peptid-gebundenen Pinzetten ein erhöhtes Hemmungspotential gegenüber der Survivin–CRM1-Komplexbildung. Unerwarteterweise zeigten Mutationen der vermutlich an der Pinzettenbindung beteiligten basischen Aminosäuren K90/91 und K103 zu Serin eine erhöhte Bindungsaffinität für die unmodifizierte sowie die ELTL-verknüpfte Pinzette. Da diese Survivin-Mutante aber erhebliche strukturelle, die ITC-Ergebnisse beeinflussende Defekte aufwies, ist hier der Einbau von besser geeigneten Mutationen erforderlich. Gleichwohl zeigten Untersuchungen mit dieser Survivin-Mutante in Zelllysaten, dass hier keine der drei Pinzetten die Survivin–CRM1-Wechselwirkung zu beeinflussen vermochte. Dies lässt vermuten, dass die Pinzetten ihre inhibitorische Wirkung tatsächlich über die gezielte Bindung von Lysinen in Survivins NES und Dimerisierungsregion vermitteln.

Zukünftig wird die Etablierung zellulärer Experimente zum Nachweis der Survivin–CRM1-Co-Lokalisation sowie zur Analyse der nukleären Exportaktivität weiterführende Untersuchungen der biologischen Funktion von Survivin ermöglichen. Der Nachweis der zellulären Aufnahme der supramolekularen Pinzetten wird weiterhin Analysen möglicher Interferenzeffekte erlauben. Eine weitere Verbesserung der Bindungsaffinität sowie der Spezifität könnte durch Multivalenz erreicht werden, beispielsweise mit einem supramolekularen Liganden, welcher beispielsweise zwei Pinzetteneinheiten kombiniert. Diese könnten an zwei Bindestellen im NES und der Dimerisierungsregion verankert und über eine ausgedehnte Peptidsequenz verbunden sein, die das NES größtenteils nachahmt und dadurch flankiert. Darüber hinaus würden Nanopartikel sowie Präzisionsmakromoleküle, die kovalent mit verschiedenen NES-spezifischen Liganden dekoriert sind, zusätzliche Hetero- und Multiavidität erzeugen.

Zusammenfassend stellt die Modifikation der supramolekularen Pinzetten mit Peptiden als zweites Bindemotiv eine vielversprechende Strategie dar, um deren Affinität sowie Spezifität und damit ihr inhibitorisches Potential gegenüber der Survivin–CRM1-Interaktion zu verbessern.

1 INTRODUCTION

1.1 Supramolecular chemistry

The field of supramolecular chemistry begins right beyond the well-established field of molecular chemistry which started nearly 200 years ago with the synthesis of urea (Wöhler, 1828). Since molecular chemistry constructs molecular structures only by formation of covalent bonds between atoms, supramolecular chemistry was defined in 1978 by Jean-Marie Lehn as “the chemistry of molecular assemblies and of the intermolecular bond” (Lehn, 1978).

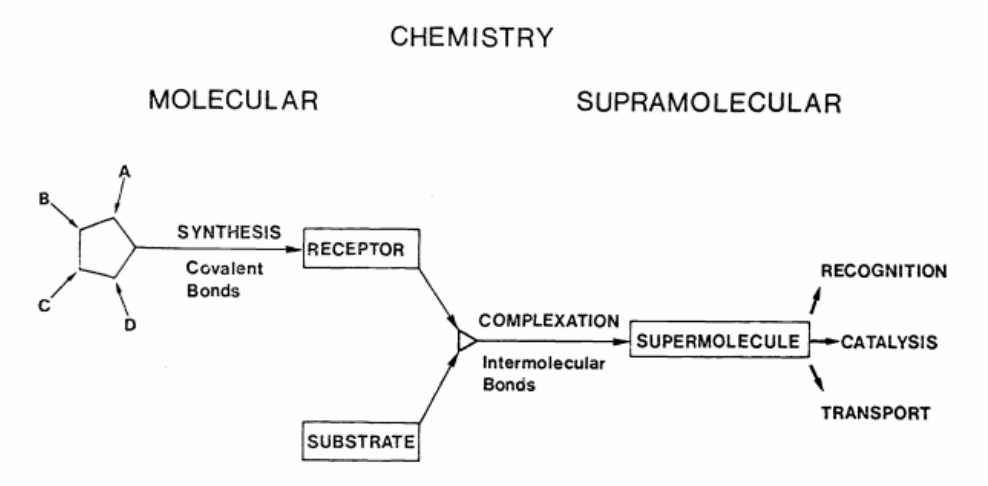

Figure 1.1: From molecular to supramolecular chemistry.
Schematic summary of general considerations regarding supramolecular chemistry (Lehn, 1978).

Supramolecular chemistry examines the weaker and reversible non-covalent interactions between molecules. These intermolecular interaction forces include electrostatic interactions, hydrogen bonding, π-π interactions, dispersion interactions and hydrophobic or solvophobic effects. Non-covalent interactions range from 2 kJ mol^{-1} for dispersion interactions to 300 kJ mol^{-1} for ion-ion interactions and are therefore weaker than single covalent bond interactions (150–450 kJ mol^{-1}). However, using these weaker non-covalent interactions in a co-operative manner will help to construct supramolecular complexes, which are stable enough to exist (Steed *et al.*, 2007). Table 1.1 summarizes the non-covalent supramolecular interactions and their strengths.

Table 1.1: Supramolecular bonds.
Overview of non-covalent interactions with their corresponding force strength (Steed *et al.*, 2007).

Interaction	Strength (kJ mol^{-1})
ion-ion	200-300
ion-dipole	50-200
dipole-dipole	5-50
hydrogen bonding	4-120
cation-π	5-80
π-π	0-50
van der Waals	< 5, but variable depending on surface area
hydrophobic	related to solvent-solvent interaction energy

The breakthrough of the relatively young field of supramolecular chemistry came in the 1960s and 1970s with the understanding and development of selective alkali metal cation binding by natural and synthetically produced macrocyclic and macropolycyclic ligands (Lehn, 1993). The most prominent representatives are the crown ethers developed by Pedersen (Pedersen, 1967), the cryptands developed by Lehn (Dietrich *et al.*, 1969) and the spherands developed by Cram (Cram *et al.*, 1979). In 1987 all three researchers Donald J. Cram, Jean-Marie Lehn and Charles J. Pedersen received the Nobel Prize in Chemistry "for their development and use of molecules with structure-specific interactions of high selectivity" (Nobel Media AB, 2018) awarding their work in the established field of supramolecular chemistry (Steed *et al.*, 2007).

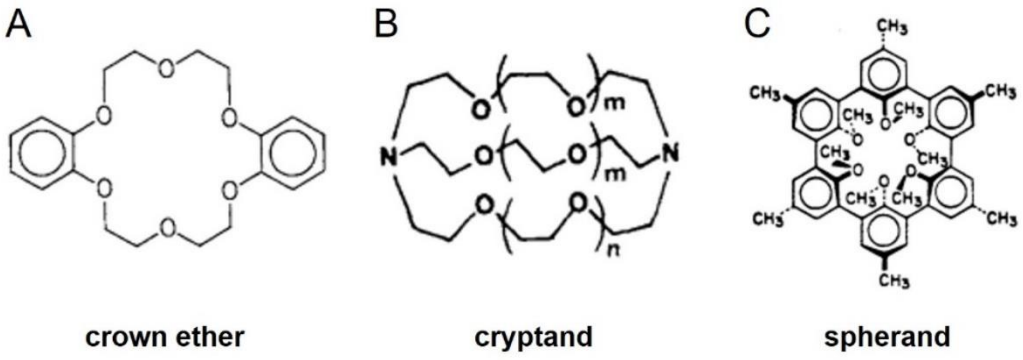

Figure 1.2: First supramolecular ligands selectively binding alkali metal cations.
Chemical structures of **A)** crown ether (Pedersen, 1988), **B)** cryptand (Lehn, 1988) and **C)** spherand (Cram, 1988).

Although the term supramolecular chemistry was defined not until 1978 by Jean-Marie Lehn (Lehn, 1978), the basic intermolecular forces have been well known for a long time. Already in 1873, Johannes Diderik van der Waals postulated, the existence of weak intermolecular forces (van der Waals, 1873) and in 1920 Latimer and Rodebush described the non-covalent hydrogen bonding (Latimer and Rodebush, 1920). However, it was Emil Fischer who made the first attempt towards the concept of supramolecular chemistry in 1894 by postulating its 'lock and key' model for the enzyme-substrate interaction (Fischer, 1894).

This model perfectly describes the basic principle of molecular recognition and host-guest chemistry, one broad concept in the nowadays mature field of supramolecular chemistry. The second concept is the self-assembly. The concept of host-guest chemistry studies a large host molecule which is able to enclose a smaller guest molecule via non-covalent interactions. If there is no significant difference in size, two or more molecules can associate in the second concept via non-covalent interactions to form larger aggregates. They self-assemble. This self-assembly can be spontaneous or influenced by solvent or template effects and is reversible (Steed *et al.*, 2007). Figure 1.3 depicts both main concepts of supramolecular chemistry, which only differ in size and shape of the involved molecules.

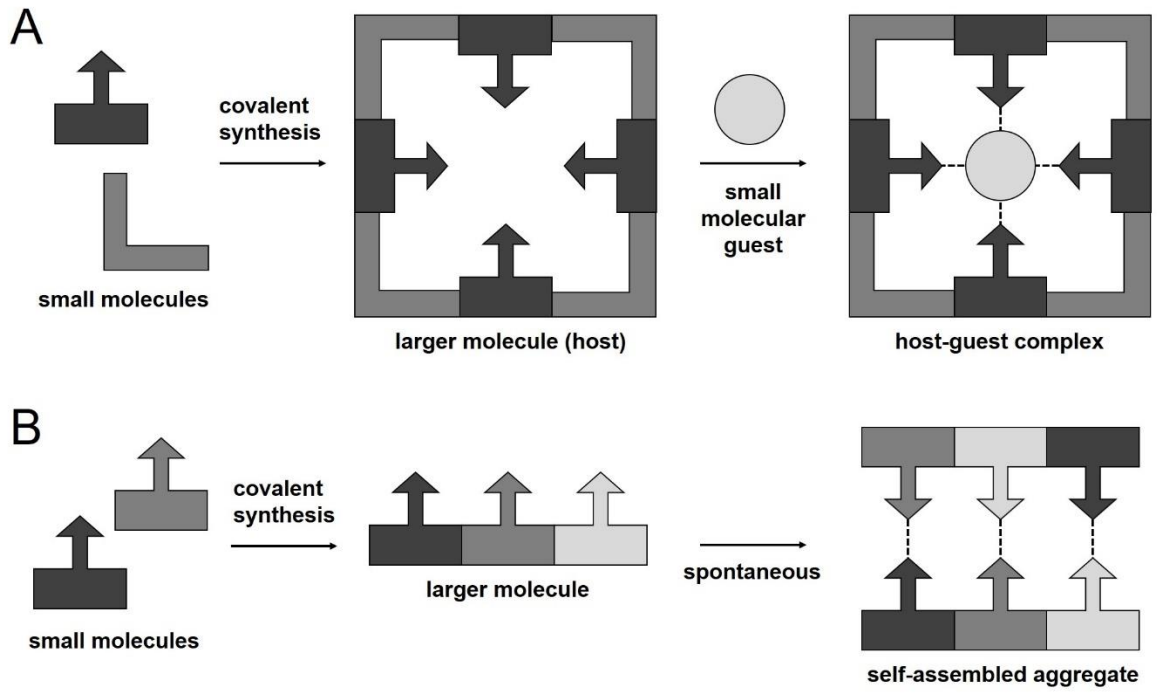

Figure 1.3: Two main concepts of supramolecular chemistry.
Construction of supramolecular systems from molecular building blocks by **A)** host-guest chemistry and **B)** self-assembly. Modified after (Steed *et al.*, 2007).

Nowadays, a variety of supramolecular systems exists which differ in shape, compositions, conditions and functionalities. Therefore, supramolecular systems are also widely used in diverse fields of science, like chemistry, physics, material science and even biology. Indeed, the initial inspiration for supramolecular chemistry came from biology with its fascinating natural molecules such as proteins, oligonucleotides, lipids and their multimolecular complexes. However, application of supramolecular chemistry for investigations in biological systems is challenging, because synthetic systems assembling in water are required (Uhlenheuer *et al.*, 2010). On the one hand the host molecule must be water-soluble, which limits the usable building blocks for formation, and on the other hand the strong competitive influence of water molecules must be overcome, which form an infinite and dynamic network of hydrogen bonds and are therefore involved in non-covalent processes important for supramolecular assembly (Oshovsky *et al.*, 2007). However, in recent years these challenges were accomplished with the design and development of a variety of supramolecular architectures that assemble in water. One of those water-stable supramolecular systems is the molecular tweezer (Oshovsky *et al.*, 2007).

1.1.1 Molecular tweezer – a lysine- and arginine-specific supramolecular ligand

The term “molecular tweezer” was introduced in 1978 by Chen and Whitlock for a molecule consisting of two caffeine moieties linked via a rigid diyne unit which prevents self-association of the two caffeine moieties. The attained distance of approximately 7 Å between the caffeine rings in the syn conformation allows the insertion of small aromatic molecules which are representing π-systems (Chen and Whitlock, 1978).

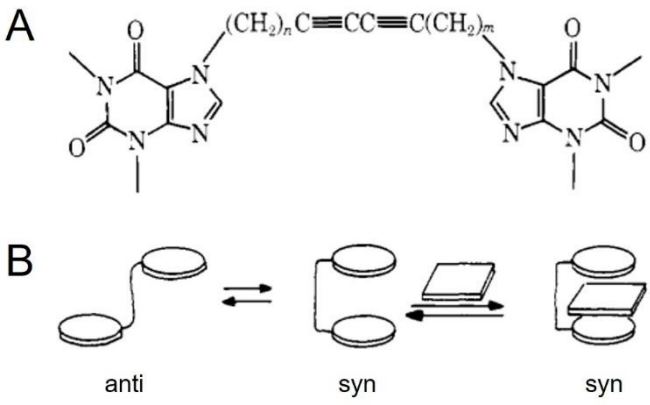

Figure 1.4: First molecular tweezer as a simple model for bifunctional intercalation.
A) Chemical structure of molecular tweezer consisting of two caffeine moieties linked via a rigid diyne unit. **B)** Schematic model of bifunctional intercalation. Syn conformation of molecular tweezer allows the insertion of a π-system (Chen and Whitlock, 1978).

After several different supramolecular host-guest systems of molecular tweezers were developed over the last years (Zimmerman and VanZyl, 1987; Harmata *et al.*, 1994; Valdes *et al.*, 1995), Klärner and his colleagues established a new type of molecular tweezer in 1996, which represents the basis of the supramolecular tweezer molecules which are used in this work. Klärner's molecular tweezer consists of alternating aromatic and norbornadiene units making it perfectly preorganized for supramolecular host-guest binding of small aromatic molecules. On the one hand the aromatic units can interact with the guest molecules via aren-aren interactions and on the other hand the norbornadiene units ensure a certain flexibility of the system, providing a geometrical fit to the structure of the guest molecule (Klärner *et al.*, 1996).

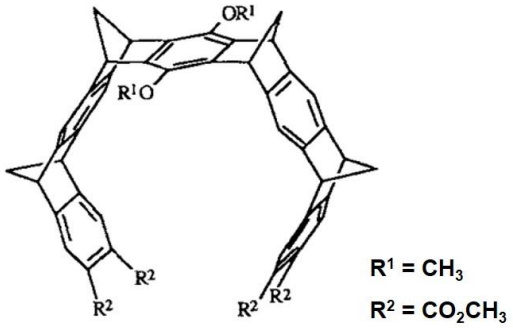

Figure 1.5: Molecular tweezer as synthetic receptor in host-guest chemistry.
Chemical structure of new molecular tweezer type (dimethoxy-tweezer) consisting of alternating aromatic and norbornadiene units making it perfectly preorganized for supramolecular host-guest binding of small aromatic molecules (Klärner *et al.*, 1996).

As a result of a collaboration between Klärner and Schrader in 2005, the molecular tweezer (Figure 1.5) was further improved by adding two rotatable peripheral anionic phophonate groups at the central spacer unit (Fokkens *et al.*, 2005).

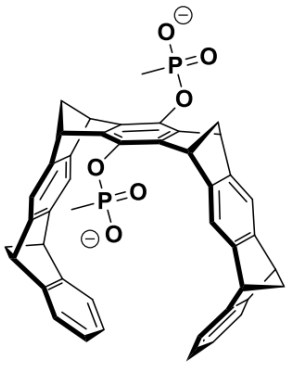

Figure 1.6: Chemical structure of molecular biphosphonate-tweezer.
Klärner's molecular tweezer (Figure 1.5) was improved by adding two rotatable peripheral anionic phophonate groups at the central spacer unit (Fokkens *et al.*, 2005).

The addition of the functional phosphonate groups has two decisive advantages. On the one hand, the water solubility of the tweezer molecule increases to a considerable extend which makes it highly attractive for biological applications. On the other hand, basic amino acids such as lysine or arginine are complexed with high binding constants (K_A = 5000 M^{-1} for lysine and 2000 M^{-1} for arginine) while other amino acids are not bound (Figure 1.7 A). This special selectivity for these two basic amino acids is achieved by threading the whole side chains of lysine as well as arginine through the cavity while the positively charged ammonium group of lysine or guanidino group of arginine is fixed by the negatively charged phosphonate groups of the molecular tweezer via hydrogen and ionic bonding (Fokkens *et al.*, 2005).

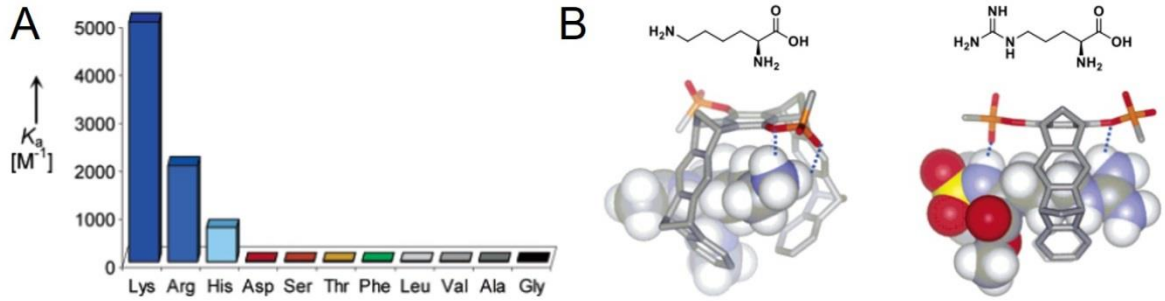

Figure 1.7: Selectivity of molecular bisphosphonate-tweezer for basic amino acids.
A) Selectivity of molecular biphosphonate-tweezer for N/C-protected amino acids. K_A values in buffered aqueous solution (c = 0.1 mM in 25 mM NaH_2PO_4, pH = 7.0). **B)** Monte Carlo simulations (MacroModel 7.1, Amber, water, 5000 steps) of the complexes between molecular biphosphonate-tweezer and lysine (left) as well as arginine (right) (Fokkens *et al.*, 2005).

In the following years, the molecular tweezer was improved. The anion groups at the central spacer unit were varied. As a result, the molecular tweezer bearing two phosphate groups (Figure 1.8) shows the best affinity (K_D = 17 µM) for lysine being even three times better than the bisphosphonate-tweezer (K_D = 68 µM) (Dutt *et al.*, 2013a).
In addition to varying the anion of the spacer unit, exchanges of one phosphate group with various linker units were studied, making the symmetrical molecular tweezer systematically unsymmetrical. However, the monophosphate tweezer with a hydroxy group shows a decreased affinity towards lysine and arginine because of an entropic effect. The amino acid can enter the monophosphate tweezer cavity unlike the diphosphate tweezer only on one site, the phosphate site, because the cationic side chain must be complexed for good threading.
Other linkers totally block or at least drastically lower lysine and arginine binding. Long alkyl chains for example block the entrance of the cavity by forming van der Waals interactions

between CH groups, and alkoxyalkyl units self-include their side chain into the cavity and block it for other guests. Ester and carboxylate moieties on the other hand keep the cavity open due to the highly polarized electron-rich carbonyl group (Dutt *et al.*, 2013b).

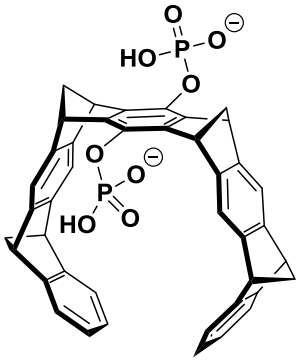

Figure 1.8: Chemical structure of molecular diphosphate-tweezer.
The molecular tweezer bearing two phosphate groups shows three times better affinity (K_D = 17 µM) for lysine than the bisphosphonate tweezer (K_D = 68 µM) (Dutt et al, 2013a).

As a water-soluble lysine- and arginine-specific supramolecular host-guest system the molecular tweezer is usable for biological applications and investigations.
The first successful application of the biphosphonat-tweezer (Figure 1.6) was the enzyme inhibition of alcohol dehydrogenase (ADH). By lysine binding around the active site, the molecular biphosphonat tweezer was able to prevent the binding of the co-factor nicotinamide adenine dinucleotide (NAD^+), thus reducing enzyme activity in a non-competitive way. Subsequent adding of lysine derivates led to a displacement of tweezer molecule and therefore to a regaining of enzymatic activity (Talbiersky *et al.*, 2008).
Furthermore, the improved molecular diphosphate-tweezer was discovered to inhibit the aggregation and toxicity of amyloid proteins by binding to lysine residues and thus disrupting hydrophobic and electrostatic interactions which are important for fibril formation (Sinha *et al.*, 2011). Moreover, in 2012, first *in vivo* experiments treating transgenic mice suffering from Alzheimer's disease with the molecular diphosphate tweezer over a period of 28 days showed a decrease of amyloid aggregation in the brain with no signs of tweezer toxicity (Attar *et al.*, 2012). Since these amyloid fibrils are associated with neurodegenerative diseases such as Alzheimer's disease, Parkinson's disease and dementia but also non-neuropathic diseases like type II diabetes (Chiti and Dobson, 2006), the molecular tweezer might be a promising novel therapy for amyloidosis.
In 2013, it was further demonstrated that molecular tweezer molecules can even modulate protein–protein interactions in a specific manner. The lysine-specific molecular diphosphate tweezer was shown to inhibit binding between the small adapter protein 14-3-3 and its two

partner proteins cellular rapidly accelerated fibrosarcoma (c-Raf) and exoenzyme S (ExoS) by binding to only one single lysine residue 214 exposed on the surface of the 14-3-3 protein. Tweezer binding on lysine residue 214, which lies in the proximity of the central channel of 14-3-3 proteins responsible for partner protein binding, results in steric conflicts and hinders protein association (Bier *et al.*, 2013).

1.2 Nucleocytoplasmic transport

A decisive property of all eukaryotic cells is their separation into nucleus and cytoplasm, which is maintained by the nuclear envelope at interphase. While deoxyribonucleic acid (DNA) replication and ribonucleic acid (RNA) transcription take place in the nucleus, protein synthesis occurs in the cytoplasm. Consequently, a large number of metal ions, small molecules and macromolecules must be transferred between both compartments reaching their place of action. For example, RNA transcripts are transferred from the nucleus to the ribosomes in the cytoplasm while proteins like histones, polymerases and transcription factors are transferred from the cytoplasm into the nucleus to reach the DNA (Görlich and Kutay, 1999; Fried and Kutay, 2003; Cook *et al.*, 2007). All nucleocytoplasmic transport processes occur only via transport channels passing through the nuclear envelope, the nuclear pore complexes (NPCs) (Fahrenkrog and Aebi, 2003; Tran and Wente, 2006; Sakiyama *et al.*, 2017). NPCs are large and complex protein assemblies with a highly selective permeability for different molecules. While metal ions and small molecules can pass by passively diffusion, the NPCs are impermeable to most larger macromolecules except the soluble nucleocytoplasmic transport factors, known as karyopherins (Kaps), which are able to actively shuttle through the NPCs in an energy-dependent manner. By carrying other macromolecules across, they help to overcome the permeability barrier of the NPCs (Keminer and Peters, 1999; Fried and Kutay, 2003; Tran and Wente, 2006; Cook *et al.*, 2007; Wente and Rout, 2010). Cargo macromolecules include proteins, transfer ribonucleic acids (tRNAs), ribosomal subunits, and viral particles (Macara, 2001).

1.2.1 The nuclear pore complex and the translocation mechanism

Representing one of the largest protein complexes, the nuclear pore complex (NPC) is easily recognizable using scanning electron microscopy. In human cells, a high number of 3000-5000 NPCs exists (Görlich and Kutay, 1999; Kabachinski and Schwartz, 2015). The NPC has an overall conserved eightfold symmetrical architecture and consists of a cylindrical central framework residing within the nuclear envelope, eight cytoplasmic filaments and a nuclear basket which is formed by eight filaments converging into a distal ring (Lim *et al.*,

2008). First reconstructions of the peripheral, flexible components of the NPC, the cytoplasmic filaments and the nuclear basket, are gained from cryoelectron tomography studies of nuclei isolated from *Dictoyostelium discoideum*. Cryoelectron tomography results revealed lengths of approximately 35 nm for the cytoplasmic filaments, 60 nm for the nuclear basket and 50 nm for the central framework. Taken together, the NPC has an overall length of about 150 nm and an outer diameter of 125 nm (Beck *et al.*, 2004; Beck *et al.*, 2007). The central framework, also known as the spoke complex, contains eight spokes surrounding an hourglass-shaped central pore with a diameter of 60-70 nm at its cytoplasmic and nuclear periphery and approximately 45 nm in the midplane (Panté and Kann, 2002; Fahrenkrog and Aebi, 2003; Stoffler *et al.*, 2003; Beck *et al.*, 2004; Beck *et al.*, 2007; Lim *et al.*, 2008). This central pore acts as the connection between cytoplasm and nucleoplasm enabling nucleocytoplasmic transport (Lim *et al.*, 2008). Moreover, the central framework is perforated by eight peripheral channels (Maimon *et al.*, 2012), whose functionality is still not completely resolved and a subject of scientific research.

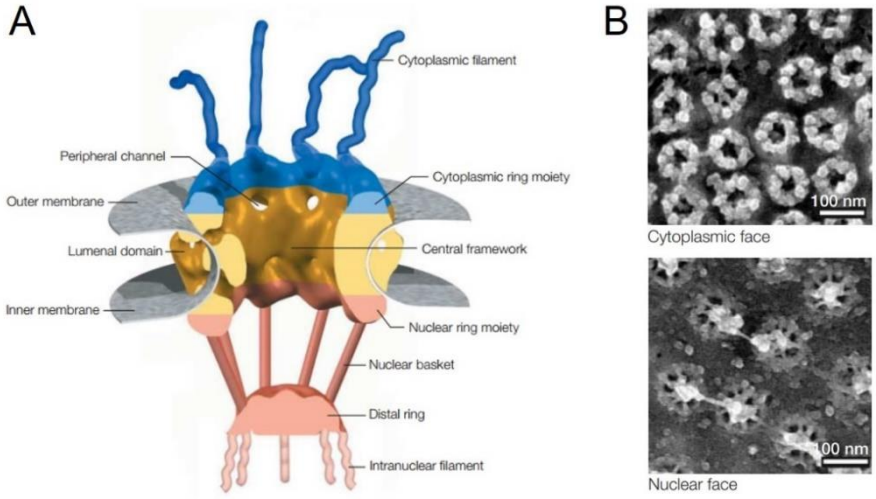

Figure 1.9: Structure of the nuclear pore complex.

A) Schematic representation of the NPC. The main structural components include the central framework (yellow), the cytoplasmic ring moiety (blue) and cytoplasmic filament (blue) as well as the nuclear ring moiety (red) and nuclear basket (red). **B)** Images of NPCs visualized by electron microscopy. Negatively stained (with heavy metal salts) NPCs show the typical eightfold rotational symmetry. Cytoplasmic face image (top) expose the cytoplasmic filaments while the nuclear face image (bottom) expose the nuclear basket structure of the NPCs (Fahrenkrog and Aebi, 2003).

Despite its enormous molecular mass of approximately 125 MDa in vertebrates (Reichelt *et al.*, 1990), the NPC is assembled by only a small number of approximately 30 nucleoporins (NUPs) that are largely conserved throughout eukaryotic evolution. Because of the eightfold symmetry of the NPC, all nucleoporins are present in at least eight copies per NPC

(Cronshaw *et al.*, 2002; Lim *et al.*, 2008). Based on amino acid sequence motifs, structural characteristics and their position within the NPC, nucleoporins can be grouped into four distinct classes. The first class, the transmembrane NUPs, anchor the NPC to the nuclear envelope and are important for its assembly. The second class, the scaffold NUPs consist of outer and inner ring NUPs as well as linker NUPs and connect the FG NUPs to the transmembrane NUPs. The third class, the barrier-forming FG NUPs are named for their conserved sequence motif of phenylalanine-glycine (FG) repeats domains and line the whole NPC from the cytoplasmic filaments via the central pore until the distal ring. NUPs forming the peripheral cytoplasmic filaments and nuclear basket represent the fourth class (Sakiyama *et al.*, 2017).

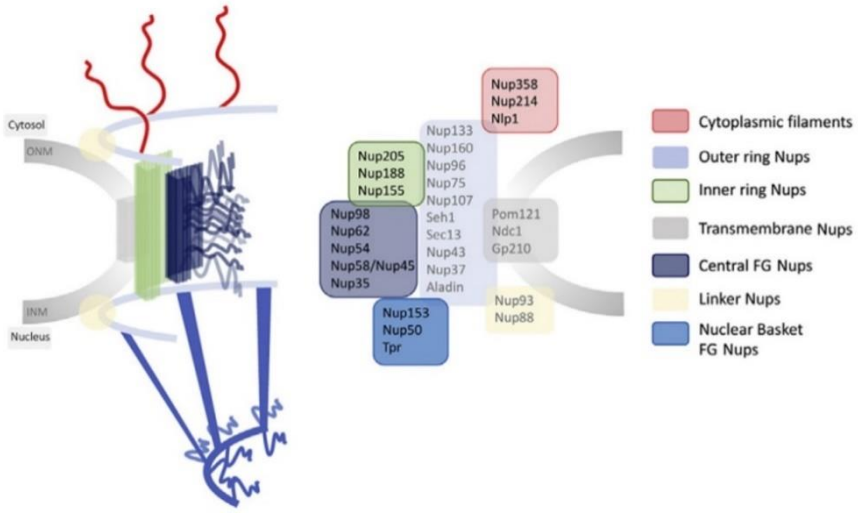

Figure 1.10: Schematic representation of nucleoporin sub-structures within a vertebrate NPC. Strong colors depict dynamic components including the barrier-forming FG NUPs (grey), the inner ring NUPs (green) and the peripheral cytoplasmic filaments (red) and nuclear basket (blue) whereas pale colors depict more rigid components including transmembrane NUPs (light grey), outer ring NUPs (light blue) and linker NUPs (light yellow). ONM: outer nuclear membrane, INM: inner nuclear membrane (Sakiyama *et al.*, 2017).

Covering nearly one-third of all nucleoporins, the FG NUPs form a selective transport barrier in the central pore which impedes the translocation of large non-specific macromolecular cargoes (Lim *et al.*, 2008; Sakiyama *et al.*, 2017). Metal ions as well as small molecules can freely diffuse through the NPC. The general diffusion limit set by the NPC was long time believed to be 9-12 nm in diameter thus interpreted as a maximal size of 60 kDa for proteins. However, recent studies showed that this limit may extend to at least 100 kDa and even larger (Wang and Brattain, 2007; Timney *et al.*, 2016). Nevertheless, the majority of larger macromolecules requires the assistance of soluble transport receptor proteins known as karyopherins to be effectively transported through the NPC. The transport selectivity for

these karyopherins is thereby accomplished by the FG repeat domains which represent specific binding sites for Kaps (Lim *et al.*, 2008; Sakiyama *et al.*, 2017). However, the exact mechanism how the FG repeat domains contribute to the selective gating of the NPC is still not completely revealed (Lim *et al.*, 2008). In recent years, several models have been proposed on how FG-NUPs form this selective transport barrier. On the one hand all these models will have to consider that the NPC is strongly bidirectional *in vivo*, mediating both import and export, on the other hand transport as a rapid process with first-order kinetics occurring at a rate of about 1000 translocations every second must be explainable (Ribbeck and Görlich, 2001; Kabachinski and Schwartz, 2015).

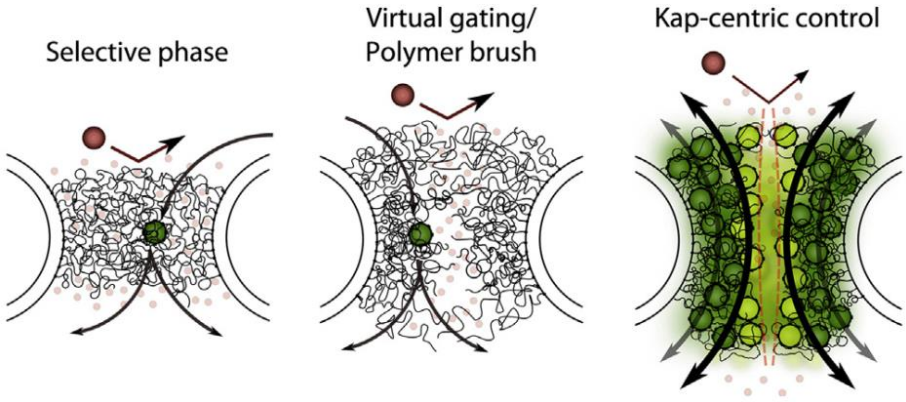

Figure 1.11: Schematic representation of NPC barrier models.
Selective phase model (left), virtual gating / polymer brush model (center) and Kap-centric control model (right) differently explain the formation of the selective transport barrier in the central pore. Small molecules (small pale red circles) diffuse freely through the barrier while large non-specific molecules (red circle) are restrained. Kaps (slow-phase: green circle; fast-phase: light green circle) can pass the barrier due to their interaction with FG repeat domains (Sakiyama *et al.*, 2017).

In 2003, Rout and colleagues proposed the “virtual gate model” in which the bristling motions of the FG NUPs in the NPC would restrict non-specific macromolecules from crossing while FG NUP-binding of Kaps would enhance the probability of Kap-cargo complexes to translocate (Rout *et al.*, 2003). This model was supported in 2006 by Lim and colleagues who detected a polymer brush-like behavior of Nup153 by extending beyond its hydrodynamic radius (Lim *et al.*, 2006). Currently the most prominent model is the “selective-phase model” by Görlich and colleagues, proposed already in 2001 and improved over the years. In this model, FG NUPs line the central pore and extend their FG repeat domains into the middle of the channel. The FG domains attract each other via hydrophobic interactions and generate a hydrogel with a mesh size that sets the cutoff limit for non-specific cargoes. By binding FG domains, Kaps are locally melting the FG-mediated hydrogel and therefore able to cross the channel (Ribbeck and Görlich, 2001; Ribbeck and Görlich, 2002; Frey and

Görlich, 2007). A recent model proposed by Lim and colleagues in 2014 termed the "Kap-centric control model" considers the Kaps as integral components of the FG barrier regulating transport selectivity and speed. In this model, strongly bound Kaps saturate FG domains located in the peripheral region of the channel. Because of the strong binding, they translocate slowly through the channel (slow-phase). Thereby, a narrow aqueous channel along the NPC axis is formed which sets the passive size limit but remains selective for further Kaps (fast-phase) which bind weakly enough to diffuse along the mostly saturated peripheral FG domains ensuring a rapid cargo translocation (Kapinos *et al.*, 2014).

1.2.2 Transport signals for nuclear import and export

The majority of larger macromolecular cargoes requires the assistance of soluble transport receptor proteins known as karyopherins to be effectively transported through the selective barrier of the NPC. In case of proteins, cargo binding with karyopherins – more specifically with importins and exportins – is mediated via specific transport signals. Thereby, nuclear localization signals (NLS) are recognized by importins and mediate nuclear import of cargo proteins while nuclear export signals (NES) in cargo proteins are recognized by exportins and mediate nuclear export through the NPC (Lim *et al.*, 2008).

So far, two established classes of NLS are known. The classical NLS contain either monopartite or bipartite signals which are recognized by importin-α. These highly frequent and conservative signals are clusters of basic, positively charged amino acid residues like lysine and arginine, one for monopartite and two separated by a spacer for bipartite signals (Sorokin *et al.*, 2007; Kim *et al.*, 2017). The first characterized classical monopartite NLS is ^{126}PKKKRKV^{132}, the NLS of simian virus 40 (SV40) large T antigen of the SV40 virus (Kalderon *et al.*, 1984b; Kalderon *et al.*, 1984a; Kim *et al.*, 2017). The first characterized classical bipartite NLS ^{155}KRPAATKKAGQAKKKK^{169} was found in nucleoplasmin, of *Xenopus laevis* (Dingwall *et al.*, 1988; Kim *et al.*, 2017). For nuclear import, classical NLS containing cargo proteins requires binding of the adapter molecule importin- α, which enables the association with importin- β. Subsequently, importin-β is specifically recruited to the NPC via direct interactions with the FG NUPs (Görlich and Kutay, 1999).

The PY-NLS, representing the second class, have diverse sequences and large structures and are recognized by importin-β. These signals consist of a loose amino (N)-terminal hydrophobic motif and a C-terminal $RX_{2-5}PY$ motif. Representative signals are the NLS ^{270}SSNFGPMKGGNRFFRSSGPY^{289} of the human heterogeneous nuclear ribonucleoprotein A1 (hnRNP A1) as well as the NLS ^{506}RSGGNHRRNGRGGRGGYNRRNNGYHPY^{532} of the yeast heterogeneous nuclear ribonucleoprotein 1 (Hrp1) (Kim *et al.*, 2017). Besides these two NLS classes there are many other quite divers NLS types. NLS may be very arginine-

glycine (RG) rich, sequences may be relatively large and sometimes only the three-dimensional structure may form a recognizable NLS. This diversity often complicates NLS identification in potential cargo proteins (Sorokin *et al.*, 2007).

The best characterized and most common NES are the hydrophobic leucine-rich NES which are recognized by the ubiquitous export receptor CRM1. Their consensus sequence is $LX_{2-3}LX_{2-3}LXL$, where "L" representing a hydrophobic residue (often leucine (L) but also isoleucine (I), phenylalanine (F), methionine (M) or valine (V) and "X" representing any amino acid. The most prominent signals are the first identified mammalian protein kinase A inhibitor (PKI) NES ^{37}LALKLAGLDI^{46} as well as the human immunodeficiency virus 1 (HIV-1) Rev (reversionless) protein NES ^{75}LPPLERLTL^{83}. However, hydrophobic leucine-rich NES were identified in many more eukaryotic proteins including a variety of transcription factors and cell cycle regulators (Wen *et al.*, 1995; Sorokin *et al.*, 2007; Kim *et al.*, 2017).

1.2.3 GTPase Ran dependent nucleocytoplasmic transport

Since the NPC is, despite its asymmetry, bidirectional and not able to distinguish between import and export, the directionality of transport is mediated by the small rat sarcoma (Ras)-like guanosine triphosphatase (GTPase) Ran (Wente and Rout, 2010; Kabachinski and Schwartz, 2015; Kim *et al.*, 2017).

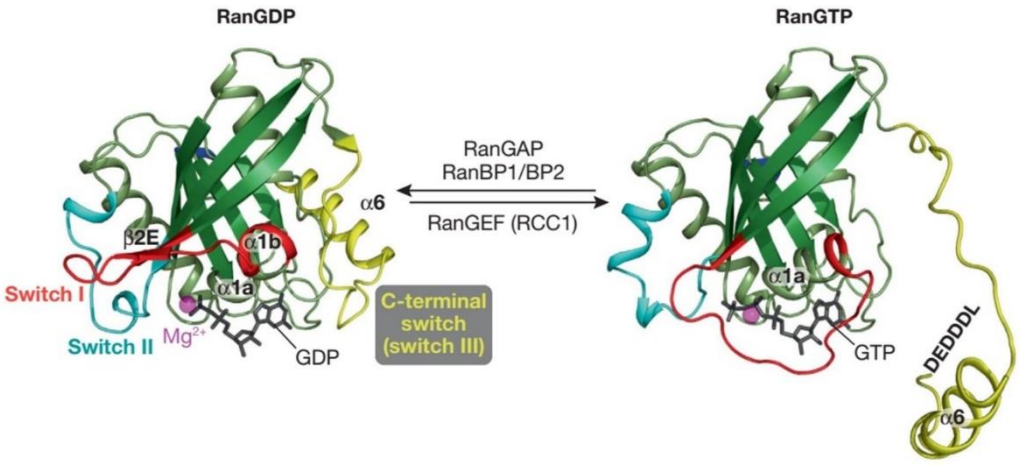

Figure 1.12: The guanine nucleotide switch of the GTPase Ran.
Structure of Ran bound to GDP (left) and GTP (right). Depicted are the central six-stranded β-sheets of Ran's guanine nucleotide-binding domain (dark green), peripheral α-helices and loops (light green), the nucleotide (grey sticks) and the Mg^{2+} ion (magenta sphere), respectively. When Ran switches between its nucleotide states, the so-called Switch regions (red Switch I: Ran30-47, cyan Switch II: Ran65-80 and yellow Switch III: Ran177-216) undergo drastic conformational changes (Güttler and Görlich, 2011).

The **Ra**s-related **n**uclear protein Ran belongs to the Ras superfamily and consists of 216 amino acids and a corresponding molecular weight of 24.4 kDa. In contrast to the majority of the Ras superfamily members, Ran localizes predominantly in the nucleus due to facilitated nuclear import mediated by nuclear transport factor 2 (NTF2) (Smith *et al.*, 1998). However, similar to other Ras-like GTPases, Ran switches between a guanosine diphosphate (GDP)-bound and a guanosine triphosphate (GTP)-bound state inside the cell (Joseph, 2006; Güttler and Görlich, 2011).

The molecular guanine nucleotide switch causes conformational changes of the protein especially in the Switch I and Switch II regions of the catalytic domain as well as in the C-terminal extension of Ran resulting in different binding potentials for partner proteins (Fahrenkrog and Aebi, 2003; Güttler and Görlich, 2011).

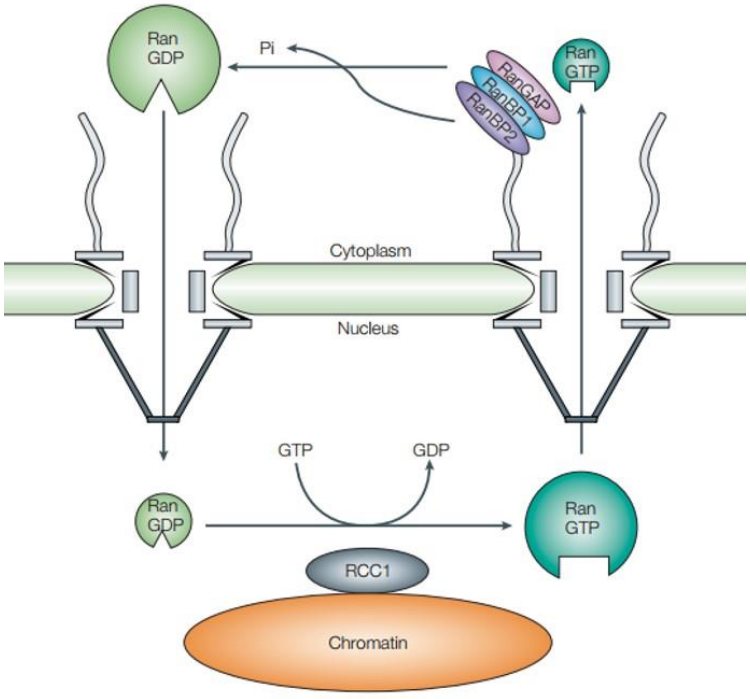

Figure 1.13: The RanGTPase cycle gives directionality to nucleocytoplasmic transport.
The RanGTPase cycle regulates the binding and release of signal-bearing cargos from their transport receptors. The Ran gradient in the cell is achieved by an asymmetric distribution of the Ran regulators, which determines the nucleotide-bound state of Ran. In the nucleus, RCC1 (grey) is bound to chromatin (orange) and promotes the dissociation of GDP from Ran, thereby allowing GTP-binding. Nuclear Ran is therefore predominantly in its GTP-bound form (cyan). Leaving the nucleus, RanGAP (pink) induces GTP hydrolysis to GDP and inorganic phosphate (Pi) in cooperation with RanBP1 (blue) and RanBP2 (violet) at the cytoplasmic filaments of the NPC. Cytoplasmic Ran is therefore predominantly in its GDP-bound form (green). See main text for details (Fahrenkrog and Aebi, 2003).

Two main regulators of Ran, which are asymmetrically distributed within the cell, are responsible for these guanine nucleotide switches since Ran exhibits only low intrinsic GTP-hydrolysis und nucleotide exchange activity. On the one hand, the guanine exchange factor (GEF) termed regulator of chromosome condensation 1 (RCC1) is bound to chromatin in the nucleus, promotes the dissociation of GDP from Ran and allows GTP binding. Therefore, nuclear Ran is predominantly GTP-bound. On the other hand, the GTPase-activating protein (GAP) RanGAP1 induces GTP hydrolysis to GDP and inorganic phosphate (Pi) in cooperation with two RanGTP-binding proteins (RanBP1 and RanBP2) at the cytoplasmic filaments of the NPC. Therefore, cytoplasmic Ran is predominantly GDP-bound (Görlich and Kutay, 1999; Macara, 2001; Fahrenkrog and Aebi, 2003; Joseph, 2006; Wente and Rout, 2010). However, to sustain the required nucleocytoplasmic traffic, at the end of each Ran-dependent transport cycle RanGDP returns to the nucleus via facilitated import mediated by NTF2 (Smith *et al.*, 1998). Overall, the described RanGTPase cycle (Figure 1.13) creates a RanGTP gradient across the nuclear envelope with high levels in the nucleus and low levels in the cytoplasm. This gradient directs nucleocytoplasmic transport by regulating the assembly and disassembly of import and export complexes (Görlich and Kutay, 1999; Macara, 2001; Fahrenkrog and Aebi, 2003; Joseph, 2006; Wente and Rout, 2010). The fact of RanGTP gradient being the key component for transport direction is supported by a study, in which an increased cytoplasmic RanGTP level of permeabilized HeLa cells could partially invert the direction of transport (Nachury and Weis, 1999). Moreover, amino acid mutation of glutamate 69 to leucine in Ran protein results in a drastically reduced GTPase activity which cannot be stimulated by RanGAP1, thus producing a constitutively active RanQ69L mutant once bound to GTP (Klebe *et al*., 2002).

Beside Ran's role in directing the nucleocytoplasmic transport of macromolecules across the nuclear envelope, studies also revealed a critical function of Ran for other cellular processes including mitotic spindle assembly and post-mitotic nuclear envelope assembly, thereby using exactly the same molecular mechanism (Macara, 2001; Melchior, 2001; Dasso, 2002; Joseph, 2006). Similar to the nuclear transport, a RanGTP gradient in the mitotic cells represents the key component for regulating the assembly of mitotic spindle as well as nuclear envelope (Dasso, 2002; Joseph, 2006). This gradient is generated by chromatin-bound RCC1, which mediates a local increased concentration of RanGTP near the choromosomes, while the RanGTP concentration is low throughout the rest of the mitotic cell (Kalab *et al.*, 2002).

The spindle assembly factors (SAFs) controlling many aspects of microtubule behavior, including nucleation, stabilization and bundling, are necessary for mitotic spindle assembly. At low RanGTP concentrations, SAFs are inactivated by binding to importin-α/β via their NLS. The increased RanGTP concentrations near the chromosomes locally disrupt the

inhibitory complexes by RanGTP-binding to importin-β and therefore allowing fully restored SAF activity. Far from chromosomes, RanGTP undergoes nucleotide hydrolysis mediated by RanGAP in cooperation with RanBP1, recycling importin-β and allowing it to re-establish inhibition of SAFs (Figure 1.14 A) (Dasso, 2002).

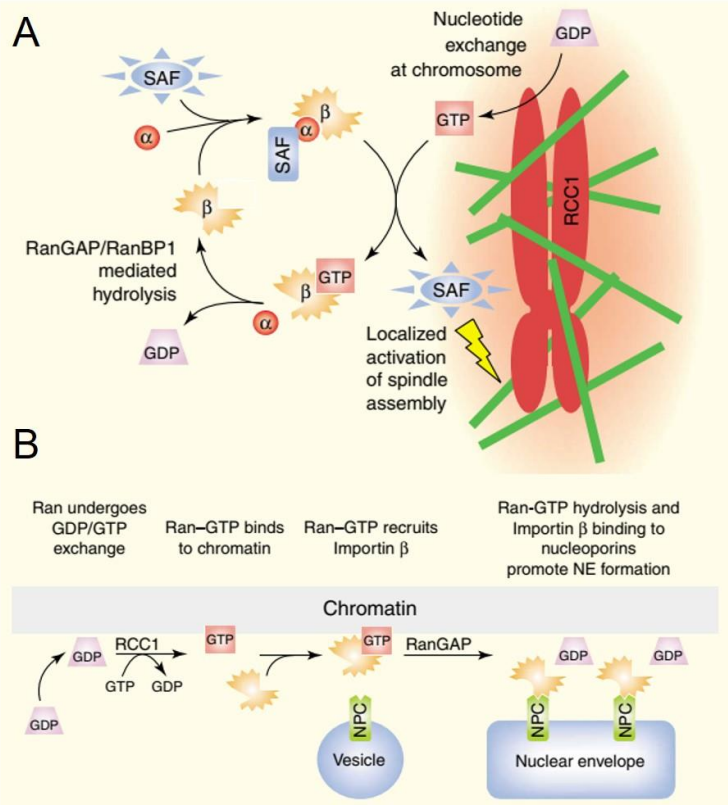

Figure 1.14: Ran promotes the assembly of the mitotic spindle and the nuclear envelope.
A) Increased RanGTP levels near the chromosomes promote the assembly of the mitotic spindle, composed of chromosomes (red) and a variety of proteins particularly microtubules (green). Spindle assembly factors (blue) are bound and inhibited by importin-α (red circle) and importin-β (orange) at low RanGTP (light red) concentrations. Close to the chromosomes, associated RCC1 generates an increased concentration of RanGTP by exchange of GDP (violet), locally disrupting the inhibitory complexes by binding to importin-β and therefore allowing full activity of SAFs (yellow flash). Finally, a RanGAP/RanBP1 complex mediates GTP-hydrolysis, releasing importin-β. **B)** Ran promotes nuclear envelope assembly. RCC1, bound to chromatin (light blue), generates an increased local concentration of RanGTP (red) by exchange of GDP (violet) allowing its direct binding to chromatin. This chromatin-associated RanGTP recruits importin-β (orange) and membrane vesicles (blue) with NPC proteins (green). RanGAP-mediated hydrolysis of RanGTP is required for fusion of the vesicles and therefore nuclear envelope formation. Modified after (Dasso, 2002).

Additionally, the re-formation of the nuclear envelope around the segregated DNA at the end of mitosis involves the RanGTPase cycle (Dasso, 2002; Joseph, 2006). RCC1 generates an increased RanGTP concentration allowing its interaction to chromatin either in an RCC1-

dependent fashion or by direct binding to nucleosomes and histones H3 and H4 (Bilbao-Cortés *et al.*, 2002). Upon association, RanGTP recruits the karyopherin importin-β which in turn binds to membrane vesicles with NPC proteins (NUPs). Finally, vesicle-fusion, enabled by RanGAP-mediated hydrolysis of RanGTP (Hetzer *et al.*, 2000; Zhang and Clarke, 2001), results in nuclear envelope assembly (Figure 1.14 B).

1.2.4 Mechanism of facilitated nuclear import and export cycle

Facilitated transport of large macromolecules through the barrier of the NPC is mediated by a superfamily of transport receptors, the β-karyopherins, which are characterized by an N-terminal Ran-GTP binding domain. Currently, at least 20 karyopherins are known in humans splitting up in importins responsible for nuclear import and exportins responsible for nuclear export. These receptors bind their transport substrates either directly or via adapter molecules via a transport signal and cooperate with the RanGTPase cycle to regulate the cargo interactions (Macara, 2001; Cook *et al.*, 2007; Sorokin *et al.*, 2007; Kim *et al.*, 2017).
Depending on the NLS type of the cargo molecule, different importins are involved in the import cycle. The best investigated, representative importin-β can directly recognize proline-tyrosine (PY) NLS and forms an import complex with these cargoes in the cytoplasm as a first step of the import cycle (Figure 1.15 B). However, recognition of classical NLS requires the adapter molecule importin-α, which binds on the one hand the NLS-containing cargo and on the other hand importin-β in the cytoplasm forming a trimeric import complex (Figure 1.15 A). The interaction of importin-α with importin-β is mediated via its N-terminal importin-β binding domain (Görlich and Kutay, 1999). Following assembly of the import complex in the cytoplasm, importin-β is specifically recruited to the NPC via direct interactions with the FG-repeat domains of the FG NUPs. Translocation is terminated in the nucleoplasm via binding of Ran-GTP to importin-β, which releases the complex from the NPC and facilitates its dissociation. The transported cargo is released, and the RanGTP-bound importin-β is exported back to the cytoplasm for another import cycle. However, recycling of the adapter molecule importin-α is mediated by a nuclear export receptor, the cellular apoptosis susceptibility protein (CAS) bound to Ran-GTP (Macara, 2001; Cook *et al.*, 2007; Wente and Rout, 2010; Kim *et al.*, 2017).
The export cycle mediates transport processes in the opposite direction with the help of exportins. So far, eight exportins have been identified in higher eukaryotes which are differentiated according to their substrates. While Exportin 1 also known as CRM1 (chromosome region maintenance 1) binds an extremely diverse number of substrates, whose recognition sequences are nuclear hydrophobic export signals, other exportins exhibit a high substrate selectivity. Exportin 2 also termed CAS, is highly selective for the retrograde

export of importin-α and transports it back to the cytoplasm. Exportin-t ensures tRNA export by selectively recognizing a part of its structure as its NES (Sorokin *et al.*, 2007; Kim *et al.*, 2017).

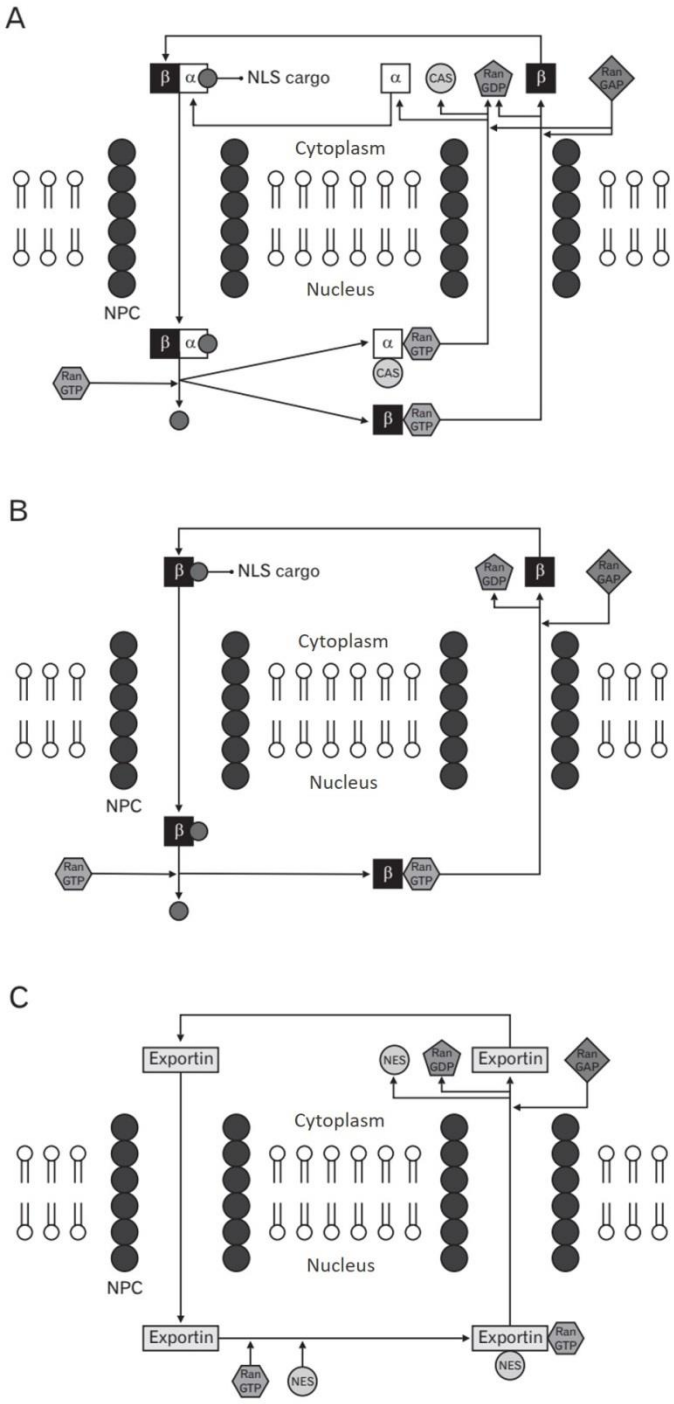

Figure 1.15: The nuclear transport cycles of proteins.

A) Import cycle for importin-β in cooperation with its adapter molecule importin-α. **B)** Import cycle for importin-β. **C)** Export cycle. See main text for details. NPC: nuclear pore complex, NLS: nuclear localization signal, NES: nuclear export signal (Kim *et al.*, 2017).

In a first step, exportins bind to the NES of their specific cargo in the nucleus by forming a trimeric complex with the high abundant nuclear RanGTP. RanGTP binding to exportins thus initially induces their high affinity for their cargo molecule. Following assembly of the export complex in the nucleus, exportins are specifically recruited to the NPC via direct interactions with the FG-repeat domains of the FG NUPs. In the cytoplasm, GTP hydrolysis results in the dissociation of the complex and the release of the transported cargo. In the end, recycling of hydrolyzed RanGDP is mediated by the nuclear transport factor 2 (Smith *et al.*, 1998) and free CRM1 reenters the nucleus to bind and export further cargo molecules (Görlich and Kutay, 1999; Macara, 2001; Cook *et al.*, 2007; Wente and Rout, 2010; Kim *et al.*, 2017).

1.2.5 CRM1-mediated nuclear export

Exportin 1 (XPO1), also known as CRM1 (chromosome region maintenance 1), is the major and most important export receptor used in the cell to transport a large number of various cargo molecules out of the nucleus (Görlich and Kutay, 1999; Sorokin *et al.*, 2007; Kim *et al.*, 2017). Currently, it is the best studied eukaryotic export receptor which mediates nuclear export via the general export cycle (section 1.2.4). In the nucleus, CRM1 binds to RanGTP and its cargo protein via a hydrophobic NES. The assembled export complex translocates through the NPC into the cytoplasm where it dissociates upon GTP hydrolysis. The cargo protein is released, and CRM1 as well as RanGDP are recycled for a next export cycle (Figure 1.16) (Dickmanns *et al.*, 2015).

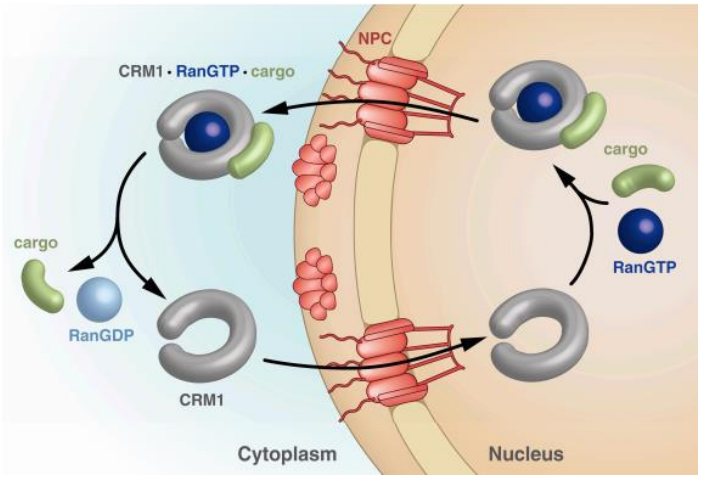

Figure 1.16: CRM1 mediated export cycle.
Nuclear CRM1 (grey) assembles together with RanGTP (dark blue) and its cargo (green) into the export complex, which passes the NPC (red). In the cytoplasm, the export complex disassembles upon GTP hydrolysis, the cargo is released and RanGDP (light blue) as well as CRM1 are relocalized to the nucleus (Dickmanns *et al.*, 2015).

In recent years, great progress has been made in the structural elucidation of CRM1 and CRM1-containing complexes which contributes to a complete understanding of the structure-function relation of CRM1 at an atomic level. This provides a more detailed insight into the export mechanism (Petosa *et al.*, 2004; Fox *et al.*, 2011; Monecke *et al.*, 2013; Monecke *et al.*, 2014; Dickmanns *et al.*, 2015).

CRM1 has a molecular weight of about 123.4 kDa (1071 amino acids) and consists of 21 tandem HEAT repeats forming an annular structure. The HEAT repeat is named after four proteins in which this repeat structure is found: **H**untingtin, elongation factor 3 (**E**F3), protein phosphatase 2A (PP2**A**) and yeast kinase target of rapamycin kinase 1 (**T**OR1). Each HEAT repeat contains a pair of anti-parallel helices A and B linked by a short loop (Figure 1.17 B). Regarding the overall structure of CRM1, the A-helices form the outer ring surface and can interact with the FG NUPs during NPC passage while the B-helices form the inner ring area and can interact with RanGTP and cargo proteins (Monecke *et al.*, 2014).

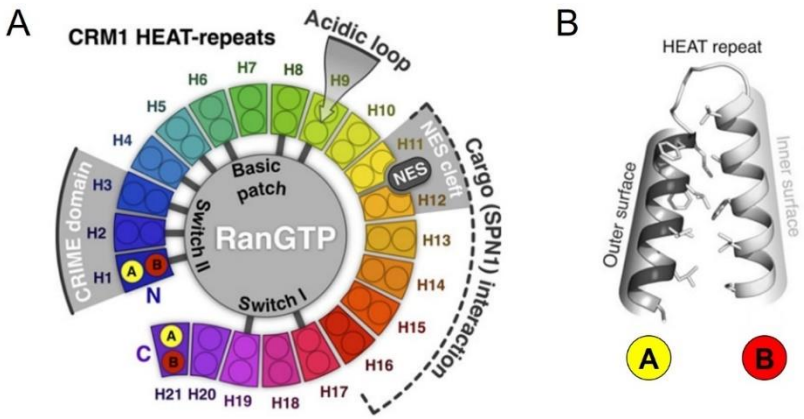

Figure 1.17: Structure of the export receptor CRM1 and its HEAT repeat motif.

A) Schematic representation of structural properties of CRM1. CRM1 consists of 21 tandem HEAT repeats (rainbow-colored) forming an annular structure. HEAT repeats predominantly bind (gray lines) to the Switch regions of RanGTP (gray circle). Important functional regions (highlighted in gray) are the N-terminal CRIME domain, the acidic or H9 loop as well as the NES cleft which is located between HEAT repeats 11 and 12 and involved in cargo interaction, e.g. snurportin 1 (SPN1). **B)** Structure of a HEAT repeat motif composed of a pair of anti-parallel helices linked by a short loop. In general, the A-helix (yellow) is located at the outer surface and the B-helix (red) lines the inner area. HEAT repeats are characterized by strong intra-HEAT-repeat hydrophobic interactions (Monecke *et al.*, 2014).

The structure of CRM1 reveals three important functional regions (**CR**M1, **im**portin-β **e**tc. (CRIME) domain, acidic loop and NES cleft). At its N-terminal part, the CRIME domain is strictly required for the association with RanGTP via Ran's Switch II region. The acidic or HEAT9 loop is another important region involved in RanGTP binding. Binding of the cargo NES occurs via the preformed hydrophobic pocket of CRM1`s NES cleft which is located

between the α-helices of the highly conserved HEAT repeats 11 and 12. Thereby, different leucine-rich NES occupy the identical five binding sites in the preformed hydrophobic pocket of CRM1 (Φ^0-Φ^4) via their α-helical or helix-like structure although they exhibit different spacing (Figure 1.18) (Monecke *et al.*, 2014; Dickmanns *et al.*, 2015). Moreover, it was recently shown that the NES peptides can bind in the CRM1 groove in both orientations which results in a large expansion in NES consensus patterns and thus in potential NES in the proteome (Fung *et al.*, 2015).

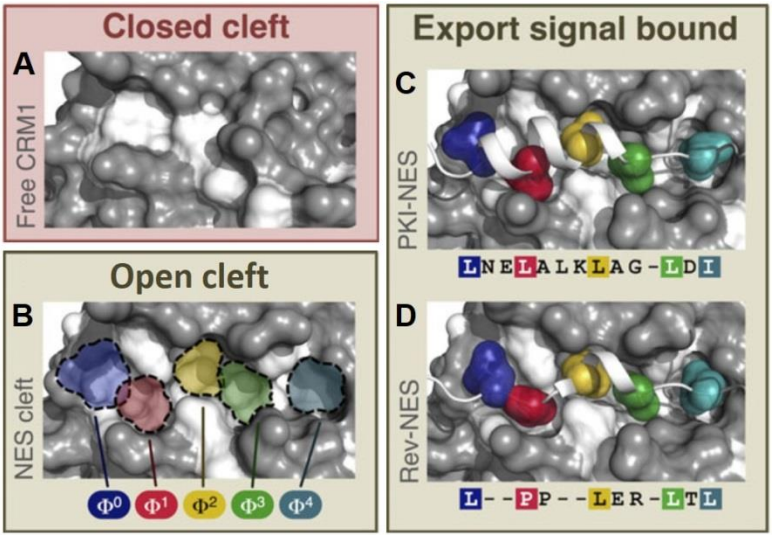

Figure 1.18: NES-binding to the hydrophobic NES cleft of CRM1 in its open state.
A) The Φ-pockets are not accessible in the closed state of the NES cleft (PDB: 4FGV). **B)** In the open state, five hydrophobic Φ-pockets (blue, Φ0; red, Φ1; yellow, Φ2; green, Φ3; teal, Φ4) are exposed (PDB: 3GJX). **C)** PKI-NES bound to the NES cleft (PDB: 3NC1). **D)** Rev (reversionless)-NES bound to the NES cleft (PDB: 3NBZ). Key residues of both NES occupy identical Φ-pockets. Different Φ-spacing is compensated by a different arrangement of the NES-peptide main chain (Monecke *et al.*, 2014).

Structural investigations revealed that CRM1 can basically adopt two different conformations, the extended (cargo-free) as well as the compact (cargo-bound) one (Figure 1.19) (Dickmanns *et al.*, 2015).
The extended (cargo-free) conformation reveals a superhelical structure with no interaction between N- and C-terminal regions. A unique property of CRM1 is the atypical arrangement of HEAT repeat 21 and especially helix 21B which shows two major orientations. In the extended conformation, helix 21B spans the molecule and touches the bases of HEAT repeat 9 thus hindering RanGTP binding. The acidic loop is oriented in a “flipped back” conformation binding to the B-helices in the NES cleft formed by HEAT repeats 11 and 12. This stabilizes the NES cleft in a closed state preventing cargo binding. The compact (cargo-bound) conformation reveals a toroidal structure. To prevent clashing RanGTP binding

requires the displacement of the helix 21B which rearranges to the outside of the molecule in parallel orientation to helix 21A. This in turn results in a tight interaction of N- and C-terminal regions. The acidic loop undergoes a conformational change, too. By contacting HEAT repeats on the opposite side of CRM1, it arranges like a “seatbelt” locking RanGTP to the N-terminal part of CRM1. This, in turn, decreases mechanical strain on the NES cleft, which stabilizes an open NES cleft state allowing cargo binding (Fox *et al.*, 2011; Monecke *et al.*, 2014; Dickmanns *et al.*, 2015).

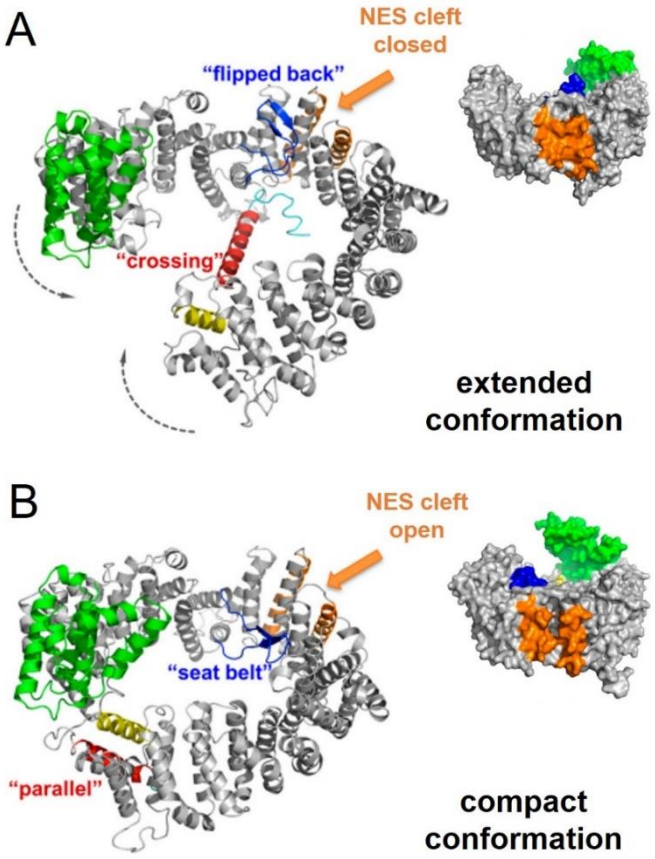

Figure 1.19: Structural changes of CRM1 between its extended and compact conformation. During the nucleocytoplasmic export cycle, the overall conformation of CRM1 (grey) changes between its **A)** extended superhelical (PDB: 4FGV) and **B)** compact toroidal structure (PDB: 3GJX) due to the local positional changes of the CRIME domain (green), the acidic loop (blue), the C-terminal HEAT helix 21B (red) and the conformation of the NES cleft (orange). See main text for details (Dickmanns *et al.*, 2015).

This structural elucidation of both CRM1 conformations enables a more detailed insight and understanding of the mechanistic processes occurring during the nucleocytoplasmic export cycle (Figure 1.20). Nuclear CRM1 in its extended conformation serves as the starting point of the export cycle. A conformational change resulting in the compact CRM1 structure

enables the export complex assembly and finally NPC passage. In the cytoplasm, RanBP1 binding results in a re-localization of the acidic loop from RanGTP to the B-helices in the NES cleft formed by HEAT repeats 11 and 12. This induces again mechanical tension leading to a constriction of the NES cleft and finally resulting in the cargo release. Subsequently, the RanGTP-RanBP1 complex dissociates from CRM1 upon GTP hydrolysis mediated by RanGAP1 in the presence of RanBP1 and RanBP2. As a last step, cytoplasmic CRM1 lacking any binding partners again exhibits the extended conformation and diffuses back into the nucleus for another export cycle (Monecke *et al.*, 2014).

Additionally, CRM1-mediated nuclear export is regulated by Ran-binding protein RanBP3, a nuclear member of the Ran-binding protein 1 family. Unlike cytosolic RanBP1 and RanBP2, which mediate export complex disassembly, RanBP3 stabilizes the export complex in the nucleus by directly interacting with CRM1. Moreover, RanBP3 also affects the cargo selectivity of CRM1 (Englmeier *et al.*, 2001; Langer *et al.*, 2011).

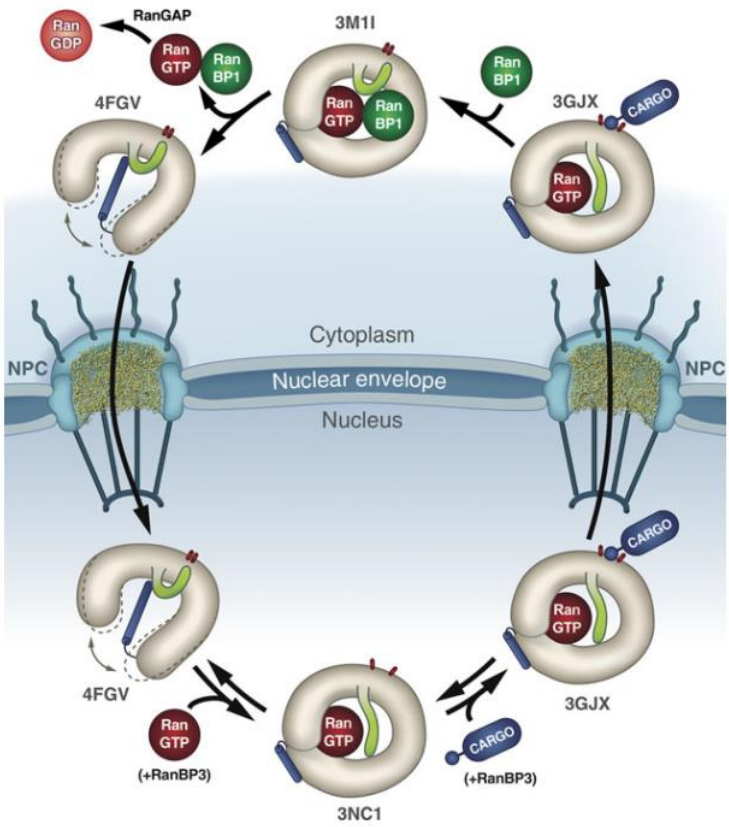

Figure 1.20: Detailed overview of CRM1's conformational changes during the individual steps of the export cycle.

The overall structure of CRM1 (grey) changes during the individual steps of the nucleocytoplasmic export cycle due to the respective orientation of the acidic loop (green) and the C-terminal HEAT helix 21B (blue) as well as the respective conformation of the NES cleft (red). The dashed lines at CRM1 indicate its high structural flexibility. PDB identities for the individual structures are stated. See main text for details (Monecke *et al.*, 2014).

Besides its established role in nuclear export, studies revealed additional functions for CRM1 in mitosis, especially in mitotic spindle assembly (Figure 1.21). CRM1, identified as a mitotic effector of RanGTP, binds to kinetochores, where it is involved in microtubule attachement. CRM1 in complex with RanGTP, which is highly concentrated near chromosomes, promotes the stable recruitment of RanGAP1 and RanBP2 to kinetochores (Arnaoutov *et al.*, 2005; Clarke, 2005). The RanGAP1-RanBP2 complex is essential for the interaction of kinetochores with microtubules *in vivo* (Joseph *et al.*, 2004). Moreover, the complex consisting of CRM1, RanGTP and the RanGAP1/RanBP2 subcomplex is proposed to work in an autoregulatory loop. After recruitment of the RanGAP1/RanBP2 complex to kinetochores, it in turn promotes hydrolysis of RanGTP and therefore catalyzes its own release from the kinetochores (Arnaoutov and Dasso, 2005). The recruitment mechanism for RanGAP1/RanBP2 is not completely elucidated but might involve a NES of RanGAP1 (Cha *et al.*, 2015). In a similar way, CRM1 might be able to recruit further SAFs via their NES to the mitotic spindle, where they achieve full activity (Clarke, 2005).

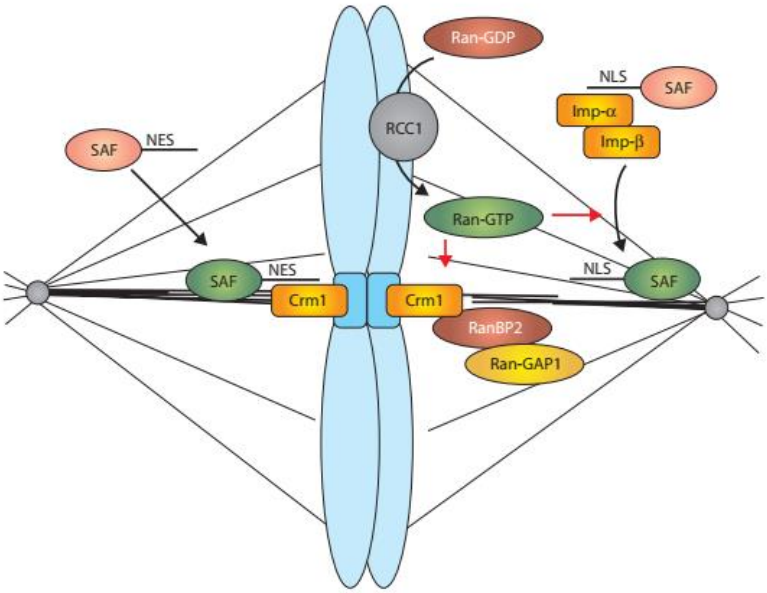

Figure 1.21: CRM1 is a critical RanGTP effector for mitotic spindle assembly and function.
CRM1 (orange) is involved in the regulation of mitotic spindle assembly by the RanGTPase cycle. Generation of RanGTP (green) from RanGDP (red) by RCC1 (grey) on chromosomes (blue) causes the release of SAFs (inactive: light red, active: green) from inhibitory complexes with importins-α/β (orange) which otherwise bind to NLS of SAFs. Moreover, RanGTP can also function through binding to its mitotic effector CRM1, which interacts with kinetochores and recruits RanBP2 (red) and RanGAP1 (yellow). The recruitment mechanism might involve a NES. The RanBP2/RanGAP1 complex is essential for the interaction of kinetochores with kinetochore fibers consisting of microtubule bundles. For additional regulation, CRM1 might recruit other NES-containing SAFs as active complexes to the spindle (Clarke, 2005).

Besides the recruitment of Ran-GAP1/Ran-BP2 to kinetochores, CRM1 bound to RanGTP was discovered to be essential for the formation of normal kinetochore fibers and for chromosome segregation at anaphase. Thus, in addition to importin-β, CRM1 is the second member of the importin-β family to act as a mitotic effector for RanGTP, and the first export receptor discovered to be involved in mitosis (Arnaoutov *et al.*, 2005).

1.2.6 Targeting CRM1-mediated nuclear export

In cancer cells, CRM1 plays a critical role in exporting various tumor suppressor proteins including p53, forkhead box O subclass (FOXO), p27, breast cancer 1 (BRCA1), adenomatous polyposis coli (APC), retinoblastoma protein (Rb) and nucleophosmin. Moreover, increased expression levels of CRM1 lead to an increased export and a cytoplasmic accumulation of those tumor suppressor proteins, which normally exert essential functions within the nucleus to prevent cancer initiation and progression or to direct the cellular response to chemotherapy in various tumor entities. Thus, targeting nuclear CRM1-mediated export represents a promising strategy to fight cancer by overcoming the disrupted physiological localization of tumor suppressors or by directing the mislocalization of proteins to inactivate oncoproteins including β-catenin, nuclear factor kappa-light-chain-enhancer of activated B cells (NF-κB) or Survivin (Gravina *et al.*, 2014; Hill *et al.*, 2014; Turner *et al.*, 2014; Stelma *et al.*, 2016).

Targeting can be envisaged at various levels including upstream regulators, the interaction between Ran regulators and the export receptor CRM1, the interaction between CRM1 and cargo proteins and the NPC. However, the respective strategy must overcome the specificity for tumor cells versus normal cells and the difficulty of interfering with protein–protein interactions (PPIs) in contrast to enzyme-substrate binding. Despite all the potential levels of targeting regarding nuclear export, the export receptor CRM1 remains the most attractive therapeutic drug target since its structure and mechanistic functions are well investigated and characterized (Hill *et al.*, 2014).

The naturally occurring compound Leptomycin B (LMB) is the first identified CRM1 inhibitor with a molecular weight of 0.54 kDa and capable of disrupting a specific protein–protein interaction. LMB was shown to bind CRM1 covalently at the conserved cysteine residue 528 of the human protein in a "Michael-type" reaction. This cysteine alkylation in the hydrophobic NES cleft prevents CRM1 binding to the leucine-rich NES of cargo proteins and thus export complex assembly (Kudo *et al.*, 1999; Sun *et al.*, 2013). The polyketide of LMB interacts with the same hydrophobic pocket residues that contact NES sequences (Gravina *et al.*, 2014; Monecke *et al.*, 2014).

Unfortunately, Leptomycin B failed in a Phase I clinical trial due to severe dose-limiting toxicity resulting in profound anorexia and malaise. LMB was no longer pursued for therapeutic use in patients (Newlands *et al.*, 1996). Consequently, attempts were made to overcome these off-target effects by developing and identifying different natural products as well as semi-synthetic and synthetic compounds with improved pharmacological properties. However, none of these improved nuclear export inhibitors including, *inter alia*, anguinomycins, goniothalamin, KOS-2464, ratjadones, the reversible PKF050-638, valtrate or acetoxychavicolacetate have entered clinical trials yet (Gravina *et al.*, 2014; Hill *et al.*, 2014).

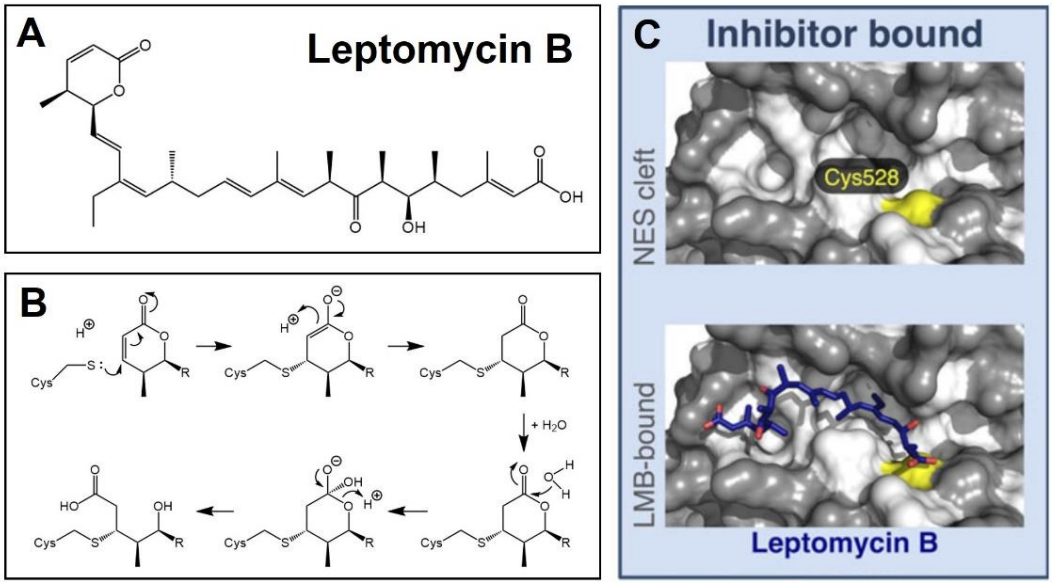

Figure 1.22: Natural export inhibitor Leptomycin B inactivates CRM1 by covalent binding at cysteine residue 528 in its conserved NES cleft.

A) Chemical structure of inhibitor Leptomycin B (Kudo *et al.*, 1999). **B)** Michael addition and hydrolysis reactions LMB performs to bind CRM1 covalently at the conserved cysteine residue 528 in the NES cleft of the human protein. Only the lactone residue of LMB is shown, the polyketide chain is displayed as R (Sun *et al.*, 2013). **C)** Blocking of the NES cleft by CRM1-specific inhibitor LMB (PDB: 4HAT). LMB has been removed in the upper image to show the dimensions of the occupied NES cleft. The interacting cysteine residue 528 is highlighted in yellow (Monecke *et al.*, 2014).

In 2012, Karyopharm Therapeutics discovered a new class of CRM1 inhibitors, the drug series of “Selective Inhibitors of Nuclear Export” (SINE) by an *in silico* molecular modelling strategy. These water-soluble small molecules covalently and irreversibly modify the cysteine residue 528 in the NES cleft of the human CRM1 with additional numerous noncovalent interactions (Lapalombella *et al.*, 2012). Although the most potent and *in vitro* studied inhibitor of the series is KPT-185, KPT-330 or Selinexor is currently under investigation in Phase I/II clinical trials, because of its more acceptable pharmacokinetics. So far, it shows

promising results in both hematological and solid tumors (Parikh *et al.*, 2014). Moreover, minimal toxicity to normal cells was observed, indicating that SINE compounds specifically and preferentially target tumor cells (Lapalombella *et al.*, 2012; Gravina *et al.*, 2014). More recently, combination therapies, thus simultaneous treatment with CRM1 inhibitors as well as available chemotherapeutic agents are proven to be effective in fighting cancer. Thereby, inhibition of nuclear export weakens the resistance mechanisms of the tumor cells and thus enhances the potency of the chemotherapeutic agent (Turner *et al.*, 2014; Stelma *et al.*, 2016).

Nevertheless, CRM1 is still the main export receptor not only in cancer cells but all kinds of cell types, facilitating export of more than 240 nuclear proteins. Thus, protein specific transport inhibitors preventing protein export by selective binding to their NES may represent a more targeted therapy and are urgently needed. In recent years, inhibitors targeting the NES peptide of topoisomerase II α or influenza A virus nucleoprotein were developed and successfully prevented protein export in a more specific and selective manner (Turner *et al.*, 2014; Kakisaka *et al.*, 2016).

1.3 Survivin

Survivin, also known as baculoviral IAP repeat-containing protein 5 (BIRC5), plays an important role in cancer disease. While it is mostly absent in normal resting adult tissues, it is highly up-regulated in almost all cancer types (Ambrosini *et al.*, 1997; Adida *et al.*, 2000). Thereby, its overexpression is associated with a resistance of tumors against chemo- and radiotherapy, frequent recurrences and decreased patient survival (Capalbo *et al.*, 2007; Engels *et al.*, 2007; Chen *et al.*, 2014; Xu *et al.*, 2014). Despite its small size (142 amino acids (aa), 16.5 kDa) and its lack of enzymatic activity, Survivin is a multitasking protein fulfilling a well characterized dual functional role within the cell (Knauer *et al.*, 2007c). As the smallest member of the inhibitor of apoptosis protein family, Survivin plays a role in the inhibition of apoptotic cell death, and as part of the chromosomal passenger complex it is also crucially involved in mitotic regulation promoting cell proliferation (Li *et al.*, 1998). For both biological functions, an interaction with the nuclear export receptor CRM1 mediated by Survivin's NES is pivotal (Knauer *et al.*, 2006; Knauer *et al.*, 2007b). Morover, Survivin has been linked to cellular DNA repair processes in recent studies but the exact molecular mechanisms are still not completely understood and a subject of scientific research (Capalbo *et al.*, 2010; Reichert *et al.*, 2011).

The gene coding for human Survivin is located at the telomeric end of chromosome 17 (17q25). So far, six splice variants of Survivin with distinct biological functions are known including Survivin (142 aa) itself as the main transcript consisting of 4 exons and 3 introns,

Survivin-2B (165 aa), Survivin-3B (120 aa), Survivin-ΔEX3 (108 aa), Survivin-2α (74 aa), Survivin-3α (78 aa) (Knauer *et al.*, 2007a; Sah and Seniya, 2015). However, the alternative splice variants are only expressed at low levels and do supposedly not interfere with the functions of the main transcript (Knauer *et al.*, 2007a).

1.3.1 Survivin's role in cancer disease

As Survivin is highly up-regulated in almost all cancer types (Ambrosini *et al.*, 1997; Adida *et al.*, 2000), it supposedly plays an important role in cancer disease. Cancer disease is the second leading cause of death globally as well as in Germany following cardiovascular diseases. In 2015, 8.8 million people worldwide and more than 200,000 people in Germany died from cancer, which correspond to 17 % and 25 % of all cases of death, respectively (Federal Statistical Office Germany, 2018; World Health Organization, 2018). Cancer is a generic term for a large group of tumor diseases suppressing and damaging healthy tissue. The tumor is characterized by the growth of abnormal cells beyond their usual boundaries and can either stay localized and invade only adjoining parts (benign) or spread to other organs and tissues, thus metastasizes (malignant) (World Health Organization, 2018).

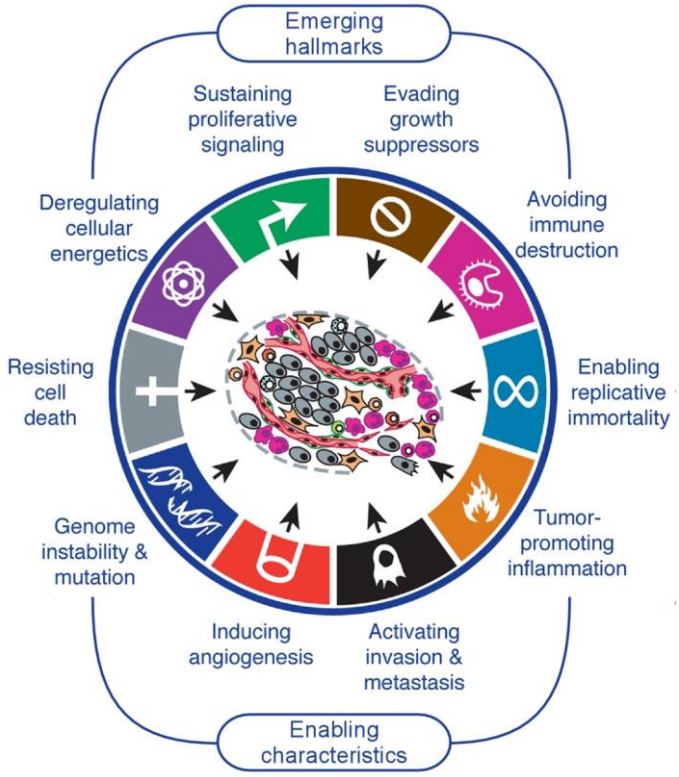

Figure 1.23: The hallmarks of cancer.
Illustrative representation of the biological capabilities acquired during the multistep development of human tumors. See main text for details. Modified after (Hanahan and Weinberg, 2011).

In 2000, Hanahan and Weinberg proposed six “hallmarks of cancer” comprising biological capabilities acquired during the multistep development of human tumors (Figure 1.23). Beside the described ability of activating invasion and metastasis the cancer hallmarks include sustaining proliferative signaling, evading growth suppressors, resisting cell death, enabling replicative immortality and inducing angiogenesis (Hanahan and Weinberg, 2000).
In 2011, the “hallmarks of cancer” concept was expanded (Figure 1.23) by two further emerging hallmarks, the ability of tumors to deregulate cellular energetics and to avoid destruction by the immune system, as well as two further enabling characteristics of tumors, namely genome instability and mutations as well as tumor-promoting inflammation (Hanahan and Weinberg, 2011).
As a key regulator in cell death inhibition and cell proliferation (Li *et al.*, 1998) and its further role in promoting angiogenesis (Sanhueza *et al.*, 2015; Li *et al.*, 2016), Survivin is strongly linked to some of the cancer hallmarks and thus to cancer disease. This cancer correlation is confirmed by Survivin’s absence in most non-proliferating healthy adult tissues on the one hand and its strong overexpression in a wide variety of cancers on the other hand (Table 1.2) (Ambrosini *et al.*, 1997; Adida *et al.*, 2000). This overexpression is correlated with advanced disease, accelerated time to recurrence, reduced patient survival and resistance to chemo- and radiotherapy (Adida *et al.*, 1998; Capalbo *et al.*, 2007; Engels *et al.*, 2007; Chen *et al.*, 2014; Xu *et al.*, 2014).

Table 1.2: Over-expression of Survivin in common human cancer types.
A variety of common human cancer types are listed with their Survivin expression (Kelly *et al.*, 2011).

Cancer	Expression	Cancer	Expression
Lung cancer	85.5 %	Colorectal cancer	63.5 %
Esophageal cancer	80 %	Hepatocellular cancer	41 %-87 %
Breast cancer	70.7 % - 90.2 %	Gastric cancer	34.5 % - 68 %
Pancreatic cancer	76.9 % - 88 %	Bladder cancer	57.8 %
Ovarian cancer	73.5 %	Acute myeloid leukemia	54.8 %
Malignant melanoma	67 %	Acute lymphocytic leukemia	68.8 %

Survivin’s overexpression in cancer is mediated in diverse ways including mutations in its promotor (Xu *et al.*, 2004), gene duplication (Tajiri *et al.*, 2001), deregulation of Survivin transcriptional repressors such as retinoblastoma protein (Rb) (Jiang *et al.*, 2004) and p53 (Hoffman *et al.*, 2002), NF-κB-induced transcription (Tracey *et al.*, 2005) and insulin-like

growth factor-1 (IGF-1)-mediated stabilization of existing messenger ribonucleic acid (mRNA) (Vaira *et al.*, 2007).

Because of its role in cancer, Survivin attracts increasing interest not only as a molecular marker for malignancies but as a potential and attractive therapeutic target for anti-cancer therapies. Various strategies exist to block the expression or function of Survivin in cancer cells including immunotherapeutic approaches to induce immune response against Survivin, small molecule inhibitors to block functions of Survivin and nucleic acid-based approaches which interfere with Survivin gene expression. By now, divers vaccination approaches using Survivin as a vaccine candidate have been evaluated in preclinical or clinical studies. The most promising small molecule inhibitor YM-155, which suppresses Survivin expression and induces apoptosis in cancer cells, is currently under investigation in phase II clinical trials as well as the antisense oligonucleotide LY2181308, a specific inhibitor of Survivin mRNA (Altieri, 2001; Kelly *et al.*, 2011; Rödel *et al.*, 2012; Coumar *et al.*, 2013; Garg *et al.*, 2016).

1.3.2 Survivin's structure and domain organization

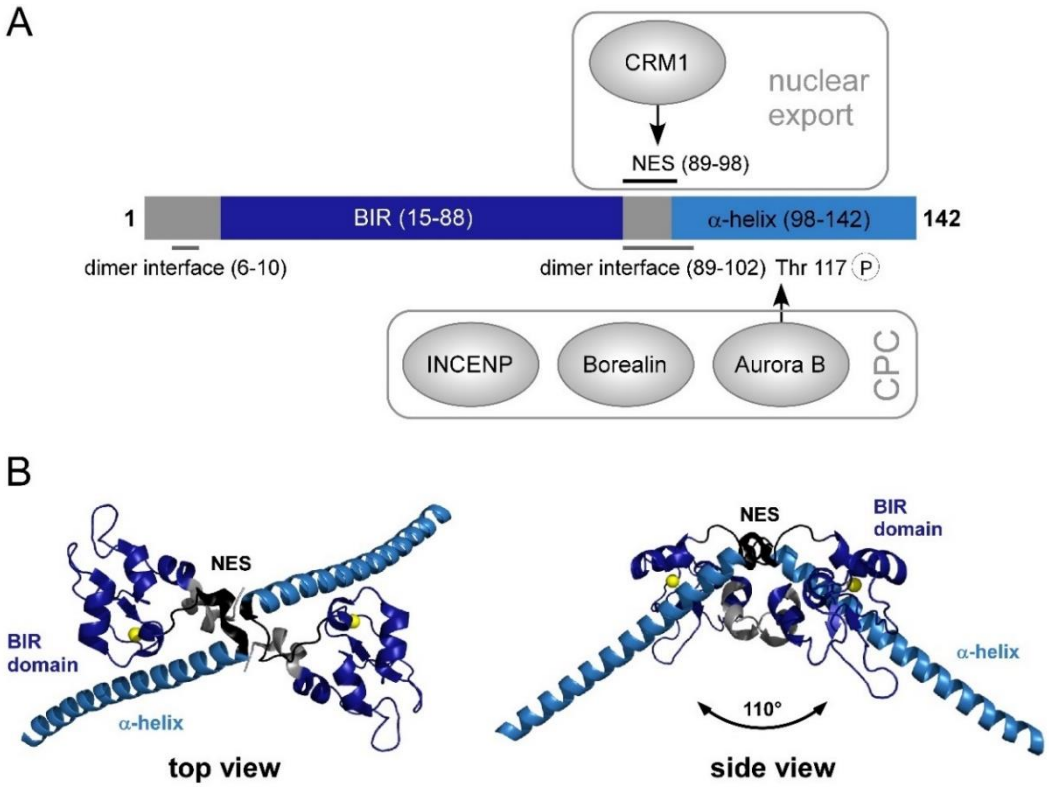

Figure 1.24: Survivin's structure and domain organization.

A) Domain organization of Survivin. See main text for details. Modified after (Altieri, 2008). **B)** Structure representation of the Survivin homodimer (PDB: 1E31) in top view (left) and side view (right). The N-terminal BIR domain is depicted in dark blue, the NES in black and the C-terminal α-helix in light blue. The Zn^{2+} ion is shown as a yellow sphere. The 110° angle is highlighted. Modified after (Chantalat et al, 2000).

The Survivin protein exhibits a unique structure and domain organization (Figure 1.24), which enable interactions to other proteins and therefore determine Survivin's various functions. The N-terminal baculovirus IAP repeat (BIR) domain (aa 15–88) classifies Survivin as a member of the IAP family since this structural motif is a characteristic feature of all IAPs. Survivin's BIR domain is a globular zinc finger domain consisting of a three-stranded antiparallel β-sheet surrounded by four small α-helices, whereby the zinc ion is coordinated by three cysteines (C57, C60, C84) and one histidine (H77). The long C-terminal α-helix (aa 98–142) extends out and away from the BIR domain. Thereby, its direction is stabilized and fixed by hydrogen bonds and hydrophobic interactions between the BIR domain and the first few turns of the helix (Chantalat *et al.*, 2000; Verdecia *et al.*, 2000). Survivin's C-terminal α-helix forms a three-helix bundle together with Borealin (aa 15–79) and inner centromere protein (INCENP) (aa 1–49) representing the basis of a stable CPC assembly (Jeyaprakash *et al.*, 2007). Moreover, the α-helix was proven to interact with microtubules (Li *et al.*, 1998). Furthermore, Survivin possesses a classical leucine rich NES (^{89}VKKQFEELTL^{98}) located between the BIR domain and the C-terminal α-helix, which mediates the interaction to the main cellular export receptor CRM1 (Knauer *et al.*, 2006). In addition to the classical NES, a further non-classical CRM1-dependent export motif was proposed in the C-terminal α-helix of Survivin, whose exact sequence has not been further defined (Rodríguez *et al.*, 2002). Another important region, partly overlapping with the classical NES, is the dimer interface (aa 6–10 and 89–102), which is responsible for the homodimerization of Survivin monomers in solution. The dimer interface is thereby formed via hydrophobic interactions of residue L98 from one monomer with a hydrophobic pocket (L6, W10, F93, F101 and L102) of the other monomer. In solution, the formed homodimer of Survivin shows a 110° angle between both C-terminal α-helices and an overall bow tie shape (Figure 1.24 B) (Chantalat *et al.*, 2000; Verdecia *et al.*, 2000).

1.3.3 Survivin's post-translational regulation

On the protein level, Survivin is also regulated by post-translational modifications (PTMs). Post-translational modifications are chemical changes, proteins undergo after their translation including specific cleavage of precursor proteins, formation of disulfide bonds or covalent addition or removal of chemical groups and peptides or small proteins. Prominent modifications are phosphorylation, acetylation, methylation, oxidation, lipidation, glycosylation, ubiquitination and sumoylation (Bürkle, 2002). These modifications play a key role in the rapid cellular regulation of protein functions including protein folding, protein stability, protein targeting to specific subcellular compartments, protein–ligand and protein–protein interactions, catalytic activity and signal transduction (Bürkle, 2002).

Survivin is mainly regulated by phosphorylation, acetylation and ubiquitination (Nogueira-Ferreira *et al.*, 2013). Survivin's four phosphorylation sites are involved in regulation of Survivin's mitotic and anti-apoptotic functions. Phosphorylation at threonine 117 by Aurora B kinase was reported to regulate localization and stability of the CPC while dephosphorylation is crucial for chromosome progression into anaphase (Wheatley *et al.*, 2004; Wheatley *et al.*, 2007). Phosphorylation at threonine 34 by cyclin-dependent kinase 1 (CDK1) was reported to be pivotal for Survivin's anti-apoptotic function (O'Connor *et al.*, 2000; Barrett *et al.*, 2009). Phosphorylation at threonine 48 by casein kinase 2 (CK2) was reported to modify the Survivin-Borealin interaction and thereby critically influence Survivin's mitotic and anti-apoptotic functions (Barrett *et al.*, 2011). Finally, phosphorylation at serine 20 by polo-like kinase 1 (Plk1) was reported to be essential for the accurate chromosome alignment and cell proliferation (Colnaghi and Wheatley, 2010). Survivin's C-terminal region contains several lysine residues (90, 110, 112, 115, 120, 121, 122, 129 and 130) which can be acetylated by the histone acetyltransferase CREB (cyclic adenosine monophosphate response element-binding protein)-binding protein (CBP). These acetylation sites were reported to regulate the balance between cellular dimeric and monomeric forms of Survivin (Engelsma *et al.*, 2007; Jeyaprakash *et al.*, 2007; Altieri, 2008; Wang *et al.*, 2010; Nogueira-Ferreira *et al.*, 2013). Ubiquitination often promotes proteasomal degradation of proteins. Indeed, for Survivin, an increased degradation due to the ubiquitination of lysine 48 has been observed at the end of mitosis (Zhao *et al.*, 2000). Moreover, ubiquitination of Survivin regulates the dynamics of the CPC-centromere interaction and thus chromosomes segregation independently of protein degradation. While ubiquitination of lysine 63 by the ubiquitin fusion degradation protein 1 (UFD1) is required for the association of Survivin with centromeres, its de-ubiquitination mediated by human homolog of fat facet in mouse (hFAM) promotes its dissociation (Vong *et al.*, 2005).

1.3.4 Survivin's functional role in apoptosis

In its role as an apoptosis inhibitor, Survivin cytoprotectively counteracts cell death (Li *et al.*, 1998). Apoptosis is the most common and best understood form of controlled and programmed cell death and primarily occurs to preserve tissue homeostasis by maintaining the balance between cell proliferation and cell death. The term "apoptosis" was introduced in 1972 by Kerr *et al.* who were the first to describe basic morphological characteristics of apoptosis (Kerr *et al.*, 1972).

The biochemical mechanism depends on an intracellular proteolytic cascade that is mediated by cysteinyl-aspartate-specific proteases (caspases). Inactively expressed procaspases are cleaved and associate to form active heterotetrameric caspases. The first procaspases

activated by auto-proteolytic cleavage are called initiator caspases (2, 8, 9 and 10) which then activate many executioner or effector caspases (3, 6 and 7). This caspase cascade then cleaves a variety of key proteins in the cell, leading to the controlled death of the cell (Riedl and Shi, 2004).

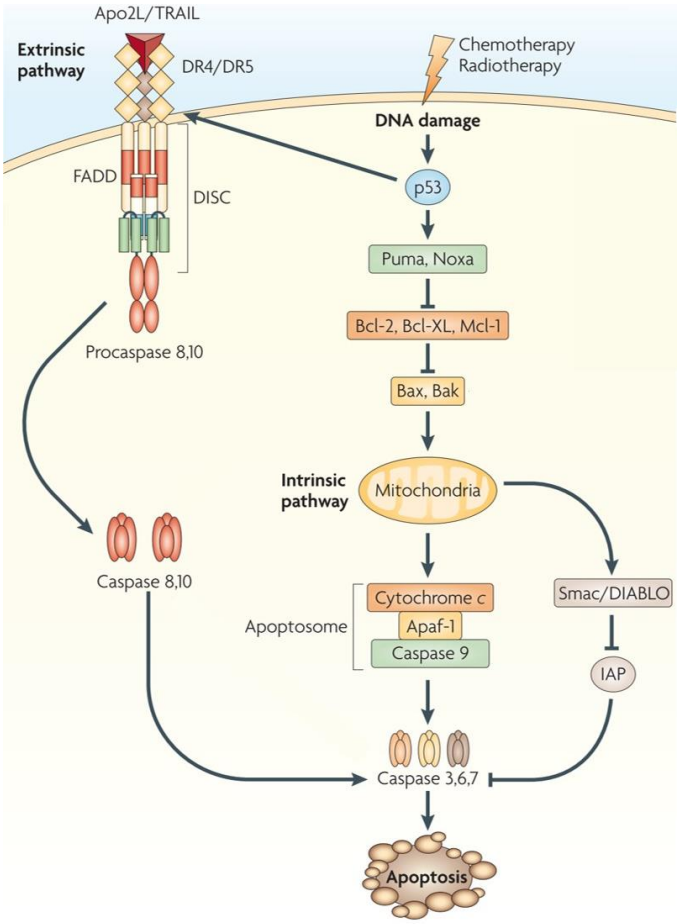

Figure 1.25: Key steps of the extrinsic and intrinsic apoptotic signaling pathways.
Extrinsic pathway: Pro-apoptotic ligands such as Apo2L/TRAIL bind to the pro-apoptotic receptors DR4 and/or DR5 on the cell surface. Ligand binding induces receptor clustering and recruitment of the adaptor protein FADD and the initiator caspases 8 and 10 as procaspases, forming a DISC complex. This triggers activation of procaspases 8 and 10 by autocatalytic processing and their release into the cytoplasm, where they activate the effector caspases 3, 6 and 7 to trigger apoptosis. Intrinsic pathway: Cellular stress, for example DNA damage induced by chemo- or radiotherapy, activates the p53 tumor suppressor protein. p53 initiates the intrinsic pathway by upregulating Puma and Noxa, which in turn inhibit Bcl-2, Bcl-XL and Mcl-1. Their inactivation leads in turn to the activation of Bax and Bak, which permeabilize the outer mitochondrial membrane. This causes a release of cytochrome c, which binds to the adaptor Apaf-1 to recruit the initiator procaspase 9 into a signaling complex, termed the apoptosome. Activated caspase 9 then cleaves and activates the effector caspases 3, 6 and 7 to trigger apoptosis. The mitochondrial protein Smac/DIABLO augments apoptosis by binding to IAPs and reversing their inhibition on several caspases. p53 mainly stimulates the intrinsic pathway, but it also upregulates some of the pro-apoptotic receptors such as DR5 and thereby augments extrinsic signaling. See main text for details. Modified after (Ashkenazi, 2008).

There are two main signaling pathways that can activate this caspase cascade: the extrinsic and the intrinsic pathway (Figure 1.25) (Ashkenazi, 2008).

The extrinsic pathway (Figure 1.25), also known as the death receptor-mediated pathway, is triggered by extracellular signal proteins, so called “death” ligands, e.g. Apo2 ligand (Apo2L) also known as tumor necrosis factor related apoptosis-inducing ligand (TRAIL). They bind to cell-surface death receptors (e.g. DR4 and/or DR5). This leads to the assembly of the death-inducing signaling complex (DISC) composed of the death receptor, fas-associated death domain (FADD), and the procaspases 8 and 10, which are activated. Downstream activation of executioner caspases 3, 6 and 7 leads at the end to cell death. The intrinsic pathway (Figure 1.25) on the other hand, also known as the mitochondrial pathway, is activated from inside the cell, in response to intracellular damage, oncogenes, injury or other stresses like DNA damage or lack of oxygen or nutrients. Induced cellular stress activates the p53 tumor suppressor protein, which upregulates Puma and Noxa. They inhibit B-cell lymphoma-2 (Bcl-2), B-cell lymphoma-extra large (Bcl-XL) and myeloid cell leukemia-1 (Mcl-1), which belong to the anti-apoptotic members of the Bcl-2 family. Their inactivation leads in turn to the activation of the pro-apoptotic Bcl-2 family members Bax and Bak, which cause altered permeability of the mitochondrial membrane resulting in the release of mitochondrial proteins into the cytosol, mainly cytochrome c, which activates the adapter protein apoptotic protease activating factor 1 (Apaf-1), causing it to oligomerize into a wheel-like heptamer and recruiting procaspase 9 molecules. This assembled apoptosome then activates the caspase cascade initiating apoptosis. Moreover, the mitochondrial protein second mitochondria-derived activator of caspase/direct inhibitor of apoptosis protein-binding protein with low pI (Smac/DIABLO) enhances apoptosis by binding to IAPs thereby reversing their inhibitory effect on several caspases. In addition to the stimulation of the intrinsic pathway, p53 upregulates some of the pro-apoptotic receptors such as DR5 and thereby also augments extrinsic signaling (Riedl and Shi, 2004; Ashkenazi, 2008).

The members of the IAP family act as intrinsic caspase-cascade regulators during apoptosis. The human IAP family consists of eight proteins (Figure 1.26): Bruce/Apollon, inhibitor of apoptosis protein-like protein 2 (ILP2), melanoma-inhibitor of apoptosis protein (ML-IAP)/Livin, Survivin, neuronal apoptosis inhibitory protein (NAIP), cellular IAP1 (c-IAP1), cellular IAP2 (c-IAP2) and X-linked inhibitor of apoptosis protein (XIAP).

IAPs are characterized by the existence of a BIR domain, a 70–80 amino acid zinc-binding domain. One to three BIR domains are located at the N-terminal region of all proteins. Furthermore, some IAPs have a C-terminal really interesting new gene (RING) domain with an E3-ubiquitin ligase activity. In addition, some members have a caspase-associated recruitment domain (CARD) of less clear function (Riedl and Shi, 2004; Altieri, 2010).

Caspase inhibition mediated by direct interaction via the BIR domain was originally proposed for all IAPs including Survivin (Tamm *et al.*, 1998; Deveraux and Reed, 1999). Recent studies, however, revealed that only XIAP is a physiological inhibitor of caspases *in vivo* (Eckelman *et al.*, 2006). Thereby, XIAP associates with executioner caspases 3 and 7 via its linker region upstream of the BIR2 domain, as well as with initiator caspase 9 through its BIR3 domain, with high affinity, shutting off their cell killing ability (Altieri, 2010).

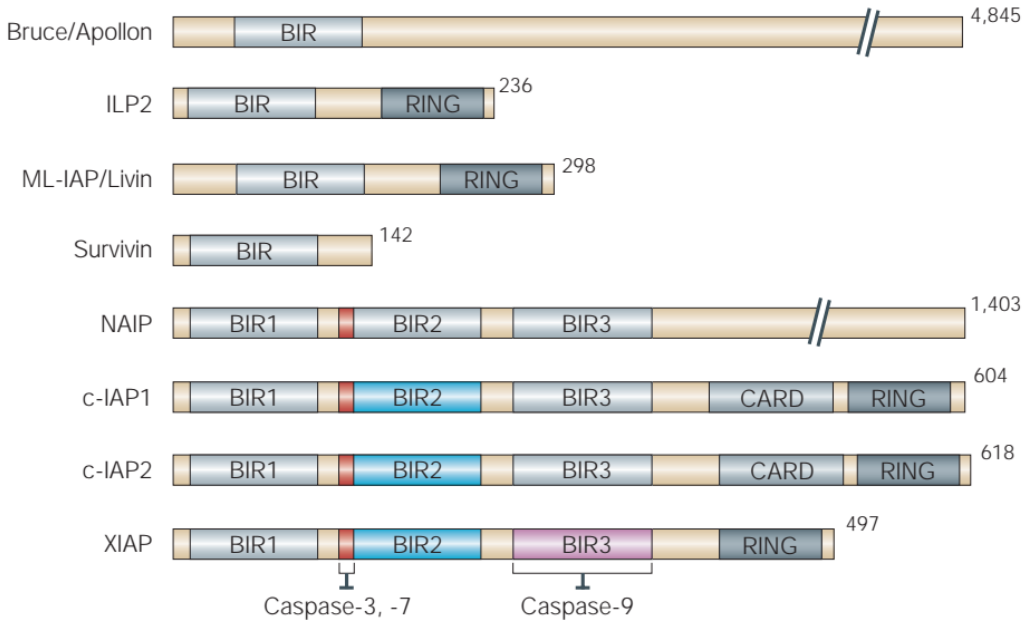

Figure 1.26: The human members of the IAP family.
Schematic representation of the human inhibitor of apoptosis proteins including Bruce/Apollon, ILP2, ML-IAP/Livin, Survivin, NAIP, c-IAP1, c-IAP2 and XIAP. A conserved linker peptide upstream of the BIR2 domain of XIAP, c-IAP1 and c-IAP2 and NAIP is responsible for binding caspases 3 and 7 (red). Only the BIR3 domain (violet) of XIAP can potently inhibit caspase 9. BIR: baculovirus IAP repeat; RING: really interesting new gene; CARD: caspase-associated recruitment domain. See main text for details (Riedl and Shi, 2004).

As the smallest member of the human IAP family, Survivin contains only one BIR domain and no further protein domains (e.g. CARD or RING) and does not directly bind caspases to execute its anti-apoptotic function (Srinivasula and Ashwell, 2008; Altieri, 2010). Instead, various modes of indirect inhibition of caspase-dependent apoptosis have been reported, especially via cooperative interactions with other partner proteins *in vivo*. For example, the IAP member XIAP was reported to form a complex with Survivin which was able to suppress caspase 9 activity. Moreover, this complex assembly results in an increased stability of XIAP against proteasomal degradation further increasing the activity of XIAP for caspase inhibition. However, the interaction is disrupted by phosphorylation of Survivin at serine 20 by protein

kinase A (PKA) (Dohi *et al.*, 2004; Dohi *et al.*, 2007). In addition to XIAP, Survivin was also reported to form a complex with the hepatitis B X-interacting protein (HBXIP). This complex was shown to bind procaspase 9 preventing its recruitment to Apaf-1 and thus formation of the apoptosome. Hereby, the Survivin-HBXIP complex selectively suppresses apoptosis initiation via the intrinsic pathway (Marusawa *et al.*, 2003). Furthermore, Survivin was also reported to bind to the pro-apoptotic factor Smac/DIABLO reducing antagonism of Smac/DIABLO to XIAP and thus allowing free XIAP to directly block caspases conducting its anti-apoptotic function (Song *et al.*, 2003).

1.3.5 Survivin's functional role in proliferation

Besides its anti-apoptotic function as an IAP, Survivin also plays an important role in cell proliferation (Li *et al.*, 1998), more specifically in cell cycle regulation. Within the cell cycle, all living cells are reproduced by replication of their DNA and division of their nucleus and cytoplasm. The cell cycle of eukaryotic cells is divided into four phases: G1 (gap 1), S (synthesis), G2 (gap 2) and M (mitosis), whereby G1, S and G2 together are named interphase and the M phase is divided into two processes, mitosis and cytokinesis. In G1 and G2 phase, the cell prepares for the upcoming critical phases of the cell cycle, the S- and the M-phase, and monitors if all extra- and intracellular conditions are favorable before it proceeds with the cell cycle. In S-phase, the DNA is replicated yielding in duplicated chromosomes. In mitosis, traditionally divided into five phases (prophase, prometaphase, metaphase, anaphase and telophase), the nucleus gets divided and the duplicated chromosomes are segregated. In prophase, the chromatin condenses, the centrosomes migrate to the opposite poles of the nucleus and the spindle apparatus forms between the two centrosomes. During prometaphase, the nuclear membrane disintegrates. The chromosomes are connected to the spindle apparatus via the kinetochore. In metaphase, the chromosomes are arranged on the equatorial plane between the two spindle poles. During anaphase, the two chromatids of a chromosome are separated and migrate to the opposite spindle poles. Separated chromatids decondens in telophase, and a new nuclear membrane is formed around each set of chromatids. Finally, in cytokinesis the division of the cytoplasm results in the formation of two daughter cells (Alberts *et al.*, 2015).

The key regulators driving the cell cycle are the cyclin-dependent kinases (CDKs). For their catalytical activity and substrate recognition, these serine/threonine kinases require cyclin-binding. During the cell cycle, temporal synthesis and degradation of cyclins result in fluctuating expression levels which in turn control CDK activation and thus cell cycle progression (Alberts *et al.*, 2015).

As a highly complex process, the cell cycle is further regulated by an internal control system to avoid deficient chromosomal distribution or other errors emerging during replication and mitosis. Five checkpoints, which are located in late G1-phase (restriction point), at the transition from G1- to S-phase, in S-phase, at the transition from the G2- to M-phase and at the transition from meta- to anaphase (spindle assembly checkpoint) in M-phase, prevent cells from entering a new phase until they have successfully completed the previous one. Among other things, successful replication and the correct connection of the chromosomes to the spindle apparatus are monitored at these points (Murray, 1992; Alberts *et al.*, 2015).

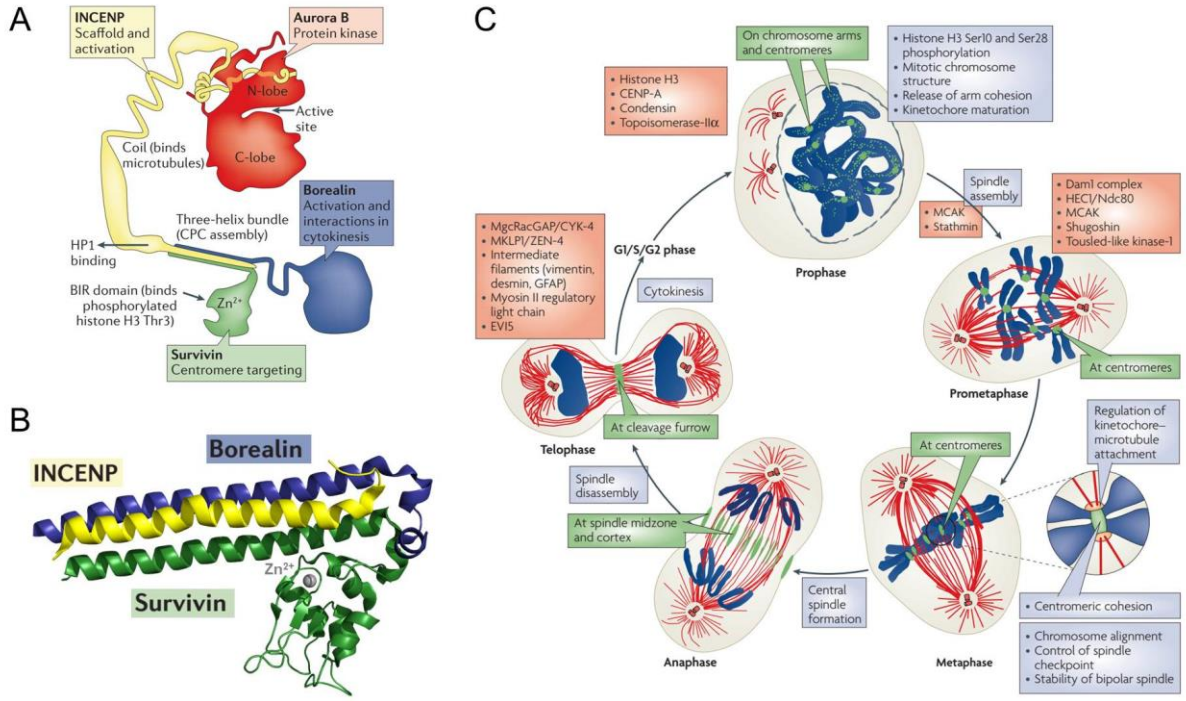

Figure 1.27: Chromosomal passenger complex structure and its localization and functions during mitosis.

A) Schematic representation of the CPC structure, which is formed by Survivin, INCENP, Borealin and the kinase Aurora B. The domains and functions for each CPC member are indicated (Carmena et al, 2012). **B)** The crystal structure (PDB: 2QFA) of the three-helix bundle of Survivin (aa 1-142, green), INCENP (aa 1–58, yellow) and Borealin (aa 10–109, blue), forming the core of the CPC, is shown (Jeyaprakash et al, 2007). **C)** Schematic representation of the CPC localization (green) correlated with its functions (blue boxes) and principle targets (red boxes) during mitosis relative to tubulin (red) and chromosome (blue) dynamics. The CPC localizes to chromosome arms and centromeres in prophase. In prometaphase, it concentrates at centromeres, where it remains during metaphase. The relocalization of the CPC to the spindle midzone and the cell cortex occurs in anaphase. In telophase, the CPC localizes to the cleavage furrow and midbody region (Ruchaud et al, 2007).

Survivin, expressed cell cycle-dependently with a maximum in the G2/M-phase (Li *et al.*, 1998), acts as a member of the CPC. During mitosis, the CPC regulates chromosome condensation, correct kinetochore-microtubule attachments as well as activation of the spindle assembly checkpoint. During cytokinesis, it controls the formation and function of the contractile ring which in turn promotes the abscission of the two daughter cells (Carmena *et al.*, 2012). Besides Survivin, the CPC is composed of the proteins INCENP, Borealin and the kinase Aurora B. Survivin's C-terminal α-helix forms a stable three-helical bundle together with similar stretched α-helices of INCENP and Borealin (Jeyaprakash *et al.*, 2007), building the core of the CPC while Aurora B kinase provides the enzymatic activity of the complex (Carmena *et al.*, 2012). During mitosis, the CPC first localizes to centromeres, later to the mitotic spindle midzone and last to the cleavage furrow and midbody region to fulfill its respective functions (Ruchaud *et al.*, 2007).

As part of the CPC, Survivin is responsible for targeting the CPC to the centromeres in early prophase. This is regulated by several means. Survivin's BIR domain for example has been demonstrated to directly bind the N-terminus of T3 phosphorylated histone H3, a specific phosphorylation mark at the inner centromer (Jeyaprakash *et al.*, 2011). Moreover, Survivin's interaction to the export receptor CRM1 has been shown to be important for tethering the CPC to centromeres as well as for CPC functions, but not for its assembly (Knauer *et al.*, 2006). Furthermore, as mentioned above, several PTMs of Survivin contribute to centromere association (ubiquitination at K63) (Vong *et al.*, 2005), accurate chromosome alignment (phosphorylation at S20) (Colnaghi and Wheatley, 2010) as well as CPC localization and stability (phosphorylation at T117) (Wheatley *et al.*, 2004; Wheatley *et al.*, 2007).

Besides its role as a member of the CPC, a distinct pool of Survivin protein is associated with polymerized tubulin and regulates microtubule formation during cell division. It depresses microtubule dynamics, supports their stability and thus the assembly of mitotic spindles (Altieri, 2006; Rosa *et al.*, 2006).

Summarizing, Survivin has a key role in proper cell proliferation, and interference with its expression or function results in mitotic defects including cell cycle arrest, aberrant spindle formation, cytokinesis failure and multinucleated cells (Li *et al.*, 1999; Conte and Altieri, 2006).

1.3.6 Survivin's functional role in further cellular processes

In addition to its dual functional role in apoptosis and proliferation, recent studies hint at other Survivin functions in further cellular processes.

Survivin has been linked to cellular DNA repair processes. Following DNA damage by irradiation, Survivin accumulation in nuclear foci and direct interactions with several

components of the DNA-double-strand break repair machinery was demonstrated. However, the exact molecular mechanisms how Survivin might assist in DNA repair are not completely understood yet (Capalbo *et al.*, 2010; Reichert *et al.*, 2011). Moreover, Survivin has been related to autophagy inhibition (Wang *et al.*, 2011; Wang *et al.*, 2014; Zhang *et al.*, 2015) as well as promotion of angiogenesis (Sanhueza *et al.*, 2015; Li *et al.*, 2016).

1.3.7 Survivin's functional role of homodimerization

Survivin's homodimerization is mediated by its dimer interface (aa 6–10 and 89–102) and post-translationally regulated by acetylation of particularly its C-terminal α-helix. Acetylation of Survivin at K129 was suggested to function as a switch between its monomeric and dimeric state. CBP-mediated acetylation should facilitate Survivins homodimerization while deacetylation by histone deacetylase 6 (HDAC6) favors Survivin's monomeric state (Wang *et al.*, 2010; Riolo *et al.*, 2012). Moreover, mutations in Survivin's dimer interface (F101AL102A) were shown to stabilize Survivin's monomeric state (Engelsma *et al.*, 2007; Pavlyukov *et al.*, 2011). However, regulation of homodimerization as well as the distinct functions of the Survivin monomer and dimer is still not completely understood. Nevertheless, recent studies have demonstrated that both the monomeric as well as the dimeric form of Survivin play distinct roles in critical cellular processes. While only monomeric Survivin has been reported to interact with the other CPC members (Jeyaprakash *et al.*, 2007), with CRM1 for its nuclear export (Engelsma *et al.*, 2007) as well as with Smac/DIABLO and XIAP for preventing caspase-dependent apoptosis (Pavlyukov *et al.*, 2011), dimeric Survivin on the other hand has been reported to stabilize microtubules (Pavlyukov *et al.*, 2011) and to inhibit the signal transducer and activator of transcription 3 (STAT3) transactivation (Wang *et al.*, 2010). In sum, the dimer-monomer balance regulation of Survivin might explain Survivin's functional diversity (Pavlyukov *et al.*, 2011).

1.3.8 Survivin's NES as attractive therapeutic target

Containing a classical leucine-rich NES (^{89}VKKQFEELTL^{98}), Survivin represents a cargo protein of the nuclear export receptor CRM1 (Knauer *et al.*, 2006). Via this NES, Survivin interacts with CRM1 and thus gets exported into the cytoplasm. However, nuclear export is antagonized by Survivin's homodimerization due to the NES overlap with part of the dimer interface (Engelsma *et al.*, 2007). Nevertheless, nuclear export seems to be required to promote Survivin's cytoprotective activity thereby inhibiting apoptosis in the cytoplasm (Knauer *et al.*, 2007b; Knauer *et al.*, 2007c). In addition, Survivin's interaction with CRM1 is

also essential for its targeting and thus CPC targeting to the centromeres in early mitosis thereby sustaining proper cell proliferation (Knauer *et al.*, 2006; Knauer *et al.*, 2007c).

Being responsible for maintaining Survivin's dual role as apoptosis inhibitor and key regulator in mitosis, Survivin's NES represents an attractive therapeutic target especially since Survivin has no enzymatic activity to interfere with. Moreover, preliminary work on a Survivin variant (SurvivinNESmut) containing a NES, in which two critical hydrophobic residues (L96 and L98) are mutated to alanine, indeed demonstrates targeting potential.

The SurvivinNESmut variant, in which the proper function of the NES is inactivated by mutations, shows decreased binding to the export receptor CRM1, and thus an inhibition of nuclear export. In addition, it loses its ability to inhibit caspase-3 activity after cellular apoptosis stimulation and therefore its anti-apoptotic function. Furthermore, SurvivinNESmut does not localize to centromeres properly, thus impairing the correct localization and function of the CPC (Knauer *et al.*, 2007b).

1.4 Aims of the thesis

In addition to conventional chemo- and radiation therapy, targeted cancer therapy provides a promising new approach to fight cancer. This involves addressing specific targets which occur preferentially or exclusively in cancer cells. A major advantage of this approach is the reduction or avoidance of harmful side effects that can occur in chemo- and radiotherapy (Baudino, 2015).

Uncontrolled cell growth, which ultimately leads to carcinogenesis, is normally prevented by a strict regulation of homeostasis between proliferation and apoptosis in healthy cells. In cancer cells this balance is disturbed (Hanahan and Weinberg, 2011). Amongst other things, an overexpression of the protein Survivin in different tumor entities may contribute to such an imbalance. Survivin acts as an inhibitor of apoptosis protein to reduce cell death of tumor cells and thus possesses cytoprotective activity, which leads to an increased resistance to conventional cancer therapies (Li *et al.*, 1998; Knauer *et al.*, 2007b; Knauer *et al.*, 2007c). Moreover, as part of the CPC, Survivin is a mitotic regulator (Li *et al.*, 1998; Knauer *et al.*, 2006; Knauer *et al.*, 2007c). However, the molecular details of this dual biological activity have not been fully elucidated yet. Survivin interacts with the cellular export receptor CRM1 via a highly conserved, leucine-rich NES, which is essential for the cytoprotective activity of Survivin. In addition, the interaction with the nuclear export receptor CRM1 is involved in targeting the CPC to the centromeres of chromosomes in mitosis (Knauer *et al.*, 2006; Knauer *et al.*, 2007c).

Thus, targeted inhibition of the Survivin–CRM1 interaction could not only help to elucidate the distinct biological functions of Survivin at the molecular level in detail but could also

provide a novel approach for targeted cancer therapy. First small molecule inhibitors of the export receptor CRM1 have already been identified (Kudo *et al.*, 1999; Gravina *et al.*, 2014; Hill *et al.*, 2014). Nevertheless, in addition to the inhibition of the Survivin–CRM1 interaction, they supposedly also interfere with the binding of CRM1 to other proteins, making them selective but not specific. However, the hypothesis-driven approach of supramolecular chemistry might bear the potential to now specifically target the Survivin–CRM1 interaction by directly addressing the Survivin protein surface.

Therefore, this work, which is integrated in the Collaborative Research Center (CRC) 1093 "Supramolecular Chemistry on Proteins", aims to investigate whether a signal-specific binding of the NES and thus a specific inhibition of the Survivin–CRM1 interaction can be achieved by supramolecular ligands. Supramolecular tweezers, which target lysine residues within or near the NES, will be developed and characterized in detail with respect to their efficacy using biochemical and cell biological methods. By establishing *in vitro* binding assays, both the binding of the supramolecular tweezer to Survivin's NES and possibly other proteins as well as their influence on the Survivin–CRM1 interaction should be quantitatively assessed. For this purpose, the development of a suitable prokaryotic expression system is required to obtain sufficient amounts of recombinant Survivin and other required proteins. In addition to the *in vitro* analyses, the effect of the supramolecular tweezer should be investigated in a cellular environment. Comprehensive cell-based assays will assess the influence of the inhibition of the Survivin–CRM1 interaction on localization, nuclear export, apoptosis inhibition, dimerization, mitotic function and CPC interactions of Survivin.

2 MATERIALS AND METHODS

2.1 Materials

2.1.1 Chemicals and reagents

The chemicals and reagents used in this work are listed in Table 2.1.

Table 2.1: Used chemicals and reagents.

Chemical / Reagent	Supplier
Acetic acid	Applichem GmbH, Darmstadt
Acrylamide solution (30 %) – Mix 37.5:1	Applichem GmbH, Darmstadt
Agarose	Applichem GmbH, Darmstadt
^{15}N-ammonium chloride	Sigma-Aldrich Chemie Gmbh, Munich
Ammonium persulfate (APS)	Applichem GmbH, Darmstadt
Antibiotic-Antimycotic	Life Technologies GmbH, Darmstadt
Bio-Rad Protein Assay Dye Reagent (5x)	Bio-Rad Laboratories GmbH, Munich
D-Biotin	Applichem GmbH, Darmstadt
Bovine serum albumin (BSA)	Applichem GmbH, Darmstadt
Bromophenol blue sodium salt	Applichem GmbH, Darmstadt
Calcium chloride dihydrate	Applichem GmbH, Darmstadt
Carbenicillin (Carb) disodium salt	Applichem GmbH, Darmstadt
Cobalt (II) chloride hexahydrate	Sigma-Aldrich Chemie Gmbh, Munich
Coomassie Brilliant Blue G-250	Applichem GmbH, Darmstadt
Copper (II) sulfate pentahydrate	Sigma-Aldrich Chemie Gmbh, Munich
Deoxyguanosine triphosphate (dGTP) sodium salt	Peqlab Biotechnologie GmbH, Erlangen
Deoxynucleotide triphosphate (dNTP) Solution Mix	New England BioLabs GmbH, Frankfurt am Main

Chemical / Reagent	Supplier
Dipotassium hydrogen phosphate anhydrous	Applichem GmbH, Darmstadt
Disodium hydrogen phosphate dihydrate	Applichem GmbH, Darmstadt
Disodium hydrogen phosphate heptahydrate	Sigma-Aldrich Chemie Gmbh, Munich
Dithiothreitol (DTT)	Applichem GmbH, Darmstadt
Dulbecco's Modified Eagle Medium (DMEM), high glucose, GlutaMax supplement	Life Technologies GmbH, Darmstadt
Dulbecco's Phosphate-Buffered Saline (DPBS)	Life Technologies GmbH, Darmstadt
Ethylenediaminetetraacetic acid (EDTA) disodium salt dihydrate	Applichem GmbH, Darmstadt
Ethanol	VWR International GmbH, Darmstadt
Ethanol technical grade	Applichem GmbH, Darmstadt
Fetal calf serum (FCS)	Life Technologies GmbH, Darmstadt
Folic acid	Applichem GmbH, Darmstadt
D-Glucose	Applichem GmbH, Darmstadt
L-Glutathione (GSH) reduced	Applichem GmbH, Darmstadt
Glutathione Sepharose 4B beads	GE Healthcare Life Sciences, Freiburg
Glycerol 87 %	Applichem GmbH, Darmstadt
Glycine	Applichem GmbH, Darmstadt
Guanidine hydrochloride	Applichem GmbH, Darmstadt
HCS CellMask™ Deep Red Stain	Life Technologies GmbH, Darmstadt
HDGreen™ Plus	INTAS Science Imaging Instruments GmbH, Göttingen
Hoechst 33342	Applichem GmbH, Darmstadt
Hydrochloric acid 1 M	Applichem GmbH, Darmstadt
Hydrochloric acid 37 %	Applichem GmbH, Darmstadt
Iron (III) chloride hexahydrate	Applichem GmbH, Darmstadt
Isopropanol	Applichem GmbH, Darmstadt

Chemical / Reagent	Supplier
Isopropanol technical grade	Applichem GmbH, Darmstadt
Isopropyl b-D-1-thiogalactopyranoside (IPTG)	Applichem GmbH, Darmstadt
Kanamycin (Kan) sulfate	Applichem GmbH, Darmstadt
Luria-Bertani (LB) agar powder	Applichem GmbH, Darmstadt
LB medium powder	Applichem GmbH, Darmstadt
Lipofectamine 2000	Life Technologies GmbH, Darmstadt
Magnesium chloride hexahydrate	Applichem GmbH, Darmstadt
Manganese sulfate monohydrat	Applichem GmbH, Darmstadt
β-Mercaptoethanol	Applichem GmbH, Darmstadt
Methanol	Applichem GmbH, Darmstadt
Methanol technical grade	Applichem GmbH, Darmstadt
Milk powder	Applichem GmbH, Darmstadt
Nicotinamide	Applichem GmbH, Darmstadt
Normal goat serum	Dako Deutschland GmbH, Hamburg
Nonidet P-40 (NP-40)	Applichem GmbH, Darmstadt
Optimized Minimum Essential Medium (Opti-MEM)	Life Technologies GmbH, Darmstadt
D-Pantothenate calcium salt	Applichem GmbH, Darmstadt
Phenylmethanesulfonylfluoride (PMSF)	Applichem GmbH, Darmstadt
Polyethylenimine (PEI)	Sigma-Aldrich Chemie Gmbh, Munich
Potassium chloride	Applichem GmbH, Darmstadt
Potassium dihydrogen phosphate	Applichem GmbH, Darmstadt
Protease inhibitor cocktail tablets Complete	Roche, Mannheim
Riboflavin	Applichem GmbH, Darmstadt
Roti-Histofix 4 %	Carl Roth GmbH & Co. KG, Karlsruhe
Sodium azide	Applichem GmbH, Darmstadt
Sodium chloride	Carl Roth GmbH & Co. KG, Karlsruhe

Chemical / Reagent	Supplier
Sodium deoxycholate	Applichem GmbH, Darmstadt
Sodium dihydrogen phosphate monohydrate	Carl Roth GmbH & Co. KG, Karlsruhe
Sodium dodecyl sulfate (SDS)	Applichem GmbH, Darmstadt
Sodium hydroxide pellets	Applichem GmbH, Darmstadt
Sodium sulfate anhydrous	Applichem GmbH, Darmstadt
N,N,N',N'-Tetramethylethylenediamine (TEMED)	Applichem GmbH, Darmstadt
Thiamine (Vitamin B1) hydrochloride	Sigma-Aldrich Chemie Gmbh, Munich
Tris(hydroxymethyl)aminomethane (Tris)	Applichem GmbH, Darmstadt
Tris acetate	Applichem GmbH, Darmstadt
Tris hydrochloride (Tris-HCl)	Applichem GmbH, Darmstadt
Triton X-100	Applichem GmbH, Darmstadt
TrypLE Express	Life Technologies GmbH, Darmstadt
Tween 20	Applichem GmbH, Darmstadt
Vitamin B12	Applichem GmbH, Darmstadt
Xylene cyanol	Applichem GmbH, Darmstadt
Zinc sulfate heptahydrate	Applichem GmbH, Darmstadt

2.1.2 Buffers, solutions and media

The buffers, solutions and media used in this work are listed in Table 2.2. Unless otherwise stated, the ingredients were dissolved in ultra-pure Milli-Q H_2O. pH values were adjusted at room temperature (RT). Buffers and solutions were sterile filtrated. Media were autoclaved for sterilization.

Table 2.2: Composition of used buffers, solutions and media.

Buffer / Solution / Medium Ingredients	Final concentration
APS	10 % (w/v)
Calcium chloride	0.1 M
Carbenicillin	100 mg/ml

Buffer / Solution / Medium	Ingredients	Final concentration
CD buffer	Sodium dihydrogen phosphate	20 mM
	Sodium sulfate	20 mM
	Zinc sulfate	10 mM
		pH 7.7
Coomassie destaining solution	Acetic acid	10 % (v/v)
	Ethanol	40 % (v/v)
Coomassie staining solution	Acetic acid	10 % (v/v)
	Ethanol	40 % (v/v)
	Coomassie brilliant blue G250	0.1 % (w/v)
DNA loading dye (10x)	Bromophenol blue	0.25 % (w/v)
	EDTA	100 mM
	Glycerol	20 % (w/v)
	Xylene cyanol	0.25 % (w/v)
DMEM++	Antibiotic-Antimycotic	1x
	FCS	10 % (v/v)
		in DMEM
DTT		1 M
Elution buffer	DTT	1 mM
	L-GSH reduced	10 mM
	Sodium chloride	25 mM
	Tris	50 mM
		pH 8.4
Gel filtration buffer	DTT	1 mM
	Magnesium chloride	2 mM
	Sodium chloride	150 mM
	Tris-HCl	50 mM
		pH 7.4
Guanidine hydrochloride		6 M
Hoechst solution	Ethanol	25 % (v/v)
	Hoechst 33342	1 mg/ml
		in PBS

Buffer / Solution / Medium	Ingredients	Final concentration
IEC buffer A	DTT	1 mM
	Sodium chloride	25 mM
	Tris-HCl	50 mM
		pH 7.5
IEC buffer B	DTT	1 mM
	Sodium chloride	1 M
	Tris-HCl	50 mM
		pH 7.5
IF antibody (Ab) dilution buffer	BSA	1 % (w/v)
	Triton X-100	0.3 % (v/v)
		in PBS
IF blocking buffer	Normal goat serum	5 % (v/v)
	Triton X-100	0.3 % (v/v)
		in PBS
IPTG		1 M
Kanamycin		50 mg/ml
LB agar	LB agar powder	40 g/l
		pH 7.5
LB medium	LB medium powder	25 g/l
		pH 7.5
Lysis buffer	Sodium chloride	150 mM
	Tris-HCl	50 mM
		pH 7.5
M9 minimal medium	Calcium chloride	0.1 mM
	Glucose	22.2 mM
	Magnesium sulfate	2 mM
	^{15}N-ammonium chloride	11.2 mM
	Salts:	
	- Disodium hydrogen phosphate	47.8 mM
	- Potassium dihydrogen phosphate	22 mM
	- Sodium chloride	8.6 mM

Buffer / Solution / Medium	Ingredients	Final concentration
M9 minimal medium	Trace metals:	
	- Calcium chloride	51 µM
	- Cobalt (II) chloride	1.1 µM
	- Copper (II) sulfate	1 µM
	- EDTA	80.6 µM
	- Iron (III) chloride	92.5 µM
	- Manganese sulfate	1.1 µM
	- Zinc sulfate	0.9 µM
	Vitamins:	
	- Biotin	81.9 nM
	- Folic acid	45.3 nM
	- Nicotinamide	409.4 nM
	- Pantothenate	104.9 nM
	- Riboflavin	132.8 nM
	- Thiamine (Vitamin B1)	148.3 nM
	- Vitamin B12	0.7 nM
Magnesium chloride		1 M
NMR buffer	DTT	2 mM
	KPi	50 mM
	Potassium chloride	90 mM
		pH 6.5
Phosphate-buffered saline (PBS)	Disodium hydrogen phosphate	10 mM
	Potassium chloride	2.7 mM
	Potassium dihydrogen phosphate	2 mM
	Sodium chloride	137 mM
		pH 7.4
PEI		10 mM
		pH 6.8
PMSF		0.2 M
		in ethanol

Buffer / Solution / Medium	Ingredients	Final concentration
Potassium phosphate buffer	DTT	2 mM
	KPi	50 mM
	Potassium chloride	150 mM
		pH 7.4
PreScission protease cleavage buffer (PCB)	DTT	1 mM
	EDTA	1 mM
	Sodium chloride	150 mM
	Tris-HCl	25 mM
		pH 7.5
PreScission protease storage buffer	DTT	1 mM
	EDTA	10 mM
	Glycerol	20 % (v/v)
	Sodium chloride	150 mM
	Tris-HCl	50 mM
		pH 8.0
Pull-down blocking buffer	BSA	1 % (w/v)
	DTT	1 mM
	Triton X-100	0.02 % (v/v)
		in PBS pH 7.4
Pull-down buffer	DTT	1 mM
	Triton X-100	0.02 % (v/v)
		in PBS pH 7.4
Radioimmunoprecipitation assay (RIPA) buffer	DTT	1 mM
	EDTA	5 mM
	NP-40	1 % (v/v)
	PMSF	1 mM
	Protease inhibitor cocktail tablet Complete	1x
	Sodium chloride	150 mM
	Sodium deoxycholate	1 % (w/v)
	Tris-HCl	50 mM

Buffer / Solution / Medium	Ingredients	Final concentration
SDS-PAGE running buffer	Glycine	192 mM
	SDS	0.1 % (w/v)
	Tris	25 mM
SDS sample buffer (5x)	Bromophenol blue	0.1 % (w/v)
	EDTA	5 mM
	Glycerol	30 % (v/v)
	β-Mercaptoethanol	7.5 % (v/v)
	SDS	15 % (w/v)
	Tris-HCl	60 mM
		pH 6.8
Separation gel buffer (4x)	SDS	0.8 % (w/v)
	Tris	1.5 M
		pH 8.8
Sodium azide		0.1 % (w/v)
		in PBS
Stacking gel buffer (4x)	SDS	0.8 % (w/v)
	Tris-HCl	0.5 M
		pH 6.8
Tris-acetate-EDTA (TAE) buffer	EDTA	1 mM
	Tris acetate	40 mM
		pH 8.3
Tris-buffered saline (TBS)	Sodium chloride	150 mM
	Tris-HCl	50 mM
		pH 7.4
Tris-buffered saline and Tween 20 (TBST)	Sodium chloride	150 mM
	Tris-HCl	50 mM
	Tween 20	0.1 % (v/v)
		pH 7.4

Buffer / Solution / Medium	Ingredients	Final concentration
Transfer buffer	Glycine	192 mM
	Methanol	20 % (v/v)
	SDS	0.01 % (w/v)
	Tris	25 mM
		pH 8.3
Washing buffer	DTT	1 mM
	Sodium chloride	150 mM
	Tris-HCl	50 mM
		pH 7.5
Western blotting (WB) blocking buffer	Milk powder	5 % (w/v) in TBST

2.1.3 Antibiotics

Antibiotics listed in Table 2.3 were sterile filtrated and added to the respective culture medium immediately before usage.

Table 2.3: Used antibiotics and their final concentrations in the culture media.

Antibiotic	Final concentration
Carbenicillin	100 µg/ml
Kanamycin	50 µg/ml

2.1.4 DNA and protein standards

The DNA and protein standards used in this work are listed in Table 2.4.

Table 2.4: Used protein and DNA standards.

Size standard	Supplier
GeneRuler 1 kb DNA Ladder	Thermo Fisher Scientific, Waltham
GeneRuler 1 kb Plus DNA Ladder	Thermo Fisher Scientific, Waltham
GeneRuler 100 bp DNA Ladder	Thermo Fisher Scientific, Waltham

Size standard	Supplier
Spectra Multicolor Broad Range Protein Ladder	Thermo Fisher Scientific, Waltham

2.1.5 Enzymes and antibodies

The enzymes used in this work are listed in Table 2.5.

Table 2.5: Used enzymes.

Enzyme class	Enzyme	Supplier / Received from
Endonucleases	*Apa*I	New England BioLabs GmbH, Frankfurt am Main
	*Bam*HI-High-Fidelity	New England BioLabs GmbH, Frankfurt am Main
Endonucleases	Deoxyribonuclease (DNase) I	Applichem GmbH, Darmstadt
	*Eco*RI-High-Fidelity	New England BioLabs GmbH, Frankfurt am Main
	*Nhe*I-High-Fidelity	New England BioLabs GmbH, Frankfurt am Main
	*Xba*I	New England BioLabs GmbH, Frankfurt am Main
Proteases	Lysozyme	Applichem GmbH, Darmstadt
	PreScission protease	Knauer group, house production

The listed specific primary (Table 2.6) and secondary antibodies (Table 2.7) were used in this work for protein detection in western blotting (section 2.5.6) and in immunofluorescence staining (section 2.4.3).

Table 2.6: Used primary antibodies.

Antigen	Origin	WB-Dilution	IF-Dilution	Supplier (order number)
CRM1	Mouse monoclonal	1:1000	1:500	Santa Cruz Biotechnology Inc, Heidelberg (sc-74454)

Antigen	Origin	WB-Dilution	IF-Dilution	Supplier (order number)
CRM1	Rabbit polyclonal	1:10000	1:1000	Novus Biologicals Ltd, Cambridge (NB100-79802)
Flag	Mouse monoclonal	-	1:300	Sigma-Aldrich Chemie Gmbh, Munich (F3165)
GST	Mouse monoclonal	1:1000	-	Santa Cruz Biotechnology Inc, Heidelberg (sc-57753)
HA	Mouse monoclonal	-	1:1000	BioLegend Inc, Koblenz (901501)
HA	Rabbit polyclonal	1:10000	-	Abcam PLC, Cambridge (AB9110)
Myc	Mouse monoclonal	1:1000	-	Cell Signaling Technology Europe, Leiden (2276)
Myc	Rabbit polyclonal	-	1:400	Cell Signaling Technology Europe, Leiden (2272)
Ran	Rabbit polyclonal	1:1000	1:500	Novus Biologicals Ltd, Cambridge (NBP1-31776)
RanBP3	Rabbit polyclonal	-	1:500	Novus Biologicals Ltd, Cambridge (NB120-2939)
Survivin	Mouse monoclonal	1:2000	1:100	OriGene Technologies Inc, Herford (TA502236)
Survivin	Rabbit polyclonal	1:1000	1:300	Novus Biologicals Ltd, Cambridge (NB500-201)
α-Tubulin	Mouse monoclonal	-	1:4000	Sigma-Aldrich Chemie Gmbh, Munich (T6074)

Table 2.7: Used secondary antibodies.

Antibody	Origin	WB-Dilution	IF-Dilution	Supplier (PON)
Anti-mouse immuno-globulin G (IgG)-Alexa Fluor (AF) 488	Goat	-	1:1000	Life Technologies GmbH, Darmstadt (A11001)
Anti-mouse IgG-AF568	Goat	-	1:1000	Life Technologies GmbH, Darmstadt (A11004)
Anti-rabbit IgG-AF488	Goat	-	1:1000	Life Technologies GmbH, Darmstadt (A11008)
Anti-rabbit IgG-AF568	Goat	-	1:1000	Life Technologies GmbH, Darmstadt (A11011)
Anti-mouse IgG-horseradish peroxidase (HRP)	Sheep	1:10000	-	GE Healthcare Life Sciences, Freiburg (NXA931)
Anti-rabbit IgG-HRP	Donkey	1:10000	-	GE Healthcare Life Sciences, Freiburg (NA934)

2.1.6 Plasmids and oligonucleotides

The plasmids used in this work are listed in Table 2.8 to Table 2.10. Vector maps of selected plasmids can be found in the appendix (section A.6). Plasmids pEYFP-C1, pEYFP-C1-YFP-CRM1, SRV100 NESmut and SRV100 WT are provided by Rodriguez group of the University of the Basque Country (UPV/EHU) in Spain (García-Santisteban *et al.*, 2016).

Table 2.8: Cloning plasmids used in this work.

Plasmid	Features	Reference
pc3-myc-Survivin142	Eukaryotic expression vector, ampicillin (Amp) R, used for cloning of full-length SurvivinK90/91/103S mutant with N-terminal myc-tag	PhD thesis of Britta Unruhe-Knauf, Knauer group, University of Essen

Plasmid	Features	Reference
pc3-Survivin142-HA	Eukaryotic expression vector, AmpR, used for cloning of CRM1 binding-deficient, full-length SurvivinL96/98A mutant with C-terminal hemagglutinin (HA)-tag	PhD thesis of Britta Unruhe-Knauf, Knauer group, University of Essen
pET41-GST-PreSc-Survivin142	Prokaryotic expression vector, KanR, used for cloning of C-terminally truncated Survivin120 and Survivin120-K90/91/103S mutant, wild type CRM1 and RanQ69L mutant with N-terminal GST-tag and PreScisson protease cleavage site	PhD thesis of Britta Unruhe-Knauf, Knauer group, University of Essen

Table 2.9: Eukaryotic expression plasmids used in this work.

Plasmid	Features	Reference
pc3-Cerulean-Survivin142	Wild type, full-length Survivin, N-terminally fused with Cerulean	Master thesis of Cecilia Vallet, Knauer group, University of Essen
pc3-CRM1-HA	Wild type, full-length CRM1, C-terminally fused with HA	Stauber group, University of Mainz
pc3-myc-Survivin142	Wild type, full-length Survivin, N-terminally fused with myc	PhD thesis of Britta Unruhe-Knauf, Knauer group, University of Essen
pc3-myc-Survivin142-K90/91/103S	Full-length SurvivinK90/91/103S mutant, N-terminally fused with myc	This work
pc3-Survivin142-DIMmut-HA	Dimerization-deficient, full-length SurvivinF101AL102A mutant, C-terminally fused with HA	PhD thesis of Britta Unruhe-Knauf, Knauer group, University of Essen
pc3-Survivin142-HA	Wild type, full-length Survivin, C-terminally fused with HA	PhD thesis of Britta Unruhe-Knauf, Knauer group, University of Essen

Plasmid	Features	Reference
pc3-Survivin142-NESmut-HA	CRM1 binding-deficient, full-length SurvivinL96/98A mutant, C-terminally fused with HA	This work
pEYFP-C1	YFP, empty vector, KanR	Rodriguez group, University of the Basque Country (UPV/EHU), Spain
pEYFP-C1-YFP-CRM1	Wild type, full-length CRM1, N-terminally fused with YFP	Rodriguez group, University of the Basque Country (UPV/EHU), Spain
SRV100 NESmut	CRM1 binding-deficient, NES mutated biosensor, modified pEGFP-N1 vector, KanR	Rodriguez group, University of the Basque Country (UPV/EHU), Spain
SRV100 WT	Wild type biosensor, modified pEGFP-N1 vector, KanR	Rodriguez group, University of the Basque Country (UPV/EHU), Spain

Table 2.10: Prokaryotic expression plasmids used in this work.

Plasmid	Features	Reference
pET41-GST-PreSc-CRM1	Wild type, full-length CRM1, N-terminally fused with GST and PreScisson protease cleavage site	This work
pET41-GST-PreSc-RanQ69L	Full-length RanQ69L mutant, N-terminally fused with GST and PreScisson protease cleavage site	This work
pET41-GST-PreSc-Survivin120	C-terminally truncated Survivin, N-terminally fused with GST and PreScisson protease cleavage site	This work

Plasmid	Features	Reference
pET41-GST-PreSc-Survivin120-K90/91/103S	C-terminally truncated SurvivinK90/91/103S mutant, N-terminally fused with GST and PreScisson protease cleavage site	This work
pET41-GST-PreSc-Survivin142	Wild type, full-length Survivin, N-terminally fused with GST and PreScisson protease cleavage site	PhD thesis of Britta Unruhe-Knauf, Knauer group, University of Essen
pET41-GST-PreSc-Survivin142-DIMmut	Dimerization-deficient, full-length SurvivinF101AL102A mutant, N-terminally fused with GST and PreScisson protease cleavage site	PhD thesis of Britta Unruhe-Knauf, Knauer group, University of Essen
pET41-GST-PreSc-Survivin142-NESmut	CRM1 binding-deficient, full-length SurvivinL96/98A mutant, N-terminally fused with GST and PreScisson protease cleavage site	Master thesis of Cecilia Vallet, Knauer group, University of Essen
pGEX-GST-PreScission protease	PreScission protease, N-terminally fused with GST	Knauer group, University of Essen

The synthetically generated DNA oligonucleotides used in this work for PCR (section 2.2.1) and SOE PCR (section 2.2.2) were purchased from Eurofins Genomics (Ebersberg) and are listed in Table 2.11. They were synthesized in 10 nmol scale, dissolved in Milli-Q H_2O and stored as 100 µM stock solutions at -20 °C. The sequencing primers were either specifically synthesized or provided by the corresponding sequencing company Laboratory of the Government Chemist (LGC) Genomics GmbH (Berlin) and are listed in Table 2.12.

Table 2.11: Primers used for PCR and SOE PCR.

Primer	Sequence (5' → 3')
ApaI_Crm1-1_f	AAAGGGCCCATGCCAGCAATTATG

Primer	Sequence (5' → 3')
ApaI_RanQL_fw	AAAGGGCCCATGGCTGCGCAGGGAG
Apa-Surv_for	AAAGGGCCCGGTGCCCCGACGTTGCCC
Bam_Crm1-1071_r	TTTGGATCCTTAATCACACATTTCTTCTGG
BamHI_RanQL_rev	TTTGGATCCTTACAGGTCATCATCCTCATCCGG
Bam-Surv120_rev	TTTGGATCCTTACTTATTGTTGGTTTCCTTTGC
pc3_seq_fw	GGAGGTCTATATAAGCAGAGCTC
pc3_seq_rev	CAACTAGAAGGCACAGTCGAG
Surv_K90+91S_fw	TCTGTCTCGTCGCAGTTTGAA
Surv_K90+91S_rev	TTCAAACTGCGACGAGACAGA
Surv_K103S_fw	GAATTTTTGTCGCTGGACAGA
Surv_K103S_rev	TCTGTCCAGCGACAAAAATTC

Table 2.12: Used sequencing primers.

Primer	Sequence (5' → 3')
CMV-F	GCAAATGGGCGGTAGGCGT
CRM1SEQFOR	GTCTCTCTGAAGTGCCTCACTGAG
CRM1SEQFOR2	CGCAGGCATTTCGTTCAGGTTCAGG
CRM1SEQREV	CAGCGACCATCTGTGGATCATTGGATCG
pGEX5	GGGCTGGCAAGCCACGTTTGGTG
T7prom	TAATACGACTCACTATAGGG
T7term	GCTAGTTATTGCTCAGCGG

2.1.7 Bacterial strains and eukaryotic cell lines

The bacterial strains used in this work are listed in Table 2.13. *Escherichia coli* (*E. coli*) XL2-Blue were used for plasmid amplification and *E. coli* SoluBL21 were used for heterologous protein expression. The respective bacteria were grown at 37 °C in LB medium or on dishes with LB agar, supplemented with the respective antibiotics (Table 2.3).

Table 2.13: Characteristics of the used bacterial strains.

Bacterial strain	Genotype	Supplier
E. coli XL2-Blue	*endA1 supE44 thi-1 hsdR17 recA1 gyrA96 relA1 lac* [F' *proAB lacI*^{q}*ZΔM15 Tn10* (TetR) Amy CamR]	Agilent Technologies, Waldbronn
E. coli SoluBL21	F^{-} *ompT hsd SB* (rB^{-} mB^{-}) *gal dcm* (DE3) + further uncharacterized mutations	Genlantis, San Diego

The eukaryotic cell lines used in this work are listed in Table 2.14. All cell lines were cultivated in DMEM++.

Table 2.14: Characteristics of the used eukaryotic cell lines.

Cell line	Origin	Growth property	Reference
HEK 293T	*Homo sapiens*, embryonic kidney	adherent	Research resource identifier: CVCL_1926 American type culture collection: CRL-11268
HeLa (Henrietta Lacks) Kyoto	*Homo sapiens*, cervical adenocarcinoma	adherent	Research resource identifier: CVCL_1922

2.1.8 Kits

All kits used in this work are listed in Table 2.15.

Table 2.15: Used kits.

Kit	Supplier
Expand High Fidelity PLUS PCR System	Roche, Mannheim
Gel Filtration low MW Calibration kit	GE Healthcare Life Sciences, Freiburg
NucleoBond Xtra Midi kit	Macherey-Nagel GmbH & Co. KG, Düren
NucleoSpin 8 Plasmid kit	Macherey-Nagel GmbH & Co. KG, Düren
NucleoSpin Gel and PCR Clean-up kit	Macherey-Nagel GmbH & Co. KG, Düren
Pierce ECL Plus Western Blotting Substrate kit	Thermo Fisher Scientific, Waltham

Kit	Supplier
PLA kit Duolink® In Situ Orange Mouse/Rabbit - Duolink® In Situ Detection Reagents Orange - Duolink® In Situ PLA® Probes	Sigma-Aldrich Chemie Gmbh, Munich
TaKaRa DNA ligation kit (version 2.1)	Clontech, Saint-Germain-en-Laye

2.1.9 Consumables

The consumables used in this work are listed in Table 2.16.

Table 2.16: Used consumables.

Item	Supplier
Beaker (different volumes)	VWR International GmbH, Darmstadt
Bottle top vacuum filter (0.45 µm, 250/500 ml)	Sarstedt AG & Co., Nümbrecht
Cell culture dish 10 cm	Sarstedt AG & Co., Nümbrecht
Cell culture flask T-75	Sarstedt AG & Co., Nümbrecht
Cell scraper 25 cm	Sarstedt AG & Co., Nümbrecht
Centricons VivaSpin® 6 (MW cutoff 10/30 kDa)	Sartorius AG, Göttingen
Centricons VivaSpin® 20 (MW cutoff 10/30 kDa)	Sartorius AG, Göttingen
Chromatography column affinity GSTrap 4B column 5 ml	GE Healthcare Life Sciences, Freiburg
Chromatography column anion exchange HiTrap Q HP 5 ml	GE Healthcare Life Sciences, Freiburg
Chromatography column size exclusion HiLoad 26/600 Superdex 75 pg	GE Healthcare Life Sciences, Freiburg
Chromatography column size exclusion Superdex 75 10/300 GL	GE Healthcare Life Sciences, Freiburg
Chromatography column size exclusion Superdex 200 Increase 5/150 GL	GE Healthcare Life Sciences, Freiburg
Cryogenic tubes	Sarstedt AG & Co., Nümbrecht
Erlenmeyer flask 25/50/250/500 ml	DURAN Group GmbH, Wertheim

Item	Supplier
Erlenmeyer flask 1000/2000 ml	VWR International GmbH, Darmstadt
Film Super RX	FUJIFILM Europe GmbH, Düsseldorf
Glass bottom dishes (35 mm)	MatTek Corporation, Ashland (MA)
PCR tubes 0.2 ml	Bio-Rad Laboratories GmbH, Munich
Pipette tip 10/20/200/1250 µl	Sarstedt AG & Co., Nümbrecht
Polyvinylidene difluoride (PVDF) transfer membrane Amersham Hybond P 0.2	GE Healthcare Life Sciences, Freiburg
Quarz glass cuvette (path length 1 mm)	Hellma Analytics, Müllheim
Reaction tubes 1.5/2 ml	Sarstedt AG & Co., Nümbrecht
Reaction tubes 15/50 ml	Sarstedt AG & Co., Nümbrecht
Rotilabo®-Blotting Papers	Carl Roth GmbH & Co. KG, Karlsruhe
Serological pipettes 2/5/10/25 ml	Sarstedt AG & Co., Nümbrecht
µ-Slide 8 well	ibidi GmbH, Planegg
Slide-A-Lyzer™ G2 Dialysis Cassettes (10 kDa, 0.5/3 ml)	Thermo Fisher Scientific, Waltham
Syringe vacuum filter Filtropur S (0.2/0.45 µm)	Sarstedt AG & Co., Nümbrecht
Syringe vacuum filter Minisart® NML (0.8 µm)	Sartorius AG, Göttingen
Ultraviolet (UV) cuvette (10 x 45 mm, 4 ml)	Sarstedt AG & Co., Nümbrecht
UV cuvette semi-micro (10 x 45 mm, 1.6 ml)	Sarstedt AG & Co., Nümbrecht

2.1.10 Laboratory devices

All laboratory devices used in this work are listed in Table 2.17.

Table 2.17: Laboratory instruments and devices.

Laboratory device	Manufacturer
Agarose gel electrophoresis chamber	Peqlab Biotechnologie GmbH, Erlangen
Autoclave vertical LVSA 40/60	Zirbus technology GmbH, Bad Grund

Laboratory device	Manufacturer
BioPhotometer Plus	Eppendorf AG, Hamburg
Calorimeter MicroCal iTC200	Malvern Panalytical GmbH, Kassel
CD spectropolarimeter J-710	Jasco Inc, Easton
Centrifuge Sorvall™ RC 6 Plus	Thermo Fisher Scientific, Waltham
Centrifuge 5417 C/R	Eppendorf AG, Hamburg
Centrifuge Allegra X-22	Beckman Coulter GmbH, Krefeld
Centrifuge ROTINA 380/380 R	Andreas Hettich GmbH & Co. KG, Tuttlingen
Chemistry pumping unit	Vacuubrand GmbH & Co. KG, Wertheim
CO_2 incubator	Binder GmbH, Tuttlingen
CO_2 incubator INC153	Memmert GmbH & Co. KG, Schwabach
Confocal laser scanning microscope (inverse) TCS SP5	Leica Microsystems GmbH, Mannheim
Confocal laser scanning microscope (inverse) TCS SP8	Leica Microsystems GmbH, Mannheim
Epifluorescence microscope (inverse) CKX41	Olympus Europa SE & Co. KG, Hamburg
Film processor Cawomat 2000 IR	CAWO, Schrobenhausen
Freezer (-80 °C) Forma 900S-RIFS	Thermo Fisher Scientific, Waltham
Freezer (-20 °C) Liebherr Premium BioFresh	Liebherr GmbH, Biberach
Gel caster	Bio-Rad Laboratories GmbH, Munich
Gel documentation system E-Box VX2	Vilber Lourmat Deutschland GmbH, Eberhardzell
GrantBio 360° vertical multi-function rotator PTR-30	Grant Instruments Ltd, Cambridge
GrantBio orbital shaking platform POS-300	Grant Instruments Ltd, Cambridge
Heating plate	Gesellschaft für Labortechnik mbH, Burgwedel

Laboratory device	Manufacturer
Heating plate	Medax GmbH & Co. KG, Rendsburg
Liquid chromatography (LC) system ÄKTApurifier	GE Healthcare Life Sciences, Freiburg
Magnetic stirrer Hei-Mix L	Heidolph Instruments GmbH & Co. KG, Schwabach
Magnetic stirrer HI 180	Hanna Instruments Deutschland GmbH, Kehl
Microscope Primo Vert	Carl Zeiss, Oberkochen
Mini centrifuge Spectrafuge	Labnet International Inc, Edison
Multichannel Pipette Plus	Eppendorf AG, Hamburg
NMR spectrometer (700 MHz Ultrashield)	Bruker Corporation, Rheinstetten
Orbital benchtop shaker MaxQ™ 4000	Thermo Fisher Scientific, Waltham
Orbital shaker POS-300	Grant Instruments Ltd, Royston
Orbital tabletop shaker Forma 420 Series	Thermo Fisher Scientific, Waltham
Peristaltic pump P-1	GE Healthcare Life Sciences, Freiburg
Pipettes Research Plus	Eppendorf AG, Hamburg
Pipetting aid Pipetus	Hirschmann Laborgeräte GmbH & Co. KG, Eberstadt
pH meter	Hanna Instruments Deutschland GmbH, Kehl
PAGE chamber Mini-PROTEAN® Tetra Cell	Bio-Rad Laboratories GmbH, Munich
Power supply peqPOWER 300	PEQLAB Biotechnologie GmbH, Erlangen
Power supply PowerPac Basic	Bio-Rad Laboratories GmbH, Munich
Precision balance	Kern & Sohn GmbH, Balingen
Refrigerator Liebherr Comfort	Liebherr GmbH, Biberach
Refrigerator Liebherr Medline	Liebherr GmbH, Biberach
Rotator PTR-30	Grant Instruments Ltd, Royston
Safety cabinet NuAire NU-437-400E	Integra Biosciences GmbH, Fernwald
Safety cabinets HERAsafe	Thermo Fisher Scientific, Waltham

Laboratory device	Manufacturer
Shaker ST5	neoLab Migge Laborbedarf-Vertriebs GmbH, Heidelberg
Spectrophotometer NanoDrop™ 2000c	Thermo Fisher Scientific, Waltham
Tank electro blotter PerfectBlue™	PEQLAB Biotechnologie GmbH, Erlangen
Thermal mixer ThermoMixer Comfort	Eppendorf AG, Hamburg
Thermal mixer MHR 11	HLC BioTech, Bovenden
Thermal printer DPU-414	Seiko Instruments GmbH, Neu-Isenburg
Thermal printer P95D	Mitsubishi Chemical Europe GmbH, Düsseldorf
Thermocycler TProfessional standard gradient 96	Biometra GmbH, Göttingen
Ultrasonic homogenizer mini20	Bandelin electronic GmbH & Co. KG, Berlin
Ultrasonic homogenizer Sonopuls HD 2070	Bandelin electronic GmbH & Co. KG, Berlin
UV Sterilizing PCR Workstation	Peqlab Biotechnologie GmbH, Erlangen
Vacuum removal system AZ 02	HLC BioTech, Bovenden
Vortexer PV-1	Grant Instruments Ltd, Royston
Vortexer Vortex-Genie 2	Scientific Industries, Bohemia
Water bath 1002-1013	Gesellschaft für Labortechnik mbH, Burgwedel
Water purification system Milli-Q® Advantage A10	Merck KGaA, Darmstadt

2.1.11 Software

The software used in this work is listed in Table 2.18.

Table 2.18: Used software.

Software	Manufacturer
Adobe Photoshop CC 2014	Adobe Systems GmbH, Munich

Software	Manufacturer
AFFINImeter for Isothermal Titration Calorimetry	S4SD – AFFINImeter (Campus Vida), Santiago de Compostela
A plasmid Editor (ApE)	Wayne Davis (University of Utah), Salt Lake City
Canvas 11	ACD Systems International Inc., Seattle
Cell Profiler	Carpenter Lab (Broad Institute of Harvard and MIT), Cambridge
Citavi 5	Swiss Academic Software GmbH, Wädenswil
Clustal W (ExPASy)	Swiss Institute of Bioinformatics, Lausanne
FileMaker Pro Advanced	FileMaker, Inc., Santa Clara
Gene Construction Kit 3.0	Textco BioSoftware, Inc., New Hampshire
GraphPad Prism 5	GraphPad Software, Inc., La Jolla
ImageJ	U.S. National Institutes of Health, Bethesda
Jasco Spectra Manager 2.0	Jasco Inc., Easton
Leica Application Suite Advanced Fluorescence (LAS-AF)	Leica Microsystems GmbH, Mannheim
Leica Application Suite X (LAS-X)	Leica Microsystems GmbH, Mannheim
MicroCal iTC200 software	Malvern Panalytical GmbH, Kassel
Microsoft Office	Microsoft Corporation, Redmond
NanoDrop 2000/2000c software	Thermo Fisher Scientific, Waltham
OriginPro	OriginLab Corporation, Northampton
PyMOL	Schrödinger LCC, Portland
SnapGene® Viewer 3.3.4	GSL Biotech LLC, Chigago
TopSpin™ 3	Bruker Corporation, Rheinstetten
Unicorn 5.20	GE Healthcare Life Sciences, Freiburg

2.2 Molecular biological methods

2.2.1 Polymerase chain reaction

The polymerase chain reaction (PCR), which is based on cyclic repetitions of denaturation, annealing and elongation steps, was applied for the amplification of selected DNA fragments (Mullis and Faloona, 1987). First, the double-stranded DNA template denatures at 94 °C. Next, primers specifically anneal onto the template at a temperature which is 2 to 5 °C lower than the melting temperature of the used primers. Finally, the elongation step requires 72 °C as optimal working temperature for the DNA polymerase which amplifies the template using dNTPs. To gain a sufficient amount PCR cycles are repeated 30 to 40 times.

Table 2.19: Composition of a 50 µl PCR reaction mixture.

Reagents	Volume
Buffer 2 (5x)	10.0 µl
Primer 1 (10 µM)	2.0 µl
Primer 2 (10 µM)	2.0 µl
dNTPs (10 mM each)	1.0 µl
DNA polymerase	0.5 µl
DNA template (10 ng/µl)	2.0–10.0 µl
Milli-Q H_2O	Add to 50 µl

Table 2.20: Standard PCR thermal profile.

Step	Temperature	Time	Cycle
Initial denaturation	94 °C	2 min	1x
Denaturation	94 °C	15–30 s	
Annealing	58–68 °C	30 s	30x
Elongation	72 °C	45–75 s	
Final elongation	72 °C	5–10 min	1x

For amplifying the DNA sequences coding for C-terminally truncated Survivin120 and Survivin120-K90/91/103S mutant, CRM1 and RanQ69L, the Expand High Fidelity PLUS PCR System from Roche was used according to the manufacturer's instructions. Table 2.19

summarizes the ingredients of a 50 µl PCR reaction mixture. The standard PCR thermal profile is displayed in Table 2.20. Plasmids usually served as DNA templates and the PCR cycle was repeated 30 times in the Thermocycler TProfessional standard gradient 96 from Biometra.
The efficiencies of the PCR reactions were subsequently analyzed by agarose gel electrophoresis (section 2.2.3).

2.2.2 Splice overlap extension PCR

The splice overlap extension (SOE) PCR is a variant of PCR suitable for introducing specific point mutations at defined sites within a nucleotide sequence e.g. for site-directed mutagenesis (Figure 2.1).

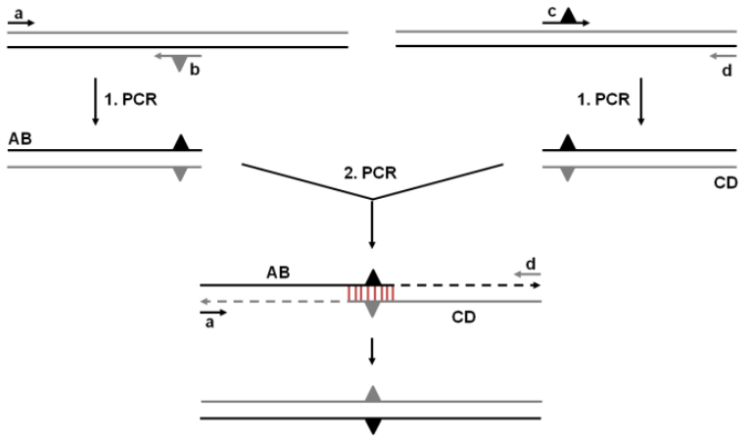

Figure 2.1: Principle of site-directed mutagenesis using the splice overlap extension PCR.

For the two-step PCR a pair of complementary mutagenesis primers bearing the mutation and a primer pair flanking the DNA template are required. In the first SOE PCR, the template is amplified in two reactions each containing one mutagenic and one flanking primer. In the second SOE PCR, both PCR products are allowed to hybridize along their complementary mutagenic region and the whole mutated DNA strand was amplified using both flanking primers.
SOE PCR was performed to introduce the point mutations K90/91/103S into the Survivin coding sequence. Thereby the same reagents and PCR thermal profile as for standard PCR (Table 2.19 and Table 2.20) were used. The efficiencies of the PCR reactions were subsequently analyzed by agarose gel electrophoresis (section 2.2.3).

2.2.3 Agarose gel electrophoresis

DNA fragments were analyzed using agarose gel electrophoresis. Thereby, an agarose gel, consisting of pores whose size depends on the agarose concentration, is placed in an electric field. Negatively charged DNA fragments migrate to the anode and are separated according to their size, since small fragments migrate faster through the pores than large ones. Finally, DNA is visualized by fluorescent DNA-binding dyes.
Agarose gels with 0.5–2 % (w/v) agarose in 40–50 ml TAE buffer were cast upon boiling and after polymerization inserted into an agarose gel electrophoresis chamber from PEQLAB filled with TAE buffer. The gels were supplemented with the DNA-staining dye HDGreen™ Plus from INTAS in 10,000-fold dilution. Before loading the DNA samples on the gel, they were mixed with DNA loading dye (10x) to increase the density and monitor the progress of electrophoresis. The samples were separated together with an appropriate DNA size standard from Thermo Fisher Scientific (section 2.1.4) by applying a constant voltage of 90–100 V for about 45–60 min with the power supply peqPOWER 300 from PEQLAB. Finally, the separated and stained DNA bands were visualized with UV light using the gel documentation system E-Box VX2 from Vilber Lourmat.

2.2.4 Purification of DNA fragments

The NucleoSpin Gel and PCR Clean-up kit from Macherey-Nagel was used according to the manufacturer's instructions to remove disturbing impurities like salts, enzymes and primers from PCR products (sections 2.2.1 and 2.2.2) and to extract DNA fragments from agarose gels (section 2.2.3). During this purification procedure, the DNA was bound to a silica membrane, washed and finally eluted with 20–30 µl Milli-Q H_2O.

2.2.5 Photometric determination of DNA concentration

The concentrations of DNA solutions were determined photometrically using the spectrophotometer NanoDrop™ 2000c from Thermo Fisher Scientific. The absorbance was measured at a wavelength of 260 nm (absorption maximum of nucleic acids). The following ratio was used to calculate the DNA concentration: A solution with a concentration of 50 ng/µl double-stranded DNA has an absorbance of 1 at a wavelength of 260 nm. The advantage of this method is the use of small sample volumes of only 1–2 µl DNA solution per measurement. In addition, absorbance was also measured at wavelengths 230 nm and 280 nm for validation of DNA purity. The A_{260}/A_{280} ratio provides information on protein or RNA contamination and should ideally exhibit values between 1.8 to 2.0 for pure DNA. The

A_{260}/A_{230} ratio informs about contamination with phenol or other organic substances and should ideally exhibit a value of 2.0 for pure DNA.

2.2.6 Restriction and ligation of DNA

Restriction enzymes, purchased from New England BioLabs GmbH (Table 2.5), were used for the restriction of plasmids and PCR products. Recognizing palindromic sites, restriction enzymes, especially those, which belong to type II endonucleases, cut double stranded DNA by hydrolysis of phosphodiester bonds within the DNA backbone yielding in either cohesive or blunt ends. For allowing following proper ligation, plasmids and PCR products must be digested with the same restriction enzymes.

For the preparation of ligatable DNA fragments a preparative restriction mixture with a final volume of 50 µl was composed. 2–10 µg DNA (PCR product or plasmid DNA) were digested with 40 units of the respective restriction enzymes in a buffer recommended by the manufacturer for 1–4 h at adequate temperature (25 °C or 37 °C). To verify successful cloning, plasmids were subjected to an analytical restriction approach with a final reaction mixture volume of 10 µl. 100–500 ng plasmid DNA were digested with 4 units of the respective restriction enzymes in a buffer recommended by the manufacturer for 1 h at 37 °C.

The restriction result was analyzed by agarose gel electrophoresis (section 2.2.3). In the case of preparative digestion, the digested DNA fragments were purified after electrophoresis with the NucleoSpin Gel and PRC-Clean-up kit from Macherey-Nagel (section 2.2.4) to remove all impurities including restriction enzymes and cutoff DNA fragments that could interfere with subsequent DNA ligation. For this purpose, the DNA bands in the agarose gel were detected by UV light, cut out and purified according to the manufacturer's instructions.

In the following ligation process, the digested DNA fragments were joined to form a plasmid by building phosphodiester bonds between adjacent 3'-hydroxy groups and 5'-phosphomonoesters of double stranded DNA molecules. The formation of these bonds was catalyzed by the T4 DNA ligase requiring adenosine triphosphate as cofactor.

Ligation of restricted vector and insert fragments after DNA clean-up was perfomed using the TaKaRa DNA ligation kit (version 2.1) from Clontech, which utilizes the T4 DNA ligase. Therefore, 0.5 µl digested plasmid, 2 µl digested insert and 2.5 µl Solution I of the kit were mixed and incubated for 30 min at RT. In order to control the re-ligation of the linearized plasmid, a second approach, in which the digested insert was exchanged by Milli-Q H_2O, was included and treated analogously. Finally, competent *E. coli* XL2-Blue cells were transformed with the ligated plasmids (section 2.3.3).

2.2.7 DNA sequencing and sequence analysis

In order to reveal undesired mutations in the coding gene sequences, the isolated and purified plasmids (section 2.3.5) were sequenced prior to their further use. Sequencing was carried out by the company LGC Genomics according to the chain-terminating or Sanger method (Sanger *et al.*, 1977). For this purpose, at least 20 µl plasmid DNA solution with a concentration of 60 to 200 ng/µl were sent to LGC Genomics while sequencing primers (Table 2.12) were synthesized or provided.
The alignments of the resulting DNA sequences as well as their translated amino acid sequences obtained from LGC Genomics with the virtual constructs were performed using the cloning software Gene Construction Kit 3.0 from Textco BioSoftware and ApE from Wayne Davis as well as the online alignment tool Clustal W (ExPASy) from the Swiss Institute of Bioinformatics.

2.3 Microbiological methods

2.3.1 Photometric determination of the optical density

In order to analyze the growth progress of bacterial cultures their optical density (OD_{600}) was photometrically determined at a wavelength of 600 nm by using the program “OD600” of the BioPhotometer Plus from Eppendorf. For this purpose, 1 ml cell suspension was transferred to a UV cuvette and measured. Thereby, fresh LB medium or Milli-Q H_2O served as reference.

2.3.2 Preparation of chemically competent *E. coli* cells

Artificial competence of *E. coli* cells used for transformation (section 2.3.3) was induced chemically. An overnight culture consisting of 5 ml LB medium without antibiotics was inoculated with the desired bacterial strain and incubated at 37 °C. The next day, 1 ml of the overnight culture was diluted with 100 ml LB medium and cultured at 37 °C. As soon as an OD_{600} of 0.2–0.4 was reached, the cell suspension was cooled down on ice for 10 min. After centrifugation (4 °C, 4000 rpm, 10 min), the pellet from 100 ml of cell suspension was resuspended in 40 ml of 0.1 M cold and sterile filtered $CaCl_2$ solution and incubated on ice for further 30 min. After another centrifugation step (4 °C, 4000 rpm, 10 min), the pellet from 100 ml of cell suspension was resuspended in 4 ml of 0.1 M cold and sterile filtered $CaCl_2$ solution supplemented with 500 µl cold glycerol. Finally, 50 µl aliquots were shock frozen in liquid nitrogen and stored at -80 °C.

2.3.3 Transformation of competent *E. coli* cells

Transformation describes the genetic alteration of competent bacterial cells by cellular uptake of exogenous plasmid DNA. Incorporation of DNA can be forced either by electroporation or heat shock causing temporary pore appearance in the cell membrane.
For a heat shock transformation, chemically competent *E. coli* cells (XL2 Blue or SoluBL21, Table 2.13) were first thawed on ice. 20–50 µl of the cell suspension were incubated with either 0.2–1 µg purified plasmid DNA or a ligation reaction mixture (section 2.2.6) for 30 min on ice. Next, heat shock was performed for 1 min at 42 °C, immediately followed by a further short incubation on ice for 2 min. After the heat shock, the cells were resuspended in preheated 150–200 µL antibiotic-free LB medium and cultivated for 1–2 h at 37 °C under shaking at 400–500 rpm. Finally, depending on the type of antibiotic resistance defined by the incorporated plasmid, 50–200 µl cell suspension were plated either on LB-Kan or LB-Carb agar plates and incubated overnight at 37 °C.

2.3.4 Long-term storage of transformed *E. coli* cells

For a long-term storage of transformed *E. coli* cells (section 2.3.3), bacterial glycerol stocks were prepared by mixing 800 µl of the respective overnight bacterial culture with 200 µl of sterile 87 % glycerol. The obtained stock solutions were shock frozen in cryogenic tubes in liquid nitrogen and stored at -80 °C.

2.3.5 Isolation of plasmids from *E. coli* cells

In order to isolate plasmid DNA from *E. coli* XL2 Blue cells, which were used for fast and easy DNA amplification, a mini or midi preparation was performed depending on the required DNA amount.
For mini preparations, overnight cultures consisting of 8 ml LB medium with either 100 µg/ml Carb or 50 µg/ml Kan (section 2.1.3) depending on the antibiotic resistance coded on the respective plasmid were inoculated with one colony from a LB agar plate (section 2.3.3) or with a sample from a bacterial glycerol stock (section 2.3.4) and incubated at 37 °C under shaking at 220 rpm in a culture tube. Next day, after centrifugation (RT, 13000 rpm, 5 min) of 6 ml cell suspension the plasmids were isolated from the cell pellets with the NucleoSpin 8 Plasmid kit from Macherey-Nagel according to the manufacturer's instructions. For midi preparations, overnight cultures consisting of 300 ml LB medium with the respective antibiotic were inoculated with 0.5–1 ml of a preculture and incubated at 37 °C under shaking at 120 rpm in a 500 ml Erlenmeyer flask with chicane. Next day, after harvesting the cells by

centrifugation (4 °C, 3900 x g, 15 min), the plasmids were isolated from the cell pellets using the NucleoBond Xtra Midi kit from Macherey-Nagel according to the manufacturer's instructions.

Both kits are based on the principle of alkaline lysis of the bacterial cells (Birnboim and Doly, 1979) in combination with subsequent chromatographic purification. For mini preparations, plasmid DNA was eluted with Milli-Q H_2O from the silica membrane-containing column while for midi preparations plasmid DNA was following elution precipitated with isopropanol, desalted with 70 % ethanol, dried and then dissolved in Milli-Q H_2O. Finally, plasmid purity and concentration were determined photometrically (section 2.2.5).

2.3.6 Heterologous expression of recombinant GST fusion proteins

The heterologous expression of recombinant proteins in *E. coli* enables a fast and high yield protein production. The most commonly used expression system is based on the bacteriophage T7 and consists of an expression vector and a suitable *E. coli* host strain. The expression vector, which is introduced into a T7 expression host strain, carries the gene of interest downstream of the T7 promoter. The chromosomal DNA of the host strain contains the gene coding for the T7 RNA polymerase. Its expression is controlled by the *lac* operon. The addition of an inducer, e.g. IPTG, leads to its binding on the *lac* repressor and thus releasing the *lac* promoter enabling the expression of the T7 RNA polymerase, which in turn binds to the likewise released T7 promoter onto the vector finally causing the expression of the target protein.

Table 2.21: Expression conditions of recombinant GST fusion proteins.

Protein	Temperature	Time
GST-PreScission protease	37 °C	4 h
GST-PreSc-CRM1	30 °C	20 h
GST-PreSc-RanQ69L	30 °C	6 h
GST-PreSc-Survivin120	30 °C	20 h
GST-PreSc-Survivin120-K90/91/103S	30 °C	20 h
GST-PreSc-Survivin142	30 °C	20 h
GST-PreSc-Survivin142-DIMmut (F101AL102A)	30 °C	20 h
GST-PreSc-Survivin142-NESmut (L96/98A)	30 °C	20 h

In this work, the used expression system comprises the *E. coli* SoluBL21 strain as well as the pET41-GST-PreSc and pGEX-GST expression vectors. Initially, *E. coli* SoluBL21 bacteria were transformed with the corresponding plasmids (section 2.3.3). A preculture consisting of 8 ml LB medium with either 100 µg/ml Carb or 50 µg/ml Kan (section 2.1.3) depending on the antibiotic resistance coded on the respective plasmid were inoculated with the transformed bacteria and incubated at 37 °C under shaking at 220 rpm in a culture tube. Next day, a 200 ml culture of fresh LB medium and the respective antibiotic was inoculated with 0.5–1 ml of the preculture and incubated overnight at 37 °C under shaking at 120 rpm in a 500 ml Erlenmeyer flask with chicane. Subsequently, 45 ml of the cell suspension were added to each of the overall four liters main culture of LB medium supplemented with the respective antibiotic. Each liter was cultured in a 2 l Erlenmeyer flask with chicane at 37 °C under shaking at 120 rpm. As soon as an OD_{600} of 0.6–0.8 was reached, protein expression was induced by adding 1 mM IPTG. The following protein expressions were carried out for time periods of 4–20 h at temperatures of 30–37 °C under shaking at 120 rpm depending on the protein of interest (Table 2.21).
Finally, after protein expression, the bacteria from 4 l main culture were harvested by ultracentrifugation (4 °C, 7000 x g, 30 min), resuspended in 40 ml of lysis buffer, shock frozen in liquid nitrogen and stored at -80 °C. Subsequently, the recombinantly produced proteins were isolated from the bacteria and purified (section 2.5.1).

2.4 Cell biological methods

2.4.1 Cultivation of eukaryotic cell lines

Eukaryotic cell lines (Table 2.14) were cultivated at 37 °C and 5 % CO_2 in approximately 90 % relative humidity. Moreover, their cell density was regulated by regular splitting and transferring to new culture vessels where they were continuously supplied with fresh growth medium. In order to prevent contaminations with viruses, bacteria and fungi, cell cultivation was performed under sterile conditions.
The eukaryotic adherent cell lines used in this work (HeLa Kyoto and 293T, Table 2.14) were cultivated in T-75 cell culture flasks in 10 ml growth medium DMEM++. When reaching a confluency of about 70 to 90 %, cells were split. After aspirating old growth medium, the cell layer was carefully washed with 5 ml DPBS from Life Technologies to completely remove enzyme-inhibiting FCS. Next, 2 ml TrypLE Express from Life Technologies, which cleaves the adhesion proteins on the cell surface, were added and cells were incubated on a heating plate until they were detached. Finally, 8 ml prewarmed DMEM++ were added, the cells were resuspended and diluted in a ratio of 1:10 to 1:20 with fresh medium up to a total volume of

10 ml in a new T-75 cell culture flask. When different dishes or flasks were used, the noted volumes of cell suspension and medium were adjusted accordingly.

2.4.2 Transient transfection of eukaryotic cells

Transient transfection describes the temporal introduction of plasmid DNA into eukaryotic cells. In order to be transcribed, DNA must be transported through the cell membrane to enter the cell and subsequently the nucleus. This can be achieved by different transfection methods. Transfection can be performed by electroporation, via nanoparticles or chemically by using cationic polymers like PEI or liposomal transfection reagents like Lipofectamine 2000 from Life Technologies. While PEI forms complexes with negatively charged DNA, which are taken up via endocytosis, Lipofectamine 2000 forms liposomes capturing DNA, which allow fusion with the cell membrane.

293T cells were transfected with PEI enabling the production of cell lysates with overexpressed proteins of interest. For this purpose, 1 ml 293T cell suspension produced during cell passage was diluted with 9 ml DMEM++ and plated on a 10 cm cell culture dish. Incubation was performed at 37 °C and 5 % CO_2. After 24 h, solution A, composed of 240 µl DPBS from Life Technologies and 40 µl 10 mM PEI (pH 6.8), and solution B, composed of 240 µl DPBS from Life Technologies and 8 µg of the desired plasmid DNA, were mixed, centrifuged and incubated for 5 min at RT. Subsequently, the transfection mixture was applied drop-wise to the cells which were incubated for further 24 h at 37 °C and 5 % CO_2.

HeLa Kyoto cells were plated in either 8 well µ-slides from ibidi or 35 mm glass bottom dishes from MatTek and transfected with Lipofectamine 2000 from Life Technologies enabling microscopic analyses. For the transfection of one well, 10 µl or 300 µl HeLa Kyoto cell suspension produced during cell passage were diluted with 200 µl or 2 ml DMEM++, seeded and incubated at 37 °C and 5 % CO_2. 24 h later, transfection solution A, composed of 12.5 µl or 100 µl Opti-MEM from Life Technologies and 0.2 µl or 3 µl Lipofectamine 2000 from Life Technologies, and solution B, composed of 12.5 µl or 100 µl Opti-MEM from Life Technologies and 100–400 ng or 1 µg of the desired plasmid DNA, were mixed, centrifuged and incubated for 5 min at RT. Subsequently, the transfection mixture was applied drop-wise to the cells which were incubated for further 24 h at 37 °C and 5 % CO_2.

2.4.3 Immunofluorescence staining

Immunofluorescence (IF) staining is performed to label endogenous or exogenous proteins within cells with fluorescence dyes in order to allow the analysis of their cellular localization and distribution by fluorescence microscopy. The method is based on the specific antigen-

antibody recognition. In this work, indirect immunofluorescence was applied by using a specific primary antibody against the protein of interest and a secondary antibody conjugated with a fluorophore recognizing the primary antibody.
The medium of the cells seeded in one well of the 8 well µ-slides was aspirated, and the cells were once washed with 200 µl PBS before fixed with 200 µl 4 % Roti-Histofix from Carl Roth for 15–20 min at RT. After washing the cells two times with PBS, they were incubated in 200 µl IF blocking buffer for 1 h at RT. Subsequently, the cells were incubated overnight at 4 °C in 100 µl primary antibody solution, which was prepared by diluting primary antibody in IF antibody dilution buffer according to Table 2.6. Next day, after washing the cells two times with PBS, 100 µl of the secondary antibody solution, consisting of fluorophore-conjugated secondary antibody diluted in IF antibody dilution buffer according to Table 2.7 and 1 µg/ml of the DNA staining dye Hoechst 33342, were applied for 1 h at RT in the dark. After removing excessive staining solution by washing the cells two times with PBS, they were stored in PBS containing 0.1 % (w/v) sodium azide at 4 °C in the dark until they were analyzed microscopically (section 2.4.7). In case of staining two different proteins, primary antibodies derived from different origins were used.

2.4.4 Proximity ligation assay

The proximity ligation assay (PLA) is a technology enabling the detecting of protein interactions in fixed cell samples. Detection is based on using two protein-recognizing primary antibodies derived from different origins on which species-specific secondary antibodies (PLA probes) bearing a unique short DNA strand can bind. In close proximity (<40 nm), both DNA strands can bind and are ligated to form a complete DNA circle after adding additional connector oligos. Subsequent DNA rolling circle amplification generates a fluorescent signal by incorporating labelled complementary oligonucleotide probes. This PLA signal can be microscopically visualized as individual fluorescent cellular foci. Therefore, protein interactions and complex formation can be quantified and assigned to a specific subcellular localization. Analysis of the endogenous Survivin–CRM1 interaction using the Duolink® PLA technology from Sigma-Aldrich was performed in cooperation with Cecilia Vallet from the Department of Molecular Biology II (Knauer group, University of Essen).
300 µl HeLa Kyoto cell suspension produced during cell passage were diluted with 2 ml DMEM++, seeded in 35 mm glass bottom dishes from MatTek and incubated at 37 °C and 5 % CO_2. 24 h later, cells were fixed, and immunostained (section 2.4.3) with primary antibody specific for the proteins Survivin (derived from rabbit) and CRM1 (derived from mouse). Immunofluorescence staining procedure was stopped at this step, in order to continue with the PLA protocol. The Duolink® In Situ Orange Starter Kit Mouse/Rabbit with

Duolink® In Situ PLA® Probes and Detection Reagents from Sigma-Aldrich was used following the manufacturer's instructions. DNA was stained with 1 µg/ml Hoechst 33342 in PBS for 15 min at RT in the dark and entire cells were stained with 2 µg/ml HCS CellMask™ Deep Red Stain from Life Technologies in PBS for 15 min at RT in the dark. Finally, cells were washed twice with PBS and covered with a PBS solution containing 0.1 % sodium azide.

Fluorescence imaging of nuclei (405 nm), PLA foci (561 nm) and cell mask (633 nm) was performed using a confocal laser scanning microscope TCS SP8 from Leica Microsystems equipped with an HCX PL Apo CS 63.0 × 1.20 water UV objective, a sensitive hybrid detector and Diode 405, Argon and diode-pumped solid-state (DPSS) 561 lasers (section 2.4.7). Quantitative image analysis was performed by Dr. Nina Schulze (ICCE, University of Duisburg-Essen) using Cell Profiler (Carpenter *et al.*, 2006; Kamentsky *et al.*, 2011). Hoechst-stained nuclei were defined as primary objects. Cell mask was used to define the entire cells as secondary objects. PLA foci within the respective cells were detected and assigned to the parental cells. Cells, which were partly out of the field of view, were not included into the analysis.

2.4.5 SRV100 biosensor assay

The SRV100 biosensor assay, adopted from literature (García-Santisteban *et al.*, 2016), is a method which enables investigation of export receptor CRM1's nuclear export activity in a cellular system.

In the biosensor assay 293T cells were used for microscopic analyses. 24 h before transfection, 20 µl 293T cell suspension produced during cell passage were diluted with 200 µl DMEM++, seeded per well of the 8 well µ-slides from ibidi and incubated at 37 °C and 5 % CO_2. Transient transfection was carried out using PEI transfection protocol (section 2.4.2). Transfection solution A, composed of 10 µl DPBS from Life Technologies and 1 µl 10 mM PEI (pH 6.8), and solution B, composed of 10 µl DPBS from Life Technologies and 300 ng of each plasmid DNA (provided by (García-Santisteban *et al.*, 2016)), were mixed, centrifuged and incubated for 5 min at RT. Subsequently, the transfection mixture was applied drop-wise to the cells which were incubated for further 24 h at 37 °C and 5 % CO_2. Thereby, plasmid DNA coding for SRV100 WT and NESmut were applied in combination with plasmid DNA coding for yellow fluorescent protein (YFP) or YFP-CRM1. 24 h later, immunofluorescence staining (section 2.4.3) of the biosensor's Flag-tag with primary anti-Flag antibody (Table 2.6) and secondary anti-mouse IgG-AF568 antibody (Table 2.7) was performed including DNA staining with Hoechst 33342. Biosensor assay was analyzed

microscopically by confocal fluorescence imaging of nuclei (405 nm), YFP/YFP-CRM1 (488 nm) and SRV100 biosensor (561 nm) (section 2.4.7).
Quantitative image analysis was performed by Dr. Nina Schulze (ICCE, University of Duisburg-Essen) using Cell Profiler (Carpenter *et al.*, 2006; Kamentsky *et al.*, 2011). Nuclei (primary objects) and cell areas (secondary objects) were defined by Hoechst staining and YFP intensity, respectively. Transfected cells were then filtered by the YFP intensity adapting a threshold of 0.07 AU. Next, SRV100 intensity in the cytoplasm as well as in the nucleus was measured only in previous filtered transfected cells. Subsequently, the nuclear/cytoplasmic intensity ratio of SRV100 was calculated of each cell. At least 450 cells were counted per sample.

2.4.6 Treatment of eukaryotic cells with TAMRA-coupled tweezer

In order to analyze the cellular uptake of molecular tweezers, eukaryotic cell treatment with a basic tweezer molecule linked to the fluorophore 5-carboxytetramethylrhodamine (TAMRA) was performed in cooperation with Cecilia Vallet from the Department of Molecular Biology II (Knauer group, University of Essen).
300 µl HeLa Kyoto cell suspension produced during cell passage were diluted with 2 ml DMEM++, seeded in 35 mm glass bottom dishes from MatTek and incubated at 37 °C and 5 % CO_2. 24 h later, cells were transiently transfected with 1 µg expression vector encoding Cerulean-Survivin142 (section 2.4.2). 6–8 h later, TAMRA-coupled tweezer in a final concentration of 10 µM was applied drop-wise to the cells which were incubated for further 20 h at 37 °C and 5 % CO_2. Live fluorescence imaging of Cerulean-Survivin142 (458 nm) and TAMRA-coupled tweezer (561 nm) was performed using confocal microscopy (section 2.4.7).

2.4.7 Confocal fluorescence microscopy

Fluorescence microscopy is based on the property of a fluorophore to enter an excited state when it absorbs light of a distinct wavelength and emits light of a longer wavelength after a short time when returning to the ground state. In this work, confocal microscopy is used to only excite one small focal volume within the cell, which is achieved by two pinholes within the light path, and subsequently to detect the emitted fluorescence. Thereby, the contrast and the optical resolution are increased compared to conventional fluorescence microscopy.
Confocal fluorescence microscopy was conducted using either the laser scanning microscope TCS SP5 or SP8 from Leica Microsystems equipped with four lasers (Argon, wavelength 458/476/488/496/514 nm; DPSS, 561 nm; HeliumNeon, 633 nm; Diode,

405 nm), various detectors (2x confocal detector img and 1x sensitive imaging hybrid detector) and controlled by the visualization softwares Leica Application Suite Advanced Fluorescence (LAS-AF) for SP5 and Leica Application Suite X (LAS X) for SP8 from Leica Microsystems. For image acquisition, the objective HCX PL APO CS 63.0 x 1.20 WATER was used. The samples were imaged by sequential scans at excitation wavelengths of 405 nm (Hoechst 33342), 458 nm (Cerulean), 488 nm (AF488 or YFP), 561 nm (AF568, PLA foci or TAMRA) and 633 nm (cell mask) with a scan speed of 200 Hz and a resolution of 1024 x 1024 pixels.

2.5 Biochemical methods

2.5.1 Purification of recombinant GST fusion proteins

This method is used to isolate and purify recombinant GST fusion proteins from bacterial lysates. Cleaning is performed in several steps including bacterial cell lysis, affinity chromatography and subsequent ion exchange chromatography. Depending on further protein application, the fused GST-tag is either removed by proteolytical cleavage or not during purification procedure.

2.5.1.1 Bacterial cell lysis

In order to obtain heterologously expressed intracellular proteins, cell disruption, hence the cell wall destruction of *E. coli* cells, must be carried out. There are various mechanical and non-mechanical cell disruption methods. In this work, a combination of enzymatic cell lysis using lysozyme and mechanical ultrasonication was performed.
Heterologous expression of recombinant GST fusion proteins in *E. coli* SoluBL21 was performed and cells of 4 l main culture were pelleted, resuspended in 40 ml lysis buffer and stored at -80 °C (section 2.3.6). After thawing 40 ml cell suspension on ice, 40 µl 1 M DTT in a final concentration of 1 mM and 200 µl 0.2 M PMSF in a final concentration of 1 mM were added and the cell suspension was incubated on ice for 10 min. Thereby, DTT functions as reducing agent preventing undesirable oxidation of cysteine residues while PMSF is a protease inhibitor. Next, 400 µl of 50 mg/ml lysozyme were added and the suspension was incubated on ice for further 20 min. Lysozyme is a hydrolase which causes lysis of the cell wall of bacteria by hydrolysis of the ß-glycosidic bond between the C1 atom of N-acetyl-muramic acid and the C4 atom of N-acetyl-glucosamine, both components of the bacterial cell wall. Afterwards, 200 µl of 10 mg/ml DNase I as well as 200 µl of 1 M $MgCl_2$ were added and the lysate was transferred to a 50 ml beaker placed on ice. As endonuclease, DNase I

hydrolyses the phosphodiester bound of bacterial DNA requiring bivalent cations provided by $MgCl_2$. In the following, complete disruption of the cells and DNA shearing was achieved by ultrasonication with the ultrasonic homogenizer Sonopuls HD 2070 and the ultrasonic probe KE76 from Bandelin electronic. Cell suspension underwent three short pulses of sonication (10 s each, 60 % intensity) and four to six long pulses of sonication (30 s each, 60 % intensity) on ice with intervals of 1 min to avoid excessive heat. Cell fragments and insoluble proteins were pelleted by centrifugation (3900 x g, 1 h, 4 °C) and the supernatant was filtered through a 0.8 µm filter into a new 50 ml reaction tube. 10 µl SDS samples of total lysate and supernatant were taken, diluted with 20 µl washing buffer, mixed with 5x SDS sample buffer and denatured at 95 °C for 10 min for further analysis by SDS-PAGE (section 2.5.4).

2.5.1.2 Affinity chromatography

This step serves to isolate the recombinant GST fused proteins from the total bacterial lysate. Due to the high affinity of glutathione-S-transferase (GST) for its substrate glutathione (GSH), the GST-tag is used to isolate GST fusion proteins via a glutathione-containing matrix (glutathione Sepharose) of a GSTrap 4B column (5 ml) from GE Healthcare.

All working steps during affinity chromatography were carried out at 4 °C. In a preliminary step, the affinity column was equilibrated using the peristaltic pump P-1 from GE Healthcare. The column was equilibrated with 15 ml Milli-Q H_2O followed by 25 ml washing buffer at a flow rate of 1–1.5 ml/min (pump stage 2–3).

After equilibration, the entire supernatant, containing the recombinant GST fusion protein of interest, was loaded onto the column at a flow rate of < 0.5 ml/min (pump stage 0.5). The slow flow rate increases the effective protein binding to the GSH matrix because of the slow kinetics of the binding. The flow through was collected and the column was subsequently washed twice with 25 ml washing buffer and once with 25 ml IEC buffer A at a flow rate of 1–1.5 ml/min (pump stage 2–3). 10 µl SDS sample of flow through diluted with 20 µl washing buffer and 30 µl SDS samples of all washing steps were taken, mixed with 5x SDS sample buffer and denatured at 95 °C for 10 min for further analysis by SDS-PAGE (section 2.5.4).

The bound GST fusion proteins can then either be eluted competitively from the GSH-column by adding reduced glutathione or, in case of GST removal, the tag-free proteins can be eluted by proteolytical cleavage (section 2.5.1.3) before directly proceeding with ion exchange chromatography (section 2.5.1.4).

After complete elution of the protein of interest, the GSTrap 4B column from GE Healthcare was regenerated before storage. Therefore, the column was first washed with 25 ml elution buffer, followed by 10 ml Milli-Q H_2O and 10 ml 6 M guanidine hydrochloride, which denatures the residual protein and thus removes it from the column. The pH value of 7.4 was

restored with 25 ml PBS and after another washing step with 20 ml Milli-Q H_2O to remove the salt, the column was finally loaded with 20 % ethanol and stored at 4 °C.

2.5.1.3 GST removal by proteolytical cleavage of fusion proteins

Depending on further protein application, the fused GST-tag was removed by proteolytical cleavage by PreScission protease during purification procedure. PreScission protease is a fusion protein of human rhinovirus 3C protease and GST. The pET41-GST-PreSc vector used to express the recombinant GST fusion proteins contains a PreScission protease cleavage site between GST and the protein of interest, so that PreScission protease is able to specifically cleave between the residues Q and G of its recognition sequence (LEVLFQ / GP) releasing the GST-free protein. Cleavage was performed directly on column. Due to its own GST-tag, PreScission protease remains bound to the column and does not contaminate the cleaved and released GST-free protein.
For GST-removal, the last washing step with 25 ml IEC buffer A (section 2.5.1.2) was replaced by a washing step with 40 ml PCB. Subsequently, a PreScission protease mix, consisting of 5 ml PCB and 50 µl PreScission protease (20 mg/ml), was loaded onto the column at a flow rate of < 0.5 ml/min (pump stage 0.5). Proteolytical digestion occurred during overnight incubation at 4 °C.
30 µl SDS samples of washing step with PCB and loading step of PreScission protease mix were taken, mixed with 5x SDS sample buffer and denatured at 95 °C for 10 min for further analysis by SDS-PAGE (section 2.5.4).

2.5.1.4 Ion exchange chromatography

As a further purification step, ion exchange chromatography was directly performed after affinity chromatography. Ion exchange chromatography (IEC) separates proteins according to their different charges. Separation of protein mixtures is achieved by electrostatic interaction between the proteins and an oppositely charged matrix. The strength of this interaction is determined by various parameters (pH, ionic strength, isoelectric point of the protein, charge density of the matrix or protein surface). Elution of the target protein can therefore be achieved by changing the pH value or increasing the ionic strength of the elution buffer. IEC of the proteins was performed at 4 °C using the HiTrap Q HP anion exchange column (5 ml) and the ÄKTApurifier system controlled by the Unicorn 5.20 control software from GE Healthcare. Due to the positive charges of the anion exchange material, negatively charged proteins are bound more strongly than positively charged proteins and elute later as the salt concentration gradient increases.

After loading and washing the supernatant (section 2.5.1.2), the GSTrap 4B affinity column from GE Healthcare was placed on top of the HiTrap Q HP anion exchange column from GE Healthcare also equilibrated with 15 ml Milli-Q H_2O and 10 ml IEC buffer A at a flow rate of 1–1.5 ml/min (pump stage 2–3). The connected columns were washed with another 20 ml IEC buffer A. The recombinant GST fusion protein was then competitively eluted from the GSTrap 4B onto the HiTrap Q HP column with 50 ml elution buffer supplemented with reduced glutathione followed by another washing step with 10 ml IEC buffer A. For proteins, whose GST-tag was removed overnight, the transfer of the protein to the HiTrap Q HP anion exchange column occurs via a second GSTrap 4B column which was also equilibrated with Milli-Q H_2O and IEC buffer A and mounted between both other columns. The recombinant GST-free protein was then rinsed from the first GSTrap 4B via the second one onto the HiTrap Q HP column with 70 ml IEC buffer A. Thereby, the intermediary affinity column restrained excessive GST fused PreScission protease as well as uncut proteins, which were not bound by the first affinity column, and hence prevented undesirable contaminations. 30 µl SDS samples of elution and washing steps were taken, mixed with 5x SDS sample buffer and denatured at 95 °C for 10 min for further analysis by SDS-PAGE (section 2.5.4).

Finally, the columns were separated again, and the HiTrap Q HP anion exchange column loaded with the protein of interest was subsequently connected under 0.3 MPa pressure limit at 1 ml/min to the previously equilibrated ÄKTApurifier system from GE Healthcare. For this purpose, the system was rinsed with 20 ml Milli-Q H_2O followed by 10 ml IEC buffer B as well as subsequent 10 ml IEC buffer A at a flow rate of 5 ml/min. The fraction collector of the ÄKTApurifier was filled with 45x 2 ml reaction tubes to collect the individual protein-containing fractions. The elution of the protein was performed with a saved program. The first 10 ml IEC buffer A (25 mM NaCl) were rinsed at a flow rate of 2 ml/min. Afterwards, using IEC buffer A and B, a salt concentration gradient of 25–1000 mM NaCl (0–100 % B) over 15 column volumes (75 ml) at a flow rate of 1.5 ml/min and a pressure limit of 0.3 MPa was applied for elution of the proteins, which were collected in 2 ml fractions. The protein elution was detected by absorbance at 280 nm. After completion of the program, the ÄKTA system and anion exchange column were regenerated under 0.3 MPa pressure limit at 2 ml/min using 20 ml of following solutions respectively, Milli-Q H_2O, 1 M NaOH, Milli-Q H_2O and 20 % ethanol. The HiTrap Q HP column was finally disconnected under 0.3 MPa pressure limit at 1 ml/min and stored at 4 °C.

The collected protein-containing fractions were further analyzed by SDS-PAGE (section 2.5.4) in order to determine the fractions with the most protein amount and the least impurities. For this purpose, 10 µl fraction sample were taken, mixed with 5x SDS sample buffer and denatured at 95 °C for 10 min.

2.5.1.5 Concentration and dialysis of protein solutions

The collected fractions with the highest eluted protein amount and the lowest impurification were combined and the protein solution was concentrated with VivaSpin® centricons from Sartorius with a 10 or 30 kDa cutoff depending on the molecular size of the protein. The centricons were equilibrated with washing buffer by centrifugation (3000 x g, 10 min, 4 °C). Subsequently, the protein solution was concentrated by applying several rounds of centrifugation steps (3000 x g, 10 min, 4 °C) until a final volume of approximately 0.5–1 ml was achieved. 5 µl SDS samples of the final purified protein were taken, diluted with 25 µl washing buffer, mixed with 5x SDS sample buffer and denatured at 95 °C for 10 min for further analysis by SDS-PAGE (section 2.5.4). After determination of the protein concentration (section 2.5.3), 50 µl protein aliquots were shock frozen in liquid nitrogen and stored at -80 °C.

Dialysis of proteins enables the replacement of protein buffer systems. For buffer exchange, the protein solution was transferred to a Slide-A-Lyzer™ G2 cassette from Thermo Fisher Scientific with a 10 kDa molecular weight cutoff and dialyzed overnight at 4 °C against at least 1 l dialysis buffer of choice under gentle stirring. Buffer exchange was e.g. necessary for long-time storage of the purified PreScission protease (PreScission protease storage buffer) or for ITC measurements (PBS) (section 2.5.9).

2.5.2 Preparation of whole cell lysates from eukaryotic cells

Whole cell lysates were prepared with a modified RIPA buffer containing different detergents like NP-40 and sodium deoxycholate to chemically lyse the eukaryotic cells. In order to prepare 293T cell lysates with overexpressed proteins of interest, the 10 cm cell culture dishes with the grown cells after transient transfection (section 2.4.2) were placed on ice for 5 min. Then, the cells were detached with a cell scraper and transferred to a 15 ml reaction tube. Cells were pelleted by centrifugation (500 x g, 5 min, 4 °C), resuspended in 1 ml cold PBS and transferred to a 1.5 ml reaction tube. After further centrifugation (500 x g, 5 min, 4 °C), the cells were lyzed by resuspending the cell pellet in 100–150 µl RIPA buffer followed by a 15 min incubation on ice. Subsequently, the cell lysate was sonicated (15 s at 90 % intensity) using the Sonopuls mini20 device with the ultrasonic probe MS 1.5 from Bandelin to shear the DNA content. Cell debris was removed by centrifugation (20000 x g, 20 min, 4 °C) and the supernatant was transferred into a new 1.5 ml reaction tube. The protein concentration was determined using the colorimetric Bradford assay (section 2.5.3). Finally, 50 µl aliquots of whole 293T cell lysate were shock frozen in liquid nitrogen and stored at -80 °C before they were used in pull-down assays (section 2.5.11).

2.5.3 Photometric determination of protein concentration

There are several methods to determine the protein concentration. In this work, the concentration of single purified proteins was quantified by measurement of the absorbance at 280 nm, while the colorimetric Bradford assay was used to determine the protein concentration of whole cell lysates.

The measurement of the absorbance at 280 nm depends on the presence of the aromatic amino acids tryptophan and tyrosine which absorb at 280 nm. Moreover, proteins absorb at 260 nm due to amino acid phenylalanine and additionally at 210 nm due to the peptide bonds. Lambert-Beer's law (Beer, 1852) is used to determine the concentration, which predicts a linear dependence of the absorbance of a protein towards its concentration in diluted solutions.

$$A_\lambda = lg\left(\frac{I_0}{I}\right) = \epsilon_\lambda \cdot c \cdot l \qquad (2.1)$$

Within this equation, A_λ is the absorbance at wavelength λ, lg is the decadic logarithm, I_0 is the intensity of the incident light, I is the intensity of the transmitted light, ϵ_λ is the molar extinction coefficient, c is the concentration and l is the path length. Protein concentration was determined with the spectrophotometer NanoDrop™ 2000c from Thermo Fisher Scientific. The respective extinction coefficient as well as the corresponding molecular weight of the protein were entered, thus taken them into account for the concentration calculation. After measuring the respective buffer as reference, only 2 µl purified protein sample solution were necessary for one measurement.

The colorimetric Bradford assay is based on the binding of the anionic triphenylmethane dye Coomassie brilliant blue G-250 to proteins under acidic conditions causing a shift in its absorption maximum from 470 nm in the unbound to 595 nm in the protein bound state. For concentration determination, 1 µl of sample lysate or 1 µl RIPA buffer as blank was diluted in 800 µl PBS and mixed with 200 µl of the 5x concentrated Bio-Rad Protein Assay Dye Reagent from Bio-Rad Laboratories in a disposable cuvette by vortexing. After incubating the mixture for 5 min at RT, the absorbance at a wavelength of 595 nm was measured using the “BRADFORD micro” program of the BioPhotometer Plus from Eppendorf. The protein concentration was determined by comparing the samples with a saved standard calibration curve of defined BSA concentrations (1–25 µg/ml).

2.5.4 SDS-polyacrylamide gel electrophoresis

SDS-polyacrylamide gel electrophoresis (PAGE) is a method for separating proteins according to their size within an electric field. Thereby, electrophoretic mobility towards the anode is mediated by the amount of negatively charged SDS detergent molecules disrupting proteins' two- and three-dimensional structures and binding to the resulting denatured and linearized polypeptide chain (Laemmli, 1970). These so received negative charges are approximately proportional to the molecular protein mass enabling the molecular size separation of proteins. In general, small proteins migrate faster through the gel than large proteins and separation properties are further depending on the gel's pore size determined by acrylamide concentration. The common use of a discontinuous system consisting of a stacking and a separation gel leads to the formation of distinct protein bands.
SDS-PAGE was used to analyze the protein samples taken during protein purification and pull-down assays. The protein samples were mixed with 5x SDS sample buffer and denatured at 95 °C for 5–10 min before gel application. Protein separation was performed in a discontinuous SDS polyacrylamide gel with a thickness of 1 mm consisting of a 4 % stacking gel and a 12.5 % separation gel (Table 2.22) using the vertical PAGE chamber Mini-PROTEAN® Tetra Cell from BioRad Laboratories.

Table 2.22: Composition of SDS-polyacrylamide gels with a thickness of 1 mm.

Components	12.5 % separation gel	4 % stacking gel
Milli-Q H_2O [ml]	1.6	2.5
4x Separation gel buffer [ml]	1.3	-
4x Stacking gel buffer [ml]	-	1.3
30 % Acrylamide solution [ml]	2.1	0.65
10 % APS [µl]	50	50
TEMED [µl]	5	5

After mixing all components, the separation gel was cast in a casting chamber. To generate a straight barrier between both gels, a layer of isopropanol was added on top of the freshly casted separation gel. After polymerization, the stacking gel was poured on top and a comb to generate wells was inserted. After polymerization, the gel was transferred to a vertical electrophoresis chamber filled with SDS-PAGE running buffer. The denatured protein samples were loaded onto the gel together with 4–8 µl of the Spectra Multicolor Broad Range protein ladder from Thermo Fisher Scientific as size standard (Table 2.4). Subsequently,

electrophoresis was performed at 180–200 V for approximately 50–80 min until the run front visualized by bromophenol blue had reached the lower end of the gel. After SDS-PAGE, separated proteins were either Coomassie-stained (section 2.5.5) or further analyzed by western blotting (section 2.5.6).

2.5.5 Coomassie-staining of polyacrylamide gels

After electrophoretic separation of proteins by SDS-PAGE, unspecific protein staining was performed using the triphenylmethane dye Coomassie brilliant blue G-250, which binds to basic amino acids under acidic conditions. After a short boiling of the polyacrylamide gels in Coomassie staining solution, staining occurred for 20–30 min at RT under shaking. Afterwards, the gels were rinsed with Milli-Q H_2O several times and incubated for at least 1 h in Coomassie destaining solution at RT under shaking in order to remove background staining. Finally, the gels were washed with Milli-Q H_2O overnight at RT under shaking, until the individual protein bands were clearly visible.

2.5.6 Western blotting

Western blotting (WB) is a widely accepted analytical technique to detect specific proteins in a given sample. By applying an electric field within this method, negatively charged proteins previously separated by SDS-PAGE (section 2.5.4) are electrophoretically transferred from a polyacrylamide gel to a suitable membrane on which they are immobilized irreversibly due to hydrophobic and electrostatic interactions. Afterwards the specificity of the antibody-antigen interaction enables the detection of target proteins in the complex protein mixture (immunoblotting).

In this work, western blotting was performed using the tank blot technique. First, the PVDF transfer membrane Amersham Hybond P 0.2 was activated by hydration in 100 % methanol for 1 min and subsequently equilibrated in transfer buffer for 10 min together with the polyacrylamide gel and four slightly larger pieces of Rotilabo®-blotting paper from Carl Roth. The pads of the blot cassette were also soaked with transfer buffer. After assembling the blot sandwich within the blot cassette from the anode- to the cathode-facing side consisting of two layers of blotting paper, the PVDF membrane, the gel and two additional layers of blotting paper together with the pads on each side, the blot cassette was inserted into the PerfectBlue™ tank electro blotter from Peqlab filled with transfer buffer. Western blotting was achieved with 350 mA for 150 min at 4 °C.

After finishing the transfer, the blot sandwich was disassembled and the PVDF membrane was shortly rinsed with TBST before it was incubated in WB blocking buffer for 1 h at RT with

gentle agitation in order to block possible binding sites on the membrane preventing unspecific binding of antibodies. Next, the membrane was incubated for 1 h at RT or overnight at 4 °C with gentle agitation in primary antibody solution, which was prepared by diluting the appropriate primary antibody in WB blocking buffer according to Table 2.6. After washing the membrane twice with TBST for 10 min each, it was incubated for 1 h at RT with gently agitation in secondary antibody solution, which was prepared by diluting the appropriate HRP-conjugated secondary antibody in WB blocking buffer according to Table 2.7. Subsequently, the membrane was again washed twice with TBST and once with TBS for 10 min each, before detection occured via enhanced chemiluminescence (ECL) by using the Pierce ECL Plus Western Blotting Substrate from Thermo Fisher Scientific according to the manufacturer's instructions. After incubating the membrane for 5 min with the substrate, it was placed into a developing cassette, exposed to a Fujifilm Super RX from Fujifilm for a maximum of 1 h followed by the development of the film using the film processor Cawomat 2000 IR from CAWO.

2.5.7 Circular dichroism spectroscopy

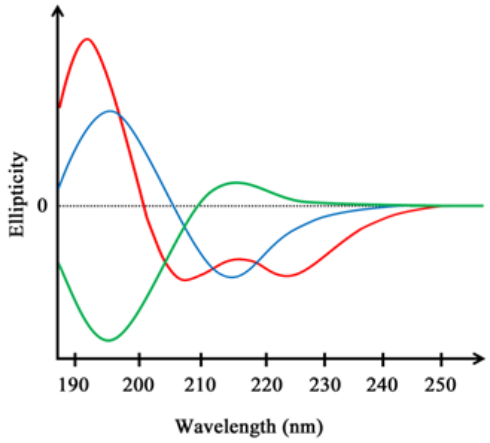

Figure 2.2: Characteristic far-UV CD spectra of the secondary protein structure elements α-helix, β-sheet and random coil.
While random coil arrangements (green) exhibit a minimum at 195 nm and a maximum of 212 nm, β-sheets (blue) show a maximum at 196 nm and a minimum at 218 nm, whereas α-helices (red) exhibit one maximum at 192 nm and two minima at 208 and 225 nm (NPTEL, 2018).

Circular dichroism spectroscopy is a method allowing the investigation of chiral molecules. Thereby, their characteristic CD, which is the difference in the absorption of left-handed and right-handed circularly polarized light, is measured over a range of wavelengths. Analysis of the structure or conformation of macromolecules, especially of proteins, is a common application for CD spectroscopy. Secondary protein structure elements can be identified by

recording far-UV CD spectra between 170 and 260 nm which show characteristic and unique minima and maxima for the different structure elements. While random coil arrangements exhibit a minimum at 195 nm and a maximum of 212 nm, β-sheets show a maximum at 196 nm and a minimum at 218 nm, whereas α-helices exhibit one maximum at 192 nm and two minima at 208 and 225 nm.

The integrity of the secondary structure of all purified proteins as well as a potential tweezer effect on Survivin's protein structure were analyzed by CD spectroscopy using the CD spectropolarimeter J-710 from Jasco. The proteins were diluted to a final concentration of 0.2 mg/ml with sterile filtered CD buffer and 200 µl protein solution were transferred to a 1 mm quartz glass cuvette from Hellma Analytics. Far-UV CD spectra were recorded between 190 and 260 nm, the data interval was set to 0.1 nm, the scanning speed to 100 nm/min, the response time to 0.5 s and the bandwidth to 2 nm. 20 spectra were recorded of each sample at 20 °C and accumulated. From each protein spectrum a buffer spectrum was subtracted and the measured ellipticity in mdeg units was converted to specific or molar ellipticity using path length and protein concentration (Equation 2.2).

$$\psi_{spec} = \frac{\psi}{l \cdot c} \tag{2.2}$$

Within this equation, ψ_{spec} is the specific ellipticity in deg cm^3 dmol^{-1}, ψ is the measured ellipticity in mdeg, l is the path length in cm and c is the concentration in mg/ml.

2.5.8 Analytical gel filtration

The principle of gel filtration (or size exclusion chromatography) is based on the separation of proteins according to their size. The used column is packed with a gel filtration medium consisting of a matrix of porous beads with a defined pore size. Proteins of different sizes are retained to varying degrees as they flow through this porous matrix. While small proteins can enter the pores, they are retained longer than larger proteins which cannot enter the beads and migrate around them. This results in a protein separation according to their size. Larger proteins pass through the column faster and elute at low retention volumes, smaller proteins pass through the column more slowly and elute at high retention volumes. In this work, analytical gel filtration was applied to analyze the molecular weight of purified proteins, the oligomerization state of Survivin variants, effects of tweezers on Survivin's dimerization as well as export complex formation.

Analytical gel filtration was performed at 4 °C using either the Superdex 75 10/300 GL column with a volume of 24 ml and a pressure limit of 1.8 MPa or the Superdex 200 Increase

5/150 GL column with a volume of 3 ml and a pressure limit of 3 MPa together with the liquid chromatography system ÄKTApurifier controlled by the Unicorn 5.20 control software from GE Healthcare. The columns and the LC system were equilibrated with an appropriate volume of Milli-Q H_2O followed by gel filtration buffer, both sterile filtered and degassed beforehand. Next, the respective protein sample was injected bubble-free via a sample loop into the LC system. For the Superdex 75 10/300 GL column a 500 µl sample loop was used to load 400–500 µl protein sample solution of a final concentration of 0.8–1 mg/ml onto the column and for the Superdex 200 Increase 5/150 GL column a 15 µl sample loop was used to load 15 µl of the prepared and injected 100 µl protein sample solution of a final concentration of 3–4 mg/ml onto the column. The samples passed through the column with a flow rate of 0.4 or 0.45 ml/min and protein elution was monitored by measuring the absorbance at 280 nm. In the end, the columns were regenerated with appropriate volumes of 0.5 M NaOH, Milli-Q H_2O, gel filtration buffer, again Milli-Q H_2O and finally 20 % ethanol for column storage at 4 °C. For calibration, a Gel Filtration low MW Calibration kit from GE Healthcare consisting of the globular proteins ribonuclease A (13.7 kDa), carbonic anhydrase (29 kDa), ovalbumin (44 kDa), conalbumin (75 kDa), aldolase (158 kDa) as well as blue dextran 2000 (>2,000 kDa) was analyzed under the same conditions.

2.5.9 Isothermal titration calorimetry

Isothermal titration calorimetry (ITC) is a technique to determine binding constants by measuring the heat produced during a chemical reaction for example ligand binding to a protein. By reference comparison, a calorimeter, as an isolated system, records changes in temperature and thus heat absorbance or release upon titration. By stepwise titration of only small amounts, many data-points are collected which allow a subsequent model fitting revealing information about the enthalpy, the binding affinity as well as the stoichiometry of the investigated reaction.

ITC measurements were performed to investigate tweezer binding on Survivin proteins. Thereby, tweezer molecules were provided by Christian Heid (AG Schrader). ITC experiments were performed with the calorimeter MicroCal iTC200 controlled by the MicroCal iTC200 software from Malvern Panalytical at 25°C using PBS pH 7.4. After purification of Survivin120, the protein was dialyzed overnight at 4 °C in PBS pH 7.4 (section 2.5.1.5). The concentration was carefully determined (section 2.5.3), immediately before starting each data collection. Moreover, all tweezer molecules were freshly dissolved in dialysis buffer (PBS pH 7.4) before measurements.

In a primary ITC experiment, 300 µl solution of 33.3 µM Survivin120 was placed in the sample cell and subjected to stepwise titration with 1 µl aliquots of a 5 mM solution of

unmodified tweezer molecule for a total of 39 injections. The reference power was set to 5 µcal/s, the initial delay to 60 s and the stirring speed to 750 rpm. Each injection occurred in a period of 2 s and the equilibration time between pairs of injections was 120 s. In further ITC experiments, 300 µl solution of either 100 µM unmodified tweezer, Tweezer-ELTL or Tweezer-ELTLGEFL molecules were placed in the sample cell and subjected to stepwise titration with 1.5 µl aliquots of a 1.2 mM solution of Survivin120 protein or a 0.92 mM solution of Survivin120-K90/91/103S protein for a total of 25 injections. The reference power was set to 5 µcal/s, the initial delay to 60 s and the stirring speed to 750 rpm. Each injection occurred in a period of 3 s and the equilibration time between pairs of injections was 120 s.
Blank titration of either the tweezer or the protein solution into the buffer was performed in order to provide a control for possible dilution effects. The control heating power, obtained in this way, was subtracted respectively from the measured corresponding raw heating power. Finally, data evaluation was carried out by Christian Heid using the software AFFINImeter for Isothermal Titration Calorimetry from S4SD-AFFINImeter. The integrated and normalized heat values, except those for the primary ITC experiment, were fitted to a one-site binding model.

2.5.10 NMR spectroscopy and tweezer titration experiments

Nuclear magnetic resonance (NMR) spectroscopy and tweezer titration experiments were performed to provide structural information about binding sites of tweezer molecules on the surface of Survivin. To record NMR protein spectra, proteins must be isotopically labelled.
Purification of isotopically labeled Survivin proteins as well as NMR spectroscopy and tweezer titration experiments were performed in cooperation with Dr. Christine Beuck from the Department of Structural and Medicinal Biochemistry (Bayer group, University of Essen).
Survivin was expressed and isotopically labeled by inoculating 4 l LB medium with an overnight culture of *E coli* SoluBL21, grown at 37 °C until OD_{600} reached 1.0–1.2. The cells from 4 l LB medium were then pelleted and resuspended in 1 l M9 minimal medium supplemented with 1 g/l ^{15}N-ammonium chloride. After another incubation for 30 min at 37 °C, expression was induced by adding 0.2 mM IPTG. Cells were incubated for 20 h at 30 °C. Afterwards, cells were pelleted, lysed with lysozyme in PBS (pH 7.4) supplemented with 2 mM DTT and 1 mM PMSF and finally sonicated. The cell lysate was centrifuged (142000 x g, 60 min, 4 °C) and filtrated supernatant was used for further purification. The supernatant containing Survivin was applied to a GSH-column from GE Healthcare in PBS pH 7.4 supplemented with 2 mM DTT, washed with PBS containing 2 mM DTT, high salt buffer (PBS pH 7.4 with 2 mM DTT and 0.5 M NaCl) and again with PBS containing 2 mM DTT. The GST-tagged protein was eluted using PBS pH 7.4 supplemented with 2 mM DTT

and 20 mM GSH. Cleavage of the GST-tag was done with PreScission protease and subsequent preparative size exclusion chromatography was performed with a HiLoad 26/600 Superdex 75 pg column and a downstream mounted GSH-column from GE Healthcare in potassium phosphate buffer at a flow rate of 0.8 ml/min. Finally, Survivn protein was dialyzed for NMR spectroscopy against NMR buffer.

NMR experiments were performed using a 700 MHz Ultrashield NMR spectrometer from Bruker equipped with a 5 mm CPTCI ^{1}H-$^{13}C/^{15}N/D$ cryoprobe with z-gradient. NMR samples contained 400 µM of ^{15}N-labeled Survivin (90 % H_2O : 10 % D_2O). ^{1}H-^{15}N-band-selective excitation short-transient (BEST)-transverse relaxation optimized spectroscopy (TROSY)-heteronuclear single quantum correlation (HSQC) spectra were recorded with 32 scans and 2k x 0.256k data points. Data were processed with TopSpin™ 3 from Bruker. Titration experiments with unmodified tweezer and Tweezer-ELTL molecules were performed at 25 °C by stepwise addition of up to 400 µM tweezer solution to Survivin. Assignments of Survivin (residues 2–117) were obtained from the BMRB data base (BMRB # 6342). Intensity changes of the signals as well as chemical peak shifts were analyzed and plotted against the Survivin sequence.

2.5.11 GST pull-down assay

The GST pull-down assay was used to investigate the *in vitro* assembly of the export complex consisting of the export receptor CRM1, its cofactor RanQ69L as well as its cargo protein Survivin and to analyze the effect of the tweezer molecules on complex formation.

All GST pull-down assays were performed at RT in pull-down buffer. GST fusion proteins were immobilized on 50 µl GSH-coated Sepharose 4B beads from GE Healthcare and used as bait proteins to capture putative binding partners. As a control, in one sample of each experiment no bait protein was added. First, the GSH-beads were equilibrated twice by washing with 500 µl pull-down buffer for 5 min under rotation and subsequent centrifugation (500 x g, 5 min). Next, the GSH-beads were either directly blocked to prevent unspecific binding or GST fusion proteins were bound to the beads first. Blocking was performed by incubating the GSH-beads in 500 µl pull-down blocking buffer for 1 h under rotation.

After blocking, 500 µl protein mixture, consisting of 2 mM dGTP and all three export complex members or all missing members, in case of prebinding of one GST fusion protein member, diluted in pull-down buffer, was added to the GSH-beads and incubated for 2 h under rotation.

For complex assembly investigation with recombinant Survivin, 40 µg Survivin, 35 µg GST-CRM1 and 55 µg RanQ69L were mixed. In experiments with overexpressed

Survivin-HA in 293T cell lysate (section 2.4.2 and 2.5.2), 200 µg lysate, 80 µg GST-CRM1 and 55 µg RanQ69L were mixed.

For investigation of tweezer effects on complex assembly with recombinant Survivin120, 40 µg Survivin were pre-incubated with no ligand or 100 µM unmodified tweezer for 1 h and then mixed with 35 µg GST-CRM1 and 55 µg RanQ69L. When using 293T cell lysate with overexpressed Survivin-HA (section 2.4.2 and 2.5.2), 200 µg lysate were pre-incubated with either no ligand, 100 µM unmodified tweezer, Tweezer-ELTL or, as control, ELTL peptide for 1 h and then mixed with 55 µg RanQ69L alone, since GST-CRM1 was prebound to the GSH-beads before blocking. Prebinding occurred by incubating the equilibrated GSH-beads in 500 µl pull-down buffer containing 140 µg GST-CRM1 for 1.5 h under rotation, followed by three washing steps with 500 µl pull-down buffer. For analysis of the effective tweezer concentration, 200 µg 293T lysate with overexpressed Survivin-HA (section 2.4.2 and 2.5.2) were pre-incubated with no ligand or different concentrations (10 nM to 200 µM) of unmodified tweezer or Tweezer-ELTL for 1 h and then mixed with 35 µg GST-CRM1 and 55 µg RanQ69L. To investigate an effect of tweezer molecules on complex formation with overexpressed myc-Survivin142 and myc-Survivin142-K90/91/103S in 293T cell lysate (section 2.4.2 and 2.5.2), 200 µg lysate were pre-incubated with either no ligand or 50 µM unmodified tweezer, Tweezer-ELTL or Tweezer-ELTLGEFL for 1 h and then mixed with 35 µg GST-CRM1 and 55 µg RanQ69L.

In the changed pull-down setup for removal of unbound tweezer, 40 µg GST-Survivin120 or GST-Survivin120-K90/91/103S mutant were prebound to equilibrated GSH-beads in 500 µl pull-down buffer, containing additionally either no ligand or 50 µM unmodified tweezer, Tweezer-ELTL, Tweezer-ELTLGEFL or peptide ELTL, for 1 h under rotation. After washing and blocking, GSH-beads were incubated with a protein mixture consisting of 2 mM dGTP, 50 µg CRM1 and 50 µg RanQ69L for 2 h under rotation.

30 µl SDS samples of input, supernatant and beads were taken during pull-down assays, mixed with 5x SDS sample buffer and denatured at 95 °C for 10 min for further analysis by SDS-PAGE (section 2.5.4) and western blotting (section 2.5.6). Input samples were taken from the protein mixtures before adding them to the beads, supernatant samples were taken after pelleting the beads (500 x g, 5 min) upon 2 h incubation and beads samples were taken after three final washing steps. Western blots were analyzed by densitometric analysis with ImageJ from U.S. National Institutes of Health. Therefore, the mean grey intensity of protein bands was measured.

2.6 Bioinformatical methods

2.6.1 Molecular dynamic simulations of Survivin

For investigation of a potential flexibility and instability of Survivin's C-terminal α-helix, *in silico* analysis was performed in cooperation with Jean-Noël Grad from the Department of Bioinformatics and Computational Biophysics (Hoffmann group, University of Essen). Molecular dynamic (MD) simulations of monomeric and dimeric Survivin were measured.
Therefore, an initial structure for Survivin was generated in Modeller v9.17 (Sali and Blundell, 1993) using the Uniprot protein sequence O15392-1 (human BIRC5 isoform alpha) as target and PDB entries 1E31, 1F3H, 3UEG, 3UEH, 3UEI and 1XOX as templates. The best model was selected to minimize the DOPE and molpdf scores and was validated with PROCHECK (Laskowski *et al.*, 1993) from the online Swiss-Model Workspace (Arnold *et al.*, 2006). The same procedure was used for the dimeric Survivin.
MD simulations were carried out with Gromacs 4.6.7 (Pronk *et al.*, 2013) using the Amber ff99SB force field (Hornak *et al.*, 2006) extended with ZAFF to model the zinc finger (Peters *et al.*, 2010). Topology files were created with the TLEaP module of Amber v12.21 (Case *et al.*, 2012) and converted to Gromacs topologies by ACPype (Sousa da Silva and Vranken, 2012). Proteins were solvated in a dodecahedron box of SPC/E water molecules (Berendsen *et al.*, 1987) with a 10 Å minimum separation between the protein and the box boundaries. The system was neutralized by addition of Na^+ and Cl^- ions to a final ionic strength of 0.15 mol/l, energy-minimized by steepest-descent to a total force of 2000 kJ mol^{-1} nm^{-1} and equilibrated for 4 ns in the NVT ensemble with restrained heavy atoms, and for 4 ns in the NPT ensemble without restraints. Production simulations were performed in the NPT ensemble for 50–500 ns depending on the system (WT monomer: 1 x 500 ns, 2 x 200 ns, 2 x 250 ns; WT dimer: 3 x 50 ns, 2 x 80 ns). Temperature was stabilized at 300 K in the NVT and NPT ensembles by the V-rescale thermostat (Bussi *et al.*, 2007), while the pressure was stabilized at 1 atm in the NPT ensemble by the Berendsen barostat (equilibration) or Parinello-Rahman barostat (data production) (Parrinello and Rahman, 1981). Simulations were carried out on a GPU (GeForce 970 and GeForce 1070, CUDA 6.5) using a time step of 2 fs, the Verlet scheme (Páll and Hess, 2013) for neighbor search with a 10 Å cutoff, the Particle Mesh Ewald method (Darden *et al.*, 1993) for electrostatic calculations, and the LINCS algorithm (Hess *et al.*, 1997) for bond constraints.
Representative structures were extracted from trajectories based on mutual RMSDs, using the g_rms tool in Gromacs to produce 2D RMSD plots, the PAM (partition around medoids (Kaufman and Rousseeuw, 1987)) tool from R package cluster, version 2.0.6, in R v3.3.1 (R

Core Team, 2016) to find clusters, and the cluster.stats function of R package fpc, version 2.1.10, to validate the clustering based on silhouette coefficients (Rousseeuw, 1987).

2.6.2 Molecular dynamic simulations of tweezer binding to Survivin

Before synthesis of peptide-linked tweezer molecules, molecular dynamic (MD) simulations of basic Tweezer, Tweezer-ELTL and Tweezer-ELTLGEFL were performed in cooperation with Christian Heid from the Department of Organic Chemistry (Schrader group, University of Essen) to study their binding to Survivin.

The peptides were each minimized in presence of monomeric Survivin (based on PDB: 1XOX) by force field calculations (OPLS 2005 force field). Then the Tweezer unit was placed on the lysine residue 103, so that it encloses the lysine side chain inside the tweezers' cavity and an ionic interaction occurs between the negatively charged phosphate groups of the tweezers and the positively charged ammonium groups of the lysine. This overall structure was first minimized and then a Monte Carlo simulation was carried out (2500 steps). The thermodynamically most energy-efficient structure was then used for further simulations. The peptide with its azide function and the tweezers with the alkyne function were then linked together by a click reaction to form a triazole. A simple minimization was then carried out again, followed by another Monte Carlo simulation. Subsequently, MD simulations (Desmond 2015.4–2016.3, 100 ns, 300 K, 0.15 mM NaCl) were performed, based on the thermodynamically most favorable structure. Resulting ligand interaction diagrams and energy profiles during simulation time reveal requested information about tweezer binding on Survivin monomer (Heid, 2018).

2.6.3 MD and QM/MM studies of tweezer binding to lysine residues of Survivin

Molcular dynamic (MD) simulations and quantum mechanics/molecular mechanics (QM/MM) optimizations to confirm and explain the experimental NMR titration results were performed in cooperation with Dr. Yasser B. Ruiz Blanco from the Department of Computational Biochemistry (Sánchez-García group, University of Essen).

The geometry of the Survivin monomer was taken from the PDB structure 1XOX. The isolated structure of Tweezer-ELTL was first simulated in water solution by doing three short (10 ns) MD runs. The two most populated, sterically free geometries along the 30 ns of MD simulation were extracted to build the complexes with the lysine sites in following MD simulations.

MD-setup: Each MD simulation was executed using NAMD (Phillips *et al.*, 2005) with the CHARMM force field (Klauda *et al.*, 2010; Vanommeslaeghe *et al.*, 2010). The NPT

ensemble at 1 atm and 300 K was settled by means of a temperature and pressure control obtained from Langevin dynamics with a damping constant of 5 ps^{-1} (Feller *et al.*, 1995). The simulations were conducted in a solvent box built with a padding of 20 Å beyond molecules' dimensions. The water molecules were represented by the TIP3P model. The solvent box was neutralized with sodium ions. A cutoff of 12 Å was used for Van der Waals interactions and long-range electrostatics were evaluated using the Particle Mesh Ewald method (Darden *et al.*, 1993). Geometries where initially minimized and equilibrated at 300 K using short NVT and NPT simulations, both equilibrium and production runs used time steps of 2 fs.

Here, Survivin monomer was used for the MD simulations. Harmonic constraints on collective variables representing distances and angles were used to maintain the geometry of the tetrahedral zinc finger.

Four replicas of 20 ns of MD simulations were executed for each complex Tweezer – lysine residue of Survivin. Regarding Tweezer-ELTL, two replicas of 40 ns of MD simulations were run, starting at the complexes derived from the two geometries simulated in water solution.

QM/MM-setup: QM/MM optimizations were performed using ChemShell (Sherwood *et al.*, 2003) with the DL-FIND geometry optimizer (Kästner *et al.*, 2009) and Turbomole (Ahlrichs *et al.*, 1989) to handle the QM region. The QM region is defined by the tweezers and the methylene groups in positions δ and ε of lysine's sidechain while the MM region contains the rest of the protein atoms, solvent and ions within 30 Å from the tweezers. An electrostatic embedding (Cisneros *et al.*, 2006) was used. The MM region is modeled with the CHARMM version force-field and the QM region at the DFT(B3LYP-D3)/Def2SVP level (Grimme, 2011). Five QM/MM optimizations were carried out for each geometry, taking the three outcomes with more similar energy values to estimate the final average results.

3 RESULTS

Survivin plays an important role in cancer. While it is mostly absent in normal resting adult tissues, it is up-regulated in almost all cancer types (Adida et al, 2000; Ambrosini et al, 1997). Thereby, its overexpression is associated with a resistance of tumors against chemo- and radiotherapy, frequent recurrences and decreased patient survival (Capalbo et al, 2007; Chen et al, 2014; Engels et al, 2007; Xu et al, 2014), making Survivin an attractive target for novel therapeutic strategies. As a member of the IAP family, Survivin plays a role in the inhibition of cell death, but as part of the CPC it is also crucially involved in mitotic regulation (Li et al, 1998). For both biological functions, an interaction with the nuclear export receptor CRM1 mediated by Survivin's NES is pivotal (Knauer et al, 2006; Knauer et al, 2007b). Thus, interference with this interaction should lead to a loss of Survivin's functions and therefore to an inhibition of cancer cell proliferation.
Novel supramolecular tweezer molecules targeting Survivin's NES on the surface of the protein should be characterized by a quantitative assessment of its binding affinity and its potential to inhibit the Survivin–CRM1 interaction as well as a thorough analysis of the resulting cellular biological effects.

3.1 Purification and characterization of wild type Survivin protein

To begin with, sufficient amounts of recombinant Survivin as well as other proteins are required for *in vitro* investigations. For this purpose, a suitable prokaryotic expression system was established.
After transformation of the expression strain *E. coli* SoluBL21 with the prokaryotic expression vector pET41-GST-PreSc-Survivin142, the protein GST-PreSc-Survivin142 was expressed. Cell disruption was performed by sonication followed by centrifugation to separate cell debris from the soluble protein fraction. Survivin's fused GST-tag allowed GSH affinity chromatography as a first purification step. After several washing steps, the GST-tag was cleaved on the column by loading recombinantly expressed and purified PreScission protease (appendix A.1), followed by an overnight incubation. The next day, the cleaved product Survivin142 was rinsed onto an ion exchange chromatography column (Figure 3.1).

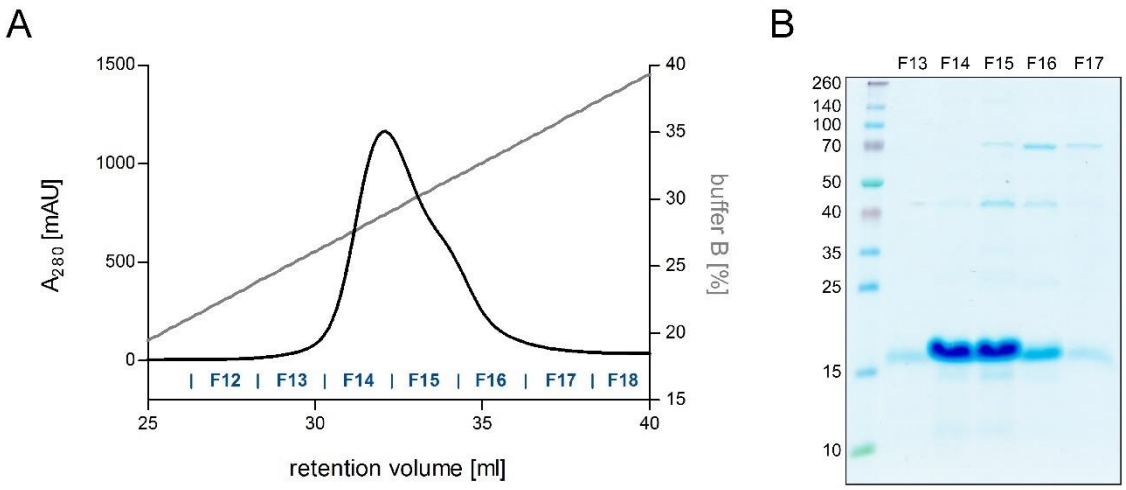

Figure 3.1: Purification of Survivin142 by ion exchange chromatography.
A) Absorbance chromatogram at 280 nm of the ion exchange chromatography following GSH affinity purification and GST-tag cleavage. The elution gradient (0–100 % ion buffer B, 25 mM to 1 M NaCl, 75 ml, grey) and the collected elution fractions (F12–F18, blue) are included. **B)** Coomassie-stained SDS gel of protein-containing elution fractions. Fractions F13–F17 contain Survivin142 with few impurities. They were pooled, concentrated and used for subsequent experiments.

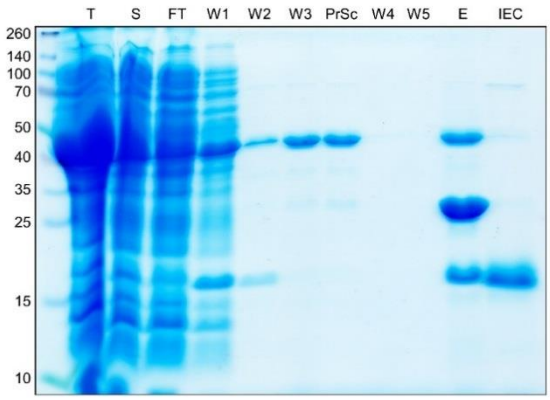

Figure 3.2: Overview of the purification procedure of Survivin142.
Coomassie-stained SDS gel of samples taken after the respective purification steps (T: total lysate, S: supernatant, FT: flow through of GSH column loading, W1–W3: wash fractions after loading the GSH column, PrSc: flow through of PreScission protease loading onto the GSH column, W4–W5: flow through of rinsing protein from the GSH column onto an ion exchange column, E: final GSH-elution of GSH column, IEC: pooled and concentrated protein after ion exchange chromatography).

Survivin142 eluted at a retention volume of 32 ml and 29 % buffer B which corresponded to a salt concentration of roughly 315 mM NaCl. The purity and protein content of the collected fractions F13–F17 were controlled by SDS-PAGE. Considering both, purity and protein

amount, fractions F13–F17 were pooled, concentrated to 4 mg/ml and stored at -80 °C. Finally, the GSH affinity column was regenerated with 10 mM GSH elution buffer. Samples taken after each purification step were analyzed by SDS-PAGE to control the purification process (Figure 3.2).

During the purification procedure, a significant proportion of the expressed Survivin142 protein was detected in the insoluble protein fraction after centrifugation, ended up in the flow through and wash fractions or remained on the GSH affinity column as uncleaved or cleaved protein. However, Survivin142 reached a purity of more than 95 %, only a few impurities by *E. coli* proteins, most likely heat shock proteins, were detectable. The overall protein yield amounted to 1.5 mg per liter of bacterial culture.

The purified wild type protein Survivin142 was biochemically characterized. Its secondary structure was analyzed by CD spectroscopy (Figure 3.3), dimerization was assessed by analytical gel filtration (Figure 3.4 A), and an NMR spectrum was recorded (Figure 3.5; Dr. Christine Beuck, AG Bayer) to firmly establish the peak – amino acid correlation for titration experiments.

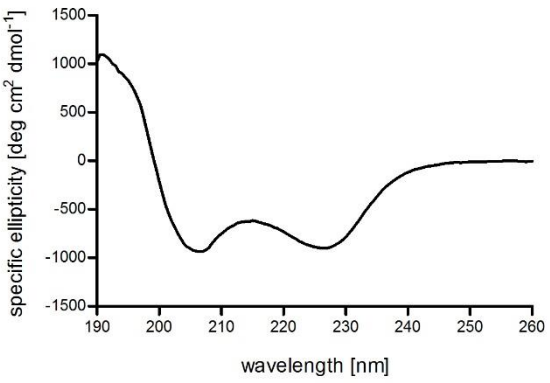

Figure 3.3: Far-UV CD spectrum of Survivin142.

The shape of the far-UV CD spectrum of tag-free Survivin142 recorded at 20 °C in 20 mM phosphate buffer containing 10 µM Zn^{2+}. Especially the minima at 207 nm and 227 nm hint at a correctly folded protein with a high α-helical content.

The CD spectrum exhibited two minima at 207 nm and 227 nm with equal ellipticity, plus a maximum at 191 nm. These correlated with the minima at 208 nm and 225 nm and the maximum at 192 nm of the α-helix spectrum, respectively. Thus, Survivin142 can be considered as correctly folded.

Analytical gel filtration was performed to study Survivin's dimerization (Figure 3.4 A). The column was calibrated with proteins whose molecular weight (MW) range covered the size of monomeric (16.4 kDa) and dimeric protein (32.8 kDa). Next, the influence of amino acid mutations in Survivin's NES or dimer interface on its dimerization was studied by analytical

gel filtration experiments of wild type protein compared to Survivin mutants (Figure 3.4 B; (Vallet, 2014)).

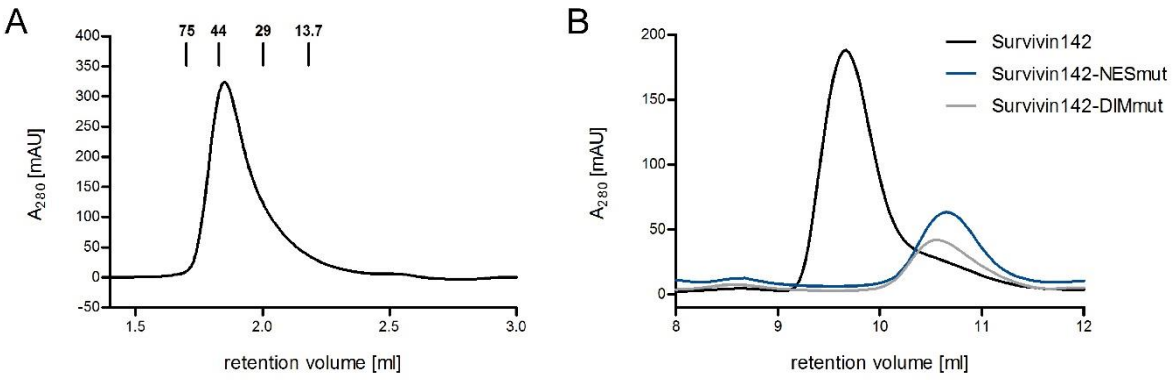

Figure 3.4: Analytical gel filtration of Survivin142 wild type and mutants.
A) Analytical gel filtration absorbance chromatogram measured at 280 nm on a calibrated Superdex 200 Increase column reveals that wild type Survivin142 elutes in the range of 29–44 kDa, corresponding to a homodimer. **B)** Analytical gel filtration absorbance chromatograms of Survivin142 WT (black) and two Survivin mutants, Survivin142 NESmut (L96AL98A, blue) and DIMmut (F101A L102A, grey), measured at 280 nm on a Superdex 75 10/300 GL column reveal that mutations in Survivin's NES or dimer interface seem to abolish Survivin's homodimerization in solution (Vallet, 2014).

Survivin142 eluted at nearly the same retention volume as ovalbumin, which has a protein size of 44 kDa. This better matches the dimeric protein size of 32.8 kDa than its monomeric size of 16.4 kDa. The deviation can be explained by Survivin's dynamic radius, which has to be considered in this gel filtration experiment and which is enhanced compared to globular proteins because of Survivin's C-terminal α-helix. Thus, in solution wild type Survivin142 is stable as a homodimer. Mutations in Survivin's NES (NESmut-L96AL98A) or dimer interface (DIMmut-F101AL102A) led to a higher retention volume compared to the wild type protein. Since the DIMmut Survivin protein is supposed to form a monomer in solution, it served as a control in this gel filtration experiment. The NESmut protein eluted in the same range as the DIMmut protein, so mutations in Survivin's NES seem to abolish Survivin's homodimerization in solution.
Next, NMR spectroscopic analysis was performed to get structural access to Survivin for further titration experiments with molecular tweezer molecules. Here, in cooperation with Dr. Christine Beuck from the Department of Structural and Medicinal Biochemistry (Bayer group, University of Essen) a ^{1}H-^{15}N-HSQC NMR spectrum of ^{15}N-labeled wild type Survivin142 was recorded (Figure 3.5).

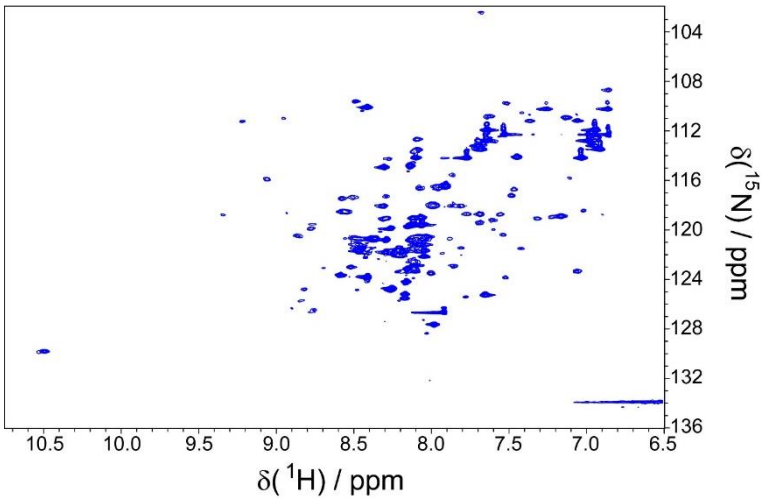

Figure 3.5: ^{1}H-^{15}N-HSQC NMR spectrum of Survivin142.

^{1}H-^{15}N-HSQC spectrum of ^{15}N-labeled wild type Survivin142 measured in NMR buffer. A peak – amino acid residue assignment was not possible for the resulting NMR signals (^{15}N-labeled protein purification and NMR measurements by Dr. Christine Beuck, Department of Structural and Medicinal Biochemistry, Bayer group, University of Essen).

Unfortunately, wild type Survivin142 did not give evaluable NMR signals. A correlation of visible peaks to distinct amino acids of Survivin142 was not possible for the resulting spectrum, most probably due to instability of the protein. Since the truncated protein version Survivin120 is the only solved and published NMR structure in solution (Sun *et al.*, 2005), Survivin's C-terminal α-helix might destabilize the full-length protein.

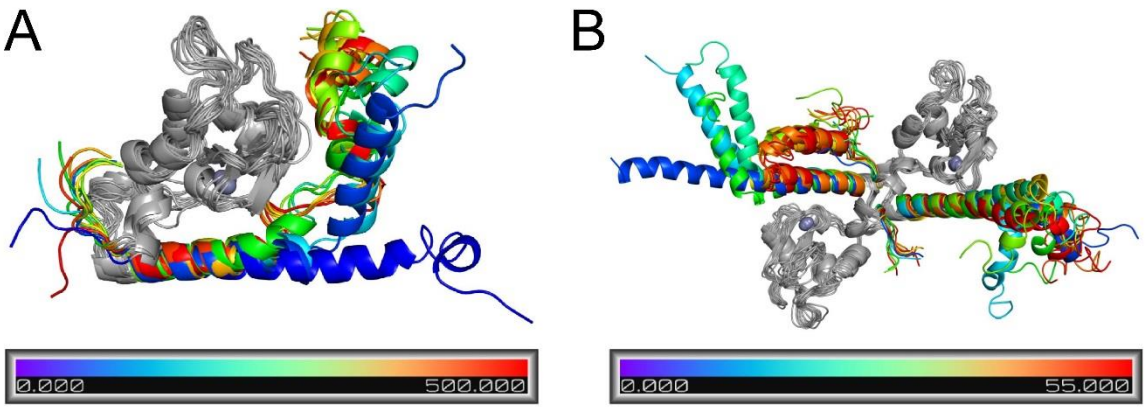

Figure 3.6: *In silico* simulation trajectories of Survivin protein dynamics.

Structurally stable regions are colored in grey. The color bar represents the time in nanoseconds. The representative simulation trajectories of the **A)** monomeric and **B)** dimeric Survivin system reveal a flexibility and instability of Survivin's C-terminal α-helix (simulations by Jean-Noël Grad, Department of Bioinformatics and Computational Biophysics, Hoffmann group, University of Essen).

To investigate this hypothesis, an *in silico* analysis was performed in cooperation with Jean-Noël Grad from the Department of Bioinformatics and Computational Biophysics (Hoffmann group, University of Essen). Protein dynamics of a monomeric and dimeric Survivin system were investigated over time. Each Survivin system was simulated five times with non-consistent durations (monomer: 1×500 ns, 2×200 ns, 2×250 ns; dimer: 3×50 ns, 2×80 ns) and simulation trajectories of the monomeric and dimeric system were visualized (Figure 3.6). In these dynamic simulations Survivin's C-terminus was observed to be consistently bending on multiple spots in the second half of the C-terminal α-helix, but especially in the region around aa 120. This was the case for the monomeric and the dimeric simulation system. These results demonstrated a flexibility and instability of Survivin's C-terminal α-helix while other regions of the protein kept stable over time.
As the simulations confirmed the hypothesis of an instable Survivin C-terminus which might be the problem for NMR measurements of Survivin, the protein was truncated to Survivin120 in analogy to the solved and published NMR structure.

3.2 Purification and characterization of truncated Survivin protein

The coding sequence of the truncated Survivin120 protein was amplified by PCR, digested and finally ligated into the expression vector. After verifying the DNA sequence, the expression strain *E. coli* SoluBL21 was transformed with the correct prokaryotic expression vector pET41-GST-PreSc-Survivin120. Following expression of the truncated protein Survivin120, bacterial cells were disrupted by sonication and cell debris was separated from the soluble protein fraction by centrifugation. Survivin's fused GST-tag allowed GSH affinity chromatography as a first purification step. After several washing steps, the GST-tag was cleaved on the column by loading recombinantly expressed and purified PreScission protease (appendix A.1), followed by an overnight incubation. The next day, the cleaved product Survivin120 was applied to an ion exchange chromatography column (Figure 3.7).
Survivin120 eluted at a retention volume of 31 ml and 27.5 % buffer B which corresponded to a salt concentration of roughly 300 mM NaCl. The purity and protein content of the collected fractions F11–F18 were controlled by SDS-PAGE. Considering both, purity and protein amount, fractions F12–F14 were pooled, concentrated to 49 mg/ml and stored at -80 °C. Finally, the GSH affinity column was regenerated with 10 mM GSH elution buffer. Samples taken after each purification step were analyzed by SDS-PAGE to control the purification process (Figure 3.8).

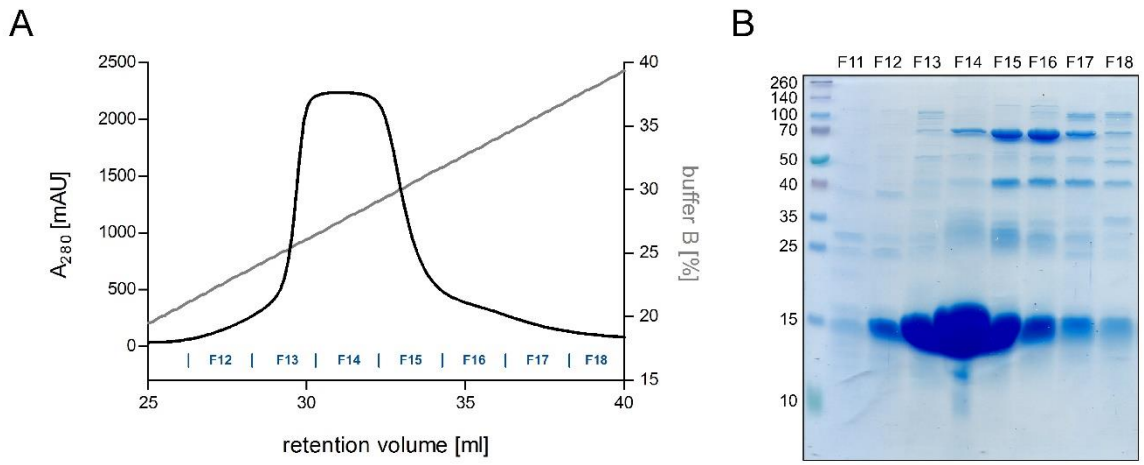

Figure 3.7: Purification of Survivin120 by ion exchange chromatography.

A) Absorbance chromatogram at 280 nm of the ion exchange chromatography following GSH affinity purification and GST-tag cleavage. The elution gradient (0–100 % ion buffer B, 25 mM to 1 M NaCl, 75 ml, grey) and the collected elution fractions (F12–F18, blue) are included. **B)** Coomassie-stained SDS gel of protein-containing elution fractions. Fractions F12–F14 contain Survivin120 with few impurities. They were pooled, concentrated and used for subsequent experiments.

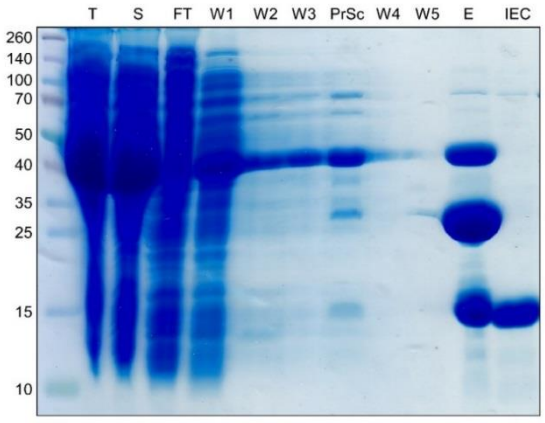

Figure 3.8: Overview of the purification procedure of Survivin120.

Coomassie-stained SDS gel of samples taken after the respective purification steps (T: total lysate, S: supernatant, FT: flow through of GSH column loading, W1–W3: wash fractions after loading the GSH column, PrSc: flow through of PreScission protease loading onto the GSH column, W4–W5: flow through of rinsing protein from the GSH column onto an ion exchange column, E: final GSH-elution of GSH column, IEC: pooled and concentrated protein after ion exchange chromatography).

During the purification procedure, a significant portion of the expressed Survivin120 protein was detectable in the wash fractions or remained on the GSH affinity column as uncleaved or cleaved protein. However, Survivin120 reached a purity of more than 99 %, only a few

impurities by *E. coli* proteins, most likely heat shock proteins, were detectable. The overall protein yield amounted to 5.3 mg per liter of bacterial culture.

Subsequently, in cooperation with Dr. Christine Beuck from the Department of Structural and Medicinal Biochemistry (Bayer group, University of Essen) an ^{1}H-^{15}N-BEST-TROSY-HSQC NMR spectrum of ^{15}N-labeled truncated Survivin120 was recorded (Figure 3.9).

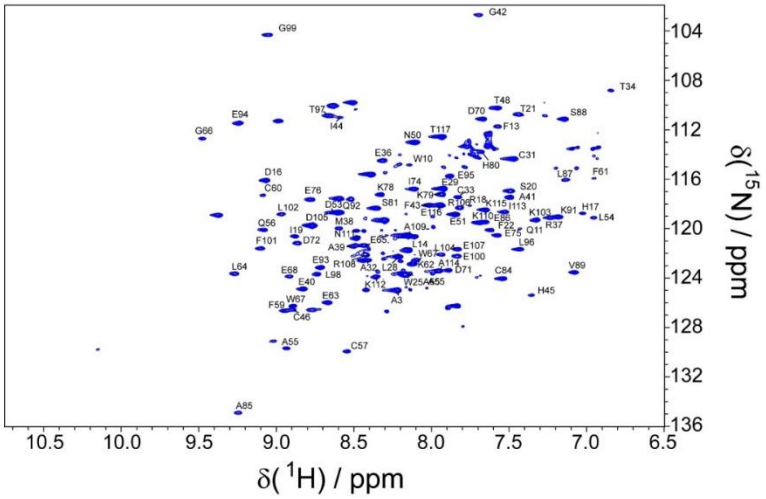

Figure 3.9: ^{1}H-^{15}N-BEST-TROSY-HSQC NMR spectrum assignment of Survivin120.

^{1}H-^{15}N-BEST-TROSY-HSQC spectrum of ^{15}N-labeled truncated Survivin120 measured in NMR buffer. A peak – amino acid residue assignment was possible for the resulting NMR signals. The amino acid residue label corresponding to the respective signal (blue) is depicted in black (^{15}N-labeled protein purification and NMR measurements by Dr. Christine Beuck, Department of Structural and Medicinal Biochemistry, Bayer group, University of Essen).

The strategy to shorten Survivin's C-terminal α-helix most probably responsible for protein instability was indeed successful for NMR analysis as Survivin120 gave evaluable signals. With the corresponding spectrum, a visible cross peak could be perfectly correlated to almost every amino acid in the sequence. This set the stage for following titration experiments with the molecular tweezer molecules.

Next, to assure Survivin's correct secondary protein structure even with a truncated helix, CD spectroscopy was performed in comparison to full-length Survivin142 (Figure 3.10).

The CD spectrum of truncated Survivin exhibited the same two minima at 207 nm and 227 nm and the maximum at 191 nm as detected for full-length Survivin. However, compared to the equal ellipticity of both minima for the Survivin142, the minima for Survivin120 showed different ellipticities. For Survivin120, the minimum at 207 nm was not as low as that of Survivin142. Since this minimum strongly indicates α-helical structures, an increased ellipticity suggested a reduced α-helical content of Survivin120 perfectly in line with the

truncated C-terminal α-helix. Thus, Survivin120 can be considered as correctly folded with a minor α-helical content.

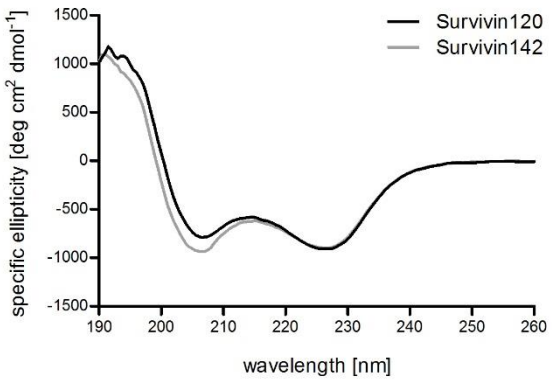

Figure 3.10: Far-UV CD spectrum of Survivin120.

The shape of the far-UV CD spectrum of tag-free Survivin120 (black) recorded at 20 °C in 20 mM phosphate buffer containing 10 µM Zn^{2+}. Especially the minima at 207 nm and 227 nm, hint at a correctly folded protein with a high α-helical content. Compared to far-UV CD spectrum of Survivin142 (grey), Survivin120 revealed a minor α-helical content due to its truncated α-helix.

For analytical gel filtration of Survivin120 (Figure 3.11) the column was calibrated with proteins whose MW range covered the size of monomeric (14 kDa) and dimeric Survivin120 (28 kDa).

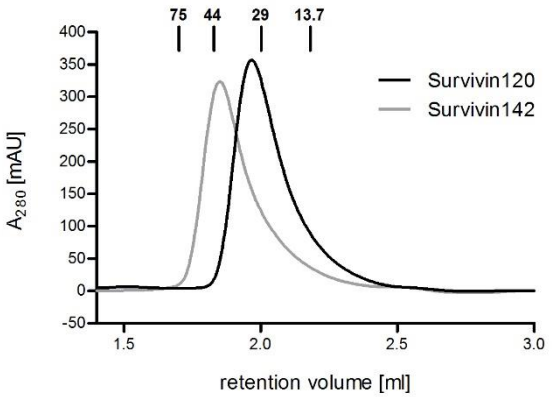

Figure 3.11: Analytical gel filtration of Survivin120.

Analytical gel filtration absorbance chromatogram measured at 280 nm on a calibrated Superdex 200 Increase column reveals that truncated Survivin120 elutes in the range of 29–44 kDa, corresponding to a homodimer. Compared to full-length Survivin142 it elutes at a higher retention volume due to its truncated α-helix.

Compared to full-length Survivin142, Survivin120 eluted at a higher retention volume due to its truncated C-terminal helix. Regarding its dimerization, Survivin120 eluted little earlier than the calibration protein carbonic anhydrase, which has a protein size of 29 kDa. This rather matched the dimeric protein size of 28 kDa than its monomeric MW of 14 kDa. The deviation can be explained by Survivin's dynamic radius, which is enhanced compared to globular proteins like carbonic anhydrase because of Survivin's C-terminal α-helix even though truncated. Thus, also truncated Survivin120 is stable as a homodimer in solution.

3.3 Supramolecular tweezer binding to Survivin

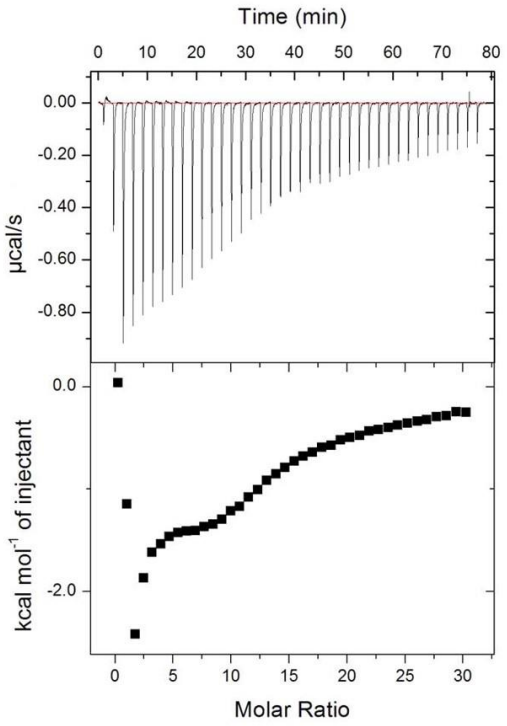

Figure 3.12: ITC measurement of tweezer binding to Survivin.
For the ITC experiment a solution of 33.3 µM Survivin120 was placed in the sample cell and subjected to stepwise titration with 1 µl aliquots of a 5 mM solution of unmodified tweezer molecule for a total of 39 injections. The equilibration time between two injections was 120 s. **Top:** raw heating power over time. **Bottom:** integrated energy values normalized to injected tweezer. The exothermic binding reaction displays a more-phase course hinting at a minimum of two binding events with different affinities (tweezer kindly provided by Christian Heid, Department of Organic Chemistry, Schrader group, University of Essen).

Having the purified and well-characterized Survivin120 protein at hand, a first binding experiment was performed with the unmodified molecular tweezer to testimate the potential

of generating new peptide-linked tweezer molecules with additional binding motifs to enhance affinity and selectivity.

In an initial ITC experiment, Survivin120 was placed in the sample cell and subjected to stepwise titration with the unmodified molecular tweezer (Figure 3.12). In this experimental ITC setup, more than one binding event could be observed. Binding of the unmodified molecular tweezer to Survivin120 definitely occurred, but saturation could not be achieved, and a suitable fitting model was difficult to determine because of these several observed binding events. Nevertheless, based on this first promising ITC result, the molecular tweezer molecules were further improved.

3.3.1 Design and generation of new peptide-linked tweezer molecules

The idea is to design novel tweezer molecules, which should exhibit an enhanced affinity and selectivity towards Survivin. Since the overall aim is to interfere with Survivin's dual functional role, Survivin's NES, which allows binding to the export receptor CRM1, can be regarded as a prime target for such supramolecular ligands. The NES (V89–L98) partially overlaps with Survivin's dimer interface (V89–L102) localized right at the bend preceding the C-terminal α-helix. Since this dimer interface moreover represents another natural binding region of Survivin, the idea was to utilize it for the design of new tweezer molecules.

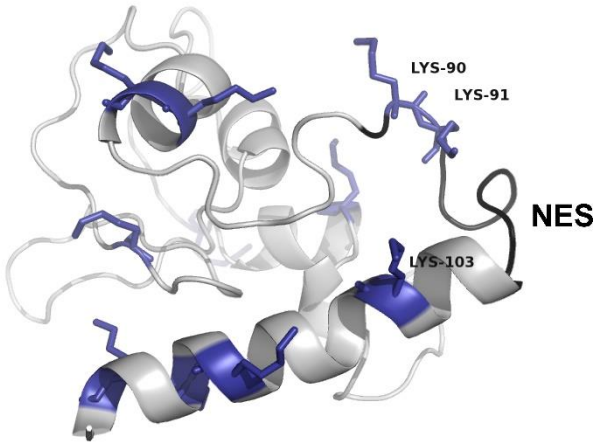

Figure 3.13: Position of Survivin's lysine residues.
Location of lysine residues (blue) of monomeric Survivin (grey) (PDB: 1XOX). K90, K91 and K103 are in close proximity to Survivin's NES (black).

The basic tweezer molecule binds surface accessible basic amino acids, preferably lysine residues. Survivin contains a total of 16 lysine residues, four of them located at the truncated part of the C-terminal α-helix and therefore not visible in the crystal structure of monomeric

Survivin (Figure 3.13). Most of Survivin's lysine residues are well accessible and sterically hardly shielded. However, lysines K90, K91 and K103 are particularly attractive since they reside within or are in very close proximity to the targeted NES and dimer interface.

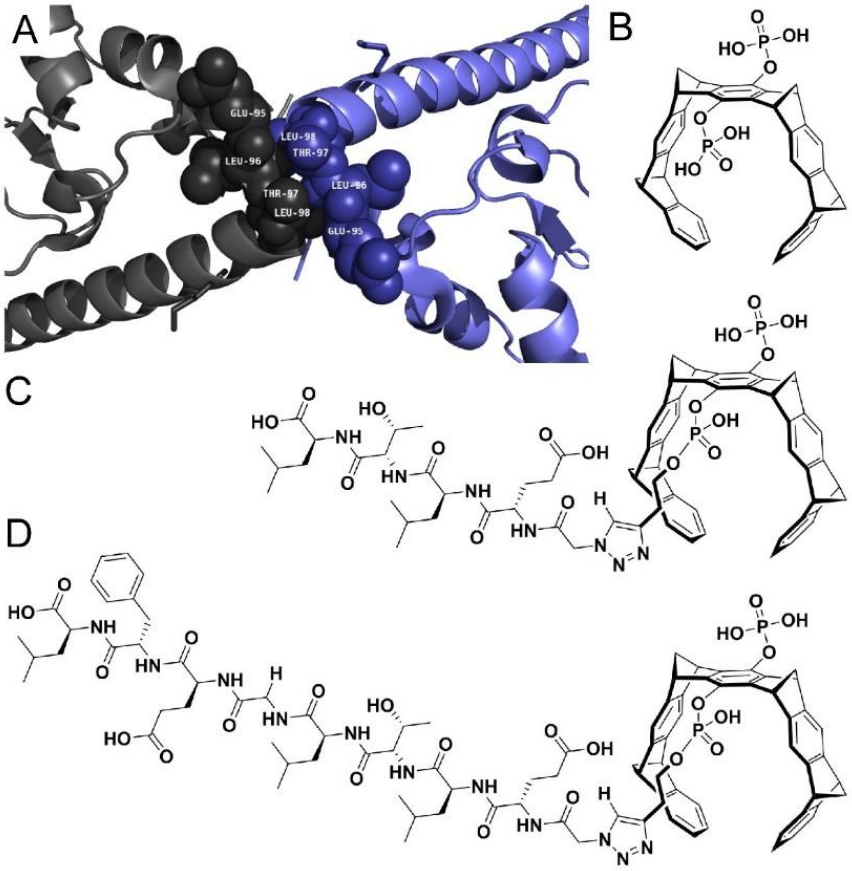

Figure 3.14: Design of new peptide-linked supramolecular tweezer molecules.
A) Representation of Survivin's dimer interface based on the dimeric Survivin structure (PDB: 1E31). Both monomers are depicted in black and blue interact mainly via the ELTL sequence (spheres) in the dimer interface. This peptide sequence, which is responsible for the interaction between two Survivin monomers, inspired the design of new tweezer molecules with a linked peptide as a second binding motif. The chosen anchor lysine residue K103 for the tweezer cavity is shown as a stick model in both monomers. **B)** Chemical structure of the unmodified basic molecular tweezer molecule. **C)** Chemical structure of an asymmetrical molecular tweezer molecule linked to the short peptide ELTL. **D)** Chemical structure of an asymmetrical molecular tweezer molecule linked to the elongated peptide ELTLGEFL.

For further design, K103 was chosen as the anchor lysine for the basic tweezer cavity. As a second binding motif, a peptide should be linked to the basic tweezer molecule, which mimics the dimer interface of the Survivin homodimer. As such, affinity and selectivity towards Survivin should be enhanced, and the NES would be shielded to avoid any

interaction with the export receptor CRM1. Two peptides with different lengths were selected, one short peptide (ELTL), which mimics the main overlapping interface between both monomers, and an elongated peptide (ELTLGEFL), which covers a larger region of the dimer interface and should provoke more pronounced effects compared to the short peptide (Figure 3.14). At its N-terminus, the peptides were linked to the basic molecular tweezer molecule via click chemistry.

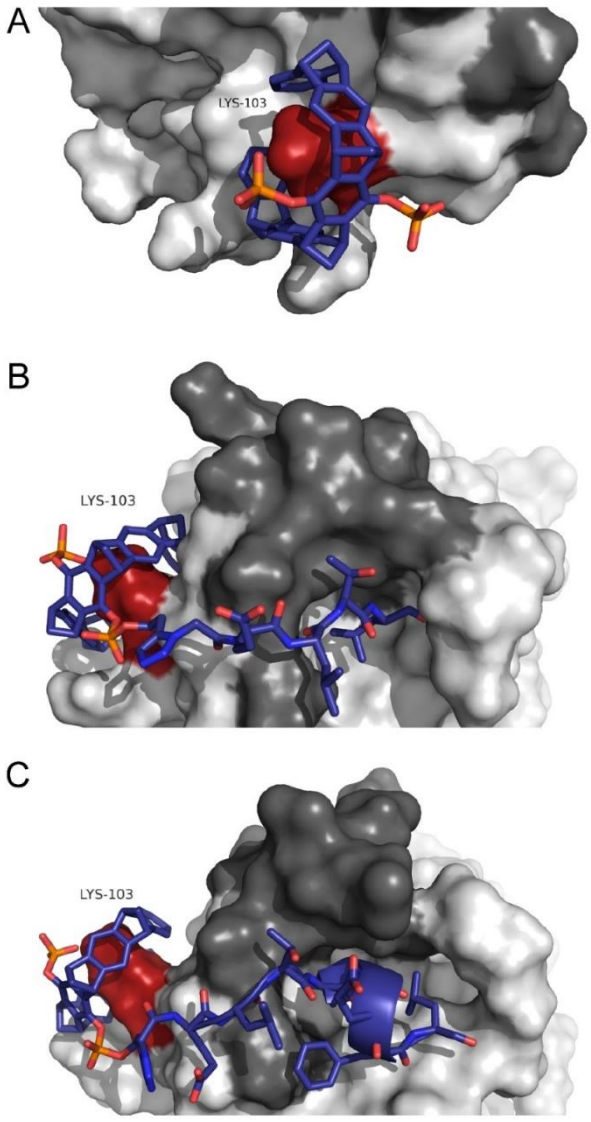

Figure 3.15: MD simulations of basic and newly designed peptide-linked molecular tweezer molecules bound to Survivin.

MD simulation results after 100 ns for the basic tweezer **(A)**, Tweezer-ELTL **(B)** and Tweezer-ELTLGEFL **(C)** binding to Survivin. The surface of Survivin, based on the monomeric structure in solution (PDB: 1XOX), is shown in light grey. Survivin's NES is depicted in dark grey. The tweezer molecules (blue) bind with their cavity to the anchor lysine residue K103 (red) on Survivin's surface (MD simulations and tweezer synthesis and provision for subsequent experiments by Christian Heid, Department of Organic Chemistry, Schrader group, University of Essen).

Before synthesis of these new peptide-linked tweezer molecules, MD simulations (100 ns, 300 K, 0.15 mM NaCl) were performed in cooperation with Christian Heid from the Department of Organic Chemistry (Schrader group, University of Essen) to study their binding properties to Survivin. The 100 ns-simulation (Figure 3.15) was based on the monomeric structure of Survivin in solution (PDB: 1XOX).
During the whole MD simulation time, the π-cation-interactions between K103 and the cavity of the different tweezer molecules were maintained. This indicated a strong complexation of K103 by each tweezer molecule. Additionally, the free negatively charged phosphate group interacted with the positively charged ammonium group of K103 and enforced binding. The linked peptides interacted with amino acid side chains of Survivin via hydrogen bonds. Thereby, they partly shielded the NES of Survivin during the whole simulation time. Within the elongated peptide ELTLGEFL, even intramolecular hydrogen bonds were formed, thus indicating the formation of a secondary α-helical structure. During the simulation time, an energy decrease could be observed, suggesting that the structure was running into a stable energetic minimum. Based on the MD simulation results that indicated a stable binding to Survivin's protein surface and a partial shielding of its NES, both newly designed peptide-linked tweezer molecules were synthesized by Christian Heid from the Department of Organic Chemistry (Schrader group, University of Essen) for experimental evaluation.

3.3.2 Characterization of binding affinities by isothermal titration calorimetry

To study the direct binding of the basic tweezer molecule and both newly synthesized peptide-linked tweezer molecules to Survivin120 and to determine binding affinities, ITC measurements were performed. Binding of the basic tweezer molecule was already observed in an initial ITC experiment (Figure 3.12). However, a suitable fitting model was difficult to determine, since several binding events occurred. Therefore, in contrast to the initial experiment, the unmodified tweezer molecule was now placed in the sample cell and subjected to stepwise titration with the protein Survivin120 (Figure 3.16).
An exothermic binding reaction was observed when titrating Survivin120 to a solution of basic tweezer molecule. The respective binding isotherm revealed a one-phase course. Correspondingly, this time a one-site model could be used to fit the experimental data. The resulting fit revealed a dissociation constant K_D of 29.6 µM.

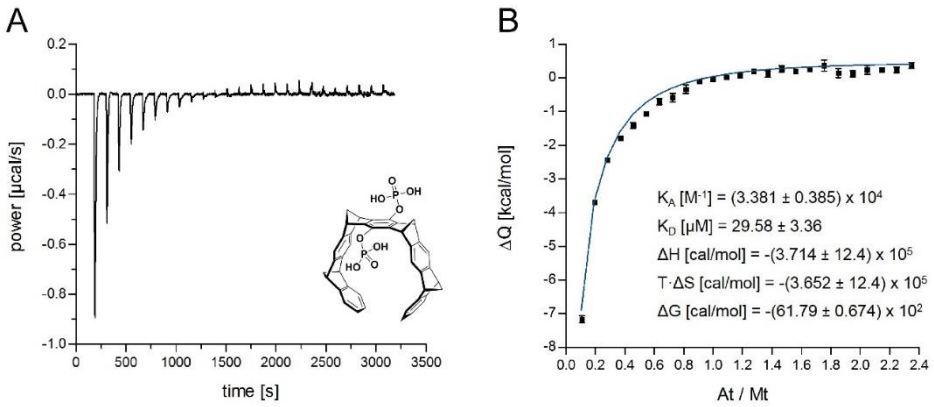

Figure 3.16: Verification of unmodified tweezer binding to Survivin120 via ITC.

For the ITC experiment, a solution of 100 µM unmodified tweezer molecule was placed in the sample cell and subjected to stepwise titration with 1.5 µl aliquots of a 1.2 mM solution of Survivin120 protein for a total of 25 injections at 25 °C using PBS pH 7.4. The equilibration time between two injections was 120 s. **A)** Raw heating power over time substracted by control heating power of Survivin120 titration into PBS, as well as the chemical structure of unmodified molecular tweezer. **B)** Fit of the integrated energy values normalized to injected Survivin120. The exothermic binding reaction displays a one-phase course hinting at a single binding event. Fitting of the ITC data to a one-binding-site model reveals a dissociation constant K_D of 29.6 µM (tweezer synthesis and data evaluation by Christian Heid, Department of Organic Chemistry, Schrader group, University of Essen).

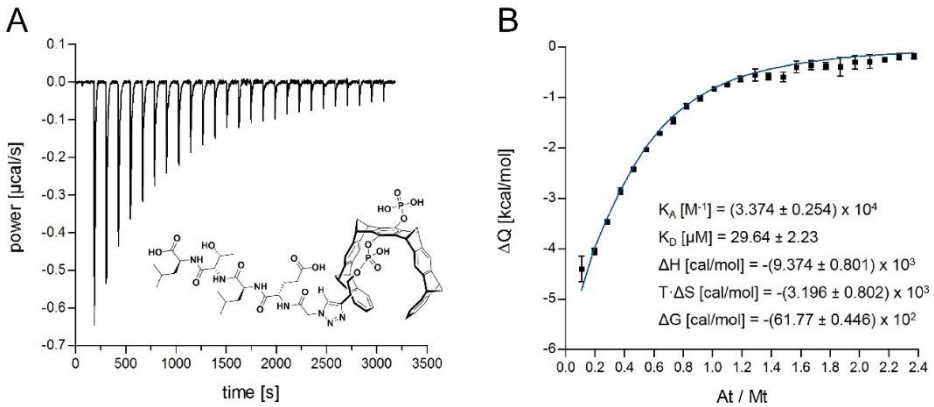

Figure 3.17: Verification of Tweezer-ELTL binding to Survivin120 via ITC.

For the ITC experiment, a solution of 100 µM Tweezer-ELTL molecule was placed in the sample cell and subjected to stepwise titration with 1.5 µl aliquots of a 1.2 mM solution of Survivin120 protein for a total of 25 injections at 25 °C using PBS pH 7.4. The equilibration time between two injections was 120 s. **A)** Raw heating power over time substracted by control heating power of Survivin120 titration into PBS, as well as the chemical structure of Tweezer-ELTL. **B)** Fit of the integrated energy values normalized to injected Survivin120. The exothermic binding reaction displays a one-phase course hinting at a single binding event. Fitting of the ITC data to a one-binding-site model reveals a dissociation constant K_D of 29.6 µM (tweezer synthesis and data evaluation by Christian Heid, Department of Organic Chemistry, Schrader group, University of Essen).

Survivin120 titrations to the short (Figure 3.17) and long (Figure 3.18) peptide-linked tweezer molecules also resulted in exothermic binding reactions. Their binding isotherms revealed one-phase courses, so that their data-points were fitted with a one-site model. The resulting dissociation constants were also a K_D of 29.6 µM for the short peptide-linked tweezer and a slightly lower K_D of 21.2 µM for the elongated peptide-linked tweezer.

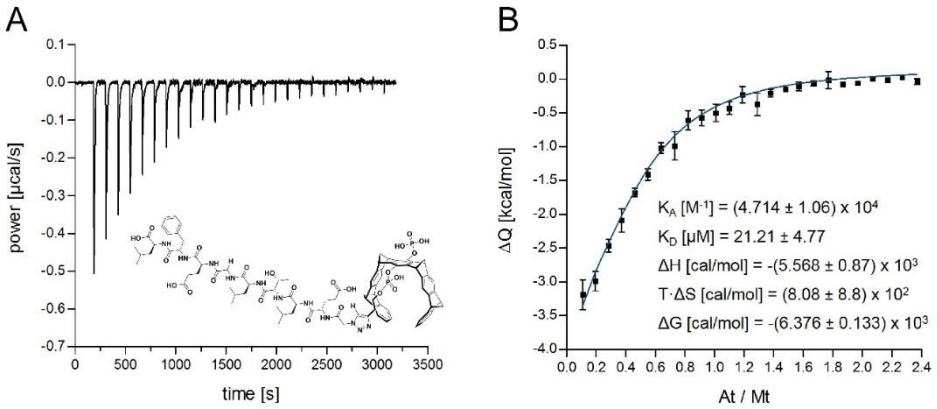

Figure 3.18: Verification of Tweezer-ELTLGEFL binding to Survivin120 via ITC.
For the ITC experiment, a solution of 100 µM Tweezer-ELTLGEFL molecule was placed in the sample cell and subjected to stepwise titration with 1.5 µl aliquots of a 1.2 mM solution of Survivin120 protein for a total of 25 injections at 25 °C using PBS pH 7.4. The equilibration time between two injections was 120 s. **A)** Raw heating power over time substracted by control heating power of Survivin120 titration into PBS, as well as the chemical structure of Tweezer-ELTLGEFL. **B)** Fit of the integrated energy values normalized to injected Survivin120. The exothermic binding reaction displays a one-phase course hinting at a single binding event. Fitting of the ITC data to a one-binding-site model reveals a dissociation constant K_D of 21.2 µM (tweezer synthesis and data evaluation by Christian Heid, Department of Organic Chemistry, Schrader group, University of Essen).

ITC measurements confirmed a direct binding of tweezer molecules to Survivin with affinities in the micro molar range. Whereas modification of the tweezer with the short peptide motif ELTL did not affect binding, the elongated peptide motif ELTLGEFL moderately enhanced binding affinity.

3.3.3 Mapping tweezer binding to Survivin by NMR titration experiments

Since the ^{1}H-^{15}N-BEST-TROSY-HSQC NMR spectrum of ^{15}N-labeled Survivin120 was already established (Figure 3.9), NMR titration experiments were used to analyze tweezer binding to Survivin (Dr. Christine Beuck, Department of Structural and Medicinal Biochemistry, Bayer group, University of Essen).

First, a ^{1}H-^{15}N-BEST-TROSY-HSQC NMR spectrum of a solution of 400 µM ^{15}N-labeled Survivin120 was recorded. Next, equimolar amounts of both the basic tweezer molecule and the short peptide-linked tweezer molecule were titrated to the Survivin solution, and ^{1}H-^{15}N-BEST-TROSY-HSQC NMR spectra were measured (Figure 3.19). Following signal correlation to Survivin's amino acid sequence, comparison of the corresponding spectra with and without tweezer including chemical shift perturbations and signal intensities allowed to determine the respective binding region. Thus, tweezer binding could indeed be mapped to specific amino acids in the Survivin sequence.

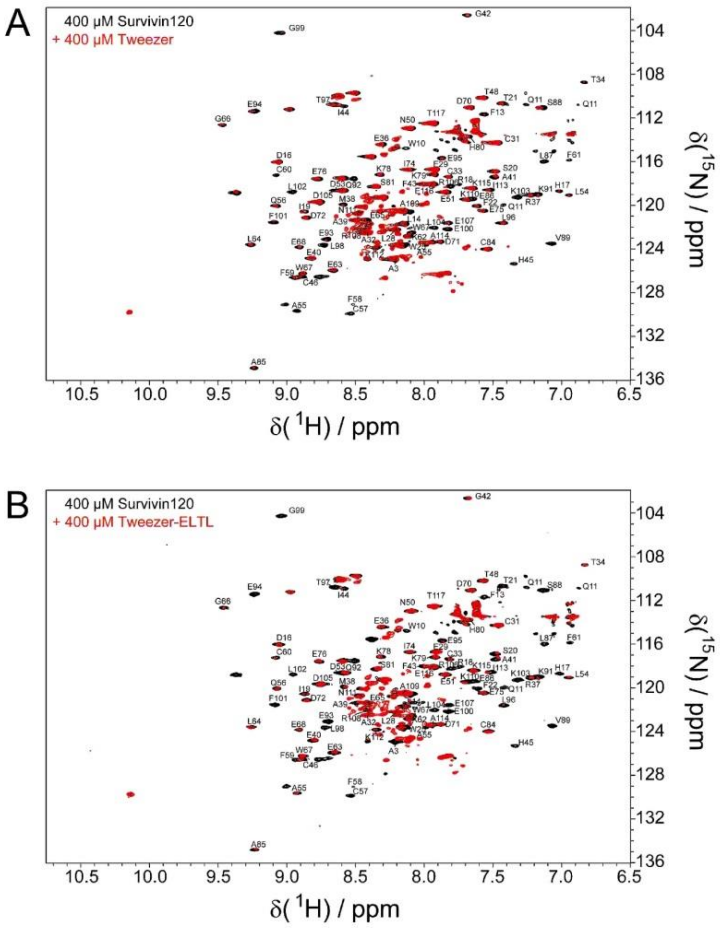

Figure 3.19: ^{1}H-^{15}N-BEST-TROSY-HSQC NMR spectra assignment of Survivin120 upon tweezer titrations.

^{1}H-^{15}N-BEST-TROSY-HSQC spectra of 400 µM ^{15}N-labeled truncated Survivin120 measured in NMR buffer with (red) and without (black) titration of 400 µM unmodified tweezer **(A)** and Tweezer-ELTL **(B)** are shown. A peak – amino acid residue assignment was possible for the resulting NMR signals. (^{15}N-labeled protein purification and NMR measurements by Dr. Christine Beuck, Department of Structural and Medicinal Biochemistry, Bayer group, University of Essen).

Chemical shift perturbations (Figure 3.20) and signal intensities (Figure 3.21) of each amino acid peak were plotted against the Survivin amino acid sequence for tweezer titrations.

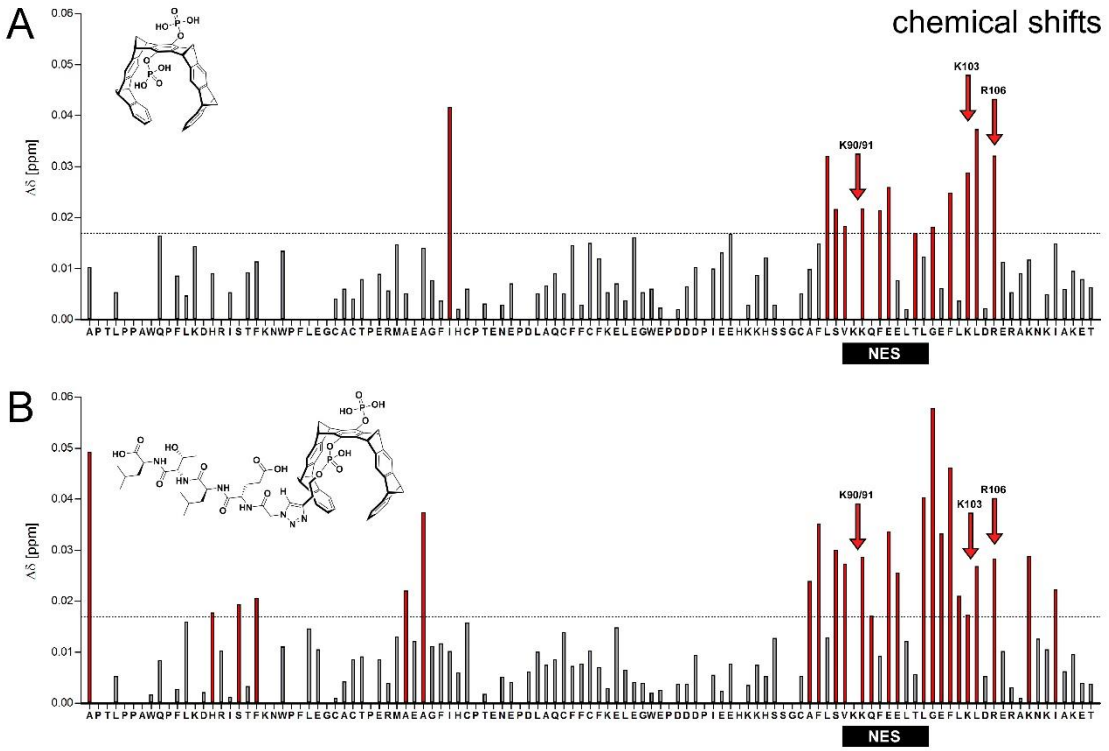

Figure 3.20: Chemical peak shift analyses allow to map binding of molecular tweezers to Survivin120.

^{1}H-^{15}N-BEST-TROSY-HSQC spectra of 400 µM ^{15}N-labeled Survivin120 titrated without and with either unmodified tweezer molecule **(A)** or Tweezer-ELTL **(B)** up to one equivalent. Chemical peak shifts are identified for each signal and plotted against the Survivin sequence (residues 2–117 as assigned in the data-base). The cutoff (dashed line) was arbitrarily set to 0.017 ppm. Chemical shifts exceeding the cutoff, are highlighted in red. Lysine and arginine residues with a prominent shift perturbation are clustered around Survivin's NES (black box) and marked with a red arrow (^{15}N-labeled protein purification and NMR measurements by Dr. Christine Beuck, Department of Structural and Medicinal Biochemistry, Bayer group, University of Essen).

Titration of the unmodified tweezer clearly resulted in chemical shift perturbations up to 0.04 ppm for the potential tweezer cavity binding sites K91, K103 and R106. Interestingly, more amino acids significantly shifted when the tweezer with the ELTL peptide was used. These not only included the potential tweezer-cavity binding sites K91, K103 and R106, but also amino acids in and near Survivin's NES, the latter also being part of its dimer interface located at the beginning of its C-terminal helix. This indicated that the modified ELTL-linked tweezer molecule was able to bind those regions more specifically. Since amino acid peaks

sometimes already shift in NMR, when ligands are rather just passing by and only interact for a very limited time, signal intensities were evaluated in addition. A decrease in signal intensity indicates for a robust and stable interaction.

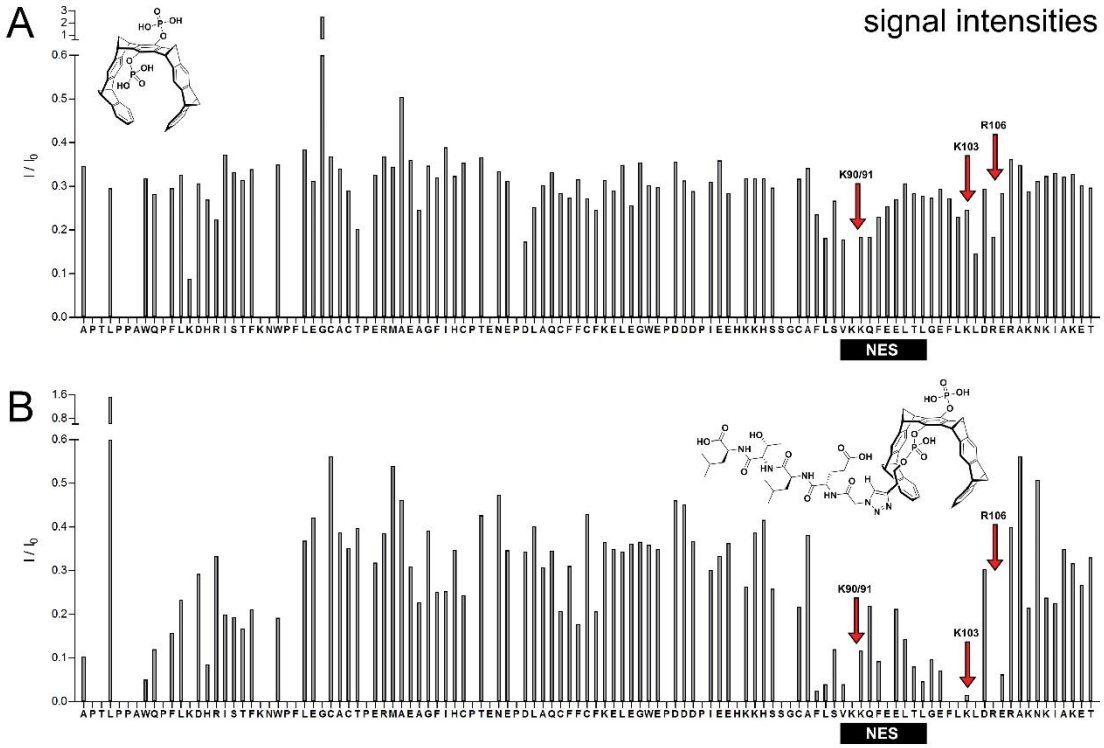

Figure 3.21: Signal intensity analyses allow to map binding of molecular tweezers to Survivin120.

^{1}H-^{15}N-BEST-TROSY-HSQC spectra of 400 µM ^{15}N-labeled Survivin120 titrated without and with either unmodified tweezer molecule **(A)** or Tweezer-ELTL **(B)** up to one equivalent. Normalized signal intensities for each signal are plotted against the Survivin sequence (residues 2–117 as assigned in the data-base). Lysine and arginine residues with a reduced intensity are present around Survivin's NES (black box) and marked with a red arrow. Especially upon titration with Tweezer-ELTL, signal intensities collapse around the NES region (^{15}N-labeled protein purification and NMR measurements by Dr. Christine Beuck, Department of Structural and Medicinal Biochemistry, Bayer group, University of Essen).

Following titration of the unmodified tweezer molecule, loss of signal intensity in the region around K90, K103 and R106, the potential binding sites for the tweezer cavity, was already observed. Likewise, titrating the ELTL-linked tweezer molecule resulted in strongly decreased signal intensities not only for K90/91, K103 and R106, but also for the complete NES region and the dimer interface. In line with the chemical shift perturbation analyses, the

modified tweezer molecule was demonstrated to indeed bind more specifically and with a higher affinity in the NES region compared to the unmodified tweezer.
NMR titration experiments thus allowed a precise mapping of the molecular tweezers, especially when modified with the short peptide ELTL, to specific basic amino acids (K90/91, K103 and R106) within or near Survivin's NES (Figure 3.22).

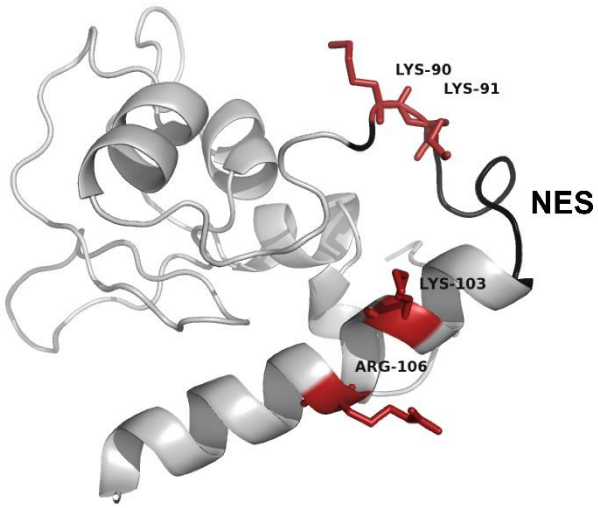

Figure 3.22: Shifting residues with reduced intensities mapped to the monomeric structure of Survivin.
Based on the monomeric structure of Survivin in solution (PDB: 1XOX), surface accessible lysine and arginine residues, which strongly shifted and had reduced intensities in NMR measurements upon tweezer titration, are highlighted in red. K90, K91, K103 as well as R106 are in close proximity to Survivin's NES (black).

Thus, results gained from NMR titration experiments were in perfect agreement with the initial design of the novel peptide-linked tweezer molecules, indeed targeting the basic amino acids initially chosen as anchor binding sites.

3.3.4 *In silico* analysis of tweezer binding to Survivin by MD and QM/MM studies

To confirm the experimental NMR results and to receive more detailed information about tweezer binding to Survivin, MD and QM/MM studies were performed in cooperation with Dr. Yasser B. Ruiz Blanco from the Department of Computational Biochemistry (Sánchez-García group, University of Essen).
Different complexes between four lysine residues (K23, K90, K91 and K103) and two tweezer molecules, the unmodified and the ELTL-linked tweezer, were analyzed for monomeric Survivin. As a starting point for the MD simulations, the tweezer cavity

complexed the lysine residue on Survivin's surface, respectively. Next, MD simulations were performed and the distance between the ammonium nitrogen of the lysine and the center of mass of the tweezer were measured over 16000 frames collected every 5 ps along the 80 ns of simulation, respectively (Figure 3.23).

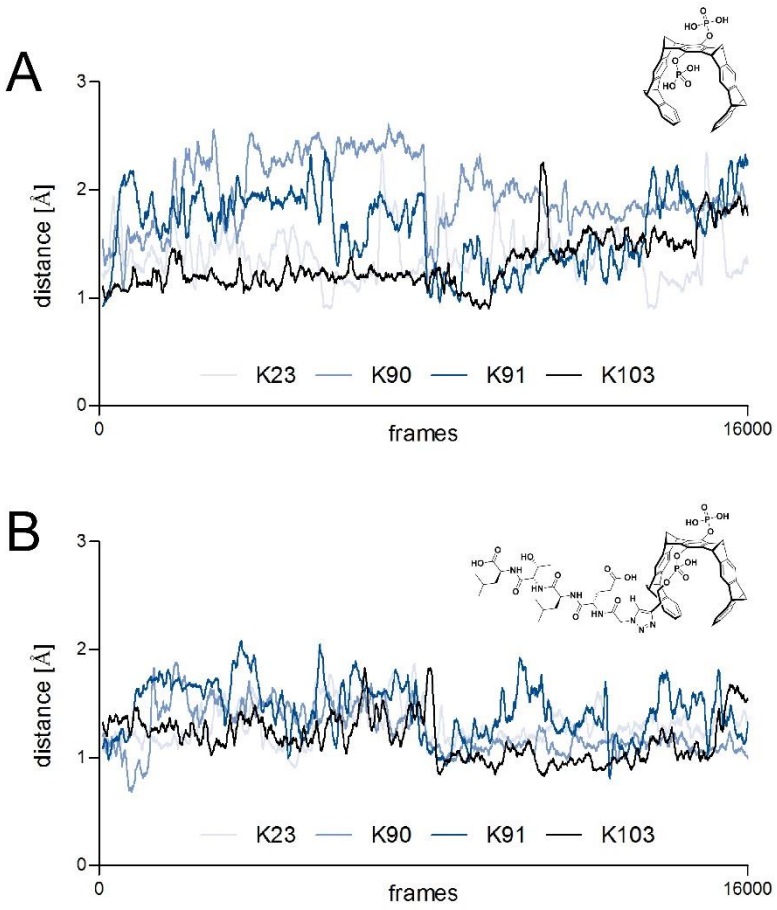

Figure 3.23: The unmodified and ELTL-linked tweezers form stable complexes with four lysine residues (K23, K90, K91 and K103) of monomeric Survivin.
Distance between the ammonium nitrogen of the respective lysine (K23, K90, K91 and K103) of Survivin monomer and the center of mass of Tweezer **(A)** or Tweezer-ELTL **(B)** over 16000 frames collected every 5 ps along the 80 ns of MD simulation (MD simulations by Dr. Yasser B. Ruiz Blanco, Department of Computational Biochemistry, Sánchez-García group, University of Essen).

The distance fluctuations did not surpass 1 Å in most parts of the trajectories, which evidenced the stability of the complexes. Moreover, Tweezer-ELTL showed a lesser amplitude in the fluctuations, which suggest that the interactions of the linked peptide served to stabilize the conformation of the inclusion complexes. Such more rigid binding might be responsible for the larger effects on the NMR shifts (Figure 3.20) produced by this tweezer. However, during the simulations, permanent and specific interactions of the peptide tail of Tweezer-ELTL with a distinct protein region were not detected. Nevertheless, one unique

long-lasting interaction between the tail of Tweezer-ELTL and the homologous segment in the protein (E95–L98) took place when the complex was located on K103 (Figure 3.24). This particular site, found upstream along the ELTL sequence, was the only one among the studied sites that permitted the anti-parallel pairing observed in the original binding mode of the Survivin dimer. The other sites did not show any sustainable binding mode that could resemble the interface of the Survivin dimer structure. Despite the effective anti-parallel binding between the fragment E95 to L98 of Survivin and the tail of Tweezer-ELTL linked to K103, this interaction was not stable over the whole simulation time. Nonetheless, the arrangement was preserved for about 10 ns, which indicated that this binding mode populates a region of low energy content in the potential energy surface of this system.

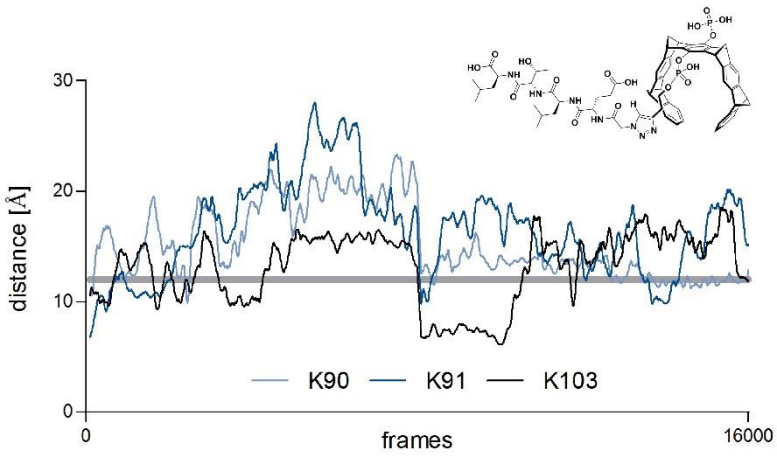

Figure 3.24: The peptidic tail of Tweezer-ELTL shows a long-lasting binding mode that resembles the anti-parallel binding of the Survivin dimer, uniquely when located at lysine residue K103 of monomeric Survivin.

Distance between the centers of masses of the peptide tail of Tweezer-ELTL and the analogous segment of monomeric Survivin associated to residues E95 to L98 over 16000 frames collected every 5 ps along the 80 ns of MD simulation. The gray bar located at a distance of 12 Å represents a cutoff above which no effective interaction occurs (MD simulations by Dr. Yasser B. Ruiz Blanco, Department of Computational Biochemistry, Sánchez-García group, University of Essen).

Furthermore, the results of the QM/MM optimizations (Table 3.1) conclude for monomeric Survivin that K23 is the least favored site for tweezer binding. This matches the effects of the NMR signals and is an evidence of the role of addtional interactions between the protein and the tweezers in the region that gathers the sites K90, K91, K103 and the interfacial segment in the dimer structure. Moreover, the complex of Tweezer-ELTL on site K103 resulted the one with the lowest energy content which can obey to the more effective binding of its tail to the analogous peptide segment in the protein.

Table 3.1: The calculated QM/MM energies for all analyzed tweezer–lysine complexes.
(QM/MM study by Dr. Yasser B. Ruiz Blanco, Department of Computational Biochemistry, Sánchez-García group, University of Essen).

Complex	Energy [AU]	Relative energy [kcal/mol]	Error [kcal/mol]
Tweezer – K90	-3036.18	0	2.1
Tweezer – K91	-3036.16	17.6	3.7
Tweezer – K103	-3036.16	18.3	6.1
Tweezer – K23	-3036.10	54.3	5.7
Tweezer-ELTL – K103	-5147.89	0	2.8
Tweezer-ELTL – K91	-5147.87	9.4	13.2
Tweezer-ELTL – K90	-5147.84	28.5	4.3
Tweezer-ELTL – K23	-5147.77	71.8	3.1

Regarding Tweezer-ELTL, the interactions were more differentiated between lysine residues and the inclusion complexes were more fixed compared to unmodified tweezer, indicating a higher specificity for the ELTL-linked tweezer molecule and therefore confirming the NMR titration results (Figure 3.20 and Figure 3.21). However, the larger effects of Tweezer-ELTL over the NMR signals did not seem to obey a specific strong conserved interaction of the peptide substituent ELTL with the protein. Instead, the additional number of interactions due to the additional peptide could exert a cooperative effect leading to a higher specificity of Tweezer-ELTL compared to unmodified tweezer, thus maximizing the effect over the sites. With the monomeric form of the protein, the complexes formed on sites K90, K91 and K103 possessed lower energy content than the separated K23, which agreed with the magnitude of the effects over the NMR signals and confirmed the monomeric form during the NMR experiments. The design of the ELTL-linked tweezer, whose peptide emulates the interface of the dimer structure, permitted that at least the complex on K103 could adopt a binding conformation that closely resembles the original interface of the dimer. This structure, although not preserving over the whole simulation, represented the only long-lasting arrangement for approximately 10 ns observed in the trajectories. Thus, it is expected to contribute significantly on the properties of the complex between Tweezer-ELTL and K103 and its differentiation with those on the other sites.

However, results for monomeric Survivin showed stable complexation with both lysine residues K90 and K91, thus requiring further analysis whether Tweezer-ELTL is able to

distinguish between the adjacent lysine residues. For a complete assignment of the NMR data, the arginine residues or at least R106 should be also considered in the calculations. Furthermore, the elongated ELTLGEFL-linked tweezer has to be analyzed by MD and QM/MM studies as well as experimental NMR titration experiments checking for an enhanced affinity, stability and specificity of its binding to Survivin compared to Tweezer-ELTL.

3.3.5 Influence of tweezer molecules on Survivin's folding and dimerization

Following proof of tweezer binding to Survivin by ITC and mapping the tweezer binding site to specific basic amino acids by NMR, the influence of the tweezer molecules on Survivin folding and dimerization was investigated.

To analyze potential effects on secondary structure, Survivin120 was incubated with 100 µM of each tweezer molecule for 30 min on ice and subjected to CD measurements (Figure 3.25 B). Survivin120 without tweezer incubation served as a control, and additional CD spectra of all three different tweezer molecules were recorded separately (Figure 3.25 A). This allowed to exclude any potential effects caused by the tweezer molecules, especially those which are peptide-linked.

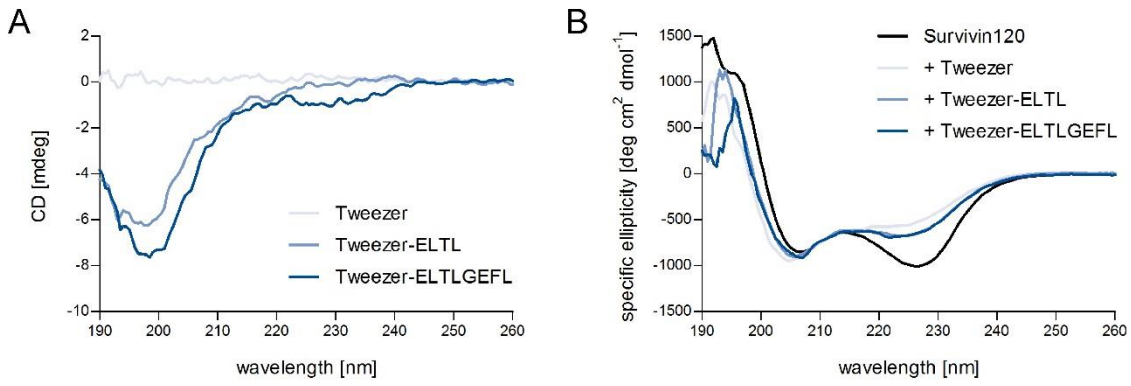

Figure 3.25: Far-UV CD measurements allow investigation of tweezer effects on Survivin's secondary structure.

A) While the far-UV CD spectrum for the basic tweezer shows no extrema, both spectra of the peptide-linked tweezers exhibit a minimum at around 200 nm hinting towards a random coil arrangement. **B)** The far-UV CD spectrum of tag-free Survivin120 (black) changes upon 100 µM tweezer pre-incubation. The ellipticity of the minima at 227 nm clearly increases, indicating a change in secondary structure of Survivin120. All spectra were recorded at 20 °C in 20 mM phosphate buffer containing 10 µM Zn^{2+}.

The CD spectrum of the basic molecular tweezer (Figure 3.25 A) showed no differences compared to the buffer baseline. However, both spectra of the peptide-linked tweezer molecules exhibited a minimum at around 200 nm. The minimum at around 200 nm is a typical signal for random coil arrangements, which are no defined structural elements but rather a conformation with a random orientation. These random coil signals were caused by the peptides, which were linked to the basic tweezer molecule. The spectrum of the elongated peptide even exhibited a slight minimum at around 225 nm, indicating the formation of a secondary α-helical structure. This observation matched with the MD simulation result (Figure 3.15 C). All secondary structures, stemming from the individual tweezer molecules themselves, were subtracted from the CD spectra for Survivin120 incubated with the respective tweezer molecule.

Nevertheless, changes in the CD spectrum and therefore in the secondary structure of Survivin120 could be observed upon incubation with all tweezer molecules (Figure 3.25 B). The ellipticity of the minimum at 227 nm increased upon tweezer binding. This shift led to a lower minimum at 207 nm compared to 227 nm and therefore definitely to a change in Survivin's secondary structure. The data suggest that tweezer binding results in a lower content of α-helical structures.

Although tweezer molecules influenced Survivin's secondary structure, they did not denature the protein. The CD spectra showed that Survivin retained a defined secondary structure and was not randomly folded.

To analyze the influence on dimerization, Survivin120 was incubated with 100 µM of each tweezer molecule, with the control peptide ELTL or without tweezer for at least 1 h on ice, and analytical gel filtration experiments were performed (Figure 3.26).

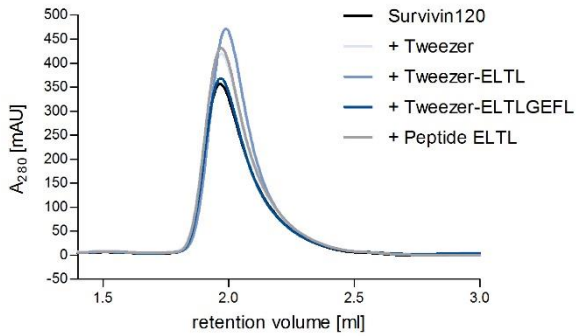

Figure 3.26: Analytical gel filtration allow investigation of tweezer effects on Survivin's dimerization.

Analytical gel filtration absorbance chromatograms of Survivin120 without (black) or with pre-incubation of 100 µM tweezers (blue) and peptide (grey) measured at 280 nm on a Superdex 200 Increase column reveal that ligand pre-incubation does not affect the retention volume of Survivin120.

As chromatograms revealed no changes in the retention volume of Survivin120 independently of tweezer or peptide pre-incubation, tweezer binding had either no influence on Survivin's dimerization or was not stable in the experimental setup. Binding affinities might be too weak to induce measurable effects in gel filtration experiments because of the strong dilution of the tweezer molecules during the run.

3.4 Study of export complex assembly *in vitro*

Expression and purification of both other export complex members, the export receptor CRM1 and its cofactor Ran in its constitutive active GTP-bound variant RanQ69L, enabled the study of export complex assembly *in vitro*.

3.4.1 Purification and characterization of export complex members

Following transformation of the expression strain *E. coli* SoluBL21 with the prokaryotic expression vector pET41-GST-PreSc-CRM1 for expression of the receptor protein and pET41-GST-PreSc-RanQ69L for expression of the cofactor protein, four liters of bacterial culture were harvested, respectively. The purification of one batch for each protein is shown exemplarily. Cell disruption by sonication was followed by centrifugation to separate cell debris from the soluble protein fraction. The fused GST-tag allowed GSH affinity chromatography as a first purification step. After several washing steps, the GST-tag could be cleaved on column by loading recombinantly expressed and purified PreScission protease (appendix A.1), followed by an overnight incubation. The next day, the cleaved protein products, either CRM1 (Figure 3.27) or RanQ69L (Figure 3.28), were transferred onto an ion exchange chromatography column.

CRM1 eluted at a retention volume of 28.1 ml and 23.5 % buffer B, which corresponded to a salt concentration of roughly 260 mM NaCl. The purity and protein content of the collected fractions F11–F15 were controlled by SDS-PAGE. Considering both, purity and protein amount, fractions F11–F13 were pooled, concentrated to 37.7 mg/ml and stored at -80 °C. Finally, the GSH affinity column was regenerated with 10 mM GSH elution buffer. Samples of each purification step were analyzed by SDS-PAGE to control the purification process (Figure 3.29 A).

RanQ69L eluted at a retention volume of 20.7 ml and 13.7 % buffer B, which corresponded to a salt concentration of roughly 162 mM NaCl. The purity and protein content of the collected fractions F7–F12 was controlled by SDS-PAGE. Considering both, purity and protein amount, fractions F7–F10 were pooled, concentrated to 1.8 mg/ml and stored at -80 °C. Finally, the GSH affinity column was regenerated with 10 mM GSH elution buffer.

Samples of each purification step were analyzed by SDS-PAGE to control the purification process (Figure 3.29 B).

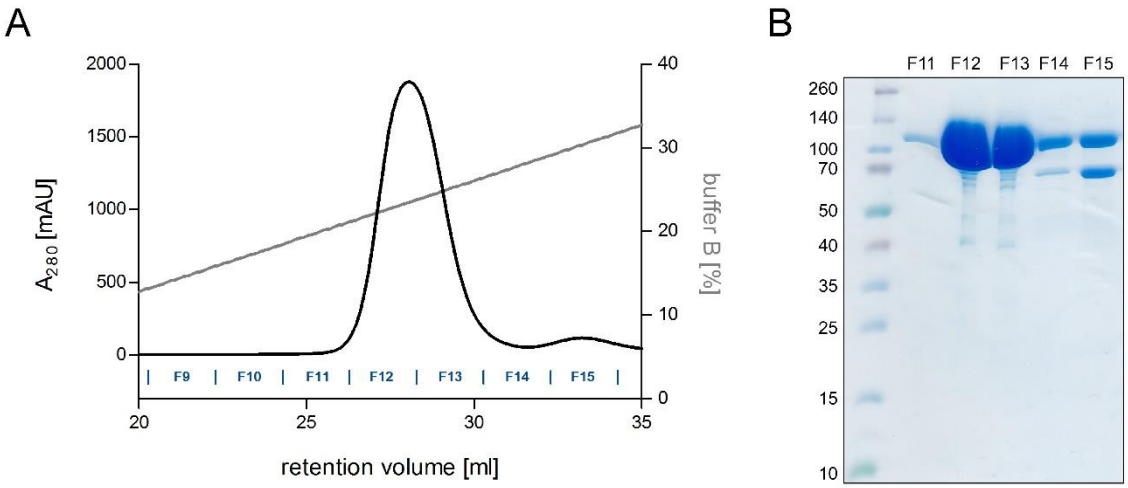

Figure 3.27: Purification of CRM1 by ion exchange chromatography.

A) Absorbance chromatogram at 280 nm of the ion exchange chromatography following GSH affinity purification and GST-tag cleavage. The elution gradient (0–100 % ion buffer B, 25 mM to 1 M NaCl, 75 ml, grey) and the collected elution fractions (F9–F15, blue) are included. **B)** Coomassie-stained SDS gel of protein-containing elution fractions. Fractions F11–F13 containing CRM1 with few impurities were pooled, concentrated and used for subsequent experiments.

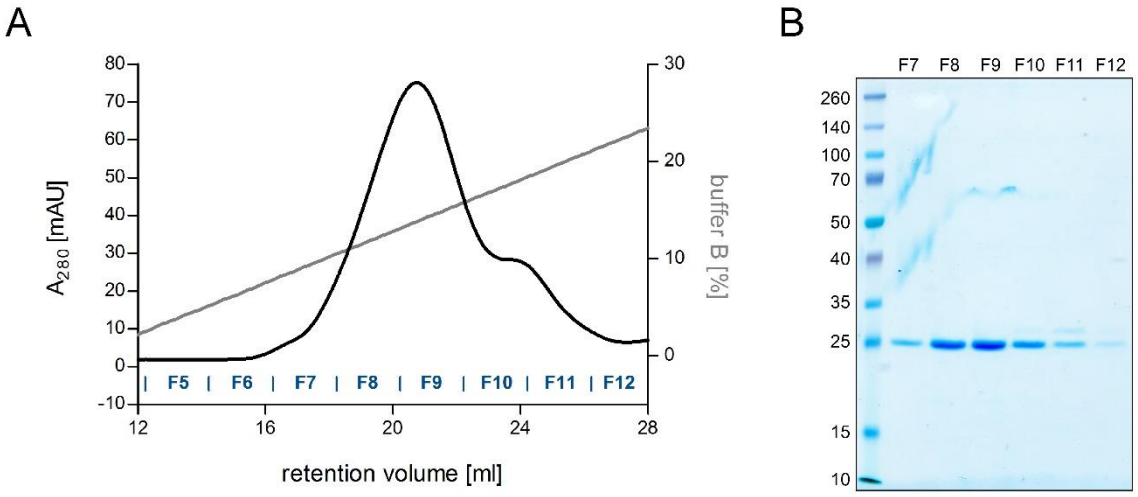

Figure 3.28: Purification of RanQ69L by ion exchange chromatography.

A) Absorbance chromatogram at 280 nm of the ion exchange chromatography following GSH affinity purification and GST-tag cleavage. The elution gradient (0–100 % ion buffer B, 25 mM to 1 M NaCl, 75 ml, grey) and the collected elution fractions (F5–F12, blue) are included. **B)** Coomassie-stained SDS gel of protein containing elution fractions. Fractions F7–F10 containing RanQ69L with few impurities were pooled, concentrated and used for subsequent experiments.

During the purification procedure, a portion of both expressed proteins, CRM1 and RanQ69L, were detected in the insoluble protein fraction after centrifugation, ended up in the flow through and wash fractions or remained on the GSH affinity column as uncleaved or cleaved protein. However, purity of CRM1 as well as RanQ69L could finally be assigned to more than 95 %, only a few impurities were detectable in the final IEC fractions. The overall protein yield amounted to 2.4 mg per liter of bacterial culture for CRM1 and 0.1 mg per liter of bacterial culture for RanQ69L.

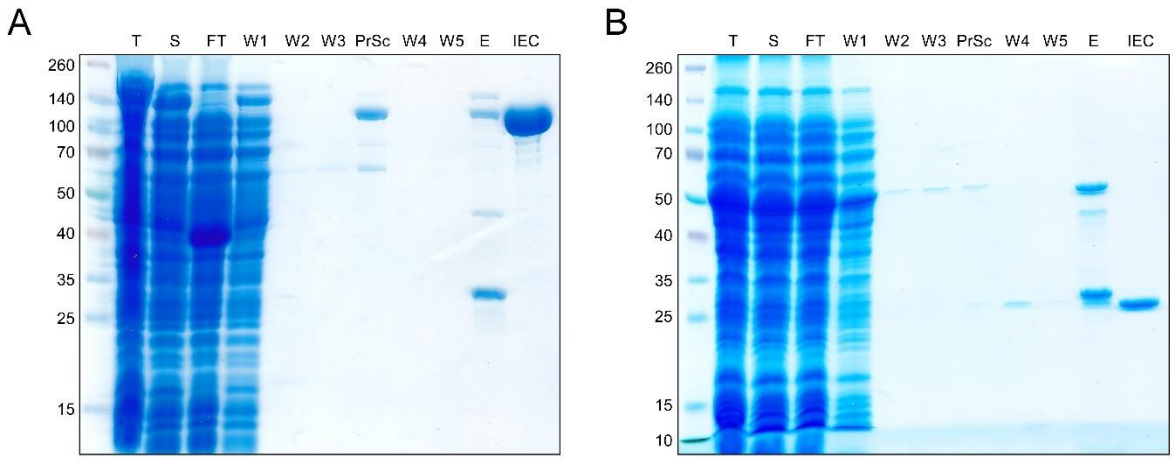

Figure 3.29: Overview of the purification procedure of CRM1 and RanQ69L.
Coomassie-stained SDS gels of samples taken after the respective CRM1 **(A)** and RanQ69L **(B)** protein purification steps (T: total lysate, S: supernatant, FT: flow through of GSH column loading, W1–W3: wash fractions after loading the GSH column, PrSc: flow through of PreScission protease loading onto the GSH column, W4–W5: flow through of rinsing protein from the GSH column onto an ion exchange column, E: final GSH-elution of GSH column, IEC: pooled and concentrated protein after ion exchange chromatography).

Additionally, for all recombinantly expressed and purified export complex members, the export receptor CRM1, its cofactor RanQ69L as well as the cargo protein Survivin in its full-length and truncated form, a Coomassie-stained SDS-PAGE gel as well as a specific immunoblot staining were performed (Figure 3.30).
In analogy to the cargo protein Survivin (full-length and truncated), the other purified export complex members were characterized in more detail by CD spectroscopy (Figure 3.31 A) and analytical gel filtration (Figure 3.31 B) to ascertain their correct protein folding and size.
The CD spectra of CRM1 and RanQ69L also exhibited two minima at 209 nm and 222 nm for CRM1 and at 207 nm and 218 nm for RanQ69L with equal ellipticity, plus a maximum at 192 nm for CRM1 and at 190 nm for RanQ69L. These correlated with the minima at 208 nm

and 225 nm and the maximum at 192 nm of the α-helix spectrum. Thus, both other export complex members can also be considered as correctly folded.

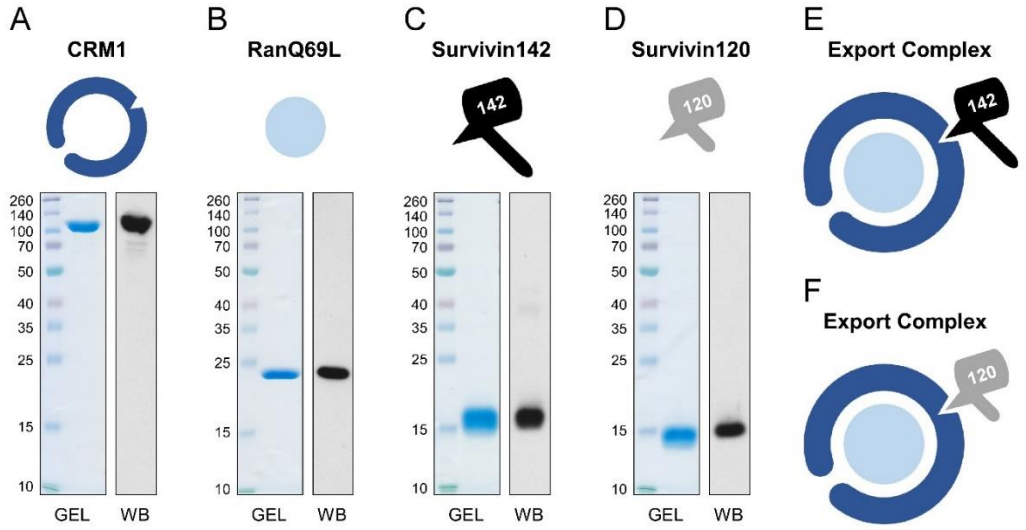

Figure 3.30: Representation of all recombinantly expressed and purified export complex members.

Coomassie-stained SDS-PAGE gels and specific immunoblot results of purified export receptor CRM1 **(A)**, cofactor protein small GTPase RanQ69L **(B)**, cargo protein Survivin142 **(C)** and cargo protein Survivin120 **(D)**. Schematic representation of assembled export complex with Survivin142 **(E)** or Survivin120 **(F)** as cargo protein.

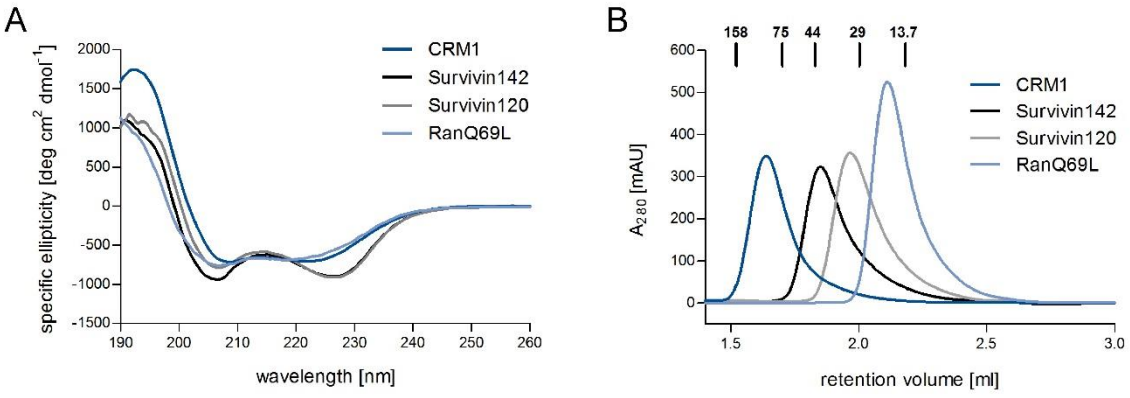

Figure 3.31: Far-UV CD spectra and analytical gel filtration of export complex members.

A) Far-UV CD spectra of all tag-free export complex members, recorded at 20 °C in 20 mM phosphate buffer containing 10 µM Zn^{2+}, hint at correctly folded proteins. **B)** Analytical gel filtration absorbance chromatograms measured at 280 nm on a calibrated Superdex 200 Increase column reveal that the actual protein sizes of CRM1 and RanQ69L match the theoretical molecular weight of their monomers while the actual protein sizes of full-length Survivin142 and truncated Survivin120 correspond the theoretical weight of their homodimer.

Analytical gel filtration revealed the actual protein sizes of CRM1 and RanQ69L. CRM1 eluted between the calibration proteins aldolase (158 kDa) and conalbumin (75 kDa). This observation matched CRM1's theoretical molecular weight of 123.5 kDa. RanQ69L eluted between the calibration proteins carbonic anhydrase (29 kDa) and ribonuklease A (13.7 kDa). Again, this matched RanQ69L's theoretical molecular weight of 24.6 kDa. The chromatograms of full-length and truncated Survivin are displayed to compare their size to CRM1 and RanQ69L. The fact that both Survivin variants eluted earlier than RanQ69L indeed confirmed their homodimerization in solution. Monomeric forms would elute later than RanQ69L.

3.4.2 Export complex assembly *in vitro*

In the context of the cell, Survivins's dual role crucially depends on its binding to the export receptor CRM1. As such, modulation of Survivin's functions can be achieved by targeting this interaction. To test if the tweezer molecules, which bind to Survivin within or near its NES, are also able to functionally influence the Survivin–CRM1 interaction, novel quantitative *in vitro* assays need to be established.

3.4.2.1 Analysis of complex assembly by gel filtration experiments

One method to analyze the assembly of the export complex consisting of the export receptor CRM1, its cofactor RanQ69L and Survivin is the analytical gel filtration. Since this method distinguishes between different proteins based on their molecular weight, an assembled protein complex should be identified by a lowered retention volume compared to its single protein members. Export complex formation with full-length (Figure 3.32 A) and truncated Survivin (Figure 3.32 B) were analyzed by analytical gel filtration in comparison to the export complex members on their own. Therefore, the same amount of export complex members was mixed in a molar ratio of 1:6:9 CRM1:RanQ69L:Survivin and allowed to assemble over an incubation time of at least 1 h. As a cofactor for RanQ69L, 2 mM dGTP were added to the mixture.

Both gel filtration chromatograms showed three peaks for the complex mixtures. Those corresponded to those for the single complex members. The prominent additional peak at a retention volume of 2.58 ml represented the elution of dGTP, which also gives a signal in the UV 208 lane. The absence of peak shifts and additional peaks at a low retention volume suggests that formation of the export complex was unsuccessful for both Survivin variants. Explanations could be that on the one hand, no export complex was formed and on the other hand export complexes were formed in the mixture but were not stable in the chosen gel

filtration method. The binding affinities might be too weak to be stable enough in the experimental setup because of sub-optimal salt concentrations and pH or simply because of the high dilution during the run. Moreover, the separation potential of the used column might be unsuited for the detection of the complex and therefore the column might not be able to distinguish little molecular weight changes in the elution range of CRM1 and the potentially formed complex.

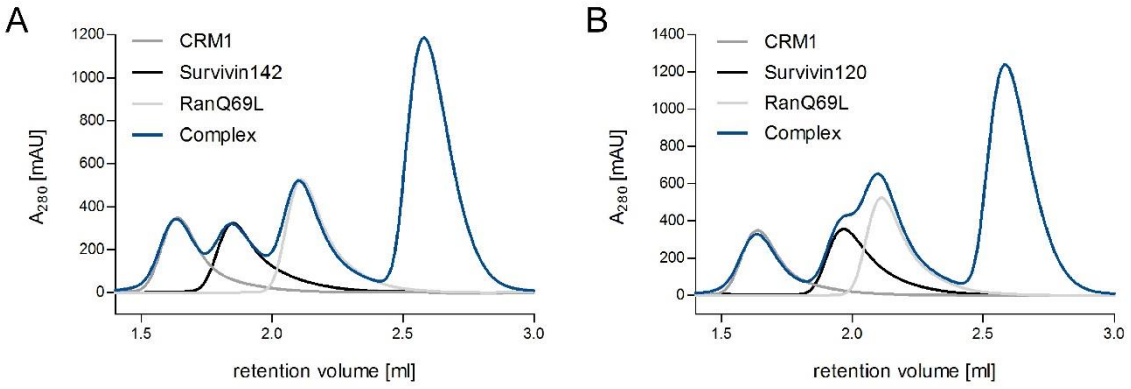

Figure 3.32: Analytical gel filtration allows analysis of export complex assembly.
Analytical gel filtration absorbance chromatograms are measured at 280 nm on a Superdex 200 Increase column. Chromatograms for all export complex members alone are shown together with the chromatogram for a mixture of export complex proteins and an excess of 2 mM cofactor dGTP. Proteins are mixed in a molar ratio of 1:6:9 CRM1:RanQ69L:Survivin. An additional peak at a low retention volume, indicating an export complex formation for wild type Survivin142 **(A)** or truncated Survivin120 **(B)**, does not appear.

3.4.2.2 Analysis of complex assembly by pull-down experiments

Since gel filtration obviously was not the right method to observe export complex assembly, a pull-down assay should be established. Here, a strong dilution of the proteins could be avoided, and less sample material was needed. Moreover, immunoblotting is a very specific and sensitive detection method for visualization of proteins.
CRM1 was chosen as bait protein in the pull-down assay because it directly interacts with both other export complex members. Moreover, as the export member with the highest molecular weight, it should not be drastically influenced in its conformation by fusion to the affinity tag GST. GST-CRM1 was expressed and purified (Sichelschmidt, 2016) similar to tag-free CRM1 (appendix A.2), just omitting GST-tag cleavage by the PreScission protease. The recombinantly expressed and purified bait protein was incubated with the other recombinantly expressed and purified export members, the cofactor RanQ69L and the prey

protein Survivin in its full-length and truncated form, respectively. With GSH-Sepharose beads, GST-CRM1 was pulled out of the solution and immunoblotting was performed for all export complex proteins (Figure 3.33). A sample lacking the bait protein GST-CRM1 should control for any unspecific binding to the beads.

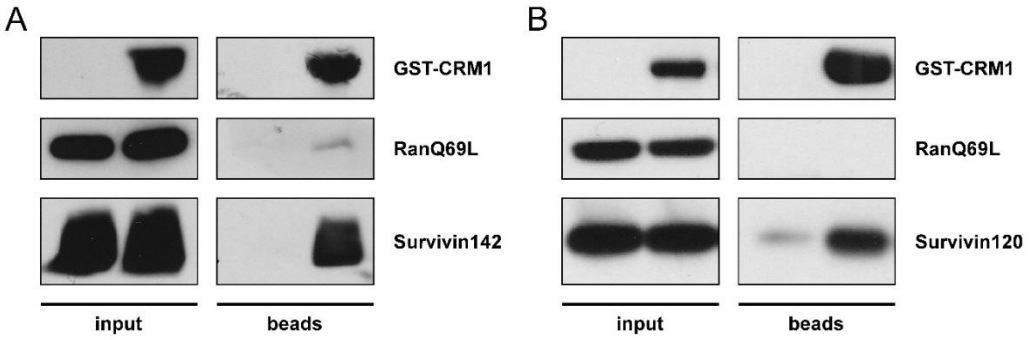

Figure 3.33: Export complex assembles *in vitro*.
Recombinant GST-CRM1 bait protein was incubated with either recombinant wild type Survivin142 **(A)** or truncated Survivin120 **(B)** in the presence of recombinant RanQ69L and dGTP to allow export complex assembly. GST-CRM1 as well as interacting proteins were pulled out of solution by GSH-Sepharose beads and a mixture without GST-CRM1 was used as control. Proteins present in the input and beads samples were analyzed via immunoblotting with antibodies specific for GST, Ran or Survivin.

The bait protein GST-CRM1 as well as both prey proteins Survivin142 and Survivin120 were pulled out of solution successfully. In contrast, controls lacking the bait protein showed no or only minor amounts of Survivin protein binding to the beads, indicating that Survivin did not bind unspecifically.
Furthermore, it was tested if CRM1 is also able to complex with Survivin even in the presence of other potential cargo proteins as present in total cell lysates.Therefore, wild type Survivin protein bearing a HA-tag at its C-terminus and two Survivin mutants with mutations in the NES region (NESmut-L96AL98A) and dimer interface (DIMmut-F101AL102A), which should have a reduced binding affinity to CRM1, were overexpressed in the eukaryotic cell line 293T. Cell lysates were incubated with the bait protein GST-CRM1 and its cofactor RanQ69L and subjected to a pull-down assay (Figure 3.34).
The bait protein GST-CRM1, its cofactor RanQ69L as well as the prey proteins wild type Survivin142-HA and both Survivin mutants could be successfully detected on the beads in contrast to the controls. However, binding was significantly reduced for the Survivin mutants where the NES and the dimer interface responsible for CRM1-binding were mutated.
To conclude, both pull-down assays, *in vitro* and from whole cell lysates, were suitable to assess the Survivin–CRM1 interaction.

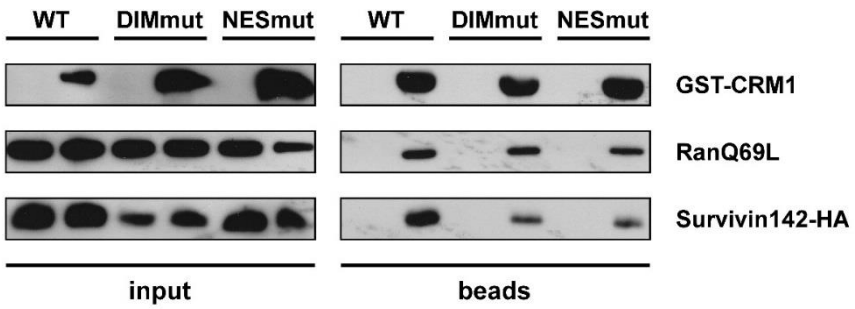

Figure 3.34: Binding of CRM1 to Survivin appearing even in the presence of other potential cargo proteins is counteracted by mutations of Survivin's NES or dimerization interface.
Recombinant GST-CRM1 bait protein was incubated in 293T cell lysate with either overexpressed wild type Survivin142-HA, mutated Survivin142-F101AL102A-HA (DIMmut) or mutated Survivin142-L96AL98A-HA (NESmut) in the presence of recombinant RanQ69L and dGTP to allow export complex assembly. GST-CRM1 as well as interacting proteins were pulled out of solution by GSH-Sepharose beads and a mixture without GST-CRM1 was used as control. Proteins present in the input and beads samples were analyzed via immunoblotting with antibodies specific for GST, Ran or HA.

3.4.3 Effects of supramolecular binding on export complex assembly

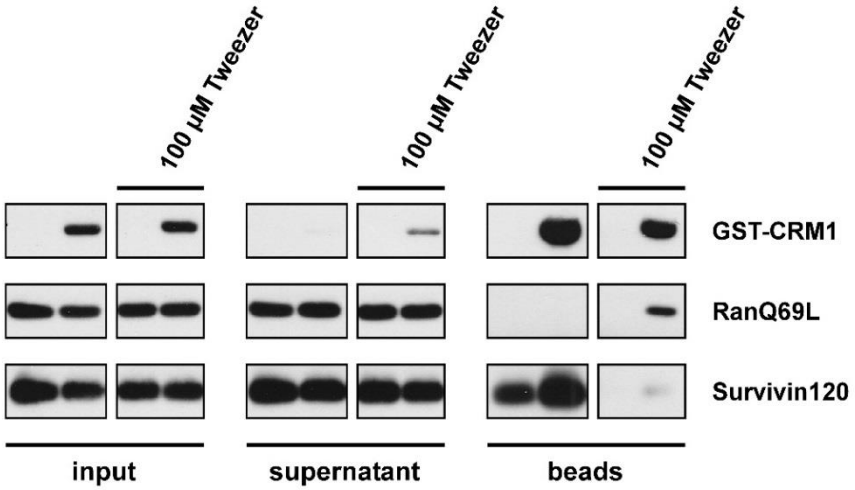

Figure 3.35: The basic tweezer molecule interferes with export complex assembly *in vitro*.
Recombinant Survivin120 prey protein was pre-incubated with a 100 µM solution of the basic tweezer molecule. Next, recombinant GST-CRM1 bait protein was mixed with either pre-incubated or pure prey protein Survivin120 in the presence of recombinant RanQ69L and dGTP to allow export complex assembly. GST-CRM1 as well as interacting proteins were pulled out of solution by GSH-Sepharose beads and a mixture without GST-CRM1 was used as control. Proteins present in the input, supernatant and beads samples were analyzed via immunoblotting with antibodies specific for GST, Ran or Survivin.

Since the pull-down assay now enables robust assessment of the Survivin–CRM1 interaction, effects of the unmodified and modified tweezer molecules containing the NES interacting peptides were analyzed. Thus, the respective tweezer molecules were included in the pull-down procedure. First, the effect of the unmodified tweezer molecule was tested on the export complex assembly *in vitro* with truncated Survivin120 as cargo protein. To allow binding, Survivin120 was pre-incubated for 1 h with 100 µM unmodified tweezer before addition of the other components (Figure 3.35). Again, a control lacking the GST-CRM1 bait protein was included.
Indeed, the unmodified tweezer successfully inhibited the interaction of Survivin120 to CRM1.

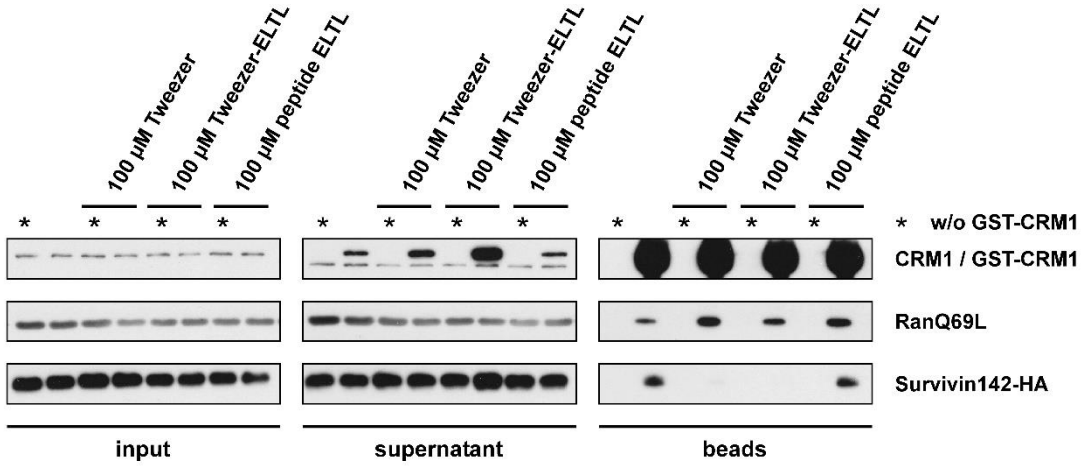

Figure 3.36: The assembly of the export complex in eukaryotic cell lysates is disturbed by basic and short peptide-linked tweezer molecules.
Recombinant GST-CRM1 bait protein was immobilized on GSH-Sepharose beads and a sample without GST-CRM1 immobilization was used as control. 293T cell lysate with overexpressed Survivin142-HA was pre-incubated with a 100 µM solution of either basic tweezer molecule, Tweezer-ELTL or the ELTL peptide alone as control. Binding to pure or GST-CRM1 coated beads was allowed in the presence of recombinant RanQ69L and dGTP. GST-CRM1 as well as interacting proteins were pulled out of solution by GSH-Sepharose beads. Proteins present in the input, supernatant and beads samples were analyzed via immunoblotting with antibodies specific for CRM1, Ran or HA.

To test, if the tweezer molecules were also able as well as specific enough to inhibit the Survivin–CRM1 interaction in cell lysates, wild type Survivin protein bearing an HA-tag at its C-terminus was overexpressed in eukaryotic 293T cells. The respective cell lysate was pre-incubated with either the unmodified tweezer, the short peptide-linked tweezer molecule, the ELTL peptide alone as a control or without any ligand. Here, the GSH-Sepharose beads were pre-loaded with the GST-CRM1 bait protein. Pre-incubated cell lysates were mixed with

the cofactor RanQ69L and added to the pre-loaded GSH-Sepharose beads. Export complexes were allowed to assemble before pull-down analysis (Figure 3.36).

In contrast to the positive control, Survivin142-HA was not detectable upon tweezer addition. Thus, both the unmodified and ELTL-peptide modified tweezer molecules, but not the peptide alone, effectively hindered export complex assembly at a concentration of 100 µM. Although unspecific binding to the beads could be successfully avoided, the tweezer molecules seemed to enhance the removal of the bound GST-CRM1 protein from the GSH-Sepharose beads. A significantly increased amount of protein could be observed in the supernatant upon unmodified tweezer incubation, even more pronounced for the peptide-linked ligand. This suggests that tweezer molecules might also bind to GST to some extent, thereby interfering with binding to the GSH-beads.

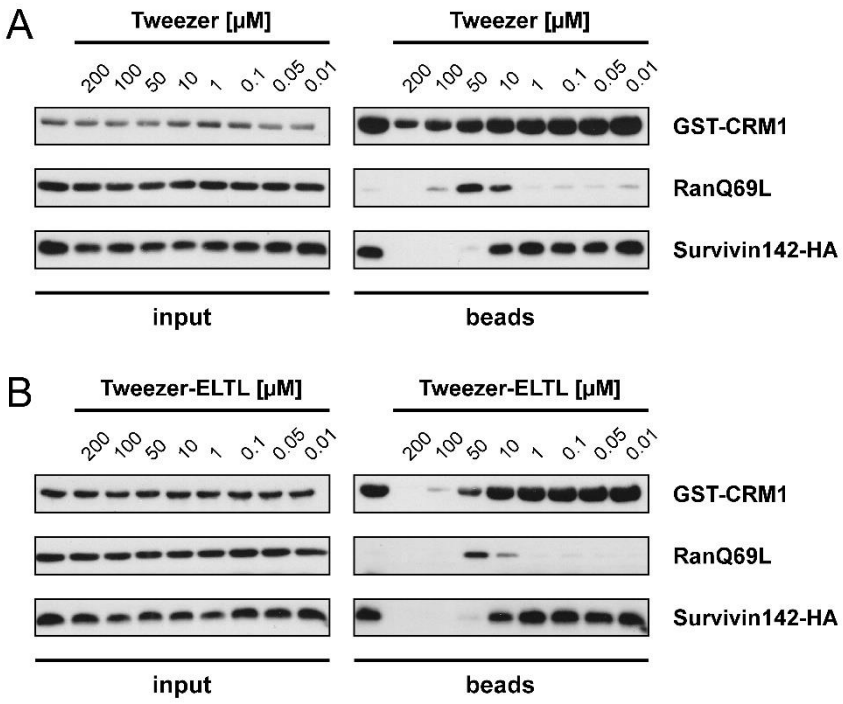

Figure 3.37: The assembly of the export complex in eukaryotic cell lysates is disturbed by basic and short peptide-linked tweezer molecules at an effective concentration between 10–50 µM.

293T cell lysate with overexpressed Survivin142-HA was pre-incubated with either basic tweezer molecule **(A)** or Tweezer-ELTL **(B)** at concentrations ranging from 0.01–200 µM. Recombinant GST-CRM1 bait protein was mixed with either non- or pre-incubated cell lysates in the presence of recombinant RanQ69L and dGTP to allow export complex assembly. GST-CRM1 as well as interacting proteins were pulled out of solution by GSH-Sepharose beads. Proteins present in the input and beads samples were analyzed via immunoblotting with antibodies specific for GST, Ran or HA.

As no differences between unmodified and ELTL modified tweezer were detected at least at a concentration of 100 µM, lower tweezer concentrations ranging from 10 nM up to 200 µM were included (Figure 3.37).

For both tweezer molecules, Survivin142-HA was successfully pulled out of solution at a concentration of 10 µM, while it was hardly detectable at 50 µM. Thus, the effective concentration of both tweezer molecules for the inhibition of the Survivin–CRM1 interaction was determined to be between 10–50 µM matching the ITC results, which revealed a K_D of 29.6 µM, respectively. Unfortunately, differences between unmodified and peptide-linked tweezer was not observed, indicating similar interference potential. However, at higher concentrations (50–200 µM), both tweezers hindered binding of GST-CRM1 to GSH-Sepharose beads. The peptide-linked tweezer seemed to do this in a more effective manner compared to the unmodified one, which indicated that the peptide modification has indeed an additional effect.

Finally, the elongated peptide-linked tweezer was also investigated regarding its effect on the Survivin–CRM1 interaction (Figure 3.38).

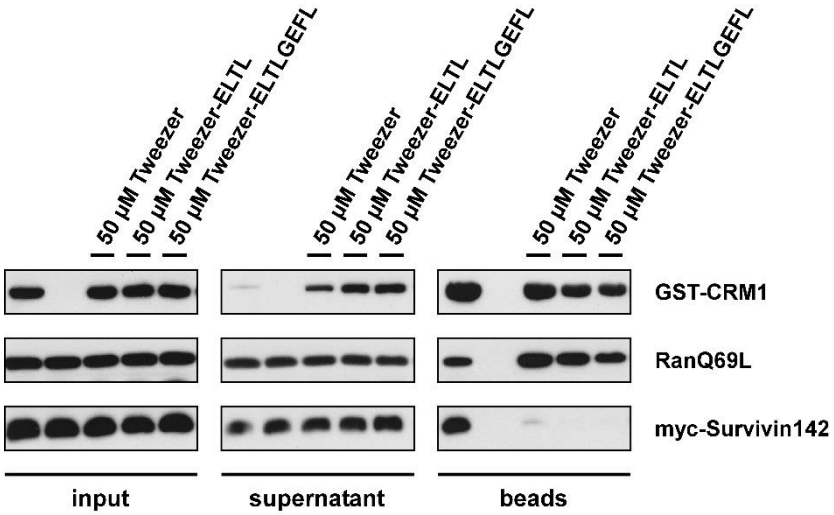

Figure 3.38: The assembly of the export complex in eukaryotic cell lysates is disturbed by basic and both peptide-linked tweezer molecules.

293T cell lysate with overexpressed myc-Survivin142 was pre-incubated with a 50 µM solution of either basic tweezer molecule, Tweezer-ELTL or Tweezer-ELTLGEFL. Recombinant GST-CRM1 bait protein was mixed with non- or pre-incubated cell lysates in presence of recombinant RanQ69L and dGTP to allow export complex assembly. GST-CRM1 as well as interacting proteins were pulled out of solution by GSH-Sepharose beads and a mixture without GST-CRM1 was used as control. Proteins present in the input, supernatant and beads samples were analyzed via immunoblotting with antibodies specific for GST, Ran or myc.

Indeed, the elongated peptide-linked tweezer effectively inhibited the Survivin–CRM1 interaction at a concentration of 50 µM. Moreover, both peptide-linked tweezers showed a slightly stronger inhibitory effect compared to the unmodified tweezer. However, Tweezer-ELTLGEFL also hindered binding of GST-CRM1 to the GSH-Sepharose beads similar to the short peptide-linked tweezer.
To conclude, the established pull-down assays could successfully assess the Survivin–CRM1 interaction as well as inhibitory tweezer effects at an effective concentration ranging 10–50 µM even in the presence of other proteins competing for binding. Unfortunately, additional inhibition of the GST-CRM1 binding to the GSH-sepharose beads indicated that the peptide modifications were not sufficient enough to convey a distinct specificity of the tweezer molecules for Survivin.

3.5 Investigation of a truncated Survivin triple lysine mutant

So far, binding of tweezer molecules could be mapped to a specific region within the NES and dimer interface of Survivin by NMR titration experiments which also revealed that peptide modification triggered a more specific binding to distinct basic amino acids K90/91, K103 and R106. To further confirm this binding site, the three lysines K90/91 and K103, discovered as binding residues by NMR, were mutated to serine residues. To avoid alterations of local and moreover global structural protein conformations leading to changes in protein folding and solubility, lysines as hydrophilic amino acids on the protein surface should not be substituted by hydrophobic amino acids like alanine. Therefore, the smallest polar amino acid serine was chosen as substitution to maintain Survivin's protein structure and solubility. Mutations should hinder tweezer binding to the NES and dimer interface but should further allow binding to other surface-exposed lysine residues of Survivin. However, the peptide-modified tweezers might still bind to the NES region and dimer interface due to their mimicking peptide modifications.

3.5.1 Purification and characterization

The coding sequence harboring the desired mutations to obtain Survivin120-K90/91/103S was generated by several rounds of SOE PCRs, digested and finally ligated into the expression vector. After verifying the DNA sequence, the expression strain *E. coli* SoluBL21 was transformed with the correct prokaryotic expression vector pET41-GST-PreSc-Survivin120-K90/91/103S. Following expression of the truncated and mutated protein Survivin120-K90/91/103S, bacterial cells were disrupted by sonication and cell debris was separated from the soluble protein fraction by centrifugation. Survivin's fused GST-tag

allowed GSH affinity chromatography as a first purification step. After several washing steps, the GST-tag was cleaved on the column by loading recombinantly expressed and purified PreScission protease (appendix A.1), followed by an overnight incubation. The next day, the cleaved product Survivin120-K90/91/103S was applied to an ion exchange chromatography column (Figure 3.39).

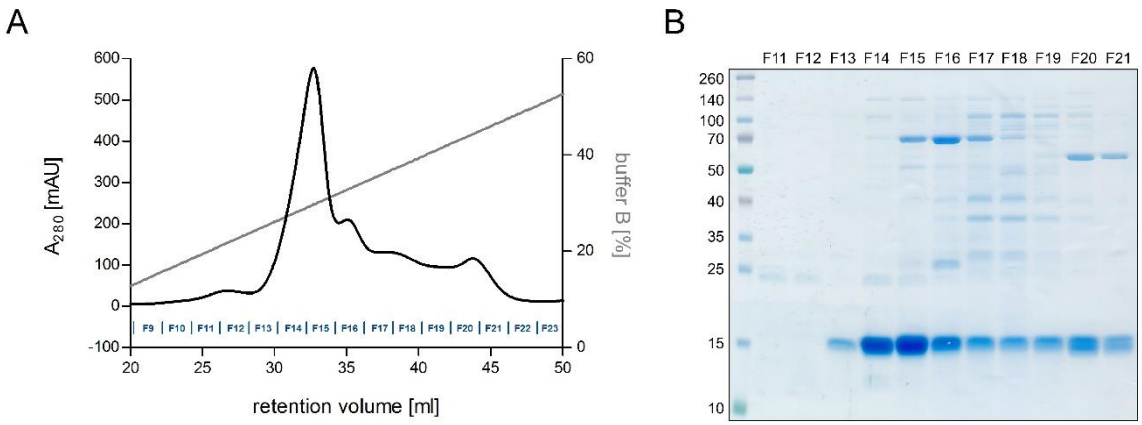

Figure 3.39: Purification of Survivin120-K90/91/103S by ion exchange chromatography.
A) Absorbance chromatogram at 280 nm of the ion exchange chromatography following GSH affinity purification and GST-tag cleavage. The elution gradient (0–100 % ion buffer B, 25 mM to 1 M NaCl, 75 ml, grey) and the collected elution fractions (F9–F23, blue) are included. **B)** Coomassie-stained SDS gel of protein-containing elution fractions. Fractions F13–F15 contained Survivin120-K90/91/103S with few impurities. They were pooled, concentrated and used for subsequent experiments.

Survivin120-K90/91/103S eluted at a retention volume of 32.7 ml and 29.7 % buffer B which corresponded to a salt concentration of roughly 322 mM NaCl. The purity and protein content of the collected fractions F11–F21 were controlled by SDS-PAGE. Regarding both, purity and protein amount, fractions F13–F15 were pooled, concentrated to 12.6 mg/ml and stored at -80 °C. Finally, the GSH affinity column was regenerated with 10 mM GSH elution buffer. Samples taken after each purification step were analyzed by SDS-PAGE to control the purification process (Figure 3.40).
During the purification procedure, a substantial fraction of the expressed Survivin120-K90/91/103S protein was detected in the insoluble protein fraction after centrifugation, ended up in the flow through and wash fractions or remained on the GSH affinity column as uncleaved protein. However, Survivin120-K90/91/103S reached a purity of more than 95 %, only a few impurities by *E. coli* proteins most likely heat shock proteins were detectable. The overall protein yield amounted to 0.7 mg per liter of bacterial culture.

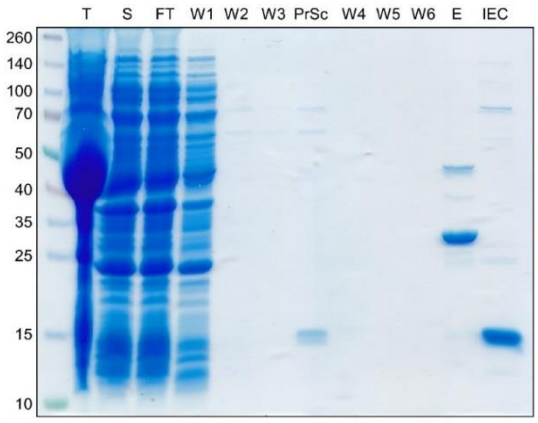

Figure 3.40: Overview of the purification procedure of Survivin120-K90/91/103S.
Coomassie-stained SDS gel of samples taken after the respective purification steps (T: total lysate, S: supernatant, FT: flow through of GSH column loading, W1–W3: wash fractions after loading the GSH column, PrSc: flow through of PreScission protease loading onto the GSH column, W4–W6: flow through of rinsing protein from the GSH column onto an ion exchange column, E: final GSH-elution of GSH column, IEC: pooled and concentrated protein after ion exchange chromatography).

In analogy to the other Survivin variants, Survivin120-K90/91/103S was biochemically characterized in more detail. Its secondary structure (A) as well as tweezer interference (B) were analyzed by CD spectroscopy (Figure 3.41), and its dimerization was studied by analytical gel filtration (Figure 3.42).

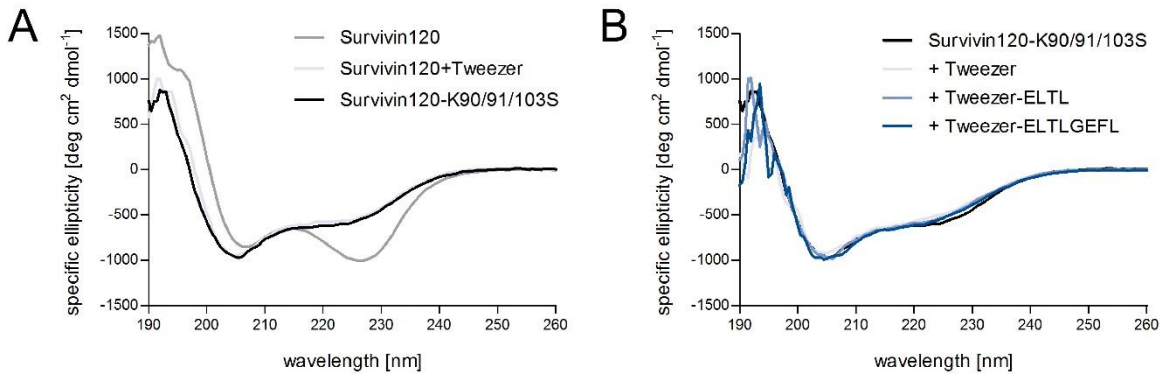

Figure 3.41: Far-UV CD spectrum of mutated Survivin120-K90/91/103S and investigation of tweezer effects on its secondary structure.
A) The far-UV CD spectrum of tag-free Survivin120-K90/91/103S (black) differed from that of Survivin120 (grey) but overlaped with the spectrum of Survivin120 pre-incubated with tweezer (light grey). **B)** The far-UV CD spectrum of tag-free Survivin120-K90/91/103S (black) hardly changed upon previous tweezer incubation. All spectra were recorded at 20 °C in 20 mM phosphate buffer containing 10 µM Zn^{2+}.

The CD spectrum showed that Survivin120-K90/91/103S retained a defined secondary structure and was not randomly folded. However, lysine to serine mutations caused changes in the CD spectrum and therefore in the secondary structure of Survivin120 (Figure 3.41 A). The ellipticity of the minimum at 227 nm increased. This shift led to a lower minimum at 207 nm compared to 227 nm and therefore definitely to a change in Survivin's secondary structure. Moreover, the spectrum of Survivin120-K90/91/103S perfectly overlapped with the spectrum of truncated Survivin120 incubated with 100 µM unmodified tweezer molecule. Thus, lysine mutations or tweezer binding seemed to lead to similar changes in the secondary protein structure, namely a lower amount of α-helical structure. The introduced negatively charged hydroxy groups, in case of the tweezer molecule by its phosphate groups and in case of the mutant by the introduced serine residues, might explain the overlap of the spectra.

Furthermore, changes in the CD spectra of Survivin120-K90/91/103S upon incubation with tweezer molecules were marginal (Figure 3.41 B). The ellipticity of the minimum at 227 nm slightly increased upon tweezer binding suggesting a lower content of α-helical structure.

Although the serine mutations influenced Survivn's secondary structure, similarly compared to tweezer binding, they did not denature the protein. The CD spectrum showed that mutated Survivin retained a defined secondary structure and was not randomly folded. Compared to Survivin120, the tweezer molecules only slightly influenced the protein folding of Survivin120-K90/91/103S.

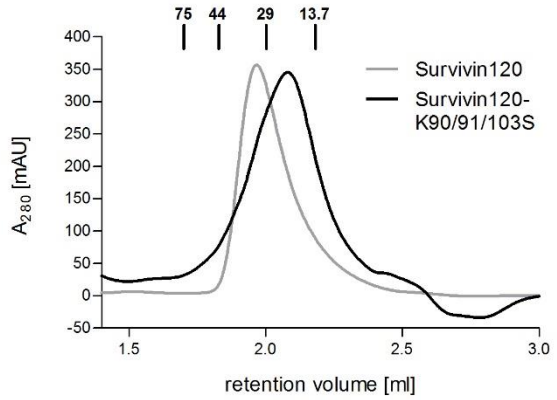

Figure 3.42: Analytical gel filtration of Survivin120-K90/91/103S.

Analytical gel filtration absorbance chromatogram measured at 280 nm on a calibrated Superdex 200 Increase column reveals that truncated and mutated Survivin120-K90/91/103S elutes in the range of 13.7–29 kDa and thereby at a higher retention volume compared to truncated Survivin120. This result did not allow to conclude the oligomeric state of Survivin120-K90/91/103S but indicated a conformational change compared to Survivin120.

Next, to analyze the influence of the serine mutations on dimerization, analytical gel filtration of Survivin120-K90/91/103S was performed (Figure 3.42). The column was calibrated with proteins whose MW range covered the size of monomeric (14 kDa) and dimeric protein (28 kDa).
Compared to Survivin120, mutated Survivin120-K90/91/103S eluted despite its similiar theoretical size at a higher retention volume between the calibration proteins carbonic anhydrase (29 kDa) and ribonuclease A (13.7 kDa). This retention volume did neither perfectly fit to its dimeric (28 kDa) nor to its monomeric protein size (14 kDa). Thus, this analytical gel filtration result did not allow to conclude the oligomeric state of Survivin120-K90/91/103S but indicated a conformational change compared to Survivin120. On the one hand, it still might form a dimer but in a more compact manner which decreased its dynamic radius. On the other hand, the amino acid mutations within the dimer interface might lead to a dimer disruption and a monomeric Survivin120-K90/91/103S. Due to Survivin's C-terminal α-helix even though truncated, its dynamic radius is enhanced compared to globular proteins like ribonuclease A and triggers its elution at a lower retention volume. To ascertain the olicomeric state of Survivin120-K90/91/103S, the DIMmut Survivin protein, which is supposed to form a monomer in solution, should serve as a monomer control in a further gel filtration experiment.

3.5.2 Characterization of binding affinities by isothermal titration calorimetry

To study the influence of the introduced lysine mutations in Survivin's NES region and dimer interface on the tweezer binding and to determine binding affinities, ITC measurments with Survivin120-K90/91/103S were performed. Therefore, the molecular tweezer molecules were placed in the sample cell and subjected to stepwise titration with the mutated protein Survivin120-K90/91/103S.
An exothermic binding reaction was observed when titrating Survivin120-K90/91/103S to a solution of basic tweezer molecule. The respective binding isotherm revealed a one-phase course. Correspondingly, a one-site model could be used to fit the experimental data. The resulting fit revealed a dissociation constant K_D of 2.2 µM (Figure 3.43). Survivin120-K90/91/103S titrations to the short peptide-linked tweezer molecules also resulted in an exothermic binding reaction. Its binding isotherm revealed a one-phase course, so that its data-points were fitted with a one-site model. The resulting fit revealed a dissociation constant K_D of 11.5 µM (Figure 3.44).

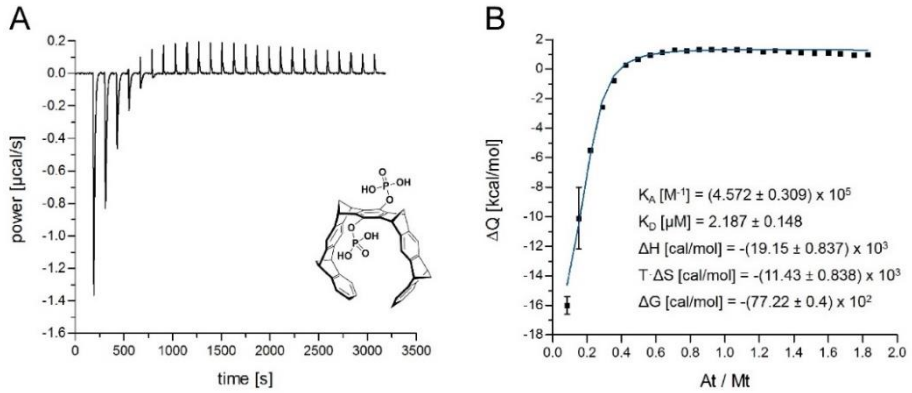

Figure 3.43: Verification of unmodified tweezer binding to Survivin120-K90/91/103S via ITC.
For the ITC experiment, a solution of 100 µM unmodified tweezer molecule was placed in the sample cell and subjected to stepwise titration with 1.5 µl aliquots of a 0.92 mM solution of Survivin120-K90/91/103S protein for a total of 25 injections at 25 °C using PBS pH 7.4. The equilibration time between two injections was 120 s. **A)** Raw heating power over time substracted by control heating power of Survivin120-K90/91/103S titration into PBS, as well as the chemical structure of unmodified molecular tweezer. **B)** Fit of the integrated energy values normalized to injected Survivin120-K90/91/103S. The exothermic binding reaction displays a one-phase course hinting at a single binding event. Fitting of the ITC data to a one-binding-site model reveals a dissociation constant K_D of 2.2 µM (tweezer synthesis and data evaluation by Christian Heid, Department of Organic Chemistry, Schrader group, University of Essen).

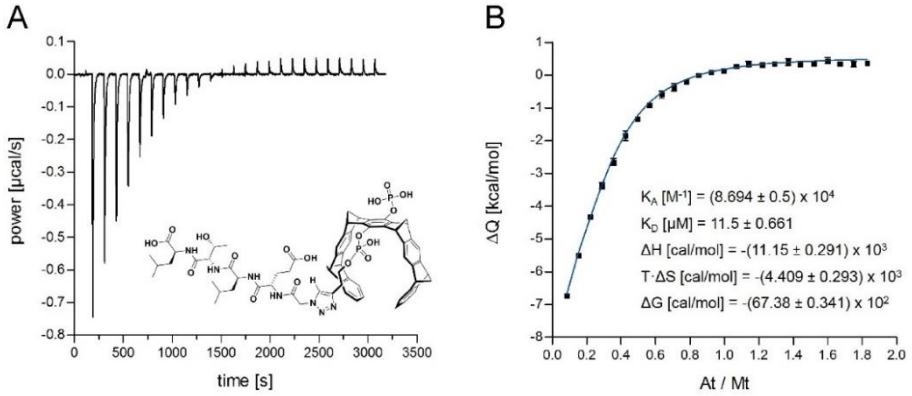

Figure 3.44: Verification of Tweezer-ELTL binding to Survivin120-K90/91/103S via ITC.
For the ITC experiment, a solution of 100 µM Tweezer-ELTL molecule was placed in the sample cell and subjected to stepwise titration with 1.5 µl aliquots of a 0.92 mM solution of Survivin120-K90/91/103S protein for a total of 25 injections at 25 °C using PBS pH 7.4. The equilibration time between two injections was 120 s. **A)** Raw heating power over time substracted by control heating power of Survivin120-K90/91/103S titration into PBS, as well as the chemical structure of Tweezer-ELTL. **B)** Fit of the integrated energy values normalized to injected Survivin120-K90/91/103S. The exothermic binding reaction displays a one-phase course hinting at a single binding event. Fitting of the ITC data to a one-binding-site model reveals a dissociation constant K_D of 11.5 µM (tweezer synthesis and data evaluation by Christian Heid, Department of Organic Chemistry, Schrader group, University of Essen).

ITC measurements confirmed a direct binding of tweezer molecules to mutated Survivin120-K90/91/103S with affinities in the low micro molar range. Unexpectedly, both tweezer molecules exhibited stronger binding affinities towards Survivin120-K90/91/103S compared to Survivin120 (K_D = 29.6 µM). Furthermore, a stronger binding affinity was detected for the basic tweezer molecule compared to the modified short peptide-linked one. Excluding tweezer binding to the three lysine residues K90/91 and K103 by mutations, other surface-exposed lysine or arginine residues of Survivn120-K90/91/103S might be assessed. However, this must be proven with additonal experiments like NMR titration or crystallization.

3.5.3 Analysis of complex assembly and tweezer effects by pull-down experiments

In addition to the potential of Survivin120-K90/91/103S to form the export complex despite its lysine mutations, the influence of these mustations on tweezer binding should be analyzed by pull-down experiments confirming a selective inhibiton of the Survivin–CRM1 interaction by tweezer binding exclusively to lysine residues in the NES region and dimer interface.
First, for the recombinantly expressed and purified cargo protein Survivin120-K90/91/103S, a Coomassie-stained SDS-PAGE gel as well as a specific immunoblot staining were performed (Figure 3.45).

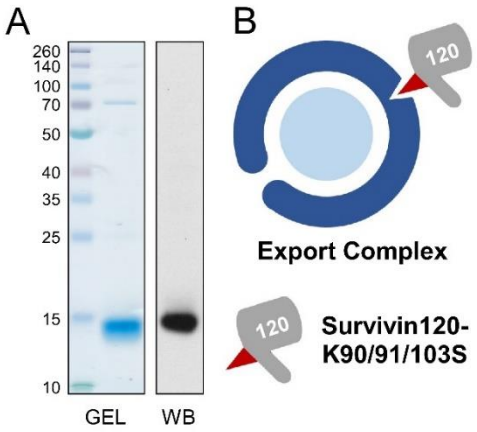

Figure 3.45: Representation of recombinantly expressed and purified cargo protein Survivin120-K90/91/103S.
A) Coomassie-stained SDS-PAGE gel and specific immunoblot result of purified cargo protein Survivin120-K90/91/103S. **B)** Schematic representation of assembled export complex with mutated Survivin120-K90/91/103S as cargo protein.

However, instead of using recombinantly expressed and purified Survivin120-K90/91/103S the pull-down experiment was directly performed in eukaryotic 293T cell lysate with

overexpressed myc-Survivin142-K90/91/103S, to ensure the competition with other potential cargo proteins.

The obtained cell lysate was pre-incubated either with a 50 µM solution of the unmodified, the short peptide-linked or the elongated peptide-linked tweezer or without any ligand. The pre-incubated cell lysate was mixed with the recombinant GST-CRM1 bait protein and its recombinant cofactor RanQ69L, respectively. Export complexes were allowed to assemble before pull-down analysis (Figure 3.46). Again, a control lacking the GST-CRM1 bait protein was included to exclude any unspecific binding onto the beads.

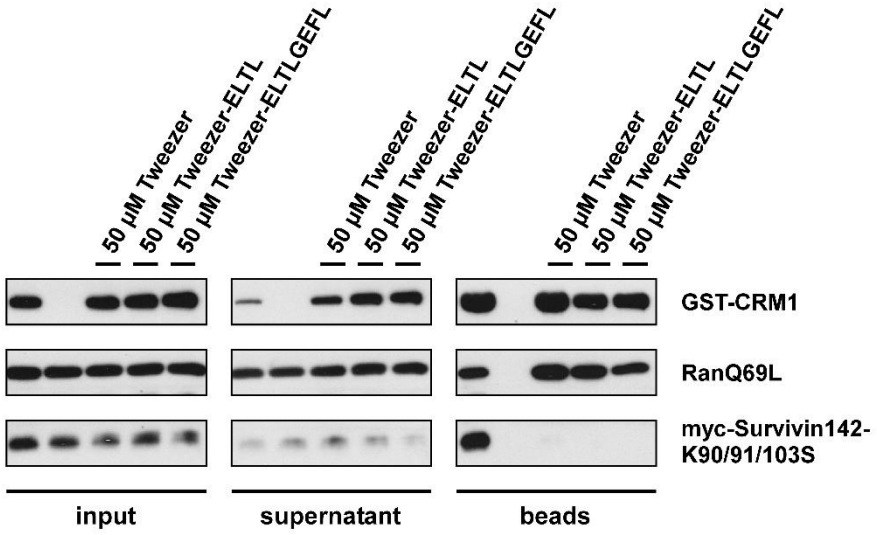

Figure 3.46: The export complex assembles in eukaryotic cell lysates despite lysine mutations in Survivin's NES region and dimer interface and seems to be disrupted by basic and both peptide-linked tweezer molecules.

293T cell lysate with overexpressed myc-Survivin142-K90/91/103S was pre-incubated with a 50 µM solution of either basic tweezer molecule, Tweezer-ELTL or Tweezer-ELTLGEFL. Recombinant GST-CRM1 bait protein was mixed with non- or pre-incubated cell lysates in presence of recombinant RanQ69L and dGTP to allow export complex assembly. GST-CRM1 as well as interacting proteins were pulled out of solution by GSH-Sepharose beads and a mixture without GST-CRM1 was used as control. Proteins present in the input, supernatant and beads samples were analyzed via immunoblotting with antibodies specific for GST, Ran or myc.

In contrast to the positive control, myc-Survivin142-K90/91/103S was not detectable upon tweezer addition. Thus, all three tweezer molecules seemed to hinder the export complex assembly at a concentration of 50 µM. Although unspecific binding to the beads could be successfully avoided, all tweezer molecules seemed to enhance the removal of the bound GST-CRM1 protein from the GSH-Sepharose beads indicating unspecific protein binding in addition to Survivin. By introducing lysine mutations, tweezer binding to Survivin's NES and

dimer interface was excluded and therefore inhibition of Survivin's interaction to CRM1 was not expected. However, an inhibition was observed. Similar to the GST-CRM1 removal from the beads, this inhibition might be caused by an unspecific tweezer binding e.g. to CRM1 near its NES cleft due to a high tweezer excess.

For removing non-bound or unspecific bound tweezers and therefore triggering specific tweezer binding exclusively to Survivin's NES and dimer interface, the experimental setup of the pull-down was changed to introduce a washing step after tweezer incubation.

Here, recombinantly expressed and purified GST-Survivin120 (appendix A.3) or GST-Survivin120-K90/91/103S (appendix A.4) bait proteins were incubated with either a 50 µM solution of each tweezer molecule or the ELTL peptide alone as a control or without any ligand and allowed to bind to the GSH-Sepharose beads. Thereby, tweezer binding at lysine residues in the NES and dimer interface was expected for GST-Survivin120 but not for GST-Survivin120-K90/91/103S. After washing the beads, to remove any unbound or unspecific bound tweezer molecules with low affinity, they were mixed with the recombinant CRM1 prey protein and its cofactor RanQ69L. Export complexes were allowed to assemble before pull-down analysis (Figure 3.47 A). Controls lacking the GST-Survivin120 or GST-Survivin120-K90/91/103S bait proteins were included.

Both bait proteins GST-Survivin120-WT and GST-Survivin120-K90/91/103S as well as the prey protein CRM1 could be successfully detected on the beads in contrast to the controls. However, binding to CRM1 was significantly increased for mutated GST-Survivin120-K90/91/103S. The binding affinity seemed to be enhanced by the introduced lysine to serine mutations. Nevertheless, the varied pull-down assay was suitable to assess the Survivin–CRM1 interaction for both Survivin variants.

Still observing CRM1 protein, tweezer incubation seemed to have no or only little inhibiting effect on the Survivin–CRM1 interaction for both Survivin variants which was expected for GST-Survivin120-K90/91/103S but not for GST-Survivin120. A reason for this might be an insufficient tweezer concentration either initially applied or remained after washing. Moreover, the different amount of detected Survivin bait protein due to an inhibition of GST binding to the beads had to be considered when comparing the pulled CRM1 prey protein.

Thus, pull-down quantification was performed by densitometric analysis. Following substraction of the CRM1 intensity signal by the signal of the negative control without bait protein, the resulting signal is in a first step normalized against the corresponding GST-Survivin intensity signal and afterwards again normalized against the CRM1 intensity of the positive control without ligand incubation (Figure 3.47 B).

Quantification revealed an inhibiting effect of all three tweezer molecules on the interaction between CRM1 and GST-Survivin120 which increased proportional to the length of peptide modification. Tweezer-ELTLGEFL exhibited the strongest inhibiting effect with a more than

50 % reduction of the pulled CRM1 amount, while peptide ELTL alone as a control only showed a little reduction. Quantification for GST-Survivin120-K90/91/103S revealed no tweezer interference with its binding to CRM1.

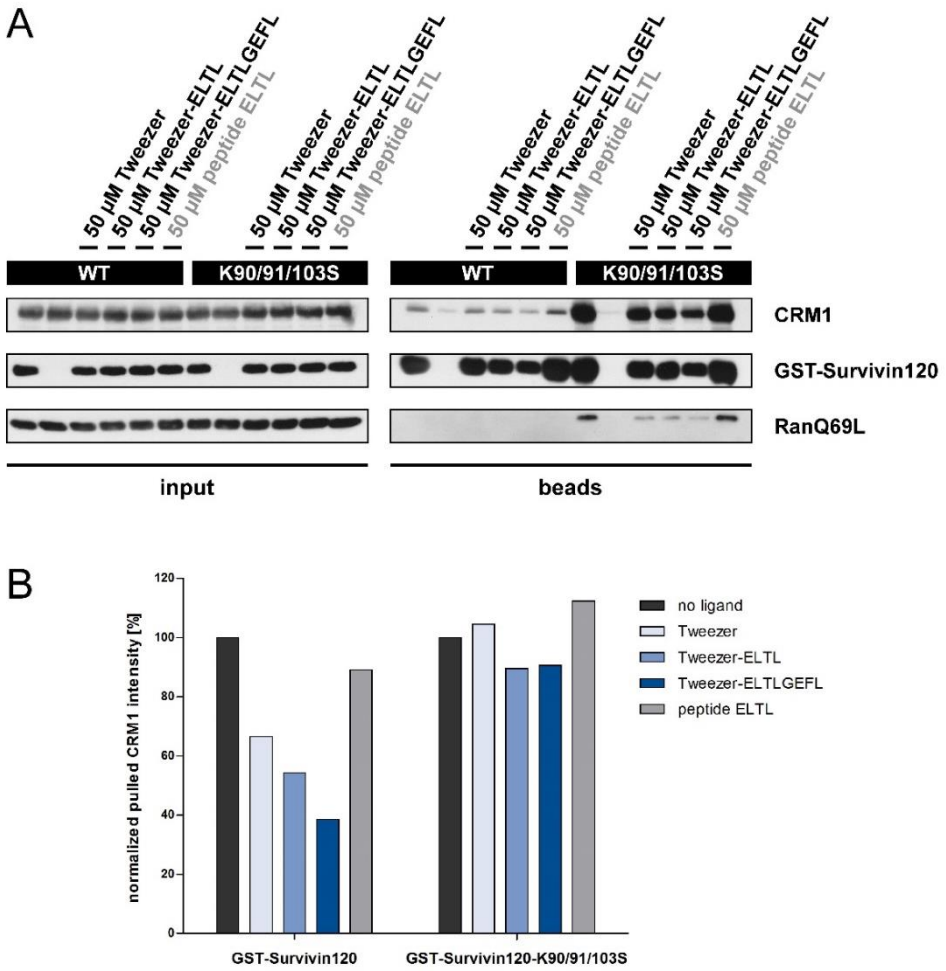

Figure 3.47: Lysine mutations in Survivin's NES and dimer interface prevent tweezer inhibition of the Survivin–CRM1 interaction.

A) Pull-down results after immunostaining. Recombinant GST-Survivin120-WT or GST-Survivin120-K90/91/103S bait proteins were incubated with GSH-Sepharose beads and a 50 µM solution of either basic tweezer molecule, Tweezer-ELTL, Tweezer-ELTLGEFL or ELTL peptide alone as control or without any ligand. After washing to remove any unbound or unspecific bound tweezer molecules, GST-Survivin120- or GST-Survivin120-K90/91/103S-loaded beads with or without ligand pre-incubation were mixed with recombinant CRM1 and RanQ69L prey proteins as well as dGTP to allow export complex assembly. GST-Survivin120-WT or GST-Survivin120-K90/91/103S as well as interacting proteins were pulled out of solution by GSH-Sepharose beads and samples without GST-Survivin120-WT or GST-Survivin120-K90/91/103S were used as controls. Proteins present in the input and beads samples were analyzed via immunoblotting with antibodies specific for CRM1, GST or Ran. **B)** Quantification of the pull-down shown in A. Pulled CRM1 intensity is substracted by negative control CRM1 intensity, then normalized by the GST-Survivin intensity and afterwards again normalized by the CRM1 intensity without ligand incubation.

To conclude, the lysine mutations of Survivin120-K90/91/103S were discovered to prevent tweezer inhibition of the Survivin–CRM1 interaction, thus confirming the supramolecular tweezer molecules as specific inhibitors interfering with the Survivin–CRM1 interaction by targeting Survivin's NES and dimer interface.
However, these findings must be confirmed by additional NMR titration experiments with Survivin120-K90/91/103S. Moreover, to gain unmistakable evidence about the exact binding site of the tweezer molecules on Survivin, crystal structures are inescapable.

3.6 Studies of Survivin's cellular export

Following thorough biochemical characterization and chemical targeting of the Survivin–CRM1–Ran export complex *in vitro*, studies on the nuclear export of Survivin should be expanded to a cellular environment.

3.6.1 Localization of export complex members

First, cellular localization of the three export complex members Survivin, CRM1 and its cofactor GTPase Ran were analyzed via immunofluorescence staining during interphase as well as in all phases during mitosis. Therefore, HeLa Kyoto cells were fixed, and endogenous proteins were stained with antibodies specific for Survivin, CRM1 or Ran, and DNA was stained with Hoechst. Microscopic analyses allowed the visualization of the cellular localization of all three export complex members (A: Survivin, B: CRM1 and C: Ran) in interphase as well as in all mitotic phases (Figure 3.48).
While Survivin was detected in the nucleus in interphase, its localization resembled the characteristics of CPC members during mitosis. It localized at the centromeres until metaphase, translocated to the spindle midzone during anaphase and finally accumulated at the midbody during telophase. As a nuclear export receptor, CRM1 was located at the nuclear membrane during interphase. During metaphase and anaphase, it seemed to accumulate at the mitotic spindle but relocalized to the developing nuclear membrane already during late telophase. For the small GTPase Ran, no distinct cell cycle-dependent localization could be observed. However, in interphase it predominantly localized in the nucleus, but was also found in the cytoplasm.

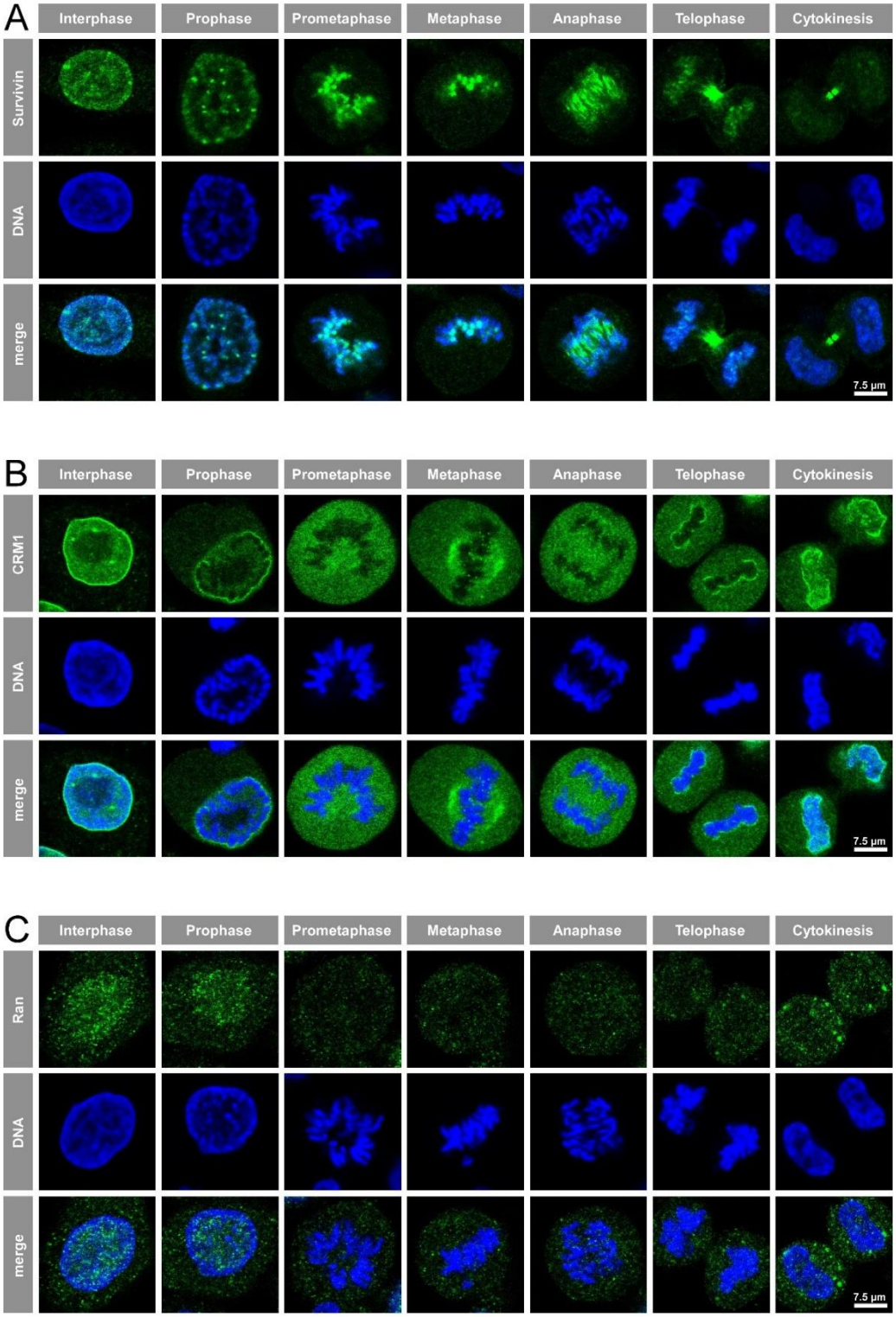

Figure 3.48: Cellular localization of export complex members.

HeLa Kyoto cells were fixed, the endogenous export complex member proteins were immunostained with antibodies specific for Survivin **(A)**, CRM1 **(B)** and Ran **(C)** (green), and DNA was stained with Hoechst (blue). Images were acquired with a Leica SP5 confocal laser scanning microscope. Scale bar, 7.5 µm.

To confirm CRM1 localization at the mitotic spindle during metaphase and anaphase, endogenous CRM1 was co-stained with endogenous α-Tubulin in HeLa Kyoto cells (Figure 3.49).

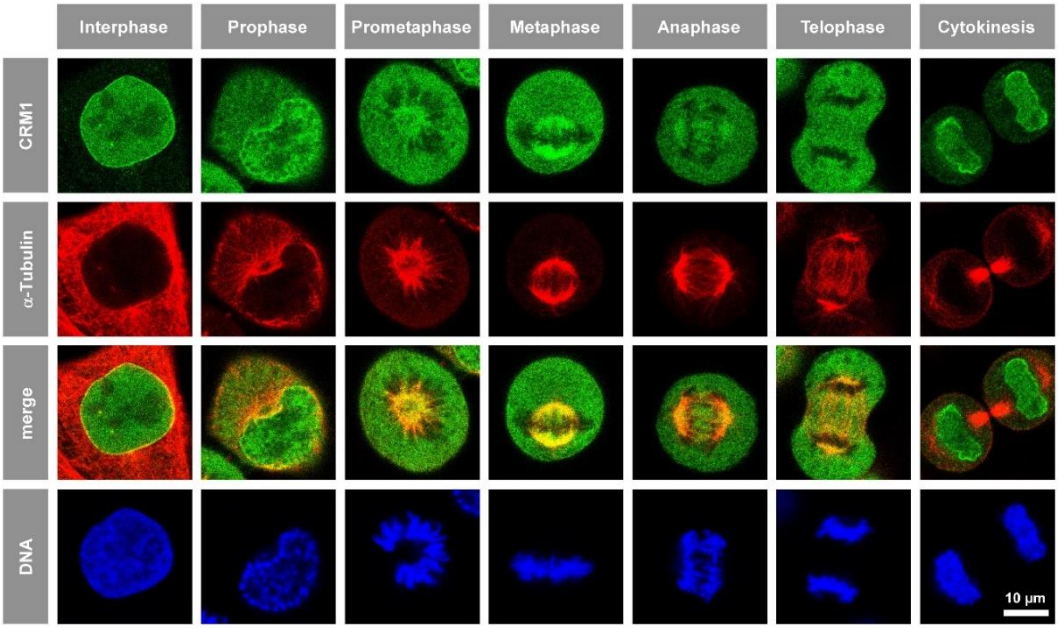

Figure 3.49: Cellular co-localization of export receptor CRM1 and α-Tubulin in mitosis.
Immunostaining of endogenous CRM1 and α-Tubulin in HeLa Kyoto cells revealed a distinct co-localization at the mitotic spindle. HeLa Kyoto cells were fixed, CRM1 (green) and α-Tubulin (red) were immunostained with specific antibodies directed against the endogenous proteins, and DNA was stained with Hoechst (blue). Images were acquired with a Leica SP5 confocal laser scanning microscope. Scale bar, 10 µm.

Indeed, CRM1 co-localizes with α-Tubulin at the mitotic spindle especially in prometa-, meta-, ana- and telophase. Following separate evaluation of the export complex members, their assembly should be assessed in a cellular system.

3.6.2 Export complex assembly in a cellular system

To visualize the Survivin–CRM1 interaction within the cell, overexpression of both proteins ensured that they are present in a high excess compared to endogenous levels, thus robustly triggering their interaction. Therefore, besides endogenous immunofluorescence staining, myc-Survivin and CRM1-HA were co-expressed in HeLa Kyoto cells (Figure 3.50).

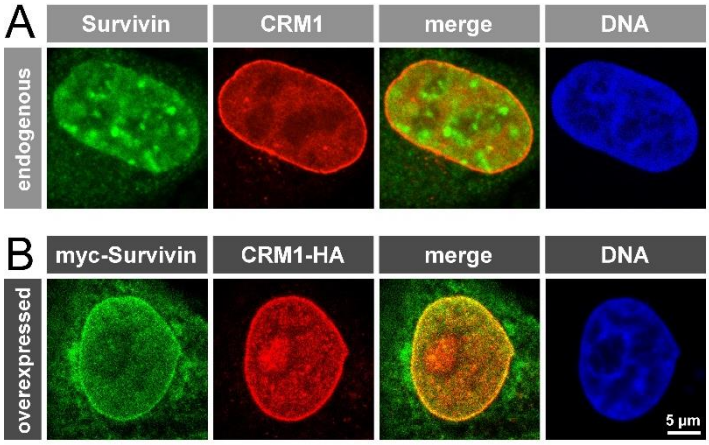

Figure 3.50: Co-localization of Survivin and CRM1 upon exogenous overexpression.
In contrast to immunostaining of endogenous Survivin and CRM1 **(A)**, transient overexpression of myc-Survivin and CRM1-HA **(B)** in HeLa Kyoto cells revealed a distinct co-localization at the nuclear membrane as well as in the nucleoplasm. **A)** HeLa Kyoto cells were fixed, endogenous proteins were immunostained with antibodies specific for Survivin (green) or CRM1 (red) and DNA was stained with Hoechst (blue). **B)** HeLa Kyoto cells were transiently transfected and fixed. Overexpressed proteins were stained with antibodies specific for myc (green) as well as for HA (red) and DNA was stained with Hoechst (blue). Images were acquired with a Leica SP5 confocal laser scanning microscope. Scale bar, 5 µm.

In interphase, endogenous Survivin exhibited a predominantly nuclear localization while the export receptor CRM1 predominantly localized to the nuclear membrane and the nucleoplasm (Figure 3.50 A). Simultaneous overexpression of both proteins resulted in an accumulation of Survivin at the nuclear membrane as well as in the nucleoplasm, where it co-localized with the export receptor CRM1 (Figure 3.50 B). To also quantitatively assess the interaction between both endogenous proteins in a cellular environment, a cell-based proximity ligation assay was established by Cecilia Vallet from the Department of Molecular Biology II (Knauer group, University of Essen). This PLA allows the detection and visualization of protein–protein interactions characterized by a distance of less than 40 nm.
HeLa Kyoto cells were fixed, and PLA (Figure 3.51) was performed with specific antibodies for Survivin and CMR1 in combination with so-called PLA probes to visualize Survivin–CRM1 interactions at a single molecule level. Thereby, PLA signals, indicating single interactions, were detected as distinct fluorescent cellular foci. Finally, cells were stained with cell mask and Hoechst to allow automated quantification by a cell profiler pipeline, which was performed by Dr. Nina Schulze from the Imaging Centre Campus Essen (ICCE, University of Essen). Samples stained with only one antibody were used to control for unspecific PLA signals.

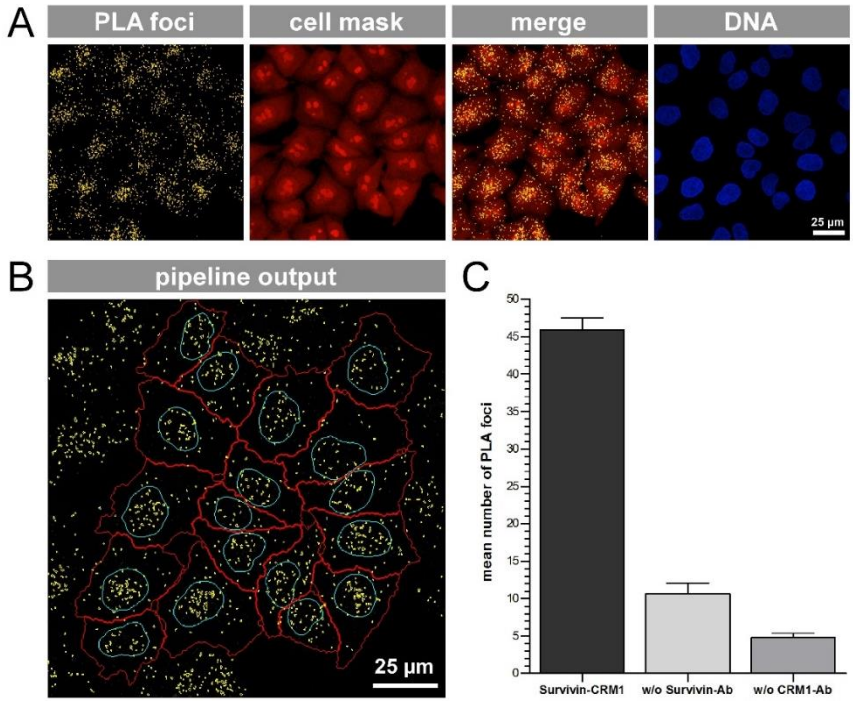

Figure 3.51: Endogenous Survivin–CRM1 interaction as revealed by PLA analysis.
Endogenous Survivin–CRM1 interactions predominantly arising in the nucleus but also detectable in the cytoplasm are quantitatively assessed by PLA analysis in HeLa Kyoto cells. **A)** Image of representative HeLa Kyoto cells with punctuate PLA signals (yellow) visualizing single cellular interactions of endogenous Survivin and CRM1, cell mask staining (red) and Hoechst staining of DNA (blue). Images were acquired with a Leica SP8 confocal laser scanning microscope. Scale bar, 25 µm (PLA assay and microscopy by Cecilia Vallet, Department of Molecular Biology II, Knauer group, University of Essen). **B)** Cell profiler pipeline output. **C)** Quantification of the Survivin–CRM1 interaction. Graphs indicate the mean number of detected PLA foci calculated by a cell profiler pipeline. At least 120 cells were counted per sample (35 cells per control sample). The error bars represent standard errors of the mean (SEM). (quantification by Dr. Nina Schulze, ICCE, University of Essen).

PLA foci indicative for single Survivin–CRM1 interactions were detectable predominantly in the nucleus, but also in the cytoplasm (Figure 3.51 A). Cell mask and Hoechst staining allowed to separate the subcellular compartments required for automated quantification (Figure 3.51 B, C). The pipeline calculated the number of PLA foci within a cell. At least 120 cells were counted per sample (35 cells per control sample). While a mean PLA foci number of 46 was calculated for the positive sample, both control samples incubated with only one of two antibodies revealed a significantly decreased number of 10 or 5 elucidating unspecific PLA signals.

Thus, with this PLA, a robust and quantitative interaction assay was established that now allows to address the endogenous Survivin–CRM1 interaction by e.g. supramolecular tweezers or other chemical ligands.

3.6.3 Localization of RanBP3 – a further export complex member

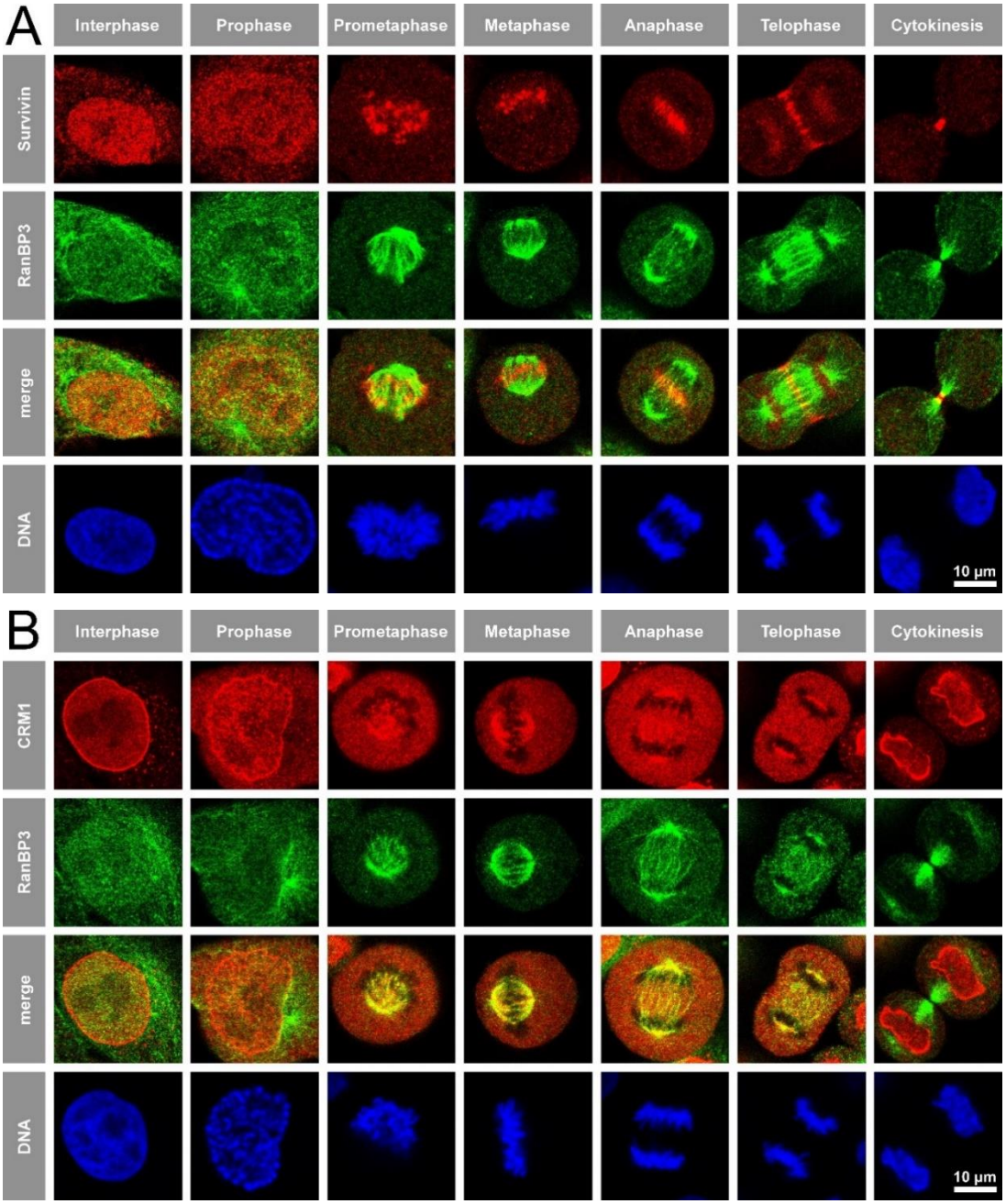

Figure 3.52: Cellular localization of RanBP3 compared to Survivin and CRM1.
Immunostaining of endogenous RanBP3 compared to Survivin and CRM1 in HeLa Kyoto cells revealed a nuclear co-localisation in interphase and a distinct one in mitosisis, respectively. Survivin co-localizes with RanBP3 at the centromeres, the spindle midzone and the midbody, while co-localization to CRM1 is detectable at the mitotic spindle. **A)** HeLa Kyoto cells were fixed, the endogenous proteins Survivin (red) and RanBP3 (green) were immunostained with specific antibodies and DNA was stained with Hoechst (blue). **B)** HeLa Kyoto cells were fixed, the endogenous proteins CRM1 (red) and RanBP3 (green) were immunostained with specific antibodies and DNA was stained with Hoechst (blue). Images were acquired with a Leica SP5 confocal laser scanning microscope. Scale bar, 10 µm.

Previous biochemical experiments indicated that the export complex formed by Survivin, CRM1 and RanQ69L was most likely not stable enough for e.g. analytical gel filtration. Thus, the question arises whether there are further components required for export complex assembly or at least might enhance its stability. RanBP3 is already known to be a further important player in nuclear export processes, stabilizing the nuclear complex and affecting cargo selectivity (Englmeier *et al.*, 2001; Langer *et al.*, 2011).

So, to verify a potential role of RanBP3 in Survivin export complex assembly, the cellular localization of RanBP3 was analyzed via immunofluorescence staining in interphase and mitosis compared to Survivin and CRM1 (Figure 3.52). Therefore, HeLa Kyoto cells were fixed, and endogenous proteins were stained with antibodies for RanBP3 and Survivin (A) or CRM1 (B). DNA was stained with Hoechst.

Indeed, the results confirmed co-localization of RanBP3 with the export receptor CRM1 especially at the mitotic spindle in prometa-, meta-, ana- and telophase, while it predominantly localized in the nucleus of interphase cells. Co-localization with the cargo protein Survivin was detectable at the centromeres, the spindle midzone and the midbody in mitosis as well as in the nucleus in interphase. This result suggested a robust interaction with CRM1 as well as a partial co-localization with Survivin, especially in but not restricted to mitotic phases. Therefore, it is worthwhile to supplement future biochemical gel filtration experiments with recombinant RanBP3 to enhance the stability of the *in vitro* export complex.

3.6.4 Biosensor assay for export activity

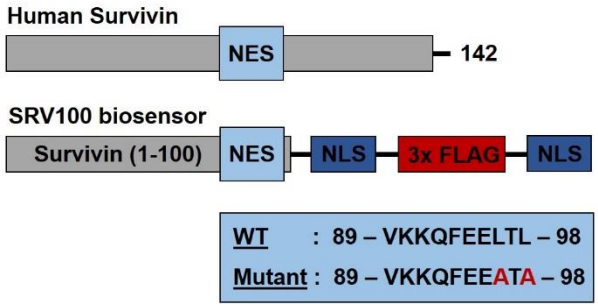

Figure 3.53: Schematic representation of human Survivin protein and the SRV100 biosensor. Deletion of the last 42 amino acids eliminated the C-terminal export motif in Survivin and disrupted its dimerization domain. Two SV40 NLS (blue) and a triple arrangement of the Flag epitope-tag (red) replaced this segment in SRV100. As a control, a mutated biosensor version beared alanine replacement for leucine residues L96 and L98 in Survivin's NES (modified after (García-Santisteban *et al.*, 2016), SRV100 WT and SRV100 NESmut plasmids were provided).

So far, successful interference of supramolecular tweezer molecules with the Survivin–CRM1 interaction in biochemical pull-down assays could be demonstrated. To now test whether the

supramolecular ligands are able to also specifically interfere with Survivin's cellular export, an already existing cell-based biosensor assay for CRM1-mediated nuclear export activity was adopted (García-Santisteban *et al.*, 2016).

In the biosensor, named SRV100, the last 42 amino acids of the Survivin protein were deleted, thus removing the C-terminal export motif and disrupting the dimerization motif. The C-terminus was replaced by two NLS sequences derived from the SV40 large T antigen and three intermitting tandem copies of the Flag epitope (3x Flag) for detection. Additionally, a biosensor variant with NES-inactivating mutations (L96+98A) was used as a control (Figure 3.53).

First, the biosensor assay was verified with the respective plasmids provided by (García-Santisteban *et al.*, 2016). 293T cells, transiently overexpressing SRV100 WT or SRV100 NESmut together with either YFP or YFP-CRM1 were fixed and immunostained with a specific Flag-tag antibody, DNA was stained with Hoechst. Indeed, the SRV100 WT biosensor accumulated in the cytoplasm of 293T cells upon co-expression with YFP-CRM1, while it stayed inside the nucleus when co-expressed with YFP alone as described (García-Santisteban *et al.*, 2016) (Figure 3.54 A). CRM1-mediated cytoplasmic relocalization of SRV100 WT was dependent on the presence of a functional NES. Upon mutation of essential amino acid residues within the NES (Figure 3.53), the respective biosensor SRV100 NESmut remained in the nucleus even when YFP-CRM1 was co-expressed (García-Santisteban *et al.*, 2016) (Figure 3.54 A).

To now adapt the biosensor system to investigate tweezer effects on nuclear export, an automated downstream quantification step was included. Thus, following image acquisition by confocal microscopy, automated data quantification was performed with a cell profiler pipeline (by Dr. Nina Schulze, ICCE, University of Essen; Figure 3.54 B). Briefly, transfected cells were only selected for analysis when exceeding a YFP intensity threshold of 0.07 AU. Next, SRV100 intensity in the cytoplasm as well as in the nucleus was measured only in previous selected cells. Thereby, nuclei were defined by Hoechst-staining and the cytoplasms were identified by YFP intensity. Subsequently, the ratio of the nuclear (N) / cytoplasmic (C) intensity of the SRV100 Flag IF signal was calculated for each cell (C>N for ratio<1, N>C for ratio>1) in at least 450 cells per sample. Percentages of co-transfected cells showing predominantly nuclear (N>C) or cytoplasmic (C>N) biosensor localization were extracted from the comprehensive cell profiler data set (Figure 3.54 B).

Here, the cytoplasmic shift of the Survivin nuclear export biosensor SRV100 WT upon CRM1 co-expression was robustly detected. Mutations of essential amino acid residues within the NES prevented such a distinct cytoplasmic shift. SRV100 NESmut predominantly localized nuclear, regardless of YFP-CRM1 co-expression. Thus, this analysis allows to easily

evaluate and quantify interference with Survivin export activity, as exemplified by the use of the NES mutant biosensor.

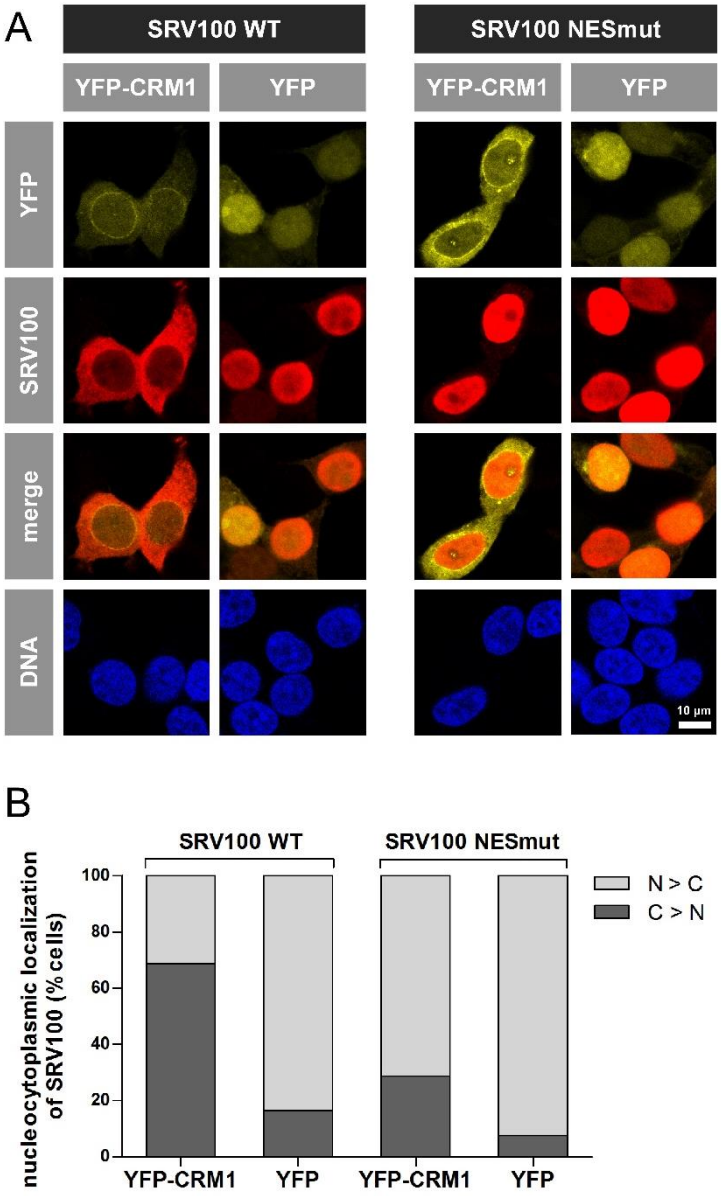

Figure 3.54: The SRV100 biosensor allows to study CRM1 nuclear export activity in a cellular system.

SRV100 WT biosensor shifted in the cytoplasm of 293T cells upon co-expression with YFP-CRM1, while SRV100 NESmut remained in the nucleus. **A)** Images show representative examples of 293T cells co-expressing SRV100 WT (left) or SRV100 NESmut (right) and either YFP or YFP-CRM1. Images were acquired with a Leica SP8 confocal laser scanning microscope. Scale bar, 10 µm (plasmids kindly provided by Jose A. Rodríguez). **B)** Quantification of the nucleocytoplasmic localization of SRV100 WT and SRV100 NESmut. Graphs indicate the percentage of co-transfected cells showing predominantly nuclear (N>C) or predominantly cytoplasmic (C>N) localization of SRV100 calculated by a cell profiler pipeline. At least 450 cells were counted per sample (quantification by Dr. Nina Schulze, ICCE, University of Essen).

Indeed, the usability of the biosensor in 293T cells was not only successfully verified by confocal microscopy (Figure 3.54 A), but its possibility of a robust automated quantification was also demonstrated (Figure 3.54 B).
These results furthermore identified the 293T cell line as a suitable cellular system to evaluate CRM1 export activity, although there might be other cell lines that better adhere to culture surfaces and might be easier to stain, e.g. HeLa Kyoto cells. However, in the HeLa Kyoto cell line, co-expression with YFP-CRM1 only marginally increased the cytoplasmic localization of SRV100 WT, making this cell line unsuitable for the biosensor assay. Differences in the nuclear transport machinery between different cell lines might lead to this observation and must be further characterized. Moreover, defining of the cell cytoplasm, so far identified by the inconsistent YFP intensity, could be optimized by a consistent cell mask staining of cells.
In the future, the biosensor has to be optimized for testing the tweezer molecules. Of note, the current biosensor comprises only aa 1-100 of the Survivin coding sequence. Since the tweezer molecules were designed and indeed shown to also bind basic residues in the C-terminus (Figure 3.20 and Figure 3.21), including K103 and R106, the biosensor has to be extended to e.g. SRV110. As a control for specificity, a biosensor relying on another, unrelated NES bearing protein should assure that tweezer molecules only affect the export of Survivin.

3.6.5 Cellular uptake of molecular tweezer molecules

To study the influence of supramolecular tweezer molecules on the Survivin–CRM1 interaction and therefore on Survivin's cellular functions, it is of utmost importance to ensure cellular uptake of molecular tweezer molecules. For this purpose, a basic tweezer molecule was linked to the fluorophore TAMRA (synthesis by Christian Heid, Department of Organic Chemistry, Schrader group, University of Essen; Figure 3.55 A). TAMRA absorbs light at a wavelength of 552 nm and emits at 579 nm. HeLa Kyoto cells, transiently overexpressing Cerulean-Survivin142 were treated with 10 µM TAMRA-coupled tweezer for 20 h and analyzed by live cell microscopy (by Cecilia Vallet, Department of Molecular Biology II, Knauer group, University of Essen; Figure 3.55 B).
Besides proving first evidence for cellular uptake of molecular TAMRA-coupled tweezer, microscopic analysis revealed an accumulation of the tweezer in vesicle-like structures inside the cell (Figure 3.55 B). Of note, tweezer uptake did not provoke obvious cellular toxic effects. However, this has to be quantitatively assessed by different cell viability assays as well as the concrete nature of the vesicles. Only if the tweezer can be released from this

vesicle-like structures into the cytoplasm and also the nucleus, it might be able to finally modulate Survivin's functions within the cell.

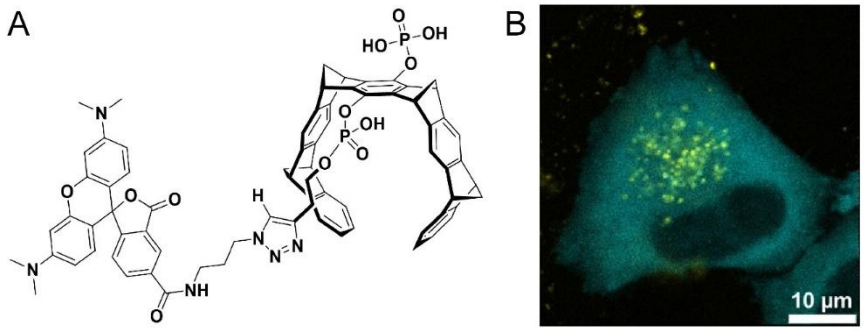

Figure 3.55: Fluorescenctly labeled tweezer localizes in vesicle-like structures inside the cell. Fluorescence labeling with TAMRA enabled visualization of cellular uptake of supramolecular tweezer and its accumulation in vesicle-like structures. **A)** Chemical structure of TAMRA-coupled tweezer (synthesis by Christian Heid, Department of Organic Chemistry, Schrader group, University of Essen). **B)** HeLa Kyoto cells, transiently overexpressing Cerulean-Survivin142 (cyan), were treated with 10 µM TAMRA-coupled tweezer (yellow) for 20 h. Image was acquired with a Leica SP8 confocal laser scanning microscope. Scale bar, 10 µm (cell treatment and microscopy by Cecilia Vallet, Department of Molecular Biology II, Knauer group, University of Essen).

4 DISCUSSION

Targeted cancer therapy provides a promising new approach to fight cancer the second leading cause of death worldwide following cardiovascular diseases (World Health Organization, 2018) and reduces or avoids harmful side effects occurring in conventional chemo- and radiotherapy. This therapy addresses specific targets which are preferentially or exclusively expressed in cancer cells (Baudino, 2015). Survivin, highly up-regulated in almost all cancer types (Ambrosini *et al.*, 1997; Adida *et al.*, 2000), represents such a target. As a multitasking protein without enzymatic activity, Survivin fulfills its dual role in inhibition of apoptosis and mitotic regulation (Li *et al.*, 1998) via an interaction with the export receptor CRM1 mediated by Survivin's highly conserved, leucine-rich NES (Knauer *et al.*, 2006; Knauer *et al.*, 2007c).

Thus, interference with the Survivin–CRM1 interaction could not only help to elucidate the distinct biological functions of Survivin in mechanistic detail but also to potentially inhibit cancer cell proliferation. Since small molecule CRM1 inhibitors supposedly also interfere with binding of CRM1 to other NES-bearing proteins, making them at most selective but clearly not specific (Kudo *et al.*, 1999; Gravina *et al.*, 2014; Hill *et al.*, 2014), Survivin's surface-exposed NES should be targeted by supramolecular tweezer molecules, which are able to bind to surface-accessible lysine and arginine residues (Fokkens *et al.*, 2005).

In contrast to the so far exploited indirect approaches to affect Survivin's functions like interference with its expression or induction of Surivivin-specific immune responses (Kelly *et al.*, 2011; Garg *et al.*, 2016), the supramolecular approach in this work represents an urgently needed direct strategy to inhibit Survivin by signal-specific binding to its NES and thus a specific inhibition of the Survivin–CRM1 interaction interfering with Survivin's cellular functions.

4.1 Robust Survivin production to enable supramolecular ligand evaluation

To enable supramolecular ligand evaluation *in vitro*, wild type Survivin142 was successfully expressed and purified (Figure 3.1 and Figure 3.2). Characterization of wild type Survivin142 by CD spectroscopy (Figure 3.3) revealed correct protein folding, and analytical gel filtration (Figure 3.4 A) demonstrated that Survivin142 homodimerizes in solution (Chantalat *et al.*, 2000; Verdecia *et al.*, 2000). Furthermore, in accordance to literature (Engelsma *et al.*, 2007) mutations in Survivin's dimer interface (F101AL102A) were shown to stabilize Survivin's monomeric state in analytical gel filtration experiments (Figure 3.4 B). Mutations in Survivin's NES (L96AL98A) also interfered with Survivin homodimerization. This can be explained by the partial overlap of Survivin's NES (^{89}VKKQFEELTL^{98}) with its dimer interface (aa 6–10 and 89–102) (Chantalat *et al.*, 2000; Knauer *et al.*, 2006).

However, wild type Survivin142 did not allow to generate evaluable NMR signals (Figure 3.5), thus precluding analysis of supramolecular tweezer binding by NMR titration experiments. Indeed, the only published NMR structure of Survivin in solution was obtained with the truncated version Survivin120 (Sun *et al.*, 2005). Moreover, *in silico* analyses of Survivin (Figure 3.6) revealed an instable and highly flexible C-terminal α-helix, specifically mediated by amino acids around residue 120. Therefore, this truncated version was used for further *in vitro* experiments.

Expression and purification of truncated Survivin120 (Figure 3.7 and Figure 3.8) resulted in a higher protein yield, supporting the hypothesis of α-helix instability. In addition, truncated Survivin120 was suitable for NMR spectroscopy (Figure 3.9), thus allowing titration of supramolecular tweezer molecules to study binding. Characterization of Survivin120 by CD spectroscopy (Figure 3.10) revealed correct protein folding with a smaller α-helical amount compared to wild type Survivin142, attributed to its shortend C-terminal α-helix. Analytical gel filtration (Figure 3.11) demonstrated that Survivin120 still forms homodimers in solution (Chantalat et al, 2000; Verdecia et al, 2000) since its dimer interface (aa 6–10 and 89–102) is not affected by the truncation.

4.2 Supramolecular tweezer binds directly to distinct surface-exposed basic amino acids of Survivin

Now, to develop an approach for Survivin inhibition by direct interaction with the protein, its surface-exposed NES should be chemically addressed by supramolecular di-phosphate tweezers (Dutt *et al.*, 2013a). As water-soluble strong lysine and arginine binders (Fokkens *et al.*, 2005), these tweezer molecules indeed revealed direct binding to recombinant Survivin

in ITC experiments (Figure 3.12). Moreover, NMR spectroscopy allowed to map supramolecular tweezer binding to distinct basic amino acid residues K90/91, K103 and R106 (Figure 3.20 A and Figure 3.21 A) within or near Survivin's NES, identifying them as potential tweezer binding sites. However, the ability of supramolecular tweezers to also bind several surface-exposed lysine and arginine residues of other proteins will cause a problem when applying these supramolecular ligands in a cellular environment. Thus, overcoming tweezer unspecificity is urgently required and was approached in this work.

4.3 Peptide modification of tweezer enhances affinity and specificity

To develop improved tweezer molecules with an even enhanced affinity and specificity towards Survivin and especially its NES, Survivin's dimer interface was selected as an additional recognition unit. As naturally occurring binding motifs, a short (ELTL) and an elongated peptide (ELTLGEFL) mimicking the dimer interface and partly overlapping with Survivin's NES were linked to the basic di-phosphate tweezer (Figure 3.14). Derived from structural data, K103 at the beginning of the C-terminal α-helix (Figure 3.13) should serve as anchor residue for the basic tweezer cavity. Here, sophisticated selection of the linker should allow perfect positioning of the peptides along the dimer interface. Indeed, MD simulations revealed a strong complexation of K103 by the tweezer cavity as well as hydrogen bond interactions between the linked peptides and the side chains of Survivin (Figure 3.15). This indicated a stable binding of the tweezer to the exposed protein surface during the whole simulation time. Moreover, the modified tweezer molecules partially shielded Survivin's NES. These promising results were thus decisive to synthesize both peptide-linked tweezer molecules as drafted by hypothesis-driven, docking-guided design.

ITC experiments indeed confirmed binding of all three supramolecular tweezer molecules to Survivin, independently of peptide-linkage (Figure 3.16 – Figure 3.18). In every case, exothermic binding reactions were observed, and the integrated data of the respective binding isotherms were fitted to a one-site binding model, which yielded K_D values of 20–30 µM. Whereas modification with the short peptide ELTL did not significantly alter the binding affinity of the basic tweezer molecule with a K_D of 29.6 µM towards Survivin, addition of the elongated peptide ELTLGEFL could increase the K_D to 21.2 µM. Thus, introducing a peptide mimicking Survivin's natural dimer interface, could indeed enhance the affinity of the molecular tweezer towards Survivin. Moreover, all binding affinities towards Survivin as determined by ITC were in good agreement with the binding affinity (K_D = 17 µM) of the basic tweezer molecule towards lysine (Dutt *et al.*, 2013a).

Next, NMR spectroscopy should allow to map supramolecular ligand binding to distinct amino acid residues (Hogeweg *et al.*, 2017). Therefore, chemical shift perturbations as well

as NMR signal intensities of Survivin were recorded upon titration with equimolar amounts of tweezer molecules (unmodified and Tweezer-ELTL) (Figure 3.19). Titration of the unmodified tweezer resulted in chemical shift perturbations especially at the basic amino acid residues K91, K103 and R106 (Figure 3.20 A). In addition, signal intensity decreased in the same amino acid region (Figure 3.21 A) identifying them as potential tweezer binding sites. However, titration of the Tweezer-ELTL even enhanced chemical shift perturbations recorded for these basic residues (Figure 3.20 B), and drastically decreased signal intensities (Figure 3.21 B). Notably, NMR data revealed that the peptide-modification enabled the tweezer molecule to additionally interfere with the complete dimer interface including the NES indicating a more specific binding with higher affinities in this area. Unfortunately, the applied NMR method is not able to distinguish between lysine residue K90 and K91 since they are in too close proximity. Nevertheless, NMR titration experiments allowed a rather precise mapping of tweezer binding to distinct basic amino acids (K90/91, K103 and R106) within or near Survivin's NES (Figure 3.22) indicating their potential for NES shielding and thus inhibition of the Survivin–CRM1 interaction. Moreover, the binding sites identified by NMR are in perfect agreement with the initial considerations when designing the new peptide-linked tweezer molecules. In future experiments, Tweezer-ELTLGEFL titration should allow to evaluate whether elongation of the peptide might even further increase binding specificity and affinity.

4.4 *In silico* analysis confirms tweezer binding sites and enhanced specificity upon peptide modification

Tweezer binding to Survivin further investigated by *in silico* MD and QM/MM studies supported experimental NMR results. Different complexes between four lysine residues (K23, K90, K91 and K103) and two tweezer molecules, the unmodified and the ELTL-linked tweezer, were analyzed for monomeric Survivin.

Distance measurements between the ammonium nitrogen of the analyzed lysine and the center of mass of the respective tweezer revealed that Tweezer-ELTL formed more fixed inclusion complexes compared to unmodified tweezer, indicating a higher specificity for the ELTL-linked tweezer molecule and therefore confirming the experimental NMR titration results (Figure 3.23). However, the larger effects of Tweezer-ELTL over the NMR signals did not seem to obey a specific strong conserved interaction of the peptide substituent ELTL with the protein. Instead, the additional number of interactions due to the additional peptide could exert a cooperative effect leading to a higher specificity of Tweezer-ELTL compared to unmodified tweezer, thus maximizing the effect over the sites.

Nevertheless, one unique long-lasting interaction between the tail of Tweezer-ELTL and the homologous segment in the protein (E95–L98) occurred when the complex is located on K103 (Figure 3.24). This particular site is the only one among the studied sites that permitted the anti-parallel pairing observed in the original binding mode of the Survivin dimer. This structure, although not preserving over the whole simulation, represented the only long-lasting arrangement for approximately 10 ns observed in the trajectories. Thus, it is expected to contribute significantly on the properties of the complex between Tweezer-ELTL and K103 and its differentiation with those on the other sites. Moreover, the complex of Tweezer-ELTL on site K103 of monomeric Survivin resulted the one with the lowest energy content (Table 3.1) which can obey to the more effective binding of its tail to the analogous peptide segment in the protein.

Furthermore, the results of the QM/MM optimizations (Table 3.1) concluded for monomeric Survivin that K23 was the least favored site for tweezer binding whereas K90, K91 and K103 were higher exposed with lower energy content. This perfectly agrees with the effects of the NMR signals, rather indicating that Survivin structure is monomeric during the NMR experiments.

Moreover, results for monomeric Survivin showed stable complexation with both lysine residues K90 and K91 (Figure 3.23), thus requiring further analysis whether Tweezer-ELTL is able to distinguish between the adjacent lysine residues, e.g. by single point mutations of either K90 or K91. For a complete assignment of the NMR data, the arginine residues or at least R106 should be also considered in the calculations. Furthermore, the elongated ELTLGEFL-linked tweezer has to be analyzed by MD and QM/MM studies as well as experimental NMR titration experiments urgently checking for an enhanced affinity, stability and specificity of its binding to Survivin compared to Tweezer-ELTL.

4.5 Influence of tweezer molecules on Survivin's folding and dimerization

The *in silico* results, which indicated a monomeric Survivin structure during the NMR experiments, initiated the experimental investigation of the tweezer molecules for a potential of dimer disruption or any other conformational changes of Survivin's structure. So far, analytical gel filtration revealed no effect of tweezer binding on Survivin dimer formation (Figure 3.26). However, this might be based on the comparatively low binding affinity of the tweezer and the high dilution in the experimental setup. Therefore, other methods, e.g. cross-linking of Survivin monomers with glutaraldehyde upon tweezer incubation and subsequent analysis of the resulting protein size via SDS-PAGE, are of utmost importance to thoroughly examine a potential effect of supramolecular tweezer binding on Survivin's dimeric state. Although dimerization did not seem to be disrupted, supramolecular binding of

tweezer molecules to Survivin influenced its secondary structure but did not induce protein denaturation (Figure 3.25 B). However, to elucidate detailed changes in Survivin's conformation X-ray crystal structures of tweezers bound to Survivin are urgently needed.

4.6 Confirming specificity of tweezer binding with a Survivin triple lysine mutant

Theoretically, mutation of the respective basic anchor residues as revealed by NMR should prevent tweezer binding and thus confirm their specific targeting to the Survivin protein surface. Therefore, a Survivin120 variant harboring three lysine to serine mutations at amino acid residues K90, K91 and K103 was generated (Figure 3.39 and Figure 3.40). Serine residues should not be bound by lysine and arginine binding tweezer molecules (Fokkens *et al.*, 2005), but as polar amino acids maintain the protein solubility and avoid undesirable effects on protein folding (Barnes and Gray, 2003; Trevino *et al.*, 2008).

Interestingly, ITC measurements revealed an increased binding of the basic tweezer (Figure 3.43) as well as the modified Tweezer-ELTL (Figure 3.44) to Survivin120-K90/91/103S compared to Survivin120. Since the tweezer molecules evidentially interact only with basic amino acids (Fokkens *et al.*, 2005), they are no longer able to bind to residues K90, K91 and K103. Thus, they must bind to other lysine or arginine residues on the protein surface. Especially R106 is not mutated and still offers an attractive binding site for the tweezer molecules. Moreover, the enhanced binding affinity could be explained by changes on Survivin's surface, due to the introduced serine mutations in the close environment of potential binding sites including R106.

Besides complexation of lysine and arginine residues by the tweezer cavity, further empirical rules exist for efficient surface lysine complexation (Bier *et al.*, 2013). First, the respective binding site must feature steric accessibility, for example be presented in the middle of an α-helix. Second, additional hydrogen bonds to neighboring residues enhance complexation. Third, a lack of multiple lysine or arginine residues in close proximity renders tweezer binding more efficient since no additional positively charged residues divert tweezers from trapping the desired lysine or arginine side chain inside their cavity (Bier *et al.*, 2013).

With respect to this work, mutations to serine decreased the quantity of lysine residues in close proximity, and the number of neighboring residues with the potential to form hydrogen bonds with the tweezer was increased. This could explain the increased binding affinity of the molecular tweezers towards the Survivin triple lysine mutant. However, to finally determine the exact binding site of tweezer molecules, additional structural experiments like NMR titration or crystallization are undoubtedly required, including different point mutants as well as modified tweezer molecules.

Since all three mutated lysine residues (K90, K91 and K103) are located in Survivin's dimer interface, mutations could also affect homodimerization and hence facilitating tweezer binding to a monomeric Survivin protein with improved steric accessibility of potential binding sites. As analytical gel filtration experiments could not clarify whether the Survivin triple lysine mutant reveals an altered dimerization behavior (Figure 3.42), the monomeric Survivin mutant SurvivinDIMmut-F101AL102A might be used as a control in further experiments.
Moreover, CD spectroscopy of Survivin120-K90/91/103S revealed structural differences compared to Survivin120 (Figure 3.41 A). This change in the CD spectrum could be explained by the additional hydroxy groups of the serine residues and thus negative charges at pH 7.7 in the CD buffer, particularly since the spectrum overlaps with that of truncated Survivin120 incubated with unmodified tweezer molecule (Figure 3.41 A). Binding of tweezer molecule also introduces negative charges due to its phosphate groups.
To conclude, specific targeting of tweezer molecules to Survivin's surface-exposed basic amino acids could so far not be confirmed with the generated triple lysine mutant because of its elucidated altered structural conformation. Thus, further attempts with a Survivin mutant harboring other lysine replacements as well as an additional replacement of R106 are required urgently.

4.7 Detection of robust export complex assembly to enable supramolecular ligand evaluation *in vitro*

Supramolecular tweezer binding was mapped at distinct lysine and arginine residues on Survivin's surface. Binding affinity and selectivity were enhanced by covalently linked peptides mimicking Survivin's dimer interface and thus providing an additional binding platform. Here, the principle of avidity was transferred from multivalent antibody–antigen interaction to protein-supramolecular ligand interaction exploiting bivalent binding via both the tweezer unit and the linked peptid ensuring a high avidity. Now, this work focused on the effect of this supramolecular tweezer binding on the Survivin–CRM1 interaction and thus export complex assembly *in vitro*. Therefore, detection of robust export complex assembly has to be ensured to enable subsequent supramolecular ligand evaluation.
Besides the cargo Survivin, the export receptor CRM1 as well as its cofactor Ran were required for *in vitro* detection of export complex assembly. To enable stable assembly of the export complex, a RanQ69L mutant was used, which has a drastically reduced GTPase activity and is, once bound to GTP, constitutively active (Klebe *et al.*, 2002). CRM1 and RanQ69L could be expressed and purified successfully (Figure 3.27 – Figure 3.29). Characterization of both export complex members by CD spectroscopy (Figure 3.31 A)

revealed their correct protein folding. Analytical gel filtration (Figure 3.31 B) confirmed their theoretical molecular weight of 123.5 kDa for CRM1 and 24.6 kDa for RanQ69L.

To now allow quantitative evaluation of the Survivin–CRM1 interaction and thus export complex assembly, two appropriate *in vitro* assays (analytical gel filtration and pull-down assay) were performed in this work.

Since assembly of multi-protein complexes is characterized by an increase in molecular weight, the proteins were first subjected to analytical gel filtration. However, under the applied experimental conditions, this method was not suitable to assess export complex assembly. Complex formation was neither detectable for full-length (Figure 3.32 A) nor for truncated Survivin (Figure 3.32 B) as a cargo. On the one hand, the separation potential of the used column might have been unsuited for the detection of the complex and therefore little molecular weight changes in the elution range of CRM1 and the potentially formed complex might not have been able to distinguish. On the other hand, the export complex might not be stable during the experiment due to either high salt concentration, a wrong pH or a high dilution factor. Moreover, since the members of the export complex undergo transient interactions, their binding affinities may be rather weak (Kutay and Güttinger, 2005) and thus too unstable to allow detection via gel filtration. This weak assembly might be overcome in future biochemical gel filtration experiments by addition of recombinant RanBP3 to enhance the stability of the *in vitro* export complex. RanBP3 is known to be involved in stabilizing the export complex and affecting its cargo selectivity (Englmeier *et al.*, 2001; Langer *et al.*, 2011). Indeed, cellular results of this work confirmed a robust interaction with CRM1 as well as a partial co-localization with Survivin, especially in but not restricted to mitotic phases (Figure 3.52), thus playing a crucial role for export complex assembly.

In addition, export complex formation might not be detected since it is a complicated mechanism with many parameters to consider, for example ensuring the compact conformation of CRM1 (Fox *et al.*, 2011; Monecke *et al.*, 2014; Dickmanns *et al.*, 2015). Specific mutations in the CRM1 protein were described to fix its conformation in the compact state even in the absence of Ran binding, thereby significantly enhancing affinity towards cargo NES (Figure 4.1). Deletion of nine amino acids at the C-terminal helix ($CRM1^{1063X}$) leads to a 10-fold higher PKI-NES affinity while alanine substitutions of three HEAT9 loop residues (430VLV > AAA) ($CRM1^{AAA}$) even enhance PKI-NES binding by a factor of 80. Importantly, combination of both alterations ($CRM1^{AAA/X}$) results in a more than 600-fold increased CRM1 binding affinity for PKI-NES compared to the wild type protein (Fox *et al.*, 2011). Using the $CRM1^{AAA/X}$ mutant and therefore downsizing the trimeric, RanGTP-containing to a dimeric complex, only constituted of Survivin and CRM1 would be a promising strategy to facilitate handling and success of the *in vitro* system. Hence, the

mutant CRM1$^{AAA/X}$ might be an attractive alternative to investigate Survivin binding via gel filtration due to its enhanced affinity even in absence of RanGTP.

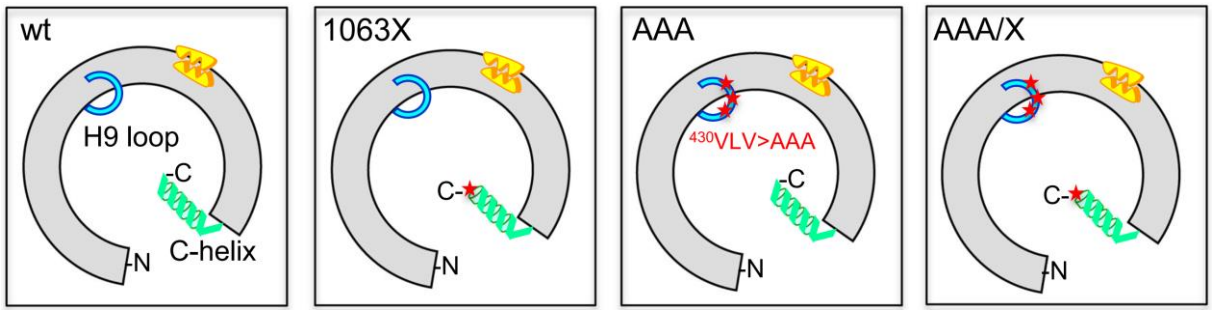

Figure 4.1: Schematic representation of CRM1 mutations increasing NES affinity in the absence of RanGTP.

CRM1^{1063X} lacks nine amino acids at the C-terminal helix. CRM1^{AAA} bears alanine substitution of three HEAT9 loop residues (430VLV > AAA). The most efficient mutant CRM1$^{AAA/X}$ combines both alterations (García-Santisteban *et al.*, 2016).

Besides analytical gel filtration, pull-down assays also allow to at least qualitatively assess protein–protein interactions. Advantages compared to e.g. gel filtration are lower protein dilution, less consumption of sample material as well as a rather sensitive detection of the proteins via immunoblot.

Pull-down assays indeed provided robust evidence of export complex assembly with recombinant proteins for full-length Survivin142 as well as truncated Survivin120 (Figure 3.33). Furthermore, CRM1 specifically interacted with wild type Survivin transiently overexpressed in eukaryotic cell lysates where binding had to compete with a variety of other cellular cargo proteins (Figure 3.34). However, binding of Survivin mutants was clearly diminished (Figure 3.34). Mutations in Survivin's NES (L96AL98A) eliminated two important hydrophobic residues for NES cleft interaction (Knauer *et al.*, 2006) and thus led to reduced CRM1 binding. Moreover, a Survivin variant mutated in its dimer interface (F101AL102A) thus forming monomers in solution (Engelsma *et al.*, 2007), also was impaired in its ability to interact with CRM1. This again underlines the importance of both Survivin regions, the NES and the overlapping dimer interface and thus the antagonism between homodimerization and nuclear export (Engelsma *et al.*, 2007), which is still not completely elucidated and a matter of controversy.

4.8 Supramolecular interference with export complex assembly *in vitro*

As proven quite robust, pull-down assays were further used to investigate the effect of supramolecular tweezer molecules on export complex assembly. Indeed, already the

unmodified basic tweezer molecule was able to hinder the interaction between recombinantly expressed Survivin and CRM1 at a concentration of 100 µM (Figure 3.35). Furthermore, the same concentration of basic tweezer and modified Tweezer-ELTL could as well specifically interfere with the Survivin–CRM1 interaction in eukaryotic cell lysates. In this experimental setting, the supramolecular ligands encounter a plethora of potential cellular target proteins including but are not limited to other potential CRM1 cargoes. Those present even more surface accessible lysine and arginine residues that represent attractive sites and thus might capture a significant proportion of tweezer molecules (Figure 3.36). Taking this unspecific binding into account, effective tweezer concentration to interfere with the Survivin–CRM1 interaction might be far lower than the applied concentration.

As a control, comparable amounts of the peptide ELTL alone did not affect export complex assembly (Figure 3.36), indicating that the tweezer unit was pivotal for specific anchorage of the peptide. Nevertheless, at concentrations of 100 µM, the peptide modification could not significantly improve the inhibitory potential of the tweezer. Thus, different tweezer concentrations ranging from 200 µM to 10 nM were now evaluated. Here, an effective concentration between 10–50 µM of basic and ELTL-linked tweezer molecules could successfully interfere with export complex assembly (Figure 3.37). This was in perfect agreement with the results of the ITC experiments (Figure 3.16 and Figure 3.17), which revealed a K_D of 29.6 µM for Survivin binding to both tweezer molecules. However, improved inhibition upon incubation with the modified Tweezer-ELTL was again not shown in pull-down experiments. Nevertheless, NMR titrations could demonstrate a more specific binding of the peptide-linked tweezer in the region around Survivin's NES (Figure 3.20 and Figure 3.21).

Further pull-down experiments additionally including the elongated peptide-linked Tweezer-ELTLGEFL at a concentration of 50 µM revealed for the first time successful export complex assembly inhibition. Here, both peptide-linked tweezers were indeed superior to the unmodified tweezer. However, to undoubtedly determine effective concentrations and thus to compare the inhibitory potential of the different tweezer molecules, the concentration range between 10–50 µM must be analyzed more precisely in e.g. 5 µM steps.

Of note, the pull-down experiments further revealed disruption of GST-CRM1 binding to GSH-Sepharose beads induced by the tweezer molecules. This indicates tweezer binding to the protein GST and suggests that current peptide modification might still not be sufficient to achieve binding specificity. Furthermore, peptide-linked tweezer might also unspecifically bind to the NES cleft of CRM1 since the linked peptides represent parts of the conserved Survivin NES. However, undesired tweezer binding to GST or CRM1 has to be further corroborated by other means, for example by ITC measurements. Nevertheless, all tweezer molecules were able to inhibit the Survivin–CRM1 interaction in competition to other proteins at an effective concentration in the range of 10–50 µM.

4.9 Confirming specificity of supramolecular interference with export complex assembly using a Survivin triple lysine mutant

To further analyze if the inhibition occurs by specific tweezer binding to lysine residues in the NES region of Survivin or rather unselectively, e.g. by tweezer binding to CRM1, pull-down assays were performed with a Survivin triple lysine mutant (K90/91/103S). Mutation of lysine residues in Survivin's NES region to serine should abolish tweezer binding in this area and thus NES shielding. However, pull-down analyses indicated that both, unmodified and peptide-linked tweezer molecules, were still able to interfere with the interaction between mutated Survivin120-K90/91/103S and CRM1 (Figure 3.46). This could possibly be explained by the high excess of tweezer molecules that might result in an unexpected unspecific binding to CRM1, thereby blocking the NES cleft. Consequently, the experimental pull-down assay set up was adapted, so that unbound tweezer molecules can be washed away to avoid unspecific binding.

Interestingly, GST-Survivin120-K90/91/103S seemed to interact with CRM1 protein more efficiently than GST-Survivin120. Thus, introducing lysine to serine mutations in Survivin's NES region might increase the binding affinity between Survivin and CRM1. Indeed, analysis of the amino acid composition of different NES sequences compared with the overall amino acid composition of the respective protein revealed a statistically significant over-representation of glutamate, aspartate, serine and leucine (La Cour *et al.*, 2004). Thus, the increase in the amount of serine residues within Survivin's NES by mutations might indeed have improved the NES binding to CRM1. To avoid this effect, other amino acid replacements have to be investigated. As another small polar amino acid threonine might be suited since it should not enhance the NES strength. Another alternative could be alanine as simplest standard substituent.

Nevertheless, the raw data from the pull-down analysis was quantified by normalizing the intensities of pulled CRM1. This now demonstrates that all three tweezer molecules revealed an inhibitory effect on the interaction between CRM1 and GST-Survivin120 in contrast to the uncoupled peptide ELTL. The inhibiting effect of the tweezers even increased proportional to the peptide length with a more than 50 % reduced interaction for Tweezer-ELTLGEFL. However, for the triple lysine mutant GST-Survivin120-K90/91/103S neither the tweezer molecules nor the peptide alone had a strong inhibiting effect on the interaction with CRM1. This indeed confirms that the tweezer molecules indeed mediate interference with the Survivin–CRM1 interaction by addressing specific lysine residues in Survivin's NES thereby shielding it from the NES cleft of CRM1. Moreover, it could be demonstrated that this shielding and inhibition were enhanced by peptide modifications. Nevertheless, these findings must be confirmed by further NMR titration experiments thereby including different

point mutants as well as other modified tweezer molecules like the elongated ELTLGEFL-linked tweezer.

Moreover, to finally reveal the exact binding site of the tweezer molecules on Survivin and hence elucidate the molecular mechanism of interference, X-ray structure analysis of Survivin bound to tweezer molecules is pivotal. Novel structural information of the Survivin–CRM1 export complex would also assist to further improve supramolecular ligands. Mutated CRM1$^{AAA/X}$ (Figure 4.1) might facilitate solving the crystal structure of the export complex, as it could be used to reduce the trimeric, RanGTP containing complex to a dimeric complex.

4.10 Robust detection of export complex assembly in a cellular environment

After demonstrating supramolecular tweezer binding to distinct lysine and arginine residues on Survivin's surface, resulting in a disruption of the Survivin–CRM1 interaction *in vitro*, interference of nuclear export should now be characterized in a cellular environment. Here, several obstacles have to be overcome, including detection of the export complex within the cell, the establishment of assays to quantitatively investigate tweezer effects on export complex formation as well as active CRM1-mediated nuclear export of Survivin and of course the proof of cellular uptake of supramolecular tweezers.

First, cellular localization of all three endogenous export complex members including the cargo protein Survivin, the export receptor CRM1 and its cofactor GTPase Ran were analyzed via immunofluorescence staining in interphase as well as during all phases of mitosis. While Survivin predominantly localized to the nucleus in interphase, it revealed the characteristic localization of the CPC in the mitotic phases (Figure 3.48 A). During prophase, Survivin localized to chromosome arms and centromeres, and concentrated at centromeres in prometa- and metaphase. In anaphase, the CPC re-localized to the spindle midzone and the cell cortex to then accumulate at the cleavage furrow and the midbody in telophase and cytokinesis (Ruchaud *et al.*, 2007). The export receptor CRM1 was predominantly concentrated at the nuclear membrane in interphase cells, where it mediates facilitated nuclear export through the NPC. Moreover, it can be detected to a minor extent in the nucleoplasm, where it promotes export complex assembly (Figure 3.48 B) (Görlich and Kutay, 1999; Sorokin *et al.*, 2007; Kim *et al.*, 2017). Interestingly, CRM1 also partially co-localized with α-Tubulin at the mitotic spindle during prometa-, meta-, ana- and early telophase (Figure 3.49). Besides CRM1's role in targeting the CPC to the centromeres in early mitosis (Knauer *et al.*, 2006; Knauer *et al.*, 2007c), these observations support its surplus involvement in mitotic spindle assembly (Wu *et al.*, 2013). Moreover, CRM1 re-localized to the developing nuclear membrane already during late telophase (Figure 3.48 B). For the small GTPase Ran, no distinct cell cycle-dependent localization could be observed.

However, in interphase it predominantly localized in the nucleus, but was also found in the cytoplasm (Figure 3.48). Dominant nuclear localization of Ran bound to GTP in interphase cells can be explained by Ran's facilitated nuclear import mediated by NTF2 (Smith *et al.*, 1998). However, cytoplasmic Ran bound to GDP was still detectable.

Using immunofluorescence staining, nuclear co-localization of CRM1 with its cargo protein Survivin and thus export complex formation could already be demonstrated at the endogenous cellular protein level. However, for a better visualization and a robust confirmation of the export complex, the Survivin–CRM1 co-localization was further triggered upon exogenous overexpressing of both proteins revealing an accumulation of Survivin at the nuclear membrane where it co-localizes with CRM1. Here, in contrast to endogenous protein levels, the export machinery was highly overloaded which resulted in the clearly observable export complex formation at the nuclear membrane. However, to further investigate the Survivin–CRM1 interaction, exogenous overexpressing of both proteins should rather be avoided as the high overload of the export machinery is not physiological and might cause undesirable side effects. Therefore, a proximity ligation assay was successfully established which allows to reliably monitor the endogenous cellular Survivin–CRM1 interaction. This assay visualizes protein–protein interactions with a maximal distance of 40 nm. Indeed, Survivin–CRM1 interactions could be visualized by single PLA foci at the molecular level. They were detected throughout the whole cell but mainly resided inside the nucleus (Figure 3.51 A), where the export complex is formed. Moreover, development of a specific imaging analysis pipeline enabled robust automated downstream quantification of PLA foci (Figure 3.51 B and C). So, this assay now allows to study the Survivin–CRM1 interaction and thus export complex assembly at the endogenous cellular protein level, and as such enables investigation of supramolecular tweezer effects in a quantitative manner.

4.11 RanBP3 contributs in Survivin export complex assembly

Furthermore, RanBP3 is known to be an important player of nuclear export, especially with regards to export complex formation. Studies revealed an involvement in stabilization of the export complex and modulation of cargo selectivity (Englmeier *et al.*, 2001; Langer *et al.*, 2011). In this work, contribution of RanBP3 in Survivin export complex assembly should be demonstrated by immunofluorescence staining of cellular endogenous RanBP3. Indeed, the results confirmed co-localization of RanBP3 with the export receptor CRM1 especially at the mitotic spindle in prometa-, meta-, ana- and telophase, while it predominantly localized in the nucleus of interphase cells (Figure 3.52 B). Co-localization with the cargo protein Survivin was detectable at the centromeres, the spindle midzone and the midbody in mitosis as well as in the nucleus in interphase (Figure 3.52 A). Thus, the results demonstrated a robust

interaction with CRM1 as well as a partial co-localization with Survivin, especially in but not restricted to mitotic phases. The observed predominantly localization of RanBP3 in the nucleus during interphase, where the export complex is assembled, suggested its contribution in complex stabilization during formation (Englmeier *et al.*, 2001; Langer *et al.*, 2011). However, robust interaction between endogenous RanBP3 and CRM1 as well as Survivin have to be further confirmed by e.g. a proximity ligation assay which represents a more reliable and quantitative alternative to visualize transient protein–protein interactions. Besides RanBP3's stabilizing function in interphase, the immunofluorescence results rather suggested an additional contribution of RanBP3 in mitosis, e.g. functioning as an additional regulator in mitotic spindle assembly (Wu *et al.*, 2013).
To further analyze and confirm the role of RanBP3 in stabilization of Survivin export complex formation as well as regulation of mitotic spindle assembly, cellular effects upon RanBP3 overexpression or knock-down have to be investigated. This would for example include a quantitative examination of the RanBP3–CRM1 interactions, preferably by PLA, as well as microscopic analysis of proper mitotic spindle assembly.

4.12 Investigation of Survivin's cellular export

Next, a cellular biosensor assay enabling the investigation of cellular nuclear export activity of CRM1 was adapted from literature (García-Santisteban *et al.*, 2016) and its evaluation was improved by an automated downstream quantification step.
Therefore, the Survivin-based biosensor SRV100 was used in its wild type form as well as harboring a mutation in its NES (Figure 3.53). As expected, the SRV100 WT biosensor accumulated inside the nucleus when co-expressed with only YFP due to its NLS but readily re-located to the cytoplasm upon co-expression with YFP-CRM1, while SRV100 NESmut remained in the nucleus even when YFP-CRM1 was co-expressed (Figure 3.54 A) (García-Santisteban *et al.*, 2016). However, quantification by García-Santisteban *et al.* was performed rather semiquantitatively by determining the biosensor localization in at least 200 co-transfected cells by manual counting, ensuring unbiased scoring only by anonymously coded slides. Here, the biosensor assay was coupled with an automated sophisticated downstream quantification step. Establishment of an automated cell profiler pipeline enabled the calculation of the nuclear (N) / cytoplasmic (C) intensity ratios of SRV100 in each co-transfected cell in a statistically significant, robust and quantitative manner. A ratio below one indicates a cytoplasmic localization while a ratio higher than one represents a predominantly nuclear localization. Cell profiler data revealed a cytoplasmic re-localization only for SRV100 WT upon YFP-CRM1 co-expression. In contrast, co-expression of YFP or NES mutation did not result in any alteration of the respective nuclear biosensor (Figure 3.54 B).

Thus, this analysis allows to easily evaluate and quantify interference with Survivin export activity, as exemplified by the use of the NES mutant biosensor.
Indeed, the usability of the biosensor in 293T cells was not only successfully verified by confocal microscopy (Figure 3.54 A), but its possibility of a robust automated quantification was also demonstrated (Figure 3.54 B).
These results furthermore identified the 293T cell line as a suitable cellular system to evaluate CRM1 export activity, although there might be other cell lines that better adhere to culture surfaces and might be easier to stain, e.g. HeLa Kyoto cells. However, in the HeLa Kyoto cell line, co-expression with YFP-CRM1 only marginally increased the cytoplasmic localization of SRV100 WT, making this cell line unsuitable for the biosensor assay. Differences in the nuclear transport machinery between different cell lines might lead to this observation and must be further characterized. Moreover, defining of the cell cytoplasm, so far identified by the inconsistent YFP intensity, could be optimized by a consistent cell mask staining of cells. Detection of cell mask staining in the near infrared avoids any interference with the other fluorophores used in the biosensor assay.
In the future, the biosensor has to be optimized for testing the tweezer molecules. Of note, the current biosensor comprises only aa 1–100 of the Survivin coding sequence. Since the tweezer molecules were designed and indeed shown to also bind basic residues in the C-terminus (Figure 3.20 and Figure 3.21), including K103 and R106, the biosensor has to be extended to e.g. SRV110. As a control for specificity, a biosensor relying on another, unrelated NES-bearing protein should assure that tweezer molecules only affect the export of Survivin. Moreover, improvement of this assay might be achieved by an exchange of the triple arrangement of the Flag-tag with a fluorescent protein-tag e.g. a red fluorescent protein. Since such a quite big fluorescent protein-tag did not affect the export behavior of the biosensor, this exchange would enable live cell analysis of nuclear export and supramolecular ligand interference.

4.13 Cellular uptake of molecular tweezer molecules

Following successful establishment of suitable cell-based assays, cellular uptake of supramolecular tweezers had to be ensured. Therefore, a TAMRA-linked tweezer (Figure 3.55 A) was generated to enable visualization in fluorescence microscopy studies. Tweezer localization in vesicle-like structures revealed first evidence for cellular uptake (Figure 3.55 B). The localization of these vesicle-like structures is concentrated to a distinct region in the cytoplasm next to the nucleus, resembling the cellular localization of the Golgi apparatus. Nevertheless, the observed vesicle-like structures might also be endosomes or lysosomes,

when tweezer uptake occurred via endocytosis. Thus, to identify the concrete nature of the vesicles, co-localization experiments with cell organelle markers have to be performed.

So far, overexpression of cell organelle markers fused to fluorescent protein-tags revealed no co-localization with the TAMRA-linked tweezer. Here, depending on low expression levels, it is conceivable that TAMRA-linked tweezer and the overexpressed organelle marker were only present in neighboring but not in the same vesicle, thus avoiding detection of co-localization. Nevertheless, demonstrating accumulation of TAMRA-linked tweezer in vesicle-like structures also after cell fixation would enable future analysis of co-localization via immunostaining of organelles with specific antibodies thus circumventing low expression barriers.

Moreover, visual inspection did not hint towards obvious cellular toxic effects of tweezer treatment. However, this has to be quantitatively assessed by different cell viability or cytotoxicity assays. While cytolysis or membrane leakage might be easily identified by staining with trypan blue, which colors dead cells after passing their membranes but cannot distinguish between apoptosis and necrosis, other assays either monitor the mitochondrial activity like the MTT (3-(4,5-dimethylthiazol-2-yl)-2,5-diphenyltetrazolium bromide) assay or measure caspase activity, a key biomarker of apoptosis. Performing a combination of several assays is urgently needed to characterize cellular tweezer toxicity in detail. Toxicity must especially be characterized after potential release of TAMRA-linked tweezer from the obvious entrapment in vesicle-like structures. Only if the tweezer can be released into the cytoplasm and reaches the nucleus, it might be able to finally modulate Survivin's functions within the cell. So far, TAMRA-linked tweezer seemed to be entrapped into vesicles, but it might also be possible that a little portion was released or that the fluorophore TAMRA induced accumulation of the tweezer molecule and TAMRA-free tweezer should therefore not be entrapped. However, due to a missing fluorescent label this hypothesis would be challenging to prove. Therefore, other strategies must be established to robustly ensure the release of the visible TAMRA-linked tweezer into the cytoplasm and also the nucleus. If the vesicles will be identified as endosomes by immunostaining of cell organelle marker, cell treatment with chemical agents e.g. chloroquine should induce endosomal escape by the proton sponge effect (Mellman *et al.*, 1986; Varkouhi *et al.*, 2011). The proton sponge effect is mediated by agents with a high buffering capacity and the flexibility to swell when protonated, like chloroquine. As relatively lipophilic molecule, it penetrates the membranes in its unprotonated form. However, upon entering an acidic environment, it becomes protonated and too polar to escape rapidly through the membrane. Moreover, its protonation induces an extensive inflow of ions and water into the endosomal environment which subsequently leads to rupture of the endosomal membrane and release of the entrapped components (Varkouhi *et al.*, 2011).

Morover, transfection reagents, either commercially available reagents like PEI or Lipofectamine 2000 or a newly developed class of artificial peptidic transfection vectors based on an anion-binding motif, the guanidiniocarbonylpyrrole cation (Samanta *et al.*, 2016; Junghänel *et al.*, 2017; Li *et al.*, 2018), might be an alternative for mediating cellular uptake of tweezer molecules. These reagents form either liposomes (Lipofectamin 2000) encapsulating the ligands or polyplex-like structures complexing the ligands. Cellular uptake of these complexes is then mediated via the endocytic pathway. But here, the transfection reagents itself should enable endosomal escape using the proton sponge effect. This should mostly avoid the entrapment of tweezer molecules in vesicle-like structures. However, endosomal escape can still fail which would lead to the digestion of endosomal content.

Thus, microinjection would allow direct delivery in different cellular compartments avoiding vesicle-involving pathways like endocytosis. Furthermore, this method would demonstrate *in vivo* relevance of tweezers for nuclear export. Promising supramolecular ligands should be pre-incubated with the established recombinant Survivin substrates (GST-Survivin-GFP, GST-SurvivinNESmut-GFP, etc.) (Knauer *et al.*, 2007b) before co-injecting the mixture directly into e.g. the nucleus and monitoring their export over time by live-cell fluorescence microscopy. Alterations in transport kinetics time upon tweezer incubation would then prove supramolecular interference with Survivin's biological export activity in a cellular environment and allow further functional studies. Here, consequences of supramolecular interference with further biological functions of Survivin should include apoptosis inhibition, mitotic regulation as well as interactions with CPC members and mitotic CPC localization.

5 CONCLUSION AND OUTLOOK

This work demonstrated that supramolecular targeting of Survivin's NES with peptide-linked tweezer molecules is a promising approach. In contrast to other strategies for Survivin inhibition, which mostly target Survivin indirectly by e.g. interfering with its expression or inducing Survivin-specific immune responses (Kelly *et al.*, 2011; Garg *et al.*, 2016), the presented supramolecular approach is based on direct interaction with Survivin. A direct inhibition strategy has the advantage to avoid interference with upstream processes, like transcription, which control and regulate a variety of other proteins, thereby limiting cellular side effects. The basic supramolecular tweezer molecule was proved to be water-soluble, leading to a good applicability in biological systems, and shown to be a strong binder for lysine and arginine residues (Fokkens *et al.*, 2005). Since these amino acids are highly surface-exposed, the supramolecular tweezer represents a useful tool to address protein surfaces rather than binding grooves. This allows interference with protein–protein interactions, which are mostly mediated via binding interfaces on their surfaces and are involved in many regulatory mechanisms. However, as a good binder for lysine and arginine residues, the supramolecular tweezer also harbors the huge drawback of unspecificity since it is able to address several surface-exposed lysine and arginine residues of a variety of proteins.

So, this work challenged to overcome its unspecificity for the model protein Survivin. Modification of tweezer molecules with additional peptidic recognition units indeed revealed enhanced specificity and affinity as well as a higher inhibition potential of the Survivin–CRM1 interaction compared to the unmodified tweezer, showing the great potential of this direct supramolecular approach.

However, unspecific binding was still detected in pull-down assays, e.g. to GST, thereby hindering its binding to GSH beads. Consequently, when thinking of a potential use for cancer therapy, affinity and specificity of supramolecular tweezers still have to be further increased towards Survivin's NES to avoid unspecific binding to other proteins. One possible strategy could be the combination of two tweezer units anchored at two opposed sites of the NES/dimer interface, K90/91 and K103. Both were already proven as binding sites in NMR titration experiments, and the binding tweezer units could be easily linked via an extended peptide sequence flanking and mimicking most of the NES. This would create multivalency in binding, not only by two aa-selective tweezer units (double-tweezer), but also by a protein-selective peptide, and thus enhance affinity as well as specificity (Figure 5.1).

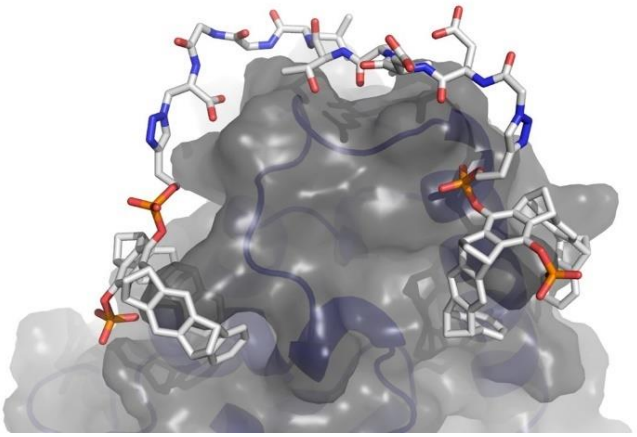

Figure 5.1: Multivalency of a double-tweezer created by anchorage of an elongated NES-mimicking peptide on two opposing lysine residues on Survivin's surface should enhance binding affinity as well as specificity.

Combination of two tweezer units anchored at two opposed sites of the NES/dimer interface, K90 (left) and K103 (right), and linked via an extended peptide sequence (GEELTLG) flanking and mimicking most of the NES should enhance affinity as well as specificity for Survivin binding. Survivin structure (ribbon structure in blue, surface in transparent grey) is based on the monomeric structure in solution (PDB: 1XOX). The double tweezer is depicted as stick representation (MD simulations and model by Christian Heid, Department of Organic Chemistry, Schrader group, University of Essen).

However, considering that the extended peptide itself is an almost complete and conserved NES, it might also bind to the NES cleft of CRM1. If an enhanced specificity towards Survivin could not be achieved, peptide sequences of other Survivin binding proteins should be considered as they might also have the potential to interfere with Survivin's biological functions. One example would be a peptide mimicking the region of Borealin or INCENP that interacts with Survivin's C-terminal helix forming the triple helix bundle (Jeyaprakash *et al.*, 2007). This would lead to an interference with correct CPC formation and thus mitotic defects. Peptides mimicking the binding interfaces of XIAP or HBXIP, which were shown to suppress apoptosis after complexing Survivin (Marusawa *et al.*, 2003; Dohi *et al.*, 2004), demonstrate another alternative. Competitive binding of those peptide-linked tweezers would inhibit the complexation of Survivin with XIAP or HBXIP, and therefore avoid the suppression of apoptosis.

To further increase the specificity and affinity of supramolecular Survivin NES ligands by multivalency, precision macromolecules and multifunctional ultrasmall metallic nanoparticles should be applied (Figure 5.2). By the use of multifunctional ultrasmall metallic nanoparticles, which can be covalently decorated, different supramolecular ligands as well as peptides can be combined on the nanoparticle surface to increase supramolecular binding (Figure 5.2 B). More precisely designed macromolecular scaffolds would furthermore allow to position and

combine different ligands, e.g. molecular tweezer units and natural peptide ligands, in defined distances and potentially orientation, thereby creating hetero- and multiavidity as well (Figure 5.2 A). Furthermore, newly developed fluorophores with aggregation-induced emission (AIE) properties should allow a simple, light-based readout upon successful protein binding, when combined with supramolecular ligands on macromolecular scaffolds or nanoparticle surfaces.

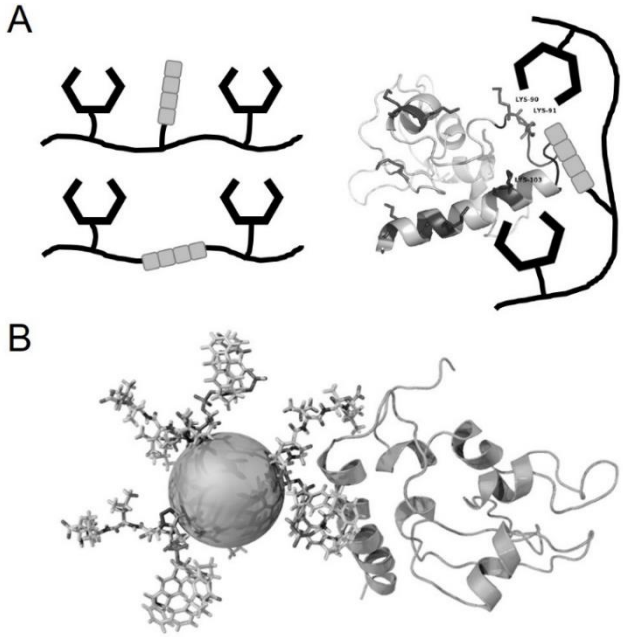

Figure 5.2: Created hetero- and multiavidity of precision macromolecules as scaffolds and multifunctional ultrasmall metallic nanoparticles should enhance binding affinity as well as specificity of supramolecular Survivin NES ligands.
Precision macromolecules **(A)** and multifunctional ultrasmall metallic nanoparticles **(B)** covalently decorated with a combination of supramolecular tweezer units and peptide ligands should strengthen the binding to Survivin by addressing several binding sites of the protein surface. Here, the ligands' NES specificity will be enhanced by rationally modifying the regognition units, concerning length, orientation and linker optimization (model of nanoparticle (B) by Mathis Kopp, Department of Inorganic Chemistry, Epple group, University of Essen).

So far, the presented supramolecular approach in this work is not applicable in a cellular environment because tweezer molecules seemed to be entrapped in vesicle-like structures not reaching their designated place of action. However, different strategies like chloroquine treatment, transfections reagents or microinjection demonstrate promising potential to ensure vesicle-escape or to circumvent ligand entrapment in vesicles. Only if the tweezer is released from these vesicle-like structures into the cytoplasm and reaches the nucleus, it will be able to finally modulate Survivin's functions within the cell.

In the future, after overcoming obstacles like unspecificity and cellular uptake of tweezer molecules, the supramolecular approach might also be adapted to interfere with other protein–protein interactions. NLS sequences on protein surfaces are outstandingly suited for supramolecular targeting since they harbor a distinct number and arrangement of lysine residues (Görlich and Kutay, 1999) that are easily addressable by tweezer molecules. Especially the precision macromolecules, which allow defined distances and orientation of supramolecular tweezer units, might enable high potential for interfering with nuclear import. They could easily be designed to address more than one of the lysine residues within NLS sequences, thus increasing binding affinity and specificity by multivalency.

LITERATURE

Adida C., Berrebi D., Peuchmaur M., Reyes-Mugica M. and Altieri D.C. (**1998**). Anti-apoptosis gene, survivin, and prognosis of neuroblastoma. *The Lancet*, 351 (9106): 882–883.

Adida C., Haioun C., Gaulard P., Lepage E., Morel P., Briere J., Dombret H., Reyes F., Diebold J., Gisselbrecht C., Salles G., Altieri D.C. and Molina T.J. (**2000**). Prognostic significance of survivin expression in diffuse large B-cell lymphomas. *Blood*, 96 (5): 1921–1925.

Ahlrichs R., Bär M., Häser M., Horn H. and Kölmel C. (**1989**). Electronic structure calculations on workstation computers: The program system turbomole. *Chemical Physics Letters*, 162 (3): 165–169.

Alberts B., Johnson A., Lewis J., Morgan D., Raff M., Roberts K., Walter P., Wilson J. and Hunt T. (**2015**). Molecular biology of the cell, New York, NY: Garland Science Taylor and Francis Group.

Altieri D.C. (**2001**). The molecular basis and potential role of survivin in cancer diagnosis and therapy. *Trends Mol Med*, 7 (12): 542–547.

Altieri D.C. (**2006**). The case for survivin as a regulator of microtubule dynamics and cell-death decisions. *Curr Opin Cell Biol*, 18 (6): 609–615.

Altieri D.C. (**2008**). Survivin, cancer networks and pathway-directed drug discovery. *Nat Rev Cancer*, 8 (1): 61–70.

Altieri D.C. (**2010**). Survivin and IAP proteins in cell-death mechanisms. *Biochem J*, 430 (2): 199–205.

Ambrosini G., Adida C. and Altieri D.C. (**1997**). A novel anti-apoptosis gene, survivin, expressed in cancer and lymphoma. *Nat Med*, 3 (8): 917–921.

Arnaoutov A., Azuma Y., Ribbeck K., Joseph J., Boyarchuk Y., Karpova T., McNally J. and Dasso M. (**2005**). Crm1 is a mitotic effector of Ran-GTP in somatic cells. *Nat Cell Biol*, 7 (6): 626–632.

Arnaoutov A. and Dasso M. (**2005**). Ran-GTP regulates kinetochore attachment in somatic cells. *Cell Cycle*, 4 (9): 1161–1165.

Arnold K., Bordoli L., Kopp J. and Schwede T. (**2006**). The SWISS-MODEL workspace: A web-based environment for protein structure homology modelling. *Bioinformatics*, 22 (2): 195–201.

Ashkenazi A. (**2008**). Directing cancer cells to self-destruct with pro-apoptotic receptor agonists. *Nat Rev Drug Discov*, 7 (12): 1001–1012.

Attar A., Ripoli C., Riccardi E., Maiti P., Li Puma D.D., Liu T., Hayes J., Jones M.R., Lichti-Kaiser K., Yang F., Gale G.D., Tseng C.-H., Tan M., Xie C.-W., Straudinger J.L., Klärner F.-G., Schrader T., Frautschy S.A., Grassi C. and Bitan G. (**2012**). Protection of primary neurons and mouse brain from Alzheimer's pathology by molecular tweezers. *Brain*, 135 (Pt 12): 3735–3748.

Barnes M.R. and Gray I.C. (ed.) (**2003**). Bioinformatics for geneticists, Chichester u.a.: Wiley.

Barrett R.M.A., Colnaghi R. and Wheatley S.P. (**2011**). Threonine 48 in the BIR domain of survivin is critical to its mitotic and anti-apoptotic activities and can be phosphorylated by CK2 in vitro. *Cell Cycle*, 10 (3): 538–548.

Barrett R.M.A., Osborne T.P. and Wheatley S.P. (**2009**). Phosphorylation of survivin at threonine 34 inhibits its mitotic function and enhances its cytoprotective activity. *Cell Cycle*, 8 (2): 278–283.

Baudino T.A. (**2015**). Targeted Cancer Therapy: The Next Generation of Cancer Treatment. *Curr Drug Discov Technol*, 12 (1): 3–20.

Beck M., Förster F., Ecke M., Plitzko J.M., Melchior F., Gerisch G., Baumeister W. and Medalia O. (**2004**). Nuclear pore complex structure and dynamics revealed by cryoelectron tomography. *Science*, 306 (5700): 1387–1390.

Beck M., Lucić V., Förster F., Baumeister W. and Medalia O. (**2007**). Snapshots of nuclear pore complexes in action captured by cryo-electron tomography. *Nature*, 449 (7162): 611–615.

Beer (**1852**). Bestimmung der Absorption des rothen Lichts in farbigen Flüssigkeiten. *Ann. Phys. Chem.*, 162 (5): 78–88.

Berendsen H.J.C., Grigera J.R. and Straatsma T.P. (**1987**). The missing term in effective pair potentials. *J. Phys. Chem.*, 91 (24): 6269–6271.

Bier D., Rose R., Bravo-Rodriguez K., Bartel M., Ramirez-Anguita J.M., Dutt S., Wilch C., Klärner F.-G., Sanchez-Garcia E., Schrader T. and Ottmann C. (**2013**). Molecular tweezers modulate 14-3-3 protein-protein interactions. *Nat Chem*, 5 (3): 234–239.

Bilbao-Cortés D., Hetzer M., Längst G., Becker P.B. and Mattaj I.W. (**2002**). Ran Binds to Chromatin by Two Distinct Mechanisms. *Current Biology*, 12 (13): 1151–1156.

Birnboim H.C. and Doly J. (**1979**). A rapid alkaline extraction procedure for screening recombinant plasmid DNA. *Nucleic Acids Res*, 7 (6): 1513–1523.

Bürkle A. (**2002**). Posttranslational Modification. In *Encyclopedia of genetics.* Brenner S., Miller J.H. and Broughton W.J. (ed.). San Diego: Academic Press, p. 1533.

Bussi G., Donadio D. and Parrinello M. (**2007**). Canonical sampling through velocity rescaling. *The Journal of Chemical Physics*, 126 (1): 14101.

Capalbo G., Dittmann K., Weiss C., Reichert S., Hausmann E., Rödel C. and Rödel F. (**2010**). Radiation-induced survivin nuclear accumulation is linked to DNA damage repair. *Int J Radiat Oncol Biol Phys*, 77 (1): 226–234.

Capalbo G., Rödel C., Stauber R.H., Knauer S.K., Bache M., Kappler M. and Rödel F. (**2007**). The role of survivin for radiation therapy. Prognostic and predictive factor and therapeutic target. *Strahlenther Onkol*, 183 (11): 593–599.

Carmena M., Wheelock M., Funabiki H. and Earnshaw W.C. (**2012**). The chromosomal passenger complex (CPC): From easy rider to the godfather of mitosis. *Nat Rev Mol Cell Biol*, 13 (12): 789–803.

Carpenter A.E., Jones T.R., Lamprecht M.R., Clarke C., Kang I.H., Friman O., Guertin D.A., Chang J.H., Lindquist R.A., Moffat J., Golland P. and Sabatini D.M. (**2006**). CellProfiler: Image analysis software for identifying and quantifying cell phenotypes. *Genome Biol*, 7 (10): R100.

Case D.A., Darden T.A., Cheatham III T.E., Simmerling C.L., Wang J., Duke R.E., Luo R., Walker R.C., Zhang W., Merz K.M., Roberts B., Hayik S., Roitberg A., Seabra G., Swails J., Götz A.W., Kolossváry I., Wong K.F., Paesani F., Vanicek J., Wolf R.M., Liu J., Wu X., Brozell S.R., Steinbrecher T., Gohlke H., Cai Q., Ye X., Hsieh M.-J., Cui G., Roe D.R., Mathews D.H., Seetin M.G., Salomon-Ferrer R., Sagui C., Babin V., Luchko T., Gusarov S. and Kovalenko, A. and Kollman, P.A. (**2012**). AMBER 12, San Francisco. URL: www.ambermd.org.

Cha K., Sen P., Raghunayakula S. and Zhang X.-D. (**2015**). The Cellular Distribution of RanGAP1 Is Regulated by CRM1-Mediated Nuclear Export in Mammalian Cells. *PLoS ONE*, 10 (10): e0141309.

Chantalat L., Skoufias D.A., Kleman J.P., Jung B., Dideberg O. and Margolis R.L. (**2000**). Crystal structure of human survivin reveals a bow tie-shaped dimer with two unusual alpha-helical extensions. *Mol Cell*, 6 (1): 183–189.

Chen C.W. and Whitlock H.W. (**1978**). Molecular tweezers: A simple model of bifunctional intercalation. *J. Am. Chem. Soc.*, 100 (15): 4921–4922.

Chen P., Zhu J., Liu D.-Y., Li H.-Y., Xu N. and Hou M. (**2014**). Over-expression of survivin and VEGF in small-cell lung cancer may predict the poorer prognosis. *Med Oncol*, 31 (1): 775.

Chiti F. and Dobson C.M. (**2006**). Protein misfolding, functional amyloid, and human disease. *Annu Rev Biochem*, 75: 333–366.

Cisneros G.A., Piquemal J.-P. and Darden T.A. (**2006**). Quantum mechanics/molecular mechanics electrostatic embedding with continuous and discrete functions. *J Phys Chem B*, 110 (28): 13682–13684.

Clarke P.R. (**2005**). The Crm de la crème of mitosis. *Nat Cell Biol*, 7 (6): 551–552.

Colnaghi R. and Wheatley S.P. (**2010**). Liaisons between survivin and Plk1 during cell division and cell death. *J Biol Chem*, 285 (29): 22592–22604.

Conte M.S. and Altieri D.C. (**2006**). Survivin regulation of vascular injury. *Trends Cardiovasc Med*, 16 (4): 114–117.

Cook A., Bono F., Jinek M. and Conti E. (**2007**). Structural biology of nucleocytoplasmic transport. *Annu Rev Biochem*, 76: 647–671.

Coumar M.S., Tsai F.-Y., Kanwar J.R., Sarvagalla S. and Cheung C.H.A. (**2013**). Treat cancers by targeting survivin: Just a dream or future reality? *Cancer Treat Rev*, 39 (7): 802–811.

Cram D.J. (**1988**). The Design of Molecular Hosts, Guests, and Their Complexes (Nobel Lecture). *Angew. Chem. Int. Ed. Engl.*, 27 (8): 1009–1020.

Cram D.J., Kaneda T., Helgeson R.C. and Lein G.M. (**1979**). Spherands - ligands whose binding of cations relieves enforced electron-electron repulsions. *J. Am. Chem. Soc.*, 101 (22): 6752–6754.

Cronshaw J.M., Krutchinsky A.N., Zhang W., Chait B.T. and Matunis M.J. (**2002**). Proteomic analysis of the mammalian nuclear pore complex. *J Cell Biol*, 158 (5): 915–927.

Darden T., York D. and Pedersen L. (**1993**). Particle mesh Ewald: An N ·log(N) method for Ewald sums in large systems. *The Journal of Chemical Physics*, 98 (12): 10089–10092.

Dasso M. (**2002**). The Ran GTPase: Theme and Variations. *Current Biology*, 12 (14): R502-R508.

Deveraux Q.L. and Reed J.C. (**1999**). IAP family proteins - suppressors of apoptosis. *Genes Dev*, 13 (3): 239–252.

Dickmanns A., Monecke T. and Ficner R. (**2015**). Structural Basis of Targeting the Exportin CRM1 in Cancer. *Cells*, 4 (3): 538–568.

Dietrich B., Lehn J.M. and Sauvage J.P. (**1969**). Les Cryptates. *Tetrahedron Letters*, 10 (34): 2889–2892.

Dingwall C., Robbins J., Dilworth S.M., Roberts B. and Richardson W.D. (**1988**). The nucleoplasmin nuclear location sequence is larger and more complex than that of SV-40 large T antigen. *J Cell Biol*, 107 (3): 841–849.

Dohi T., Okada K., Xia F., Wilford C.E., Samuel T., Welsh K., Marusawa H., Zou H., Armstrong R., Matsuzawa S.-I., Salvesen G.S., Reed J.C. and Altieri D.C. (**2004**). An IAP-IAP complex inhibits apoptosis. *J Biol Chem*, 279 (33): 34087–34090.

Dohi T., Xia F. and Altieri D.C. (**2007**). Compartmentalized phosphorylation of IAP by protein kinase A regulates cytoprotection. *Mol Cell*, 27 (1): 17–28.

Dutt S., Wilch C., Gersthagen T., Talbiersky P., Bravo-Rodriguez K., Hanni M., Sánchez-García E., Ochsenfeld C., Klärner F.-G. and Schrader T. (**2013a**). Molecular tweezers with varying anions: A comparative study. *J Org Chem*, 78 (13): 6721–6734.

Dutt S., Wilch C., Gersthagen T., Wölper C., Sowislok A.A., Klärner F.-G. and Schrader T. (**2013b**). Linker Effects on Amino Acid and Peptide Recognition by Molecular Tweezers. *Eur. J. Org. Chem.*, 2013 (34): 7705–7714.

Eckelman B.P., Salvesen G.S. and Scott F.L. (**2006**). Human inhibitor of apoptosis proteins: Why XIAP is the black sheep of the family. *EMBO Rep*, 7 (10): 988–994.

Engels K., Knauer S.K., Metzler D., Simf C., Struschka O., Bier C., Mann W., Kovács A.F. and Stauber R.H. (**2007**). Dynamic intracellular survivin in oral squamous cell carcinoma: Underlying molecular mechanism and potential as an early prognostic marker. *J Pathol*, 211 (5): 532–540.

Engelsma D., Rodriguez J.A., Fish A., Giaccone G. and Fornerod M. (**2007**). Homodimerization antagonizes nuclear export of survivin. *Traffic*, 8 (11): 1495–1502.

Englmeier L., Fornerod M., Bischoff F.R., Petosa C., Mattaj I.W. and Kutay U. (**2001**). RanBP3 influences interactions between CRM1 and its nuclear protein export substrates. *EMBO Rep*, 2 (10): 926–932.

Fahrenkrog B. and Aebi U. (**2003**). The nuclear pore complex: Nucleocytoplasmic transport and beyond. *Nat Rev Mol Cell Biol*, 4 (10): 757–766.

Federal Statistical Office Germany (**2018**). URL: https://www.destatis.de/EN/FactsFigures/SocietyState/Health/CausesDeath/CausesDeath.html.

Feller S.E., Zhang Y., Pastor R.W. and Brooks B.R. (**1995**). Constant pressure molecular dynamics simulation: The Langevin piston method. *The Journal of Chemical Physics*, 103 (11): 4613–4621.

Fischer E. (**1894**). Einfluss der Configuration auf die Wirkung der Enzyme. *European Journal of Inorganic Chemistry*, 27 (3): 2985–2993.

Fokkens M., Schrader T. and Klärner F.-G. (**2005**). A molecular tweezer for lysine and arginine. *J. Am. Chem. Soc.*, 127 (41): 14415–14421.

Fox A.M., Ciziene D., McLaughlin S.H. and Stewart M. (**2011**). Electrostatic interactions involving the extreme C terminus of nuclear export factor CRM1 modulate its affinity for cargo. *J Biol Chem*, 286 (33): 29325–29335.

Frey S. and Görlich D. (**2007**). A saturated FG-repeat hydrogel can reproduce the permeability properties of nuclear pore complexes. *Cell*, 130 (3): 512–523.

Fried H. and Kutay U. (**2003**). Nucleocytoplasmic transport: Taking an inventory. *Cell Mol Life Sci*, 60 (8): 1659–1688.

Fung H.Y.J., Fu S.-C., Brautigam C.A. and Chook Y.M. (**2015**). Structural determinants of nuclear export signal orientation in binding to exportin CRM1. *Elife*, 4.

García-Santisteban I., Arregi I., Alonso-Mariño M., Urbaneja M.A., Garcia-Vallejo J.J., Bañuelos S. and Rodríguez J.A. (**2016**). A cellular reporter to evaluate CRM1 nuclear export activity: Functional analysis of the cancer-related mutant E571K. *Cell Mol Life Sci*, 73 (24): 4685–4699.

Garg H., Suri P., Gupta J.C., Talwar G.P. and Dubey S. (**2016**). Survivin: A unique target for tumor therapy. *Cancer Cell Int*, 16 (49).

Görlich D. and Kutay U. (**1999**). Transport between the cell nucleus and the cytoplasm. *Annu Rev Cell Dev Biol*, 15: 607–660.

Gravina G.L., Senapedis W., McCauley D., Baloglu E., Shacham S. and Festuccia C. (**2014**). Nucleo-cytoplasmic transport as a therapeutic target of cancer. *J Hematol Oncol*, 7: 85.

Grimme S. (**2011**). Density functional theory with London dispersion corrections. *WIREs Comput Mol Sci*, 1 (2): 211–228.

Güttler T. and Görlich D. (**2011**). Ran-dependent nuclear export mediators: A structural perspective. *EMBO J*, 30 (17): 3457–3474.

Hanahan D. and Weinberg R.A. (**2000**). The hallmarks of cancer. *Cell*, 100 (1): 57–70.

Hanahan D. and Weinberg R.A. (**2011**). Hallmarks of cancer: The next generation. *Cell*, 144 (5): 646–674.

Harmata M., Barnes C.L., Karra S.R. and Elahmad S. (**1994**). Molecular Clefts. 4. An Approach to Structural Analogs of Echinomycin: Synthesis of a New Class of Synthetic Molecular Tweezers. *J. Am. Chem. Soc.*, 116 (18): 8392–8393.

Heid C. (**2018**). Molekulare Pinzetten zur Proteinoberflächenerkennung. *Dissertation.* University of Duisburg-Essen, Essen.

Hess B., Bekker H., Berendsen H.J.C. and Fraaije J.G.E.M. (**1997**). LINCS: A linear constraint solver for molecular simulations. *J. Comput. Chem.*, 18 (12): 1463–1472.

Hetzer M., Bilbao-Cortés D., Walther T.C., Gruss O.J. and Mattaj I.W. (**2000**). GTP Hydrolysis by Ran Is Required for Nuclear Envelope Assembly. *Mol Cell*, 5 (6): 1013–1024.

Hill R., Cautain B., Pedro N. de and Link W. (**2014**). Targeting nucleocytoplasmic transport in cancer therapy. *Oncotarget*, 5 (1): 11–28.

Hoffman W.H., Biade S., Zilfou J.T., Chen J. and Murphy M. (**2002**). Transcriptional repression of the anti-apoptotic survivin gene by wild type p53. *J Biol Chem*, 277 (5): 3247–3257.

Hogeweg A., Sowislok A., Schrader T. and Beuck C. (**2017**). An NMR Method to Pinpoint Supramolecular Ligand Binding to Basic Residues on Proteins. *Angew Chem Int Ed Engl*, 56 (46): 14758–14762.

Hornak V., Abel R., Okur A., Strockbine B., Roitberg A. and Simmerling C. (**2006**). Comparison of multiple Amber force fields and development of improved protein backbone parameters. *Proteins*, 65 (3): 712–725.

Jeyaprakash A.A., Basquin C., Jayachandran U. and Conti E. (**2011**). Structural basis for the recognition of phosphorylated histone h3 by the survivin subunit of the chromosomal passenger complex. *Structure*, 19 (11): 1625–1634.

Jeyaprakash A.A., Klein U.R., Lindner D., Ebert J., Nigg E.A. and Conti E. (**2007**). Structure of a Survivin-Borealin-INCENP core complex reveals how chromosomal passengers travel together. *Cell*, 131 (2): 271–285.

Jiang Y., Saavedra H.I., Holloway M.P., Leone G. and Altura R.A. (**2004**). Aberrant regulation of survivin by the RB/E2F family of proteins. *J Biol Chem*, 279 (39): 40511–40520.

Joseph J. (**2006**). Ran at a glance. *J Cell Sci*, 119 (Pt 17): 3481–3484.

Joseph J., Liu S.-T., Jablonski S.A., Yen T.J. and Dasso M. (**2004**). The RanGAP1-RanBP2 complex is essential for microtubule-kinetochore interactions in vivo. *Curr Biol*, 14 (7): 611–617.

Junghänel S., Karczewski S., Bäcker S., Knauer S.K. and Schmuck C. (**2017**). A Systematic Structure-Activity Study of a New Type of Small Peptidic Transfection Vector Reveals the Importance of a Special Oxo-Anion-Binding Motif for Gene Delivery. *Chembiochem*, 18 (22): 2268–2279.

Kabachinski G. and Schwartz T.U. (**2015**). The nuclear pore complex - structure and function at a glance. *J Cell Sci*, 128 (3): 423–429.

Kakisaka M., Mano T. and Aida Y. (**2016**). A high-throughput screening system targeting the nuclear export pathway via the third nuclear export signal of influenza A virus nucleoprotein. *Virus Res*, 217: 23–31.

Kalab P., Weis K. and Heald R. (**2002**). Visualization of a Ran-GTP gradient in interphase and mitotic Xenopus egg extracts. *Science*, 295 (5564): 2452–2456.

Kalderon D., Richardson W.D., Markham A.F. and Smith A.E. (**1984a**). Sequence requirements for nuclear location of simian virus 40 large-T antigen. *Nature*, 311 (5981): 33–38.

Kalderon D., Roberts B.L., Richardson W.D. and Smith A.E. (**1984b**). A short amino acid sequence able to specify nuclear location. *Cell*, 39 (3): 499–509.

Kamentsky L., Jones T.R., Fraser A., Bray M.-A., Logan D.J., Madden K.L., Ljosa V., Rueden C., Eliceiri K.W. and Carpenter A.E. (**2011**). Improved structure, function and compatibility for CellProfiler: Modular high-throughput image analysis software. *Bioinformatics*, 27 (8): 1179–1180.

Kapinos L.E., Schoch R.L., Wagner R.S., Schleicher K.D. and Lim R.Y.H. (**2014**). Karyopherin-centric control of nuclear pores based on molecular occupancy and kinetic analysis of multivalent binding with FG nucleoporins. *Biophysical Journal*, 106 (8): 1751–1762.

Kästner J., Carr J.M., Keal T.W., Thiel W., Wander A. and Sherwood P. (**2009**). DL-FIND: An open-source geometry optimizer for atomistic simulations. *J Phys Chem A*, 113 (43): 11856–11865.

Kaufman L. and Rousseeuw P.J. (**1987**). Clustering by Means of Medoids: 405–416.

Kelly R.J., Lopez-Chavez A., Citrin D., Janik J.E. and Morris J.C. (**2011**). Impacting tumor cell-fate by targeting the inhibitor of apoptosis protein survivin. *Mol Cancer*, 10 (35).

Keminer O. and Peters R. (**1999**). Permeability of Single Nuclear Pores. *Biophysical Journal*, 77 (1): 217–228.

Kerr J.F., Wyllie A.H. and Currie A.R. (**1972**). Apoptosis: A basic biological phenomenon with wide-ranging implications in tissue kinetics. *Br J Cancer*, 26 (4): 239–257.

Kim Y.H., Han M.-E. and Oh S.-O. (**2017**). The molecular mechanism for nuclear transport and its application. *Anat Cell Biol*, 50 (2): 77–85.

Klärner F.-G., Benkhoff J., Boese R., Burkert U., Kamieth M. and Naatz U. (**1996**). Molecular Tweezers as Synthetic Receptors in Host—Guest Chemistry: Inclusion of Cyclohexane and Self-Assembly of Aliphatic Side Chains. *Angew. Chem. Int. Ed. Engl.*, 35 (10): 1130–1133.

Klauda J.B., Venable R.M., Freites J.A., O'Connor J.W., Tobias D.J., Mondragon-Ramirez C., Vorobyov I., MacKerell A.D. and Pastor R.W. (**2010**). Update of the CHARMM all-atom additive force field for lipids: Validation on six lipid types. *J Phys Chem B*, 114 (23): 7830–7843.

Klebe C., Bischoff F.R., Ponstingl H. and Wittinghofer A. (**2002**). Interaction of the Nuclear GTP-Binding Protein Ran with Its Regulatory Proteins RCC1 and RanGAP1. *Biochemistry*, 34 (2): 639–647.

Knauer S.K., Bier C., Habtemichael N. and Stauber R.H. (**2006**). The Survivin-Crm1 interaction is essential for chromosomal passenger complex localization and function. *EMBO Rep*, 7 (12): 1259–1265.

Knauer S.K., Bier C., Schlag P., Fritzmann J., Dietmaier W., Rödel F., Klein-Hitpass L., Kovács A.F., Döring C., Hansmann M.-L., Hofmann W.-K., Kunkel M., Brochhausen C., Engels K., Lippert B.M., Mann W. and Stauber R.H. (**2007a**). The Survivin Isoform Survivin-3B is Cytoprotective and can Function as a Chromosomal Passenger Complex Protein. *Cell Cycle*, 6 (12): 1501–1508.

Knauer S.K., Krämer O.H., Knösel T., Engels K., Rödel F., Kovács A.F., Dietmaier W., Klein-Hitpass L., Habtemichael N., Schweitzer A., Brieger J., Rödel C., Mann W., Petersen I., Heinzel T. and Stauber R.H. (**2007b**). Nuclear export is essential for the tumor-promoting activity of survivin. *FASEB J*, 21 (1): 207–216.

Knauer S.K., Mann W. and Stauber R.H. (**2007c**). Survivin's dual role: An export's view. *Cell Cycle*, 6 (5): 518–521.

Kudo N., Matsumori N., Taoka H., Fujiwara D., Schreiner E.P., Wolff B., Yoshida M. and Horinouchi S. (**1999**). Leptomycin B inactivates CRM1/exportin 1 by covalent modification at a cysteine residue in the central conserved region. *Proceedings of the National Academy of Sciences*, 96 (16): 9112–9117.

Kutay U. and Güttinger S. (**2005**). Leucine-rich nuclear-export signals: Born to be weak. *Trends in Cell Biology*, 15 (3): 121–124.

La Cour T., Kiemer L., Mølgaard A., Gupta R., Skriver K. and Brunak S. (**2004**). Analysis and prediction of leucine-rich nuclear export signals. *Protein Eng Des Sel*, 17 (6): 527–536.

Laemmli U.K. (**1970**). Cleavage of Structural Proteins during the Assembly of the Head of Bacteriophage T4. *Nature*, 227 (5259): 680–685.

Langer K., Dian C., Rybin V., Müller C.W. and Petosa C. (**2011**). Insights into the function of the CRM1 cofactor RanBP3 from the structure of its Ran-binding domain. *PLoS ONE*, 6 (2): e17011.

Lapalombella R., Sun Q., Williams K., Tangeman L., Jha S., Zhong Y., Goettl V., Mahoney E., Berglund C., Gupta S., Farmer A., Mani R., Johnson A.J., Lucas D., Mo X., Daelemans D., Sandanayaka V., Shechter S., McCauley D., Shacham S., Kauffman M., Chook Y.M. and Byrd J.C. (**2012**). Selective inhibitors of nuclear export show that CRM1/XPO1 is a target in chronic lymphocytic leukemia. *Blood*, 120 (23): 4621–4634.

Laskowski R.A., MacArthur M.W., Moss D.S. and Thornton J.M. (**1993**). PROCHECK: A program to check the stereochemical quality of protein structures. *J Appl Crystallogr*, 26 (2): 283–291.

Latimer W.M. and Rodebush W.H. (**1920**). Polarity and Ionization from the Standpoint of the Lewis Theory of Valence. *J. Am. Chem. Soc.*, 42 (7): 1419–1433.

Lehn J.-M. (**1978**). Cryptates: Inclusion Complexes of macropolycyclic Receptor Molecules. *Pure & Appl. Chem.*, 50: 871–892.

Lehn J.-M. (**1988**). Supramolecular Chemistry-Scope and Perspectives Molecules, Supermolecules, and Molecular Devices (Nobel Lecture). *Angew. Chem. Int. Ed. Engl.*, 27 (1): 89–112.

Lehn J.-M. (**1993**). Supramolecular chemistry. *Science*, 260 (5115): 1762–1763.

Li F., Ackermann E.J., Bennett C.F., Rothermel A.L., Plescia J., Tognin S., Villa A., Marchisio P.C. and Altieri D.C. (**1999**). Pleiotropic cell-division defects and apoptosis induced by interference with survivin function. *Nat Cell Biol*, 1 (8): 461–466.

Li F., Ambrosini G., Chu E.Y., Plescia J., Tognin S., Marchisio P.C. and Altieri D.C. (**1998**). Control of apoptosis and mitotic spindle checkpoint by survivin. *Nature*, 396 (6711): 580–584.

Li M., Mosel S., Knauer S.K. and Schmuck C. (**2018**). A dipeptide with enhanced anion binding affinity enables cell uptake and protein delivery. *Org Biomol Chem*, 16 (13): 2312–2317.

Li Z., Ren W., Zeng Q., Chen S., Zhang M., Zhao Y., Cheng J. and Wang X. (**2016**). Effects of survivin on angiogenesis in vivo and in vitro. *Am J Transl Res*, 8 (2): 270–283.

Lim R.Y.H., Aebi U. and Fahrenkrog B. (**2008**). Towards reconciling structure and function in the nuclear pore complex. *Histochem Cell Biol*, 129 (2): 105–116.

Lim R.Y.H., Huang N., Köser J., Deng J., Lau K.H.A., Schwarz-Herion K., Fahrenkrog B. and Aebi U. (**2006**). Flexible phenylalanine-glycine nucleoporins as entropic barriers to nucleocytoplasmic transport. *Proc Natl Acad Sci U S A*, 103 (25): 9512–9517.

Macara I.G. (**2001**). Transport into and out of the nucleus. *Microbiol Mol Biol Rev*, 65 (4): 570-594.

Maimon T., Elad N., Dahan I. and Medalia O. (**2012**). The human nuclear pore complex as revealed by cryo-electron tomography. *Structure*, 20 (6): 998–1006.

Marusawa H., Matsuzawa S.-I., Welsh K., Zou H., Armstrong R., Tamm I. and Reed J.C. (**2003**). HBXIP functions as a cofactor of survivin in apoptosis suppression. *EMBO J*, 22 (11): 2729–2740.

Melchior F. (**2001**). Ran GTPase cycle: One mechanism - two functions. *Current Biology*, 11 (7): R257-R260.

Mellman I., Fuchs R. and Helenius A. (**1986**). Acidification of the endocytic and exocytic pathways. *Annu Rev Biochem*, 55: 663–700.

Monecke T., Dickmanns A. and Ficner R. (**2014**). Allosteric control of the exportin CRM1 unraveled by crystal structure analysis. *FEBS J*, 281 (18): 4179–4194.

Monecke T., Haselbach D., Voß B., Russek A., Neumann P., Thomson E., Hurt E., Zachariae U., Stark H., Grubmüller H., Dickmanns A. and Ficner R. (**2013**). Structural basis for cooperativity of CRM1 export complex formation. *Proc Natl Acad Sci U S A*, 110 (3): 960–965.

Mullis K.B. and Faloona F.A. (**1987**). Specific synthesis of DNA in vitro via a polymerase-catalyzed chain reaction. *Meth Enzymol*, 155: 335–350.

Murray A.W. (**1992**). Creative blocks: Cell-cycle checkpoints and feedback controls. *Nature*, 359 (6396): 599–604.

Nachury M.V. and Weis K. (**1999**). The direction of transport through the nuclear pore can be inverted. *Proc Natl Acad Sci U S A*, 96 (17): 9622–9627.

Newlands E.S., Rustin G.J. and Brampton M.H. (**1996**). Phase I trial of elactocin. *Br J Cancer*, 74 (4): 648–649.

Nobel Media AB (**2018**). The Nobel Prize in Chemistry 1987. URL: https://www.nobelprize.org/nobel_prizes/chemistry/laureates/1987/.

Nogueira-Ferreira R., Vitorino R., Ferreira-Pinto M.J., Ferreira R. and Henriques-Coelho T. (**2013**). Exploring the role of post-translational modifications on protein-protein interactions with survivin. *Arch Biochem Biophys*, 538 (2): 64–70.

NPTEL (**2018**). Circular dichroism of Proteins. URL: http://nptel.ac.in/courses/102103047/module2/lec10/1.html.

O'Connor D.S., Grossman D., Plescia J., Li F., Zhang H., Villa A., Tognin S., Marchisio P.C. and Altieri D.C. (**2000**). Regulation of apoptosis at cell division by p34cdc2 phosphorylation of survivin. *Proceedings of the National Academy of Sciences*, 97 (24): 13103–13107.

Oshovsky G.V., Reinhoudt D.N. and Verboom W. (**2007**). Supramolecular chemistry in water. *Angew Chem Int Ed Engl*, 46 (14): 2366–2393.

Páll S. and Hess B. (**2013**). A flexible algorithm for calculating pair interactions on SIMD architectures. *Computer Physics Communications*, 184 (12): 2641–2650.

Panté N. and Kann M. (**2002**). Nuclear pore complex is able to transport macromolecules with diameters of about 39 nm. *Mol Biol Cell*, 13 (2): 425–434.

Parikh K., Cang S., Sekhri A. and Liu D. (**2014**). Selective inhibitors of nuclear export (SINE) - a novel class of anti-cancer agents. *J Hematol Oncol*, 7 (78).

Parrinello M. and Rahman A. (**1981**). Polymorphic transitions in single crystals: A new molecular dynamics method. *Journal of Applied Physics*, 52 (12): 7182–7190.

Pavlyukov M.S., Antipova N.V., Balashova M.V., Vinogradova T.V., Kopantzev E.P. and Shakhparonov M.I. (**2011**). Survivin monomer plays an essential role in apoptosis regulation. *J Biol Chem*, 286 (26): 23296–23307.

Pedersen C.J. (**1967**). Cyclic polyethers and their complexes with metal salts. *J. Am. Chem. Soc.*, 89 (10): 2495–2496.

Pedersen C.J. (**1988**). The Discovery of Crown Ethers (Noble Lecture). *Angew. Chem. Int. Ed. Engl.*, 27 (8): 1021–1027.

Peters M.B., Yang Y., Wang B., Füsti-Molnár L., Weaver M.N. and Merz K.M. (**2010**). Structural Survey of Zinc Containing Proteins and the Development of the Zinc AMBER Force Field (ZAFF). *J Chem Theory Comput*, 6 (9): 2935–2947.

Petosa C., Schoehn G., Askjaer P., Bauer U., Moulin M., Steuerwald U., Soler-López M., Baudin F., Mattaj I.W. and Müller C.W. (**2004**). Architecture of CRM1/Exportin1 suggests how cooperativity is achieved during formation of a nuclear export complex. *Mol Cell*, 16 (5): 761–775.

Phillips J.C., Braun R., Wang W., Gumbart J., Tajkhorshid E., Villa E., Chipot C., Skeel R.D., Kalé L. and Schulten K. (**2005**). Scalable molecular dynamics with NAMD. *J. Comput. Chem.*, 26 (16): 1781–1802.

Pronk S., Páll S., Schulz R., Larsson P., Bjelkmar P., Apostolov R., Shirts M.R., Smith J.C., Kasson P.M., van der Spoel D., Hess B. and Lindahl E. (**2013**). GROMACS 4.5: A high-throughput and highly parallel open source molecular simulation toolkit. *Bioinformatics*, 29 (7): 845–854.

R Core Team (**2016**). R: A Language and Environment for Statistical Computing, Vienna, Austria. URL: www.R-project.org.

Reichelt R., Holzenburg A., Buhle E.L., JR., Jarnik M., Engel A. and Aebi U. (**1990**). Correlation between structure and mass distribution of the nuclear pore complex and of distinct pore complex components. *J Cell Biol*, 110 (4): 883–894.

Reichert S., Rödel C., Mirsch J., Harter P.N., Tomicic M.T., Mittelbronn M., Kaina B. and Rödel F. (**2011**). Survivin inhibition and DNA double-strand break repair: A molecular mechanism to overcome radioresistance in glioblastoma. *Radiother Oncol*, 101 (1): 51–58.

Ribbeck K. and Görlich D. (**2001**). Kinetic analysis of translocation through nuclear pore complexes. *EMBO J*, 20 (6): 1320–1330.

Ribbeck K. and Görlich D. (**2002**). The permeability barrier of nuclear pore complexes appears to operate via hydrophobic exclusion. *EMBO J*, 21 (11): 2664–2671.

Riedl S.J. and Shi Y. (**2004**). Molecular mechanisms of caspase regulation during apoptosis. *Nat Rev Mol Cell Biol*, 5 (11): 897–907.

Riolo M.T., Cooper Z.A., Holloway M.P., Cheng Y., Bianchi C., Yakirevich E., Ma L., Chin Y.E. and Altura R.A. (**2012**). Histone deacetylase 6 (HDAC6) deacetylates survivin for its nuclear export in breast cancer. *J Biol Chem*, 287 (14): 10885–10893.

Rödel F., Sprenger T., Kaina B., Liersch T., Rödel C., Fulda S. and Hehlgans S. (**2012**). Survivin as a prognostic/predictive marker and molecular target in cancer therapy. *Curr Med Chem*, 19 (22): 3679–3688.

Rodríguez J.A., Span S.W., Ferreira C.G.M., Kruyt F.A.E. and Giaccone G. (**2002**). CRM1-mediated nuclear export determines the cytoplasmic localization of the antiapoptotic protein Survivin. *Exp Cell Res*, 275 (1): 44–53.

Rosa J., Canovas P., Islam A., Altieri D.C. and Doxsey S.J. (**2006**). Survivin modulates microtubule dynamics and nucleation throughout the cell cycle. *Mol Biol Cell*, 17 (3): 1483–1493.

Rousseeuw P.J. (**1987**). Silhouettes: A graphical aid to the interpretation and validation of cluster analysis. *Journal of Computational and Applied Mathematics*, 20: 53–65.

Rout M.P., Aitchison J. D., Magnasco M. O. and Chait B. T. (**2003**). Virtual gating and nuclear transport: The hole picture. *Trends in Cell Biology*, 13 (12): 622–628.

Ruchaud S., Carmena M. and Earnshaw W.C. (**2007**). Chromosomal passengers: Conducting cell division. *Nat Rev Mol Cell Biol*, 8 (10): 798–812.

Sah N.K. and Seniya C. (**2015**). Survivin splice variants and their diagnostic significance. *Tumour Biol*, 36 (9): 6623–6631.

Sakiyama Y., Panatala R. and Lim R.Y.H. (**2017**). Structural dynamics of the nuclear pore complex. *Semin Cell Dev Biol*, 68: 27–33.

Sali A. and Blundell T.L. (**1993**). Comparative protein modelling by satisfaction of spatial restraints. *Journal of Molecular Biology*, 234 (3): 779–815.

Samanta K., Jana P., Bäcker S., Knauer S. and Schmuck C. (**2016**). Guanidiniocarbonyl pyrrole (GCP) conjugated PAMAM-G2, a highly efficient vector for gene delivery: The importance of DNA condensation. *Chem Commun (Camb)*, 52 (84): 12446–12449.

Sanger F., Nicklen S. and Coulson A.R. (**1977**). DNA sequencing with chain-terminating inhibitors. *Proceedings of the National Academy of Sciences*, 74 (12): 5463–5467.

Sanhueza C., Wehinger S., Castillo Bennett J., Valenzuela M., Owen G.I. and Quest A.F.G. (**2015**). The twisted survivin connection to angiogenesis. *Mol Cancer*, 14 (198).

Sherwood P., Vries A.H. de, Guest M.F., Schreckenbach G., Catlow C.R.A., French S.A., Sokol A.A., Bromley S.T., Thiel W., Turner A.J., Billeter S., Terstegen F., Thiel S., Kendrick J., Rogers S.C., Casci J., Watson M., King F., Karlsen E., Sjøvoll M., Fahmi A., Schäfer A. and Lennartz C. (**2003**). QUASI: A general purpose implementation of the QM/MM approach and its application to problems in catalysis. *Journal of Molecular Structure: THEOCHEM*, 632 (1-3): 1–28.

Sichelschmidt S. (**2016**). Etablierung eines biochemischen Bindungs-Assays zur Analyse des Crm1-Ran-Survivin Exportkomplexes. *Bachelor's thesis.* University of Duisburg-Essen, Essen.

Sinha S., Lopes D.H.J., Du Z., Pang E.S., Shanmugam A., Lomakin A., Talbiersky P., Tennstaedt A., McDaniel K., Bakshi R., Kuo P.-Y., Ehrmann M., Benedek G.B., Loo J.A., Klärner F.-G., Schrader T., Wang C. and Bitan G. (**2011**). Lysine-specific molecular tweezers are broad-spectrum inhibitors of assembly and toxicity of amyloid proteins. *J. Am. Chem. Soc.*, 133 (42): 16958–16969.

Smith A., Brownawell A. and Macara I.G. (**1998**). Nuclear import of Ran is mediated by the transport factor NTF2. *Current Biology*, 8 (25): 1403-1406.

Song Z., Yao X. and Wu M. (**2003**). Direct interaction between survivin and Smac/DIABLO is essential for the anti-apoptotic activity of survivin during taxol-induced apoptosis. *J Biol Chem*, 278 (25): 23130–23140.

Sorokin A.V., Kim E.R. and Ovchinnikov L.P. (**2007**). Nucleocytoplasmic transport of proteins. *Biochemistry Mosc*, 72 (13): 1439–1457.

Sousa da Silva A.W. and Vranken W.F. (**2012**). ACPYPE - AnteChamber PYthon Parser interfacE. *BMC Res Notes*, 5: 367.

Srinivasula S.M. and Ashwell J.D. (**2008**). IAPs: What's in a name? *Mol Cell*, 30 (2): 123–135.

Steed J.W., Turner D.R. and Wallace K.J. (**2007**). Core concepts in supramolecular chemistry and nanochemistry, Chichester, England, Hoboken, NJ: John Wiley.

Stelma T., Chi A., van der Watt P.J., Verrico A., Lavia P. and Leaner V.D. (**2016**). Targeting nuclear transporters in cancer: Diagnostic, prognostic and therapeutic potential. *IUBMB Life*, 68 (4): 268–280.

Stoffler D., Feja B., Fahrenkrog B., Walz J., Typke D. and Aebi U. (**2003**). Cryo-electron Tomography Provides Novel Insights into Nuclear Pore Architecture: Implications for Nucleocytoplasmic Transport. *Journal of Molecular Biology*, 328 (1): 119–130.

Sun C., Nettesheim D., Liu Z. and Olejniczak E.T. (**2005**). Solution structure of human survivin and its binding interface with Smac/Diablo. *Biochemistry*, 44 (1): 11–17.

Sun Q., Carrasco Y.P., Hu Y., Guo X., Mirzaei H., Macmillan J. and Chook Y.M. (**2013**). Nuclear export inhibition through covalent conjugation and hydrolysis of Leptomycin B by CRM1. *Proc Natl Acad Sci U S A*, 110 (4): 1303–1308.

Tajiri T., Tanaka S., Shono K., Kinoshita Y., Fujii Y., Suita S., Ihara K. and Hara T. (**2001**). Quick quantitative analysis of gene dosages associated with prognosis in neuroblastoma. *Cancer Lett*, 166 (1): 89–94.

Talbiersky P., Bastkowski F., Klärner F.-G. and Schrader T. (**2008**). Molecular clip and tweezer introduce new mechanisms of enzyme inhibition. *J. Am. Chem. Soc.*, 130 (30): 9824–9828.

Tamm I., Wang Y., Sausville E., Scudiero D.A., Vigna N., Oltersdorf T. and Reed J.C. (**1998**). IAP-family protein survivin inhibits caspase activity and apoptosis induced by Fas (CD95), Bax, caspases, and anticancer drugs. *Cancer Res*, 58 (23): 5315–5320.

Timney B.L., Raveh B., Mironska R., Trivedi J.M., Kim S.J., Russel D., Wente S.R., Sali A. and Rout M.P. (**2016**). Simple rules for passive diffusion through the nuclear pore complex. *J Cell Biol*, 215 (1): 57–76.

Tracey L., Pérez-Rosado A., Artiga M.J., Camacho F.I., Rodríguez A., Martínez N., Ruiz-Ballesteros E., Mollejo M., Martinez B., Cuadros M., Garcia J.F., Lawler M. and Piris M.A. (**2005**). Expression of the NF-kappaB targets BCL2 and BIRC5/Survivin characterizes small B-cell and aggressive B-cell lymphomas, respectively. *J Pathol*, 206 (2): 123–134.

Tran E.J. and Wente S.R. (**2006**). Dynamic nuclear pore complexes: Life on the edge. *Cell*, 125 (6): 1041–1053.

Trevino S.R., Scholtz J.M. and Pace C.N. (**2008**). Measuring and increasing protein solubility. *J Pharm Sci*, 97 (10): 4155–4166.

Turner J.G., Dawson J., Cubitt C.L., Baz R. and Sullivan D.M. (**2014**). Inhibition of CRM1-dependent nuclear export sensitizes malignant cells to cytotoxic and targeted agents. *Semin Cancer Biol*, 27: 62–73.

Uhlenheuer D.A., Petkau K. and Brunsveld L. (**2010**). Combining supramolecular chemistry with biology. *Chem Soc Rev*, 39 (8): 2817–2826.

Vaira V., Lee C.W., Goel H.L., Bosari S., Languino L.R. and Altieri D.C. (**2007**). Regulation of survivin expression by IGF-1/mTOR signaling. *Oncogene*, 26 (19): 2678–2684.

Valdes C., Spitz U.P., Toledo L.M., Kubik S.W. and Rebek J. (**1995**). Synthesis and Self-Assembly of Pseudo-Spherical Homo- and Heterodimeric Capsules. *J. Am. Chem. Soc.*, 117 (51): 12733–12745.

Vallet C. (**2014**). Molekulare Analyse der Survivin-Dimerisierung. *Master's thesis.* University of Duisburg-Essen, Essen.

van der Waals J.D. (**1873**). Over de Continuiteit van den Gas- en Vloeistoftoestand (on the continuity of the gas and liquid state). *Dissertation.* University of Leiden, Leiden, Netherlands.

Vanommeslaeghe K., Hatcher E., Acharya C., Kundu S., Zhong S., Shim J., Darian E., Guvench O., Lopes P., Vorobyov I. and Mackerell A.D. (**2010**). CHARMM general force field: A force field for drug-like molecules compatible with the CHARMM all-atom additive biological force fields. *J Comput Chem*, 31 (4): 671–690.

Varkouhi A.K., Scholte M., Storm G. and Haisma H.J. (**2011**). Endosomal escape pathways for delivery of biologicals. *J Control Release*, 151 (3): 220–228.

Verdecia M.A., Huang H., Dutil E., Kaiser D.A., Hunter T. and Noel J.P. (**2000**). Structure of the human anti-apoptotic protein survivin reveals a dimeric arrangement. *Nat Struct Biol*, 7 (7): 602–608.

Vong Q.P., Cao K., Li H.Y., Iglesias P.A. and Zheng Y. (**2005**). Chromosome alignment and segregation regulated by ubiquitination of survivin. *Science*, 310 (5753): 1499–1504.

Wang H., Holloway M.P., Ma L., Cooper Z.A., Riolo M., Samkari A., Elenitoba-Johnson K.S.J., Chin Y.E. and Altura R.A. (**2010**). Acetylation directs survivin nuclear localization to repress STAT3 oncogenic activity. *J Biol Chem*, 285 (46): 36129–36137.

Wang Q., Chen Z., Diao X. and Huang S. (**2011**). Induction of autophagy-dependent apoptosis by the survivin suppressant YM155 in prostate cancer cells. *Cancer Lett*, 302 (1): 29–36.

Wang R. and Brattain M.G. (**2007**). The maximal size of protein to diffuse through the nuclear pore is larger than 60kDa. *FEBS Lett*, 581 (17): 3164–3170.

Wang Y.-F., Zhang W., He K.-F., Liu B., Zhang L., Zhang W.-F., Kulkarni A.B., Zhao Y.-F. and Sun Z.-J. (**2014**). Induction of autophagy-dependent cell death by the survivin suppressant YM155 in salivary adenoid cystic carcinoma. *Apoptosis*, 19 (4): 748–758.

Wen W., Meinkotht J.L., Tsien R.Y. and Taylor S.S. (**1995**). Identification of a signal for rapid export of proteins from the nucleus. *Cell*, 82 (3): 463–473.

Wente S.R. and Rout M.P. (**2010**). The nuclear pore complex and nuclear transport. *Cold Spring Harb Perspect Biol*, 2 (10): a000562.

Wheatley S.P., Barrett R.M., Andrews P.D., Medema R.H., Morley S.J., Swedlow J.R. and Lens S.M.A. (**2007**). Phosphorylation by aurora-B negatively regulates survivin function during mitosis. *Cell Cycle*, 6 (10): 1220–1230.

Wheatley S.P., Henzing A.J., Dodson H., Khaled W. and Earnshaw W.C. (**2004**). Aurora-B phosphorylation in vitro identifies a residue of survivin that is essential for its localization and binding to inner centromere protein (INCENP) in vivo. *J Biol Chem*, 279 (7): 5655–5660.

Wöhler F. (**1828**). Ueber künstliche Bildung des Harnstoffs. *Ann. Phys. Chem.*, 88 (2): 253–256.

World Health Organization (**2018**). URL: http://www.who.int/cancer/en/.

Wu Z., Jiang Q., Clarke P.R. and Zhang C. (**2013**). Phosphorylation of Crm1 by CDK1-cyclin-B promotes Ran-dependent mitotic spindle assembly. *J Cell Sci*, 126 (15): 3417–3428.

Xu C., Yamamoto-Ibusuki M., Yamamoto Y., Yamamoto S., Fujiwara S., Murakami K., Okumura Y., Yamaguchi L., Fujiki Y. and Iwase H. (**2014**). High survivin mRNA expression is a predictor of poor prognosis in breast cancer: A comparative study at the mRNA and protein level. *Breast Cancer*, 21 (4): 482–490.

Xu Y., Fang F., Ludewig G., Jones G. and Jones D. (**2004**). A mutation found in the promoter region of the human survivin gene is correlated to overexpression of survivin in cancer cells. *DNA Cell Biol*, 23 (7): 419–429.

Zhang C. and Clarke P.R. (**2001**). Roles of Ran–GTP and Ran–GDP in precursor vesicle recruitment and fusion during nuclear envelope assembly in a human cell-free system. *Current Biology*, 11 (3): 208–212.

Zhang L., Zhang W., Wang Y.-F., Liu B., Zhang W.-F., Zhao Y.-F., Kulkarni A.B. and Sun Z.-J. (**2015**). Dual induction of apoptotic and autophagic cell death by targeting survivin in head neck squamous cell carcinoma. *Cell Death Dis*, 6: e1771.

Zhao J., Tenev T., Martins L.M., Downward J. and Lemoine N.R. (**2000**). The ubiquitin-proteasome pathway regulates survivin degradation in a cell cycle-dependent manner. *J Cell Sci*, 113 (23): 4363–4371.

Zimmerman S.C. and VanZyl C.M. (**1987**). Rigid molecular tweezers: Synthesis, characterization, and complexation chemistry of a diacridine. *J. Am. Chem. Soc.*, 109 (25): 7894–7896.

APPENDIX

A.1 Purification of GST-PreScission protease

PreScission protease is a fusion protein of human rhinovirus 3C protease and GST. The recombinantly expressed and purified N-terminal GST fused PreScission protease was used for GST-tag removal of proteins in this work. The cleavage was performed on the column. Thus, GST-tagged proteins can be cleaved while still bound to an affinity resin. PreScission protease specifically cleaves between the residues glutamine and glycine of the recognition sequence LEVLFQ / GP. Due to its GST-tag PreScission protease remains bound to the column and does not contaminate the cleaved protein. GST-PreScission protease is stored in GST-PreScission protease storage buffer.

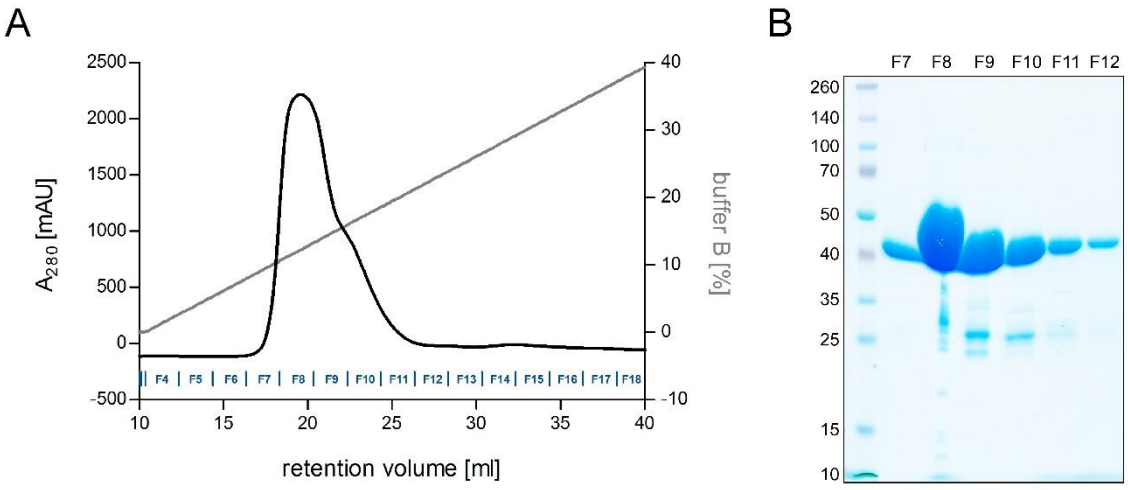

Figure A.1: Purification of GST-PreScission protease by ion exchange chromatography.
A) Absorbance chromatogram at 280 nm of the ion exchange chromatography following GSH affinity purification. The elution gradient (0–100 % ion buffer B, 25 mM to 1 M NaCl, 75 ml, grey) and the collected elution fractions (F4–F18, blue) are included. **B)** Coomassie-stained SDS gel of protein-containing elution fractions. Fractions F7–F12 contain GST-PreScission Protease with few impurities. They were pooled, concentrated and used for subsequent experiments. Yield: 9.7 mg per liter of bacterial culture.

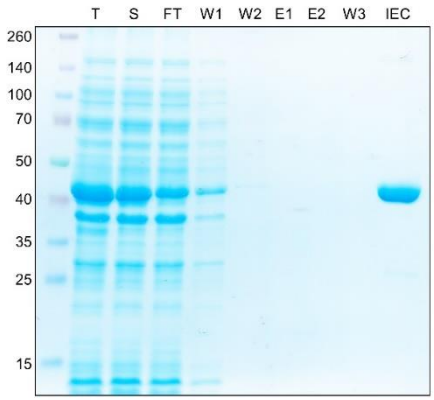

Figure A.2: Overview of the purification procedure of GST-PreScission protease.
Coomassie-stained SDS gel of samples taken after the respective purification steps (T: total lysate, S: supernatant, FT: flow through of GSH column loading, W1–W2: wash fractions after loading the GSH column, E1–E2: GSH-elution of protein from the GSH column onto an ion exchange column, W3: final wash fraction of rinsing protein from the GSH column onto an ion exchange column, IEC: pooled and concentrated protein after ion exchange chromatography).

A.2 Purification of GST-CRM1

Recombinant GST-CRM1 was used as bait protein for pull-down experiments (Sichelschmidt, 2016).

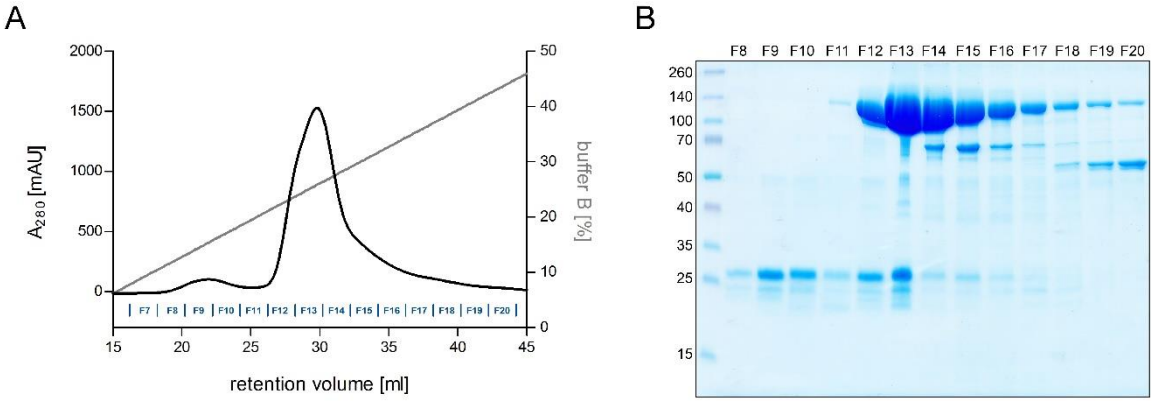

Figure A.3: Purification of GST-CRM1 by ion exchange chromatography.
A) Absorbance chromatogram at 280 nm of the ion exchange chromatography following GSH affinity purification. The elution gradient (0–100 % ion buffer B, 25 mM to 1 M NaCl, 75 ml, grey) and the collected elution fractions (F7–F20, blue) are included. **B)** Coomassie-stained SDS gel of protein-containing elution fractions. Fractions F12–F17 contain GST-CRM1 with few impurities. They were pooled, concentrated and used for subsequent experiments. Yield: 3.5 mg per liter of bacterial culture (Sichelschmidt, 2016).

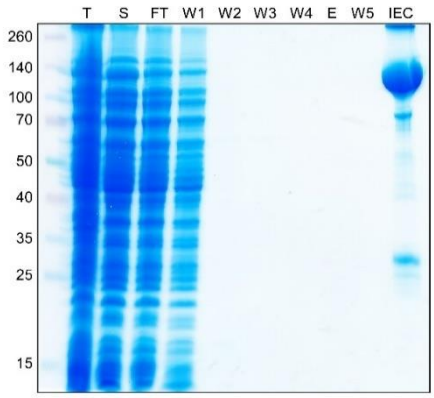

Figure A.4: Overview of the purification procedure of GST-CRM1.
Coomassie-stained SDS gel of samples taken after the respective purification steps (T: total lysate, S: supernatant, FT: flow through of GSH column loading, W1–W4: wash fractions after loading the GSH column, E: GSH-elution of protein from the GSH column onto an ion exchange column, W5: final wash fraction of rinsing protein from the GSH column onto an ion exchange column, IEC: pooled and concentrated protein after ion exchange chromatography) (Sichelschmidt, 2016).

A.3 Purification of GST-Survivin120

Recombinant GST-Survivin120 was used as bait protein for pull-down experiments.

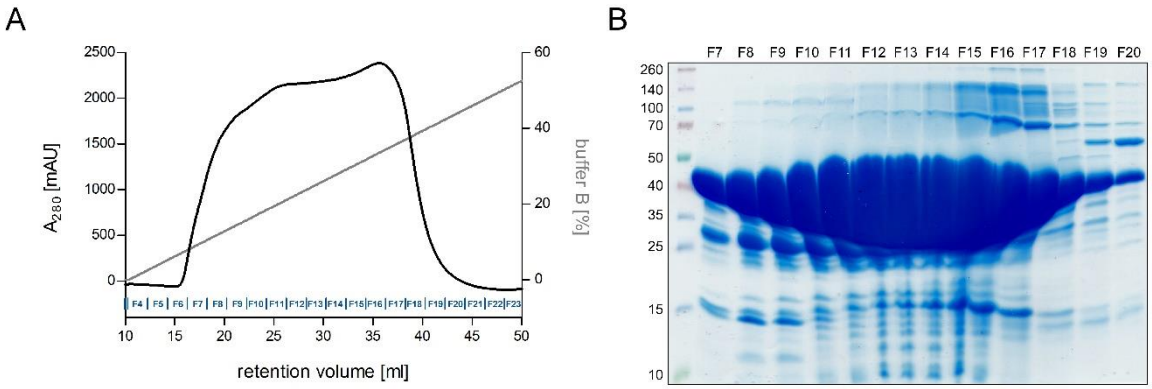

Figure A.5: Purification of GST-Survivin120 by ion exchange chromatography.
A) Absorbance chromatogram at 280 nm of the ion exchange chromatography following GSH affinity purification. The elution gradient (0–100 % ion buffer B, 25 mM to 1 M NaCl, 75 ml, grey) and the collected elution fractions (F4–F23, blue) are included. **B)** Coomassie-stained SDS gel of protein-containing elution fractions. Fractions F7–F19 contain GST-Survivin120 with few impurities. They were pooled, concentrated and used for subsequent experiments. Yield: 62.2 mg per liter of bacterial culture.

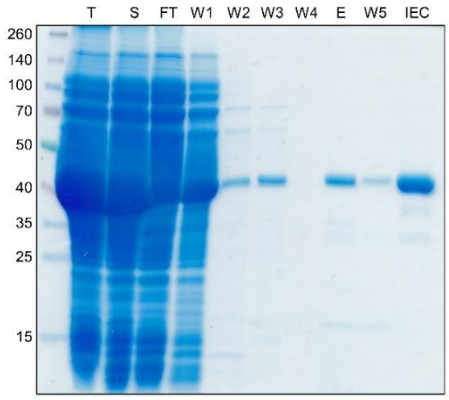

Figure A.6: Overview of the purification procedure of GST-Survivin120.
Coomassie-stained SDS gel of samples taken after the respective purification steps (T: total lysate, S: supernatant, FT: flow through of GSH column loading, W1–W4: wash fractions after loading the GSH column, E: GSH-elution of protein from the GSH column onto an ion exchange column, W5: final wash fraction of rinsing protein from the GSH column onto an ion exchange column, IEC: pooled and concentrated protein after ion exchange chromatography).

A.4 Purification of GST-Survivin120-K90/91/103S

Recombinant GST-Survivin120-K90/91/103S was used as bait protein for pull-down experiments.

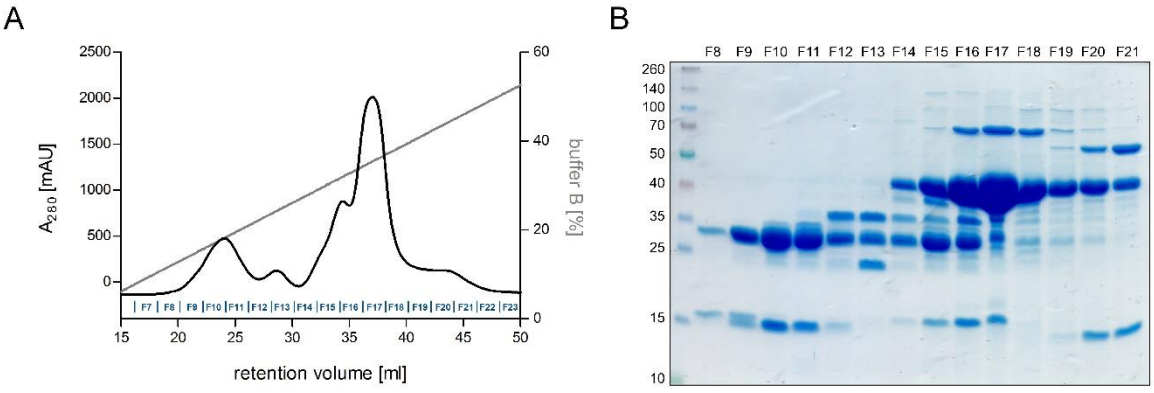

Figure A.7: Purification of GST-Survivin120-K90/91/103S by ion exchange chromatography.
A) Absorbance chromatogram at 280 nm of the ion exchange chromatography following GSH affinity purification. The elution gradient (0–100 % ion buffer B, 25 mM to 1 M NaCl, 75 ml, grey) and the collected elution fractions (F7–F23, blue) are included. **B)** Coomassie-stained SDS gel of protein-containing elution fractions. Fractions F14–F18 contain GST-Survivin120-K90/91/103S with few impurities. They were pooled, concentrated and used for subsequent experiments. Yield: 3.2 mg per liter of bacterial culture.

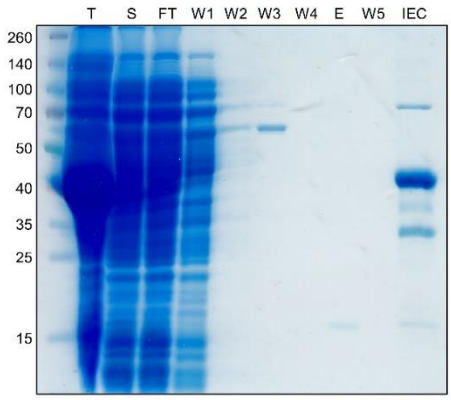

Figure A.8: Overview of the purification procedure of GST-Survivin120- K90/91/103S.
Coomassie-stained SDS gel of samples taken after the respective purification steps (T: total lysate, S: supernatant, FT: flow through of GSH column loading, W1–W4: wash fractions after loading the GSH column, E: GSH-elution of protein from the GSH column onto an ion exchange column, W5: final wash fraction of rinsing protein from the GSH column onto an ion exchange column, IEC: pooled and concentrated protein after ion exchange chromatography).

A.5 Amino acids

Table A.1: Amino acids and their letter codes.

one letter code	three letter code	amino acid	one letter code	three letter code	amino acid
A	Ala	alanine	M	Met	methionine
C	Cys	cysteine	N	Asn	asparagine
D	Asp	aspartic acid	P	Pro	proline
E	Glu	glutamic acid	Q	Gln	glutamine
F	Phe	phenylalanine	R	Arg	arginine
G	Gly	glycine	S	Ser	serine
H	His	histidine	T	Thr	threonine
I	Ile	isoleucine	V	Val	valine
K	Lys	lysine	W	Trp	tryptophan
L	Leu	leucine	Y	Tyr	tyrosine

A.6 Vector maps

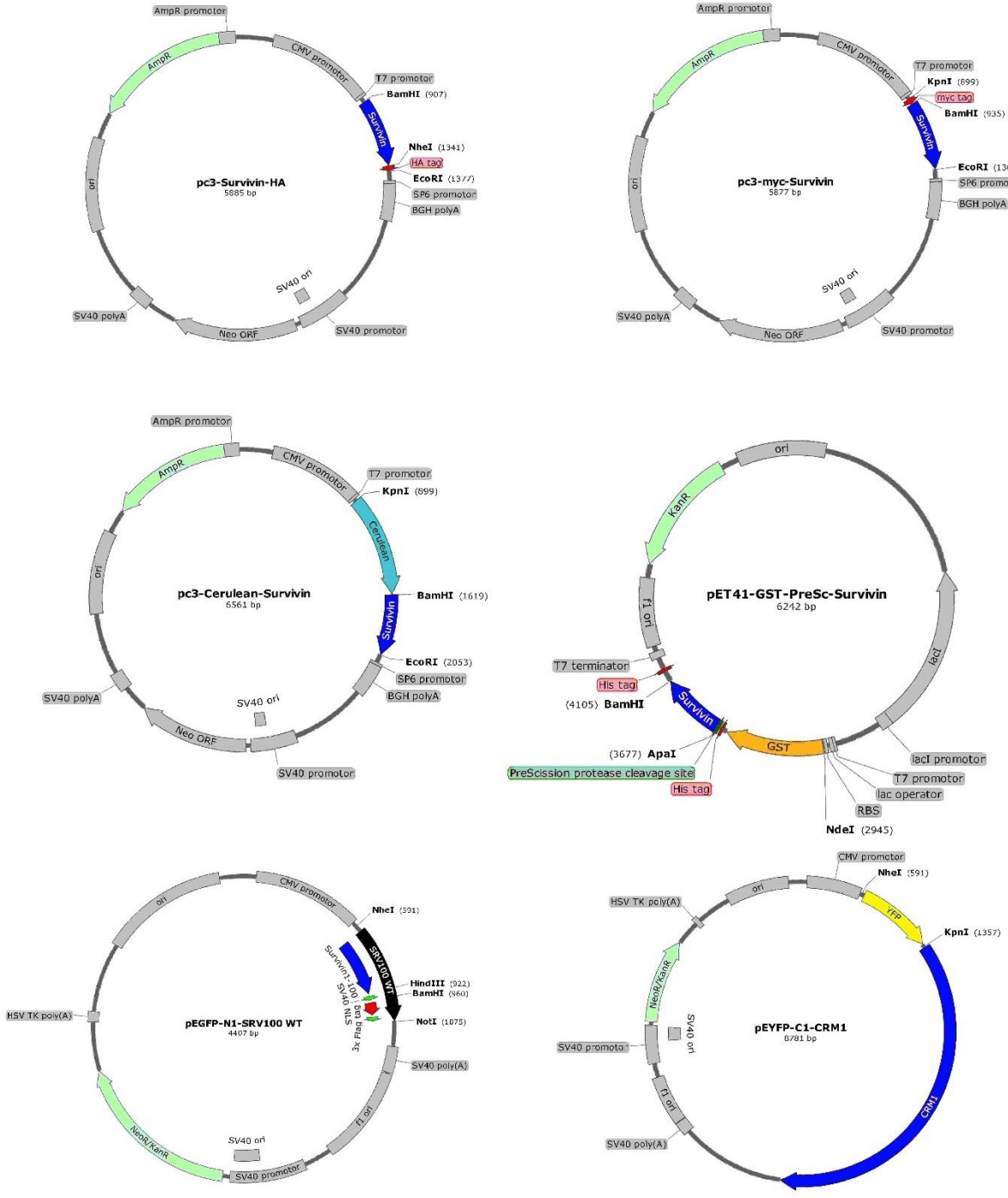

Figure A.9: Vector maps of selected eukaryotic and prokaryotic expression plasmids.

DANKSAGUNG

An dieser Stelle möchte ich allen Menschen danken, die mir in den letzten Jahren zur Seite standen, mich durch meine Promotion begleitet und zum Gelingen dieser Arbeit beigetragen haben.

Zuallererst möchte ich mich bei Prof. Dr. Shirley Knauer für die Möglichkeit bedanken, im Rahmen meiner Promotion ein interessantes und sehr interdisziplinäres Thema bearbeiten zu dürfen. Herzlich bedanken möchte ich mich für ihre wissenschaftlichen Ratschläge, aber vor allem auch für ihre persönliche Unterstützung in den letzten Jahren sowie die wertvollen Kommentare zu dieser Arbeit.

Ich danke Herrn Prof. Dr. Peter Bayer als meinen zweiten Mentor im Rahmen des CRC-1093-Graduiertenkollegs für die wissenschaftliche Unterstützung in den letzten Jahren sowie für die Übernahme des Zweitgutachtens dieser Arbeit.

Besonders möchte ich mich bei allen jetzigen aber auch ehemaligen „Shirley's Girlies und dem Quoten-Boy" (Knauer-Gruppe) bedanken: ohne euch wäre die Promotionszeit nicht das, was sie war, eine Zeit mit vielen schönen und lustigen Momenten, an die ich mich immer gerne erinnern werde. Danke zum einen für die wissenschaftlichen Diskussionen, eure Anregungen und Ideen sowie für das großartige Arbeitsklima und die große Hilfsbereitschaft im Laboralltag, aber zum anderen auch und vor allem danke für all das, was neben der Wissenschaft für den nötigen Spaß gesorgt hat.
Im Besonderen möchte ich mich bei der kleinen „CRC-1093-Mannschaft" bedanken: Cecilia danke ich für die vielen gemeinsamen Stunden bei Seminaren (mit liebevoll zubereitetem Tee!), Workshops und Symposien sowie für das PLA- und das TAMRA-Tweezer-Experiment, und Annika möchte ich für die Übernahme des Projektes danken, das bei ihr in gute Hände kommt. Ein liebes Dankeschön geht an Elisabeth: wenn jemand die Laborganisation im Griff hat, dann sie! Weiterhin möchte ich Stefanie danken für ihre großartige Unterstützung im Labor durch zahlreiche Klonierungen und Proteinreinigungen.

Im Rahmen des Survivin-Projekts danke ich Christian (Schrader-Gruppe) für die aufwendige Herstellung der supramolekularen Tweezer-Moleküle, die MD-Simulationen sowie die Auswertungen der ITC-Messungen. Christine (Bayer-Gruppe) danke ich für die Durchführung

der Proteinreinigung von isotopenmarkiertem Survivin und der NMR-Titrationsexperimente aber vor allem für ihr Interesse und ihren unermüdlichen Einsatz für den Fortschritt des Projektes. Jean-Noël (Hoffmann-Gruppe) und Yasser (Sánchez-García-Gruppe) danke ich für die MD-Simulationen und QM/MM-Berechnungen.

Speziell möchte ich Nina (Imaging Centre Campus Essen) danken für ihre ständige Hilfsbereitschaft bei aufkommenden Fragen rund ums Thema Mikroskopie sowie die automatisierte Bildauswertung von Zell-Experimenten.

Ich danke der Deutschen Forschungsgemeinschaft für die finanzielle Unterstützung meiner Dissertation und für die Teilnahme am CRC-1093-Graduiertenkolleg "Supramolekulare Chemie an Proteinen“. Ein herzliches Dankeschön möchte ich dem gesamten Team des CRC-1093 aussprechen für die hilfreichen und unbürokratischen Kooperationen. Insbesondere Dr. Lydia Didt-Koziel und Raya Schindler danke ich für die großartige Koordination und Organisation rund um den CRC-1093. Für weitere erfolgreiche Kooperationen neben dem Survivin-Projekt danke ich Sandra, Poulami und Krishna (Schmuck-Gruppe) sowie Jörg (Schlücker-Gruppe).

Robert und Johannes (Meyer-Gruppe) danke ich für ihre ständige Hilfsbereitschaft bei aufkommenden Fragen rund ums Thema Proteinbiochemie. Zudem danke ich ihnen für die technische Hilfe bei der Äkta, der ITC und der CD-Spektroskopie.

Nadine, Annika, Elisabeth, Cecilia und Papa danke ich für das Korrekturlesen dieser Arbeit.

Mein größter Dank gilt zu guter Letzt meiner Familie, besonders meinen Eltern und Geschwistern, sowie Benjamin und meinen Freunden, die mich während meiner Promotion immer unterstützt, aufgebaut und nie an mir gezweifelt haben.

PUBLICATIONS, TALKS AND POSTER PRESENTATIONS

PUBLICATIONS

Accepted:

Jan 2018 — Wissler J., Wehmeyer M., **Bäcker S.**, Knauer S. and Schlücker S. (2018). Simultaneous Rayleigh/Mie and Raman/Fluorescence Characterization of Molecularly Functionalized Colloids by Correlative Single-Particle Real-Time Imaging in Suspension. *Analytical chemistry*, 90 (1): 723–728.

Nov 2017 — Junghänel S., Karczewski S., **Bäcker S.**, Knauer S.K. and Schmuck C. (2017). A Systematic Structure-Activity Study of a New Type of Small Peptidic Transfection Vector Reveals the Importance of a Special Oxo-Anion-Binding Motif for Gene Delivery. *Chembiochem: a European journal of chemical biology*, 18 (22): 2268–2279.

Aug 2017 — Wissler J., **Bäcker S.**, Feis A., Knauer S.K. and Schlücker S. (2017). Site-Specific SERS Assay for Survivin Protein Dimer: From Ensemble Experiments to Correlative Single-Particle Imaging. *Small*, 13 (32).

Jul 2017 — Jana P., Samanta K., **Bäcker S.**, Zellermann E., Knauer S. and Schmuck C. (2017). Efficient Gene Transfection through Inhibition of β-Sheet (Amyloid Fiber) Formation of a Short Amphiphilic Peptide by Gold Nanoparticles. *Angewandte Chemie (International Edition in English)*, 56 (28): 8083–8088.

Oct 2016 — Samanta K., Jana P., **Bäcker S.**, Knauer S. and Schmuck C. (2016). Guanidiniocarbonyl pyrrole (GCP) conjugated PAMAM-G2, a highly efficient vector for gene delivery: The importance of DNA condensation. *Chemical communications*, 52 (84): 12446–12449.

May 2015 — Wünsch D., Hahlbrock A., Heiselmayer C., **Bäcker S.**, Heun P., Goesswein D., Stöcker W., Schirmeister T., Schneider G., Krämer O.H., Knauer S.K. and Stauber R.H. (2015). Fly versus man: Evolutionary impairment of nucleolar targeting affects the degradome of Drosophila's Taspase1. *FASEB journal: official publication of the Federation of American Societies for Experimental Biology*, 29 (5): 1973–1985.

Apr 2015 — Wünsch D., Hahlbrock A., Heiselmayer C., **Bäcker S.**, Schrenk C., Benne F., Schilling O. and Knauer S.K. (2015). Evolutionary divergence of Threonine Aspartase1 leads to species-specific substrate recognition. *Biological chemistry*, 396 (4): 367–376.

PUBLICATIONS

Submitted:

Samanta K., Jana P., **Bäcker S.**, Knauer S.K., Schmuck C. (2018). Vesicles formed by a PAMAM-G2 Dendrimer functionalized with Guanidiniocarbonyl Pyrrole Groups Allow the pH-controlled Encapsulation of Dyes and their Intracellular Delivery. *Angewandte Chemie (International Edition in English).*

In preparation:

Bäcker S.‡, Heid C.‡, Meiners A., Beuck C., Vallet C., Pörschke M., Grad J.-N., Ruiz-Blanco Y.B., Sánchez-García E., Hoffmann D., Bayer P., Schrader T., Knauer S.K. (2018). Specific inhibition of the Survivin-CRM1 interaction by peptide-modified molecular tweezers.
‡ equal author contribution.

Jana P., Samanta K., Ehlers M., Zellermann E., **Bäcker S.**, Knauer S.K., Schmuck C. (2018). Impact of Peptides Sequences on Their Structure and Function: Mimicking of Virus-like Nanoparticles for Gene Delivery (both DNA and siRNA).

TALKS

09/05/2017	CRC 1093 Bi-Weekly Seminar of the Integrated Graduate School, University of Essen
26/04/2017	ZMB Lunch Seminar, University of Essen
02/04/2015	ZMB Lunch Seminar, University of Essen
04/11/2014	CRC 1093 Bi-Weekly Seminar of the Integrated Graduate School, University of Essen
23/09/2014	First CRC 1093 Graduate Student Symposium 2014 “Supramolecular Chemistry on Proteins”, Schloss Gnadenthal in Kleve

POSTER PRESENTATIONS

24-26/09/2017	International Fall Meeting of the German Society for Biochemistry and Molecular Biology (GBM) 2017 “Molecular Basis of Life”, Ruhr University of Bochum
21/09/2017	Second CRC 1093 International Symposium 2017 “Supramolecular Chemistry on Proteins”, University of Essen
01/09/2016	Joint CRC 765 (Free University of Berlin) and CRC 1093 (University of Duisburg-Essen) Graduate Student Symposium 2016 “Protein–Ligand Interactions”, Hannover
29/09/2015	First CRC 1093 International Symposium 2015 “Supramolecular Chemistry on Proteins”, University of Essen
23/09/2014	First CRC 1093 Graduate Student Symposium 2014 “Supramolecular Chemistry on Proteins”, Schloss Gnadenthal in Kleve

CURRICULUM VITAE

The curriculum vitae is not included in the online version for reasons of data protection.

EIDESSTATTLICHE ERKLÄRUNGEN

Erklärung:

Hiermit erkläre ich gem. § 7 Abs. (2) d) + f) der Promotionsordnung der Fakultät für Biologie zur Erlangung des Dr. rer. nat., dass ich die vorliegende Dissertation selbstständig verfasst und mich keiner anderen als der angegebenen Hilfsmittel bedient, bei der Abfassung der Dissertation nur die angegeben Hilfsmittel benutzt und alle wörtlich oder inhaltlich übernommenen Stellen als solche gekennzeichnet habe.

Essen, den 05. Juni 2018

Sandra Bäcker

Erklärung:

Hiermit erkläre ich gem. § 7 Abs. (2) e) + g) der Promotionsordnung der Fakultät für Biologie zur Erlangung des Dr. rer. nat., dass ich keine anderen Promotionen bzw. Promotionsversuche in der Vergangenheit durchgeführt habe und dass diese Arbeit von keiner/keinem anderen Fakultät/Fachbereich abgelehnt worden ist.

Essen, den 05. Juni 2018

Sandra Bäcker

Erklärung:

Hiermit erkläre ich gem. § 6 Abs. (2) g) der Promotionsordnung der Fakultät für Biologie zur Erlangung des Dr. rer. nat., dass ich das Arbeitsgebiet, dem das Thema “Dissection and Modulation of (patho)biological Survivin Functions by supramolecular Ligands” zuzuordnen ist, in Forschung und Lehre vertrete und den Antrag von Sandra Bäcker befürworte und die Betreuung auch im Falle eines Weggangs, wenn nicht wichtige Gründe dem entgegenstehen, weiterführen werde.

Essen, den 05. Juni 2018

Prof. Dr. Shirley Knauer